NEK6 CONTROLS MITOTIC PROGRESSION THROUGH REGULATING EML3 LOCALISATION TO SPINDLE MICROTUBULES

Thesis submitted for the degree of

Doctor of Philosophy

At the University of Leicester

By

Jessica M. Montgomery BSc (Hons) (Leeds)

Department of Molecular and Cell Biology

University of Leicester

May 2016

DECLARATION

The accompanying thesis submitted for the degree of Doctor of Philosophy, entitled *'Nek6 controls mitotic progression through regulating EML3 localisation to spindle microtubules'* is based on work conducted by the author in the Department of Molecular and Cell Biology at the University of Leicester mainly during the period between October 2012 and May 2016. All work recorded in this thesis is original unless otherwise acknowledged in the text or by references. None of the work has been submitted for another degree in this or any other University.

Signed:

Date:

Department of Molecular and Cell Biology

University of Leicester

Lancaster road

Leicester

LE1 9HN

NEK6 CONTROLS MITOTIC PROGRESSION THROUGH REGULATING EML3 LOCALISATION TO SPINDLE MICROTUBULES

Jessica M. Montgomery

ABSTRACT

EMLs are a highly conserved family of microtubule-associated proteins that play a role in microtubule stability. In humans there are six EMLs. EML1, EML2, EML3 and EML4 consist of a largely unstructured basic N-terminal domain (NTD) that contains a short coiled-coil mediating trimerisation, and a highly structured C-terminal domain (CTD) named the TAPE domain. Microtubule binding is conferred through the NTD whilst the TAPE domain binds to soluble tubulin dimers. EML5 and EML6 lack the N-terminal region but have three continuous TAPE domains encoded within a single polypeptide. Previous proteomic studies had identified EML3 as a binding partner of Nek6, a serine/threonine kinase that promotes mitotic spindle assembly. In this study, we have explored the microtubule binding properties of EML3 and its regulation by Nek6. Using a stable cell line expressing YFP-EML3, fixed and time lapse imaging revealed that EML3 associates along the length of microtubules and exhibits rapid recovery following photobleaching. Whilst microtubule binding of the related EML1-NTD was reduced upon incubation of microtubules with the protease subtilisin in vitro. This suggests an electrostatic interaction between the basic EML-NTD and the acidic tubulin C-terminal tails. Immunoprecipitation experiments confirmed the interaction between EML3 and Nek6 and revealed that this interaction is increased in mitosis. Unexpectedly, while EML3 bound strongly to interphase microtubules, it exhibited much lower affinity for microtubules in mitosis. Depletion of Nek6 led to accumulation of EML3 on spindle microtubules in mitosis, whilst expression of a constitutively active Nek6 displaced EML3 from interphase microtubules. By mass spectrometry a number of phosphorylation sites were identified within the basic NTD of EML3 upon incubation with Nek6. Furthermore, introduction of acidic charge into the basic NTD of EML3 perturbed its association with interphase microtubules. Hence, we propose that phosphorylation of EML3 by Nek6 disturbs electrostatic interactions between the basic N-terminus and the acidic surface of MTs. This leads to reduced association of EML3 with microtubules in mitosis. We speculate that this decreases microtubule stability, facilitating mitotic spindle assembly and search and capture of condensed chromosomes.

ACKNOWLEDGMENTS

CONTENTS

ABBREVIATIONS

µg	microgram
µl	microliter
µM	micromolar
aa	amino acid
ab	antibody
ABL1	Abelson murine leukemia viral oncogene homolog 1
ALK	Anaplastic lymphoma kinase
APC/C	anaphase promoting complex/cyclosome
APC	Adenomatous polyposis coli
APS	ammonium persulfate
bp	base pairs
BRCA1	Breast cancer type 1 susceptibility protein
BSA	bovine serum albumin
C-	carboxy
CC	coiled-coil
Cdc20	cell division cycle 20
Cdc25	cell division cycle 25
CDK	cyclin-dependent kinase
Chk	checkpoint kinase
CKI	Cdk inhibitor
DDR	DNA damage response
DMSO	dimethylsulfoxide
DNA	deoxyribonucleic acid
EDTA	ethylene diamine tetraacetic acid
EGTA	ethylene glycol tetraacetic acid
EMAP	echinoderm microtubule-associated protein
EML	Echinoderm microtubule-associated protein-like proteins
FBS	foetal bovine serum

G418	geneticin
GDP	guanosine diphosphate
GFP	green fluorescent protein
GTP	guanosine triphosphate
HELP	hydrophobic EMAP like domain
IF	immunofluorescence microscopy
IP	immunoprecipitation
kDa	kilo Daltons
M	molar
MCC	mitotic checkpoint complex
MAPs	microtubule associated proteins
MCAK	mitotic centromere-associated kinesin
m. wt	molecular weight
mg	milligram
Mins	minutes
ml	millilitre
mM	millimolar
MT	microtubules
MTOC	microtubule organising centre
ng	nanogram
NIMA	never in mitosis A
nm	nanometer
nM	nanomolar
PBS	phosphate buffered saline
PCM	pericentriolar material
PTMs	post-translational modifications
Rpm	revolutions per minute
SAC	spindle assembly checkpoint
SDS	sodium dodecyl sulfate
SDS-PAGE	SDS polyacrylamide gel electrophoresis

siRNA   small interfering RNA

TALL   T cell acute lymphoblastic leukaemia

TAPE   Tandem atypical β-propeller

TLL   Tubulin Tyrosine Ligase

U2OS   human osteosarcoma

v/v   volume per volume ratio

TABLES AND FIGURES

CHAPTER 1   INTRODUCTION

1.1 The Eukaryotic Cell Cycle

In this section I will outline the highly complex, ordered events of the eukaryotic cell cycle that are required to produce two identical daughter cells. This is important to understand, as errors in the mechanisms regulating the cell cycle can lead to the progression of diseases, such as cancer. On the other hand, by understanding the molecular mechanisms of cell cycle control novel cancer therapies can be developed.

The eukaryotic cell cycle can be divided into two parts: interphase and mitosis (Figure 1.1). Interphase is the time the cell spends growing and replicating its DNA, whilst mitosis is the period when equal separation of the chromosomes takes place to generate two identical daughter cells. In terms of timing, a normal cell will only spend about 5% of its time in mitosis. Interphase is divided into three stages named G1, S and G2 phases. The G1 (gap 1) phase corresponds to the interval between the previous M phase and the following S phase and is when the cell synthesises proteins and organelles and takes the decision whether to commit to another round of cell division. G1 is followed by S (synthesis) phase whereby DNA replication takes place; this needs to be accurate to ensure the correct genetic material is passed on to daughter cells. Following this the cell enters the G2 (gap 2) phase, during which proteins are synthesised in preparation for mitosis and the cell ensures that DNA replication is complete. The cell will then go through mitosis and the cycle can begin again. Proliferating cells with a total cycling time of 24 hours would spend approximately 11 hours in G1, 8 hours in S, 4 hours in G2 and 1 hour in M phase. However, there is a fifth stage named G0 (quiescent stage) whereby cells exit the cell cycle from G1 and no longer divide, this can occur for a number of reasons including lack of sufficient growth factors.
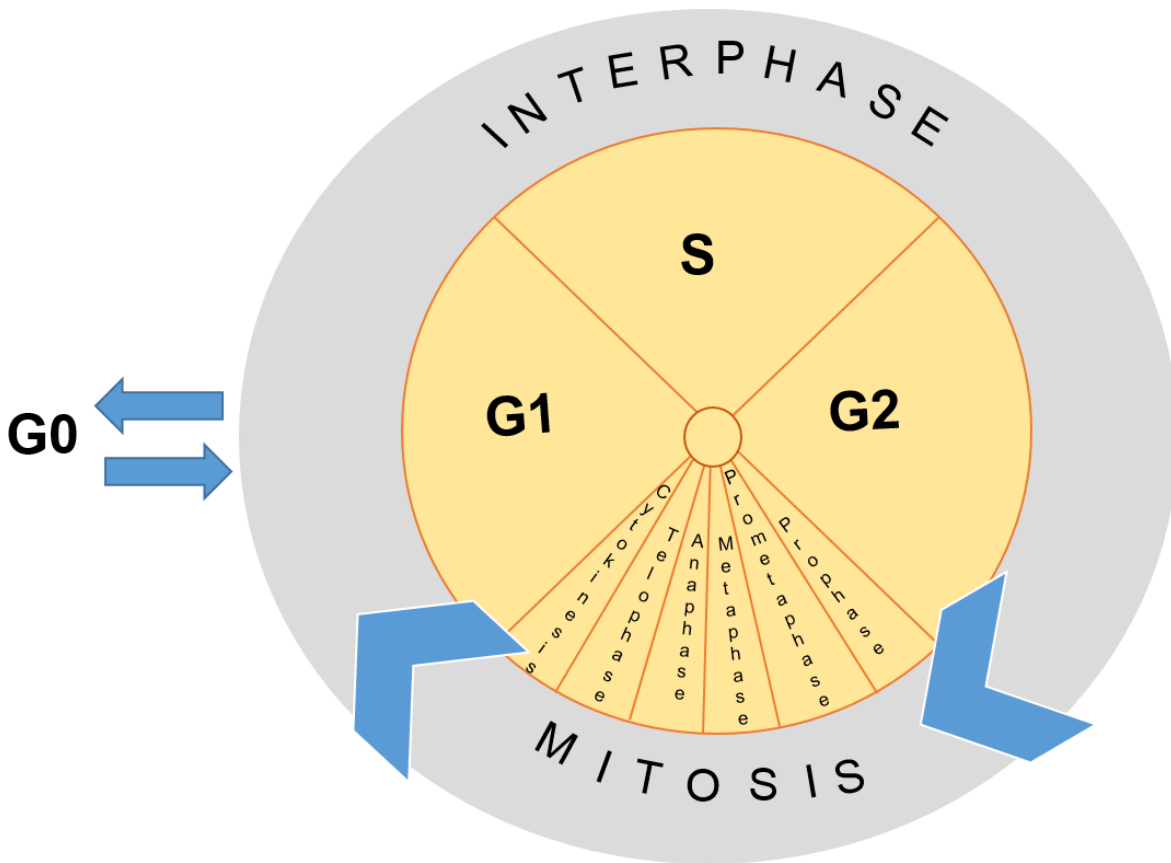
Figure 1.1 The eukaryotic cell cycle

The eukaryotic cell cycle is divided into two broad phases termed interphase and mitosis. Interphase is then split into three further phases consisting of two growth phases, G1 and G2, and a DNA synthesis phase, termed S-phase. The Mitosis or M-phase is then subdivided into six more distinct phases including cytokinesis. The quiescence phase (G0) is entered when the cell is deprived of stimulating growth factors.

1.2 Mitosis

Walther Flemming (1843-1905) coined the term "mitosis" from the Greek word for thread. This was due to his observation of fibrous structures in dividing cells. However, the existence of the microtubules (MTs) or 'spindle fibers' were disputed for a number of years (Wordeman & Asbury 2001). Mitosis itself is a highly complex process which is also sub-divided into different stages: prophase, prometaphase, metaphase, anaphase, telophase and cytokinesis (Figure 1.2). During prophase, there is the condensation of the duplicated chromosomes from a dispersed to a compact composition, whilst the centrosomes or microtubule organising centres separate and migrate to opposite poles of the cell. From here they nucleate the formation of MTs which form a highly dynamic bipolar mitotic spindle structure essential for chromosome capture. Prometaphase is characterised by the breakdown of the nuclear envelope allowing MTs access to the chromosomes.

This interaction is mediated via an interaction between the kinetochore structures found at the centromere and the MTs termed 'K fibres'. In anaphase, the sister chromatids are then 'pulled' to opposite ends of the cell, a phenomena mediated through forces exerted from the MTs. The decondensation of the chromosomes and the reformation of nuclei can be seen during telophase, followed by the physical separation of the daughter cells along with the division of the cytoplasm and organelles in cytokinesis.

As briefly highlighted, the process of mitosis is highly complex and unfortunately errors in cell division can occur, for example due to abnormal centrosome numbers or aberrant MT based spindle formation (Nigg & Raff 2009). This can result in abnormal chromosome numbers (aneuploidy), which is a typical hallmark of cancer cells. Furthermore, if during cell division, chromosomes are consistently lost or gained, this represents a property termed chromosome instability. Chromosomal instability is a common feature within malignant tumours but the exact pathogenic role has not yet been established, for this reason it is still unclear as to whether chromosomal instability is a cause or consequence of cancer progression. An increase in the number of chromosomes or chromosomal mutations will lead to higher levels of other genetic abnormalities, some of which may stimulate tumour progression. For example aneuploidy/polyploidy is associated with a worse prognosis and reduced survival rate
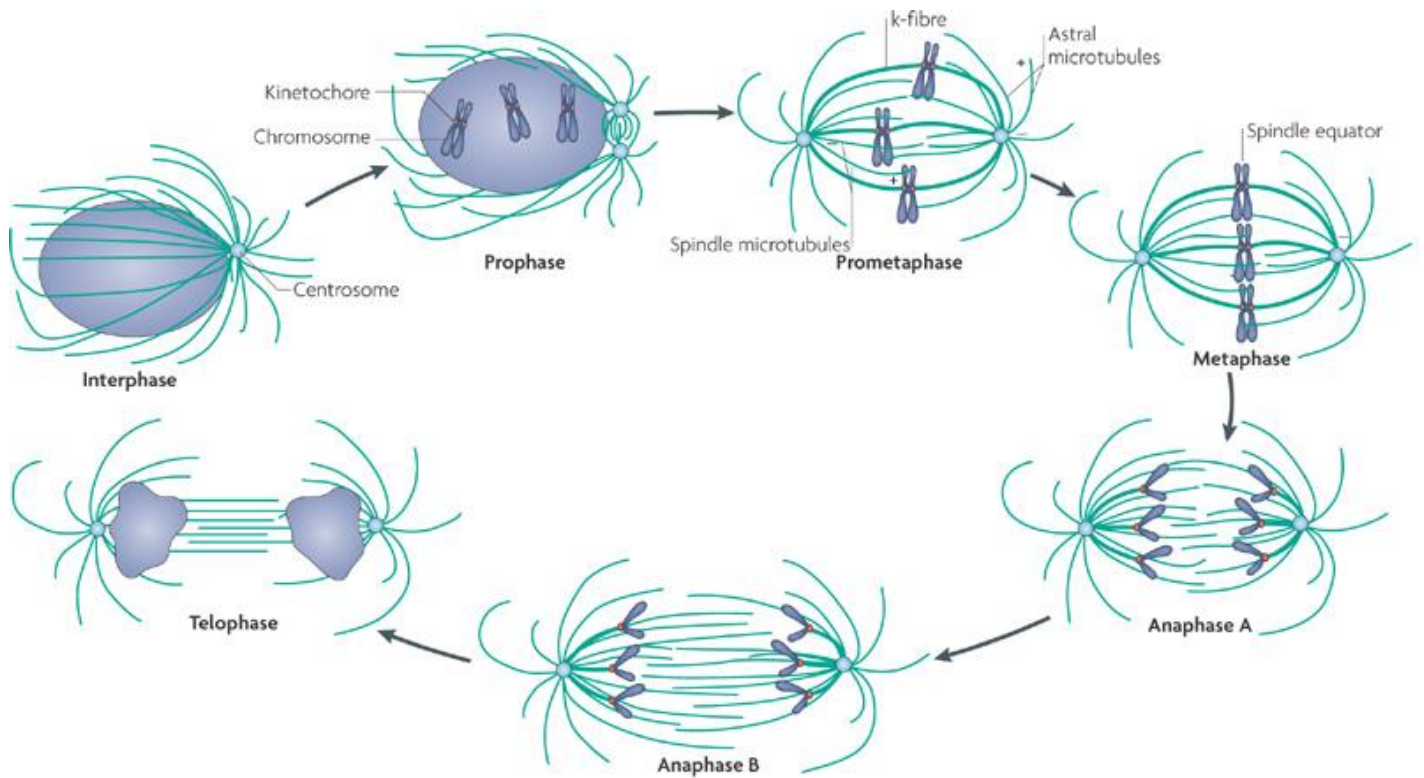
Figure 1.2 Phases of Mitosis

M-phase is divided into six distinct stages; prophase, prometaphase, metaphase, anaphase, telophase and cytokinesis. Note the rearrangement of the microtubule network at the different stages of mitosis. Taken from Walczak et al. 2010.

in patients with colorectal cancer (Walther et al. 2008). On the other hand, disruptions in proteins which control cell cycle progression could increase proliferation and stimulate rearrangements of the chromosomes. For example the inactivation of the retinoblastoma protein has been shown to slow mitotic progression and promote aneuploidy with pRB-deficient cells able to continue proliferating and exhibiting whole-chromosome gains and losses (Manning et al. 2010). Other proteins such as BRCA1 and BRCA2 have also linked chromosomal abnormalities to chromosomal instability in in pancreatic cancer mouse models (Cassidy et al. 2014). This supports the idea that aneuploidy is involved in driving tumorigenesis.

Fortunately, cells have mechanisms in place to correctly orchestrate the cell cycle, known as 'checkpoints'. These checkpoints are found at G1/S, during S-phase, G2/M and during mitosis and work via a range of mechanisms. In this section we will focus on the spindle assembly checkpoint (SAC) (Figure 1.3). The SAC is in place to prevent the entry of a cell from metaphase into anaphase without the correct capture of the chromosomes, thus preventing the development of aneuploidy. This SAC signal is produced at unattached kinetochores, multi-protein complexes critical for the attachments between chromosomes and microtubules. Screens have identified the following genes as important for SAC arrest: mitotic-arrest deficient (MAD) genes, MAD1, MAD2 and MAD3 (BUBR1 in humans), and the budding uninhibited by benzimidazole (BUB) gene, BUB1 and BUB3 (Musacchio & Salmon 2007). For mitosis to occur cell division cycle 20 (Cdc20) activates the E3 ubiquitin ligase anaphase-promoting complex/cyclosome (APC/C). This complex mediates polyubiquitylation of cyclin B and securin which in turn promotes their destruction via the 26S proteasome (Musacchio & Salmon 2007). Securin acts as an inhibitor of the separase protease and it is this protease which cleaves the cohesin complex that holds sister chromatids together (Musacchio & Salmon 2007). The unattached kinetochore recruits a number of proteins including MAD1 and MAD2 which binds to the APC/C activator Cdc20 and along with BUBR1, BUB3 and Aurora A forms the major anaphase inhibitor or MCC (Kops et al. 2012). This complex localizes in a dynamic manner to the kinetochores and within the cytoplasm whereby it binds and inhibits the APC/C.
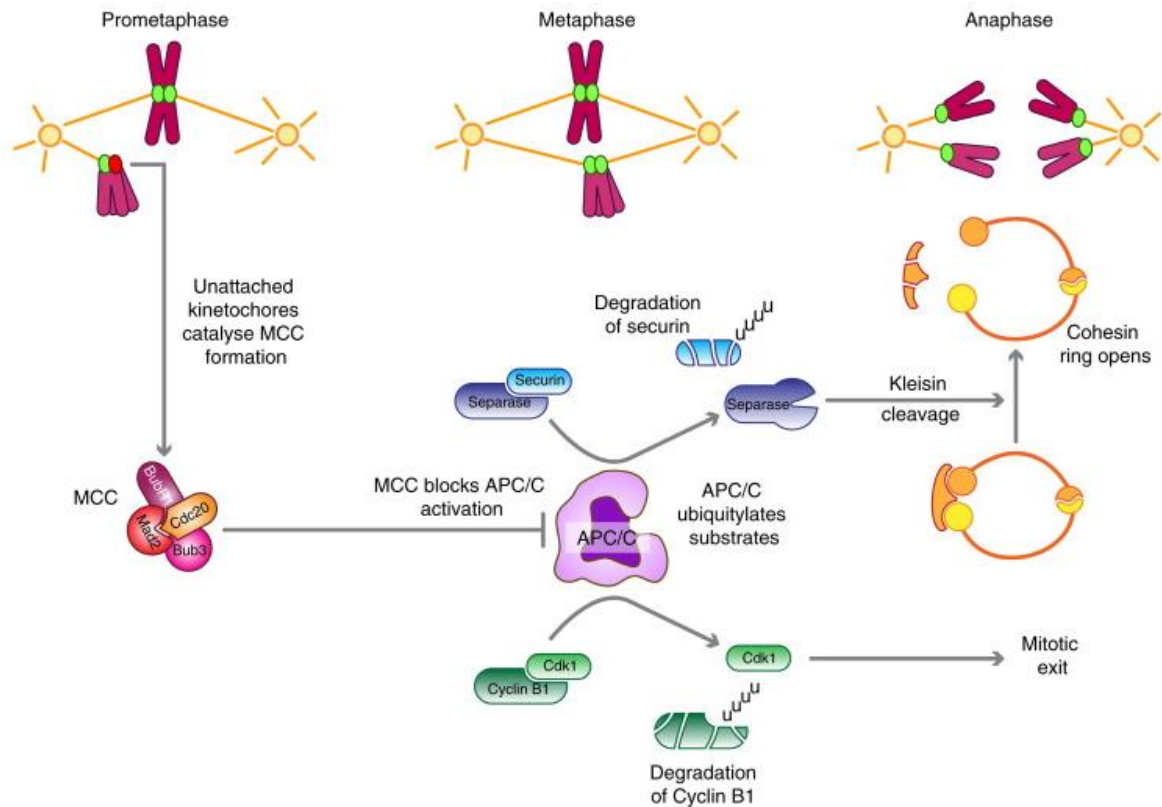
Figure 1.3 Activation of the Spindle Assembly Checkpoint (SAC)

The SAC is a protective mechanism used by the cell to prevent the entry from metaphase into anaphase until full chromosome biorientation and congression has been achieved. The key players involved include the mitotic checkpoint complex (MCC), the anaphase promoting complex (APC/C) and separase. Taken from Lara-Gonzalez et al. 2012.

During division, each chromatid has their own kinetochore to ensure that each pair is split to each daughter cell. This requires that MTs from one pole of the spindle attach to one sister and the other pole to the other sister. Recent studies have shown that this bipolar arrangement of the MTs generates physical tension between the sister kinetochores and this tension is also required to silence the SAC (Kops et al. 2012). This 'tension hypothesis' first gained support following micromanipulation studies whereby anaphase could be delayed by a single tensionless chromosome and then cell division restarted by artificially applying tension to the chromosome (Maresca et al. 2010).

1.3 Microtubules (MTs)

1.3.1 MT Structure and Dynamics

MTs are major components of the eukaryotic cytoskeleton. MTs are dynamic structures which are able to grow and shrink through assembly and disassembly depending on the requirements of the cell (Figure 1.4). In interphase they form an intricate network which maintains the cell's structure, are components of the cilia and flagella, influence both cell motility and cell polarity, and are involved in intracellular transport of secretory vesicles. In mitosis, the MT network is reorganised to form the mitotic spindle, which is responsible for capturing the chromosomes. To highlight the importance of MTs, mutations in specific tubulin genes including TUBA1A, TUBB2B and TUBB3, cause a wide spectrum of foetal brain malformations including microlissencephaly to classical lissencephaly, and in some cases polymicrogyria due to disordered cytoskeletal proteins and aberrantly located neurons (Fallet-Bianco et al. 2014).

MTs are assemblies of α and β tubulin heterodimers, which themselves have a structure of a compactly folded body and disordered negatively charged C-terminal tail (Mandelkow & Mandelkow 1994). These heterodimers then arrange longitudinally in a head-to-tail fashion to form protofilaments. Thirteen protofilaments then laterally interact to form a hollow tubular structure with a diameter of approximately 25 nm and an internal lumen (Meunier & Vernos 2012). In terms of structure, the tubulin body is

involved in tubulin-tubulin interactions whilst the C terminal tails decorate the MT exterior. The tubulin body is more conserved, sharing 80-95% sequence identity whereas the tails only share 50% identity. This allows for different interactions and biophysical properties without affecting MT polymerisation (Roll-Mecak 2014). The highly acidic C-terminal tails of tubulin are rich in glutamic and aspartic acid residues and are termed the 'tubulin E-hooks'. These E-hooks decorate the outer surface of the MTs and allow for interactions with MAPs and MT motors and undergo numerous PTMs (Figure 1.5).

Another member of the tubulin family, γ-tubulin, promotes MT nucleation. Its functions are part of the γ-TuRC (γ-tubulin ring complex) (Meunier & Vernos 2012). The γ-TURC is a component of the centrosome which acts as the major microtubule organising centre (MTOC) in human cells. Centrosomes are complex in structure consisting of two cylindrical centrioles, which are composed of nine short triplets of stabilised MTs organised in a barrel, surrounded by an extensive lattice of fibrous and globular proteins which forms the pericentriolar material (PCM). During the cell cycle the centrosomes undergo their own cycle of duplication. In S phase the centrioles begin to replicate with each of the centrioles giving rise to the growth of a new centriole. The centrosomes then become enlarged in G2 through the recruitment of additional PCM in a process termed 'maturation'. Finally, the two 'parental' centrioles become detached from each other (centrosome disjunction) and move apart to form the mitotic spindle at the G2/M transition. Additional members of the tubulin family, namely δ and ε tubulin, have also been found to localize at centrioles and be necessary for centriole duplication (Chang & Stearns 2000).

Due to the longitudinal orientation of the protofilaments, MTs have a distinct polarity with the α-tubulin exposed end being the minus end and the β-tubulin exposed end being the plus-end. Each end can exhibit distinct dynamics but the plus-end is the more dominant site for the addition of tubulin subunits and MT elongation, whereas the minus-end is usually embedded within the MTOC (Meunier & Vernos 2012). MTs undergo stochastic switching between phases of growth and shrinkage, a phenomena termed 'dynamic instability'. The terms used to describe these events are 'rescue', the transition from shortening to growing, and 'catastrophe' the transition from growth to shrinkage.
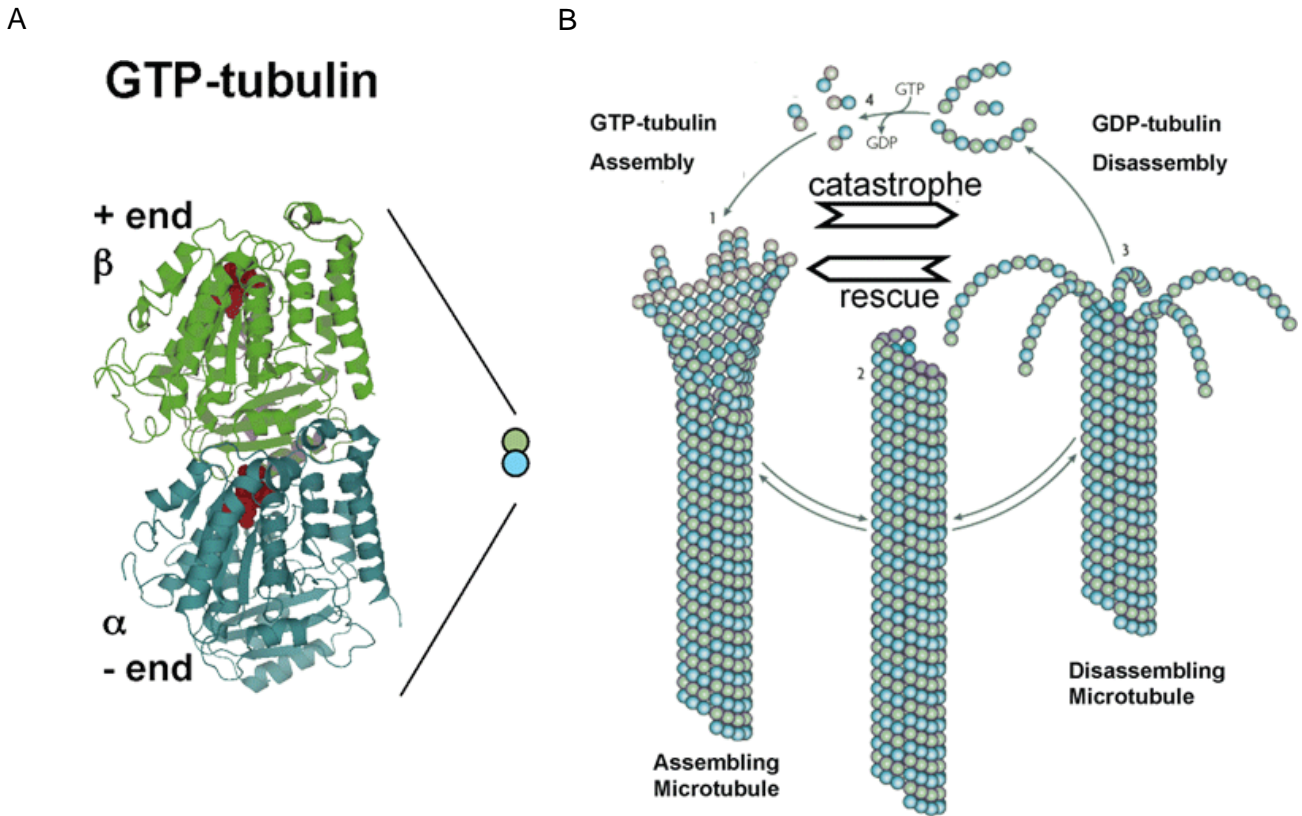
Figure 1.4: Microtubule assembly and dynamics

A. Structure of the tubulin dimer composed of α and β tubulin bound to GTP. **B.** Microtubules form cylindrical structures which are able to grow and shrink according to the needs of the cell, a phenomenon termed 'dynamic instability'. This dynamic instability is dependent on the β-tubulin capped plus ends and is mainly influenced by GTP hydrolysis. If a MT switches from a growing to shrinking phase this is called catastrophe whilst a switch from a shrinking to growth phase is termed rescue. Taken from Akhmanova & Steinmetz (2008).

There is also a phenomena called 'treadmilling' where there is addition of subunits at one end accompanied by the loss of subunits at the other. This instability is thought to be mainly driven by GTP hydrolysis with the β-tubulin subunit at the plus-end of the MT. αβ-tubulin contains two GTP-binding sites; the N-site (non-exchangeable) in α-tubulin is buried within the tubulin dimer whereas the E-site in β-tubulin is exposed on the surface (Alushin et al. 2014). Upon addition of tubulin dimers into a growing microtubule plus end, the α-tubulin subunit in the incoming dimer contacts the E-site GTP of the terminal β-tubulin subunit, completing the binding pocket that enables hydrolysis (Alushin et al. 2014). As a result a GTP cap allows MT elongation whilst exposure of GDP causes rapid shortening (Mandelkow & Mandelkow 1994). Other key factors determining MT instability are; the temperature with cold favouring shrinkage and the concentration of soluble tubulin available in the cytoplasm. Previous studies have suggested that conformational changes in tubulin allow for transitions between polymerization to depolymerisation (Alushin et al. 2014). A straight tubulin conformation is found within the body of the microtubule whereas a curved conformation is found in microtubule depolymerization peels (Alushin et al. 2014). Structural studies by Alushin et al. (2014) supports this and shows that GTP hydrolysis causes compaction of the E-site resulting in longitudinal translation of the α-tubulin intermediate domain. This leads to conformational strain that would be released by bending during depolymerization.

At the onset of mitosis there is rapid depolymerisation of the interphase MT network, with shorter, more numerous and less stable MTs nucleated from the centrosomes (Meunier & Vernos 2012). After nuclear envelope breakdown (prometaphase), the chromosomes also direct MT assembly to facilitate interaction with the kinetochores. In animal cells, there are 3 distinct subclasses of MTs which make up the mitotic spindle; astral MTs, interpolar MTs and the kinetochore fibres (K fibres). Interpolar MTs are the most dynamic (average half-life of less than 1 minute) and most abundant class of spindle MTs composing the main body of the mature spindle (Meunier & Vernos 2012). They are required for the establishment and maintenance of spindle bipolarity, as they radiate from the centrosomes and interact with the interpolar MTs radiating from the opposite spindle pole. Also they have been shown to play a role in chromosome congression through chromokinesins which push chromosome arms towards the metaphase plate (Meunier & Vernos 2012). K-fibres are bundles of MTs

that directly connect the spindle poles and kinetochore. These are much less dynamic than the interpolar MTs with a half-life of around 4-8 minutes and are composed of 20-40 MTs (Meunier & Vernos 2012). Their main function is to attach the chromosomes to the spindle poles and separate sister chromatids, with the MT bundling partially mediated by the proteins TACC3, clathrin and chTOG (Meunier & Vernos 2012). Lastly, astral MTs radiate from the centrosomes to the cell periphery and play a role in spindle positioning and cleavage furrow induction (Rankin & Wordeman 2010).

1.3.2 MT Regulation

The expression of different tubulin isoforms, MAPs and motor proteins along with specific posttranslational modifications (PTMs) of tubulin, are thought to be crucial for the diverse properties and functions of the MT network. Expression of different tubulin isoforms together with different PTMs create what has been called the 'tubulin code'. Humans have eight α-tubulin (TUBA1A, TUBA1B, TUBA1C, TUBA3C, TUBA3D, TUBA3E, TUBA4A and TUBA8) and seven β-tubulin genes (TUBB, TUBB1, TUBB2A, TUBB2B, TUBB2C, TUBB3, TUBB4, TUBB4Q and TUBB6) (Roll-Mecak 2014). Some isoforms are specific to certain tissues and developmental stages (Janke 2014). These isoforms are similar in terms of their core tubulin structure but differ in residues within their C-terminal tails which allows for specific interactions with certain MAPs. For example, the MT motors, kinesin-1 and kinesin-2, exhibit differential binding to MTs composed of different tubulin isoforms, while Katanin, an MT severing protein, preferentially binds MTs assembled with TUBB2 isoforms (Sirajuddin et al. 2014, Ghosh et al. 2012).
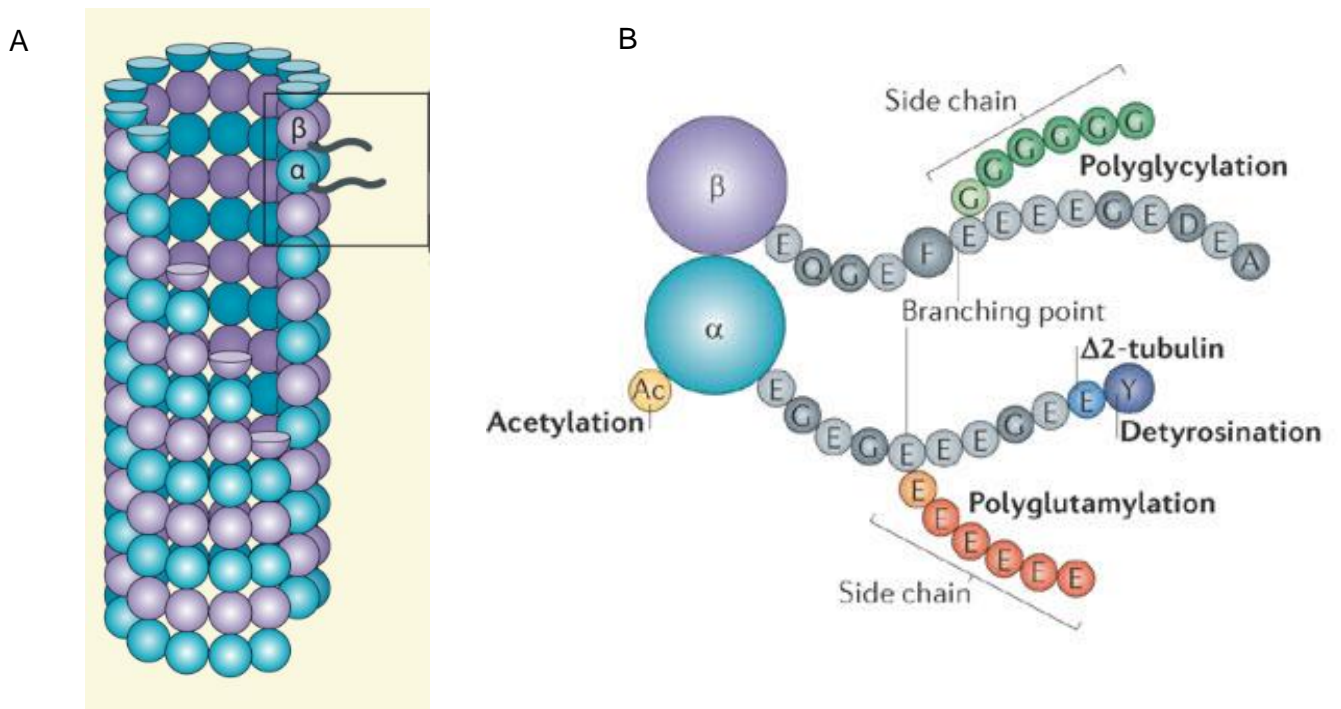
Figure 1.5 MT C-terminal 'E-hooks' and their PTMs

A. Schematic representations of the tubulin E-hooks decorating an individual MT and **B.** the residues which compose the E-hooks and their potential PTMs. Taken from Janke and Bullinski.

MT PTMs include acetylation, polyglutamylation, polyglycylation, phosphorylation, ubiquitylation, sumoylation, palmitolyation, tyrosination and detyrosination (Figure 1.4) (Kaverina & Straube 2011). It remains to be determined why tubulin undergoes such a vast range of PTMs, however some functions have been discussed. Firstly, they influence the recruitment of MAPs: for example, older microtubules which possess higher levels of modifications are hotspots for the MT severing MAP, Katanin (Sharma et al. 2007). Secondly, PTMs can directly regulate MT dynamics, for example, inhibition of the tubulin deacetylase HDAC6, has been shown to increase MT stability *in vivo* (Verhey & Gaertig 2007). The PTMs take place on tubulin subunits that are already part of the MT network and are mostly clustered within the C-terminal tails which protrude from the surface of the MTs and are thus readily accessible for interacting molecules (Wehenkel & Janke 2014).

Phosphorylation of β-tubulin can occur on serine residues within the C-terminal tails although the enzymes responsible are currently unknown. Outside of this region β-tubulin can be phosphorylated on Ser172 by Cdk1/cyclin B complexes, although the consequences of this are also unknown (Verhey & Gaertig 2007). Acetylation of α-tubulin specifically occurs on residue Lys40 within a disordered loop located within the MT lumen and is associated with stable MTs, thought to prevent MT severing (Hammond et al. 2008). Recent studies have also shown acetylation on Lys252 of non-polymerised β-tubulin (Chu et al. 2011). Two known tubulin deacetylation enzymes include the HDAC6 and SIRT2, whilst acetyltransferases shown to specifically mediate α-tubulin acetylation include ARD1-NAT1 and the elongator protein complex (Janke & Chloë Bulinski 2011). Detyronisation involves the removal of the gene-encoded C-terminal tyrosine of α-tubulin by currently unidentified carboxypeptidases and tyrosination is the enzymatic re-addition by the tubulin tyrosine ligase (TTL) of the C-terminal Tyr (Janke & Bulinski 2011).

The detyrosination/tyrosination cycle differentially recruits molecular motors and plus-end tip tracking proteins, for example kinesin-1 preferentially binds to detyrosinated MTs (2.8 fold increase), which is important for neuronal transport (Dunn et al. 2008, Janke & Bulinski 2011). Alternatively, a reduction in tyrosinated MTs causes mislocalisation of the +TIP protein CLIP170 and misorientated spindles in mitosis

(Hammond et al. 2008). Furthermore improper regulation of this cycle influences tumorigenesis and neuronal organisation, whilst TTL-null mice die right after birth (Hammond et al. 2008, Prota et al. 2013). Lastly, modifications such as glutamylation and glycylation involve the addition of glutamate and glycine residues onto the carboxyl side-chain of glutamate residues in the C-terminal tails of both α and β tubulin (Hammond et al. 2008). Loss of these modifications in the C-terminal tails of β-tubulin results in non-motile, short cilia and disruptions in intraflagella transport (Hammond et al. 2008). Tubulin polyglutamylation is also increased during neuronal differentiation (Janke 2014).

1.3.3 MT Targeting Drugs

One of the major hallmarks of cancer progression is uncontrolled cell proliferation. As a result, inducing cell cycle arrest (cytostatic) or cell death (cytotoxic) in cancer cells is a primary therapeutic objective. Many chemotherapeutic drugs induce cell death for example, alkylating agents (e.g. chlorambucil) induce DNA damage resulting in a G1/S arrest and subsequent cell death, while the topoisomerase inhibitors (e.g. irinotecan) induce single and double stranded breaks in S and G2 phase, again causing arrest and apoptosis. Other chemotherapy drugs prevent MT dynamics. These interfere with the formation of the mitotic spindle leading to prolonged activation of the SAC that ultimately induces apoptosis. These MT targeting drugs, often termed 'anti-mitotics', fall into two main classes: the vinca alkaloids, such as vincristine, vinblastine and vinorelbine, and the taxanes, such as paclitaxel and docetaxel. Vinca alkaloids are often used in combination therapies to treat haematological malignancies and lung cancers, whilst the taxane drugs are common treatments for breast and ovarian cancers (Gascoigne & Taylor 2009).

The vinca alkaloids were first isolated from *Catharanthus roseus,* more commonly known as the rosy or Madagascan periwinkle. The first–generation drugs included vincristine and vinblastine but more recently second generation vinca alkaloids have been developed such as vinorelbine and vinflunine, to overcome toxicity and resistance. In general, their mechanism of action is through an interaction with β-tubulin at a region adjacent to the GTP-binding site, meaning the vinca alkaloids bind

to tubulin at the plus-tip of microtubules (Gascoigne & Taylor 2009). This interaction at high drug concentrations induces microtubule depolymerisation by blocking the addition of tubulin subunits and triggering catastrophe and shrinkage. This disrupts spindle organisation thus preventing completion of mitosis (Jordan et al. 1991). The second generation drug, vinorelbine, shows improved efficacy and reduced toxicity and is effective in treating non-small-cell lung cancer, metastatic breast cancer and ovarian cancer with studies also proving promising for lymphoma, oesophageal and prostatic cancers (Ngan et al. 2001).

Taxol was originally derived from the bark of *Taxus brevifolia,* more commonly known as the Pacific yew. Taxol also binds to the β-tubulin subunit but can bind the length of the polymer and can to restore the longitudinal interface and the α-tubulin intermediate domain to a GTP-like state, resulting in straighter and more stable MT structures (Alushin et al. 2014). Overstabilising the MT network prevents the disassembly required at the onset of mitosis and the cell is unable to construct a mitotic spindle. However, despite the same mechanism of action, paclitaxel and docetaxel have been suggested to have significant pharmacological differences, with docetaxel having a longer plasma half-life and longer intracellular retention (Crown & O'Leary 2000).

Despite these effective drug treatments, the reality is that the overall benefit provided by these MT poisons are often limited in the patient, mainly due to the development of resistance. Patients treated with taxol in particular often have intrinsic resistance meaning the drug has little or no effect on cancer regression for that patient. Taxol resistance occurs directly at the microtubule level via tubulin mutations, changes in tubulin isotype expression, selective post-translational modifications and altered MAP expression (Orr et al. 2003). Further to this MT poisons are linked to severe toxicity with patients often showing side effects of myelosuppression, neurotoxicity inducing peripheral neuropathy, fatigue, alopecia, diarrhoea, mucosal toxicity and skin changes due to the lack of specificity for cancer cells (Gascoigne & Taylor 2009). As a result, further understanding of the molecular mechanisms involved in controlling MT dynamics and spindle organisation will potentially shed light on novel, more specific, efficacious therapeutics for the future.

1.4 MT Associated Proteins

Microtubule associated proteins or MAPs control almost every aspect of MT dynamic behaviour. By modulating in space and time the dynamics and organisation of MT assembly, this creates MTs with distinct properties in certain regions of the cell or stage of the cell cycle (Al-Bassam & Chang 2011). Originally it was assumed that all MAPs bind to and stabilise MTs, but MAPs that destabilise or sever MTs have been identified. Some of the more common stabilising and destabilising MAPS are summarised along with their effect on MT dynamics in Table 1.1.

1.4.1 Stabilising MAPs

Some of the better characterised MAPs include Tau, MAP4 and MAP2. All three vertebrate members have alternative splice isoforms, share a conserved C-terminal domain containing MT binding repeats and a N-terminal domain of varying size (Dehmelt & Halpain 2005). MAP2 and Tau are found in neurons whereas MAP4 is present in neurons and a range of other tissues, but all three possess MT stabilising activity (Dehmelt & Halpain 2005). Tau is primarily found in neurons, whereby phosphorylated of KXGS motifs (especially Ser262 and Ser356) reduces its ability to associate to MTs (Johnson & Stoothoff). Tau is crucial for neuronal polarity as well as in generating neuronal growth cones (Dehmelt & Halpain 2005). Furthermore, deregulated Tau is associated with Alzheimer's disease and a range of neurodegenerative disorders known as tauopathies. The pathological mechanism is thought to be via Tau hyperphosphorylation or 'toxic Tau' which results in a loss of normal function whilst also sequestering any normal Tau (Iqbal et al. 2005). Similarly, MAP2 is primarily found in dendritic extensions of post-mitotic cells and plays a role in neurite outgrowth and dendritic development, therefore making MAP2 a hallmark of neuronal differentiation. Moreover, MAP4 is present in all neuronal tissues, within the cerebellum Purkinje cells and the hippocampus pyramidal cells and is thought to be crucial for cytoskeletal reorganisation and regulation of MT-dependent transport within the neuron (Tokuraku et al. 2010).

Understanding the individual roles, mechanisms and regulation of MAPs will be crucial for the future development of cancer chemotherapies. Differing MAP expression in cancer tissue can cause resistance to certain chemotherapies, thus making them an important area of research. For example, alterations in MAP4 expression has been reported to modulate sensitivity to MT poisons such as taxol, with MAP4 phosphorylation and dissociation from MTs correlating with decreased taxol sensitivity in ovarian cancer cell lines. Further to this, in tissue cultured cells, paclitaxel treatment disrupts the plus tip tracking protein EB1 (Tirnauer & Bierer 2000). Consequently, further understanding of MAP expression in tumours would facilitate more effective combination therapies and even drugs with the ability to change the expression levels of relevant MAPs in the desired direction (either through up-regulation or down-regulation). MT stabilisation can occur through various mechanisms including increasing polymerisation, decreasing depolymerisation, increasing the rescue frequency and decreasing the catastrophe frequency. In this chapter I will discuss a range of stabilising MAPs with unique functions and interactions.

1.4.1.1 EMAP115

EMAP115 (*Xenopus*) / MAP7 (human) was isolated from a HeLa screen as a 220 kDa protein and unlike most other MAPs is expressed in epithelial cells (Masson & Kreis 1995). EMAP115 binds to and stabilises MTs *in vivo* and *in vitro*, by promoting growth and strongly associates with interphase MTs (Masson & Kreis 1995, Gallaud et al. 2014). However, it is disputed as to whether it is required for mitotic spindle formation (Masson & Kreis 1995, Gallaud et al. 2014). EMAP115 is abundant during mouse epithelial development and is predominantly expressed in HeLa and MCF-7 carcinoma cells (Faire et al. 1999). Moreover, *Drosophila* that are homozygous for EMAP115 gene deletion are unable to survive to adulthood, indicating that this protein is vital for survival (Barlan et al. 2013).

STABILISING	Growth	Shrinkage	Frequency of Rescue	Frequency of Catastrophe
MAP2	↑		↑	↓
Tau	↑		↑	↓
XMAP215/chTOG	↑↑	↑	↑	
EMAP115	↑			
EB-1				↓
MAP4	↑			↓
Doublecortin	↑			
DESTABILISING				
Op/18	↓			↑
Katanin				↑
MCAK		↓		↑

Table 1.1 An overview of some well characterised MAPs

MAPs are proteins which interact with the MTs and are involved in regulating the dynamic instability. MAPs can be either stabilising or destabilising and the mechanisms of some of the MAPs discussed in the following sections are outlined above.

At the onset of prophase, EMAP115 localisation is lost from MTs and as mitosis progresses EMAP115 localises only weakly to spindle poles. It then re-associates strongly with MTs of the newly established MT network during telophase (Masson & Kreis 1995). Consequently, it was postulated that EMAP115 may undergo degradation upon mitotic entry (Yen et al. 1992). However, western blot analysis revealed that this was not the case and EMAP115 is in fact phosphorylated at the onset of mitosis (Masson & Kreis 1995). This phosphorylation increases by 15 fold in mitosis, resulting in the protein becoming hyperphosphorylated and unable to interact with MTs, due to the reduction in net positive charge weakening the binding to the acidic surface of the MTs (Masson & Kreis 1995). This is similar to XMAP230, a *Xenopus* egg protein, which is hyperphosphorylated during mitosis causing dissociation from MTs at the onset of prophase and rebinding during anaphase (Andersen et al. 1994). However these results have been challenged by Faire et al. 1999 who observed that EMAP115 remained associated to MTs throughout the cell cycle and did not modulate MT dynamics *in vivo.* These differences were thought to be due to differing cell types resulting in differences in MAP expression, EMAP115 regulators or tubulin isoforms, thus highlighting the complicated nature of MAPs and microtubule dynamics.

Another role of EMAP115 is the association with kinesin-1, a major MT motor that drives transport of numerous cellular cargos towards the plus ends of MTs (Hirokawa & Tanaka 2015). Defects in kinesin-1 can cause a range of metabolic and brain disorders and thus regulation of this protein is crucial (Hirokawa & Tanaka 2015). In the cell, kinesin-1 exists primarily in its inactive state and motor activation occurs upon cargo binding to the C-terminal domain (Barlan et al. 2013). RNAi depletion of EMAP115 in *Drosophila* S2 cells resulted in lack of kinesin-1 transport and EMAP115 is therefore thought to play a role in relieving autoinhibition of kinesin-1 (Barlan et al. 2013). Recently, studies have shown this interaction is crucial during interphase to trigger centrosome separation (Gallaud et al. 2014).

1.4.1.2 XMAP215

Another well characterised stabilising MAP is XMAP215, which acts as a MT polymerase. XMAP215 is a 215 kDa protein, first studied in *Xenopus*, hence the name XMAP<u>215</u>. Cloning of XMAP215 revealed conserved members, including *Dis1* in *Schizosaccharomyces pombe* and *Stu2* in *Saccharomyces cerevisiae* both of which are important for MT stabilisation (Kinoshita et al. 2002). The human homologue is the <u>c</u>olonic and <u>h</u>epatic <u>t</u>umour <u>o</u>verexpressing <u>g</u>ene or ch-TOG, which along with XMAP215 has 5 TOG domains (Kinoshita et al. 2002). Mutations within TOG domains, especially TOG1 and TOG2, disrupt the activity of the protein whilst other TOG domains mediate MT binding and are therefore crucial for normal protein function (Widlund et al. 2011). Further to this XMAP215 is unable to bind MTs that have been subjected to subtilisin digestion, indicating that the interaction with MTs is likely mediated through the negative C-terminal tails of tubulin, termed 'E-hooks' (Widlund et al. 2011).

In vitro XMAP215 stimulates the growth rate of MTs 8 fold and is thought to stimulate the growth rate at the MT plus ends (Vasquez et al. 1994). In depletion experiments, lack of XMAP215 resulted in much shorter and more dynamic MTs in both interphase and mitotic *Xenopus* egg extracts, a phenotype rescued by the addition of purified XMAP215 (Kinoshita et al. 2002). Whilst in mitotic cells knockdown of XMAP215 leads to small, abnormally organised spindles and increased frequency of catastrophes, indicating that this protein is necessary for proper mitotic spindle formation (Al-Bassam & Chang 2011, Tournebize et al. 2000). The ability of XMAP215 to modulate catastrophe frequency is due to its ability to antagonise <u>X</u>enopus <u>k</u>inesin <u>c</u>atastrophe <u>m</u>odulator-1 (XKCM1), a member of the Kin I kinesin family which uses the energy of ATP hydrolysis to depolymerize microtubules (Walczak et al. 2002). XMAP215 binds tubulin dimers and adds them to the MT ends, making it a polymerase that directly catalyzes the addition of tubulin dimers to the growing plus end (Widlund et al. 2011, Brouhard et al. 2008) . Furthermore, XMAP215 is phosphorylated during mitosis by CDK1 (Gard & Kirschner 1987). *In vitro* phosphorylation of XMAP215 reduced its ability to promote MT elongation but it is undetermined as to whether this is the case *in vivo* (Vasquez et al. 1999).

In terms of localisation, XMAP215 localises to the MT plus ends, kinetochores and to a varying degree along the MT lengths (Al-Bassam & Chang 2011). Interestingly, biochemical analysis in *Drosophila* also revealed that this protein not only acted on MT plus ends, but the C-terminal domain of the protein localised to centrosomes, an interaction mediated by the transforming acidic coiled-coil proteins (TACC) and Aurora A kinase activity (Kinoshita et al. 2002). XMAP215 binds MTs directly with relatively low affinity. This allows for cycles of binding, release and rebinding that facilitate rapid diffusion along the MT lattice, leading to collection at the plus end (Al-Bassam & Chang 2011). This accumulation at the plus end was thought to be due to an interaction with the plus-tip tracking protein EB1, an interaction identified in frog egg extracts (Zanic et al. 2013). XMAP215 and EB1 work synergistically to increase the growth rate, with their combined effect increasing growth by 33 fold, whereas XMAP215 alone increased growth rate by only 8 fold and EB1 alone only 1.5 fold (Zanic et al. 2013).

1.4.1.3 EB1

The EB family is a highly conserved group of proteins present in yeast through to humans. In budding yeast the EB family member, *Bim1p,* regulates MT stability and is essential for the positioning of the mitotic spindle (Tirnauer & Bierer 2000). Yeast lacking the *Bim1* gene are viable but their MTs are much shorter than wild-type and they show abnormal MT dynamics (Ligon et al. 2003). In general, EB proteins localise to spindle and interphase MTs, especially at the plus tips. The number of EB proteins in the family is unknown but to date EB1, EB2, EB3 and EBF3 have been identified along with the highly related RP1, RP2 and RP3 proteins (Tirnauer & Bierer 2000).

Human EB1 is a 35 kDa protein that is mildly acidic and is present in many cell types, including neuronal, lymphocytic and epithelial (Tirnauer & Bierer 2000). It is activated by the removal of its autoinhibitory tail (aa 249-268) or by proteins that bind this tail (Zhu et al. 2009). Experiments using purified tubulin have shown EB1 regulates the dynamics and structure of MTs and can stimulate spontaneous nucleation and growth of MTs, whilst promoting both catastrophes and rescues (Vitre et al. 2008). Further to this overexpression of EB1 causes MTs to bundle and whereby EB1 is strongly associated to the bundled MTs, again indicating EB1 as a stabilising protein.

Moreover, electron cryomicroscopy showed that EB1 induces the initial formation of tubulin sheets, which close into the 13 protofilament microtubule architecture, crucial for the generation of the MT network (Vitre et al. 2008). However, the exact roles of EB1 have been disputed; for example EB1 has been shown to inhibit catastrophes in both *Xenopus laevis* egg extracts and *Schizosaccharomyces pombe* whilst in *Saccharomyces cerevisiae* and *Drosophila melanogaster* cells EB1 increases catastrophes (Vitre et al. 2008). This could, in part, be due to the position and type of tag used in these experiments as it has been shown that N-terminal His tags dramatically increase the activity of EB1 (Zhu et al. 2009).

EB1 was first cloned as an interacting partner of the adenomatous polyposis coli (APC) protein in a yeast two-hybrid screen (Tirnauer & Bierer 2000). APC is a key tumour suppressor and mutations in APC are associated with most colon cancers (Aoki & Taketo 2007). Therefore it could be that the EB1-APC complex plays a role in chromosome segregation, disruptions in which cause chromosomal instability and stimulate cancer progression.

EB1 can also interact with dynein, via the dynactin component p150Glued (Tirnauer & Bierer 2000, Ligon et al. 2003). Dynein is a minus-end directed MT based motor that is involved in Golgi dynamics and vesicle transport, mutants in which cause delayed cytokinesis due to abnormal spindle position (Tirnauer & Bierer 2000). While EB1 and p150Glued play a role in microtubule dynamics and stability, they have distinct roles as EB1 causes MT elongation whilst p150Glued influences microtubule nucleation (Ligon et al. 2003). Recent studies have shown that EB1 and p150 target the human dynein complex to growing microtubule ends via the hierarchical dynactin/CLIP-170/EB1 interaction module. CLIP-170 binds relatively efficiently to EB1 and provides new binding sites for p150, p150 then recruits the dynein complex which is essential for correct initiation of cargo transport from microtubule plus ends (Duellberg et al. 2014) .

As previously discussed EB1 can also work synergistically with XMAP215 to stabilise MTs, although these proteins are not thought to interact directly or control one another's cellular localisation (Zanic et al. 2013). Taken together this data has led to the hypothesis of a plus-end complex, yet this has not been proven (Ligon et al. 2003).

1.4.2 Destabilising MAPs

Depolymerizing activity is pivotal for spindle formation and chromosome movement. Some of the mechanisms of destabilising proteins include decreasing polymerisation, increasing depolymerisation, decreasing rescue frequencies or increasing the frequency of catastrophe. In this section I will discuss, as examples, two MT destabilising proteins, MCAK and katanin.

1.4.2.1 MCAK

Mitotic centromere-associated kinesin (MCAK) is a member of the kinesin-13 family and is a potent depolymeriser of MTs that localise to plus ends. Unlike other classical kinesins, the members of the kinesin-13 family do not use the energy from ATP turnover to move along the MTs but rather to promote depolymerisation (Sanhaji et al. 2011). Variable numbers of kinesin-13 family members exist in invertebrate species; these include Klp10A, Klp59C, and Klp59D in *Drosophila melanogaster* (Sanhaji et al. 2011). In mammals, there are three main family members, named Kif2A, Kif2B and Kif2C (or MCAK) (Sanhaji et al. 2011). Studies have shown that MCAK can also localise to MT minus ends where it acts in a similar manner to that of the plus end (Moore et al. 2005). Increased MCAK expression accelerates depolymerisation 200-fold (Helenius et al. 2006, Hunter et al. 2003). Furthermore, similar effects were observed when high levels of MCAK were added to *Xenopus laevis* extracts, resulting in shorter spindles during meiotic spindle assembly (Domnitz et al. 2012).

MCAK reaches the plus tips very quickly, making it 100 fold times faster than kinesin-1. This indicates that MCAK is probably diffusing along the length of the MTs (Helenius et al. 2006). Moreover, MCAK relies on the electrostatic interaction with tubulin E-hooks for this fast diffusion to occur (Helenius et al. 2006). Once at the plus end MCAK interacts with EB proteins allowing it to track assembling MT tips and, during mitosis, it is also localised at the centromere, centrosomes and polymerising MT tips (Domnitz et al. 2012). MCAK is thought to be concentrated at MT plus ends to provide the depolymerising activity required to limit MT length, by removing tubulin subunits and prevent long spindles during bipolar MT assembly (Domnitz et al. 2012). Research was undertaken to understand how a MT tip enriched with a destabilising protein was

able to polymerise and it was suggested that MCAK's depolymerising activities must somehow be regulated. Indeed it was found that MCAKs tip tracking capabilities are negatively regulated by phosphorylation, with Aurora B phosphorylation inactivating the protein, thus blocking MCAK accumulation at centromeres (Ohi et al. 2004). Other kinases have also been indicated to regulate MCAK, these include Aurora A, Polo-like kinase 1 and cyclin dependent kinase 1 (Sanhaji et al. 2011).

Proper regulation of MCAK is important for ensuring the segregation of chromosomes in mitosis and for safeguarding chromosome stability. Indeed, recent studies have demonstrated that MCAK is overexpressed in primary breast cancer tissues and colorectal cancers with high expression levels linked with increased cancer invasiveness and metastasis (Sanhaji et al. 2011). As a result, MCAK and its regulators such as Aurora B could be useful targets for future cancer chemotherapy (Sanhaji et al. 2011).

1.4.2.2 Katanin

Another major MT destabiliser is katanin, a heterodimeric hydrolase constituting two subunits named p60, the 60 kDa catalytic subunit and p80 the 80 kDa regulatory subunit (Ghosh et al. 2012). The p60 subunit is a 491 amino acid long protein which contains a region required for ATP associated MT severing activity and can localise to spindle poles in mitosis (Ghosh et al. 2012, Hartman et al. 1998). The 665 amino acid long p80 subunit is required for katanin localisation to centrosomes and contains six WD40 repeats (Ghosh et al. 2012, Hartman et al. 1998). Katanin is a crucial protein involved in mitotic spindle formation, spindle MTs are severed by katanin which helps to keep the optimum number of K-fibre MTs (Ghosh et al. 2012). Katanin activity increases during prophase suggesting that it is also involved in disassembly of the interphase MT network (Sharma et al. 2007).

Katanin is classified as a MT severing protein, (other MT severing proteins include Spastin and Fidgetin), which cause internal cleavage in the MT lattice (Ghosh et al. 2012). Katanin is regulated by chemical modifications such as phosphorylation by the dual specificity tyrosine phosphorylation regulated kinase 2 (DYRK2), which enhances degradation of katanin, and other MAPs including XMAP230 which inhibits katanin

(Ghosh et al. 2012). It has also been suggested that tubulin isoforms and particular posttranslational modifications favour katanin binding, as katanin prefers acetylated MTs (Ghosh et al. 2012).

Interestingly, there is an increase in p60 expression in prostate cancer, which facilitates aggressive migration. This is thought to be a result of increased MT severing and cytoskeleton reorganisation allowing the formation of cellular protrusions required for cell motility (Ghosh et al. 2012).

1.5 The EML Family of Proteins

In this section I outline the current status of EML protein research, including the founding member EMAP, the EML oncogenic fusion proteins, the newly determine crystal structures and how EMLs have been implicated in other diseases.

1.5.1 EMAP – The Founding EML Member

The founding protein of the EML family is the Echinoderm Microtubule Associated Protein (EMAP), first isolated as a major component of MT preparations from sea urchin eggs. Unfertilised sea urchin eggs contain a large store of tubulin that becomes incorporated into the first cleavage mitotic apparatus and ciliated blastula. In the study by Suprenant et al. (1993) tubulin from unfertilised sea urchin eggs was purified and a 77 kDa polypeptide (later termed EMAP) was found to readily copurify. The EMAP cDNA was isolated and found to be conserved across a range of species including cold water sea urchin species (*S. purpuratus and L. pictus*) and warm water species (*L. variegatus, A. puctulata*) and other marine organisms (Suprenant et al. 1993). Following this, the generation of an anti-77 antibody allowed the localisation of this protein to be determined in sea urchin coelomocytes. In interphase the EMAP protein colocalised clearly with DM1A (tubulin) staining and in mitosis EMAP is distributed throughout the spindle with astral regions stained much more strongly than the central spindle (Suprenant et al. 1993). It was postulated that EMAP bound to MTs via the acidic COOH terminus (E-hooks) of tubulin but subtilisin digestion of MTs did not alter EMAP binding (Hamill et al. 1998). EMAP was also identified as a novel MAP as EMAP

antiserum did not cross react with bovine brain MAPs and Tau whilst MAP-2 antibodies failed to detect EMAP (Suprenant et al. 1993). MTs are often decorated with ribosomes and it was hypothesised that EMAP may act as the 'stalk' for ribosome attachment. Indeed, electron microscopy revealed that ribosomes were absent in these MT preparations whereby the EMAP was also absent (Suprenant et al. 1993).

As discussed in previous chapters, MTs are highly dynamic structures, in interphase MTs are much longer and stable whereas in mitosis MTs become shorter and less stable. This change occurs during the G2/M transition when there is a rapid reorganisation of the MT arrays. Using video-enhanced differential interference contrast (VE-DIC) microscopy, pig brain tubulin was used to compare the effects of EMAP with XMAP125, XMAP230 and XMAP310 on MT dynamic instability (Hamill et al. 1998). In the presence of EMAP, MTs rapidly shortened and failed to regrow. This was due to a reduction in the frequency of rescue at the plus end which was shown to be 8-fold reduced compared to tubulin alone; no effect was observed on catastrophe frequency (Hamill et al. 1998). Dynamicity was also stimulated 3-fold in the presence of EMAP, calculated by measuring tubulin subunit addition and subtraction per unit time (Hamill et al. 1998). The most likely hypothesis for this decrease in rescue frequency was that EMAP is able to stabilise protofilament 'peels' during MT disassembly. During MT shortening protofilaments peel (much like a banana skin) but these peeling events must stop before MT elongation can resume. Hence, EMAP may facilitate the protofilament peels thus reducing the frequency of rescue without having an effect on the shortening velocity (Hamill et al. 1998). As EMAP is abundantly associated with the mitotic apparatus, the assumption is that this protein is somehow involved in regulating MT assembly during mitosis.

MAPs can be regulated by phosphorylation. MAP4 and EMAP-115 undergo phosphorylation and dephosphorylation as the cell enters and exits mitosis. The introduction of negative charge by phosphorylation can reduce the affinity of MAPs for MTs. Mitotic hyperphosphorylation of EMAP-115 diminishes its ability to bind MTs, whereas *in vitro* phosphorylation of MAP4 does not alter its binding (Masson & Kreis 1995). Using *S. purpuratus* eggs metabolically labelled with 32[P]orthophosphate, Brisch et al. (1998) showed that EMAP is phosphorylated in unfertilised eggs at 5 serine residues (perhaps to enable protein folding) and remains in a phosphorylated state during mitosis with the level of phosphorylation reaching its maximum during

metaphase and decreasing during the first cleavage. The kinase identified was $p34^{cdc2}$ which can co-precipitate with EMAP at every stage of the cell cycle (Brisch et al. 1996). However, localisation studies revealed that the proteins do not colocalise with EMAP on the mitotic apparatus and $p34^{cdc2}$ on the spindle poles (Brisch et al. 1996). The authors speculate that EMAP may target $p34^{cdc2}$ to the mitotic apparatus to allow for substrate interaction or to alter its activation state.

1.5.2 ELP-1 – A Homologue of Human EMLs

Human EML1 has not been functionally characterised but the *Caenorhabditis elegans* homologue ELP-1, has been shown to play a role in touch sensitivity. During larval development, ELP-1 expression was restricted to the muscles, neurons and epithelial cells; however in the adult, expression was much more varied, including the body wall muscle, spermathecal, vulval muscle, seam cells, the intestine, touch receptor neurons and inner labial 1 neurons of the head (Hueston et al. 2008). ELP-1 was found within the six touch receptor neurons responsible for detecting light touch applied to the body surface at the dendrites and ciliated endings (Hueston et al. 2008). At the subcellular level ELP-1 localised to adhesion sites (in males and hermaphrodites) and localised to the MTs, with depletion of ELP-1 causing a decrease in touch sensitivity (Hueston et al. 2008) . Mechanoreceptor neurons (TRNs) are unique as they rely on 15 protofilaments MTs rather than the normal 11 in *C. elegans,* these protofilaments are then bundled and able to act as one and it was hypothesised that they rely on ELP-1 for this bundling, hence why a reduction in ELP-1 decreases touch sensitivity (Hueston et al. 2008). ELP-1 has also been shown to act as a modifier gene in a *C. elegans* model of muscular dystrophy. Reduction in ELP-1 levels in a wild-type animal had almost no effect on muscle contractility and the animals were still viable, however loss of ELP-1 in a loss-of-function dystrophin strain (dys-1(cx18)) greatly affected motility (Hueston & Suprenant 2009). A reduction in ELP-1 in dys-1(cx18) also resulted in splayed and hypercontracted muscle with altered cholinergic signalling and the worms eventually died (Hueston & Suprenant 2009). As a result it was concluded that ELP-1 is a genetic modifier of muscular dystrophy in *C. elegans* and is involved in promoting muscle excitability. Hueston & Suprenant (2009) proposed three models of how ELP-1 could be doing this: 1. Trafficking acetylcholine receptors between the

Golgi and plasma membrane, 2. anchoring of receptors at the synapse or 3. modulating receptor activity.

1.5.3 Human EML Proteins

In humans six EMAP like proteins or EMLs are expressed (Figure 1.6). This poorly characterised protein family will be discussed in the following sections.

1.5.3.1 EML Protein Structure

The structure of EML1 (amino acids 167-815) was revealed following X-ray crystallography. This uncovered a Tandem Atypical β-Propeller in EML proteins termed the TAPE domain (Richards et al. 2014) (Figure 1.7). Residues 230-540 formed a 7 blade β-propeller domain whereby each blade was composed of a twisted four-stranded antiparallel β-sheet and encoded by a separate WD40 repeat (Richards et al. 2014). The hydrophobic EML protein (HELP) domain has been suggested to mediate MT binding but actually forms part of the hydrophobic core of the TAPE domain, and thus deleting it would disrupt the TAPE domains structure (Richards et al. 2014). It was also identified that the TAPE domain is capable of binding soluble tubulin (Richards et al. 2014). The N-terminus of the EMLs are not well conserved and often subjected to splice variation and are predicted to be the most disordered region of the proteins (Richards et al. 2015). However there is a conserved motif, which forms a coiled-coil (CC). Structural analysis has revealed that this promotes EML protein trimerisation. Within this coiled-coil, there is a conserved patch termed the ALAD (Ala-Leu-Ala-Asp) motif which helps regulate the shape of the CC (Richards et al. 2015). The N-terminal domain alone (1-174) can associate strongly to microtubules but this interaction is not dependent on the CC alone and is thought to involve the basic region between the CC and TAPE domain (Richards et al. 2015).

coiled coil HELP motif WD40 repeats

EML1 — 815aa

EML2 — 850aa

EML3 — 896aa

EML4 — 981aa

EML5&6 — ~2000aa

Figure 1.6 The EML protein family

There are six members of the human EML family with EML1, EML2, EML3 and EML4 being the most closely conserved. These four conserved proteins contain a coiled-coil within the NTD thought to play a role in protein trimerisation. This is followed by a HELP motif and then WD40 repeats within the CTD. The box represents blade12-N of the TAPE domain. EML5 and EML6 are much larger proteins which lack the coiled coil domain but that naturally contain three HELP and WD40 domains encoded within a single polypeptide. EML5 and EML6 are important in normal brain function. Schematic from Dr Mark Richards.
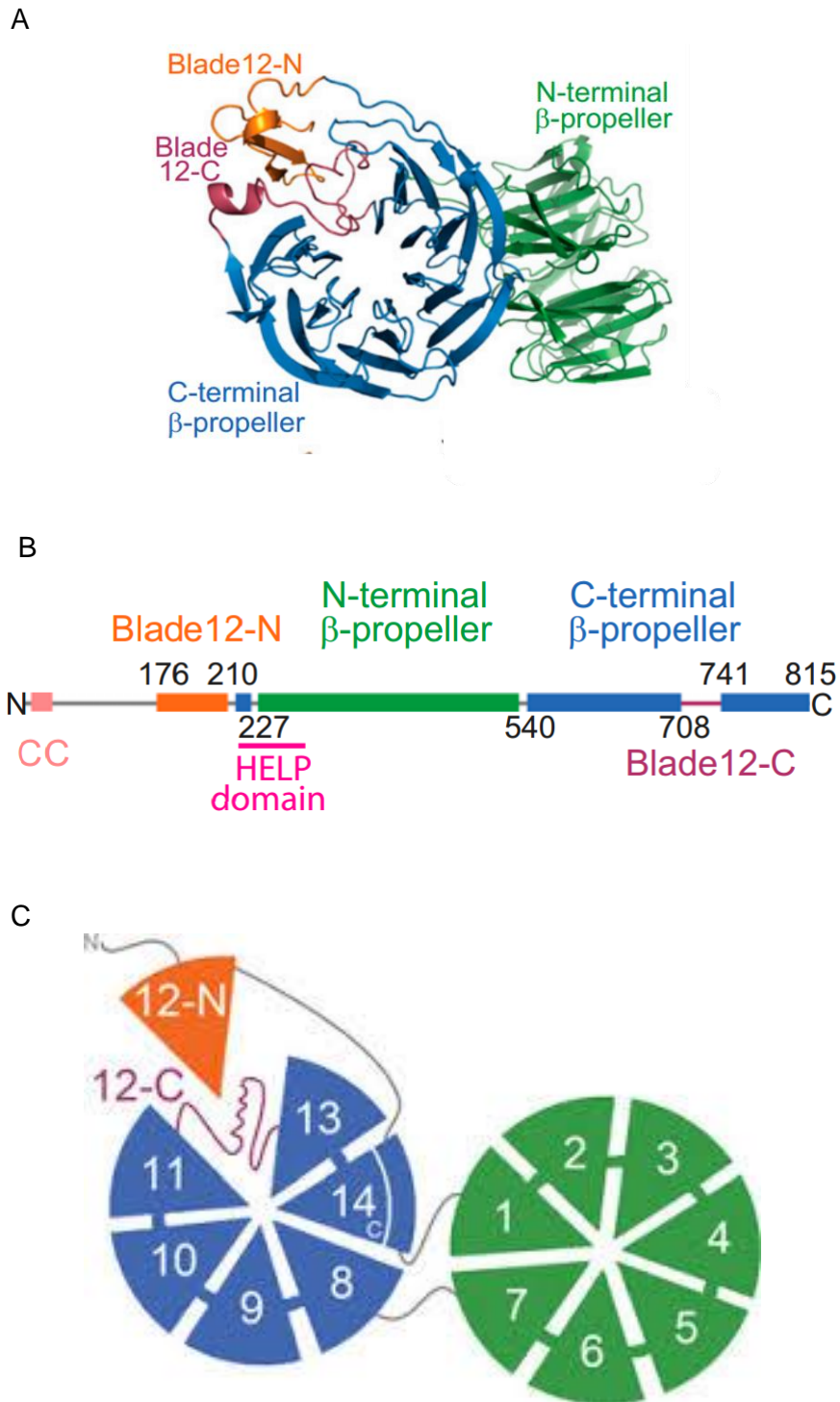
Figure 1.7 EML TAPE domain

Architecture of the EML1 TAPE domain. Throughout the figure, the subdomains are coloured as follows: orange (blade12-N), green (N-terminal propeller), blue (C-terminal propeller) and purple (blade12-C). **A)** The structure of the EML1 TAPE domain as a cartoon representation. **B)** Linear schematic of the EML1 protein. **C)** The cartoon shows the formation of the seven-bladed propellers and organisation of the blades. The HELP motif forms part of the hydrophobic core of the TAPE domain which is essential in maintaining the structure. Taken from Richards et al. 2014.

1.5.3.2 EML1 and its Associated Disorders

Human EML1 (90 kDa) shares 57% amino acid identity with the founding member of the family, EMAP. Human EML1 itself has not been functionally characterised, however it has been associated with a range of diseases. Initially, EML1 was predicted to be one of the mutated genes in Usher Syndrome, a rare genetic disorder which causes hearing loss and visual impairment, however more recently this has been disputed as other closely-linked genes have been found and mutated within this region (Eudy et al. 1997). However, EML1 has been identified as a fusion gene with ABL1 (Abelson tyrosine kinase 1) in T-cell acute lymphoblastic leukaemia. T-cell acute lymphoblastic leukaemia (T-ALL) is often characterised by chromosomal rearrangements leading to expression of chimeric proteins. ABL1 is already known to form a fusion with NUP214 (a nucleoporin protein) in 6% of all T-ALL patients. A study which screened 116 T-ALL patients for ABL1 gene rearrangements led to identification of the EML1-ABL1 gene (De Keersmaecker 2005). The EML1-ABL1 fusion occurred through fusion of exon 17 of EML1 from chromosome 14 with exon 2 of ABL1 from chromosome 9, resulting in a 190 kDa fusion protein. This protein contains the EML1 NTD (including the coiled-coil and basic region) and the kinase domain of ABL1; however, this fusion protein is unable to be associated strongly with MTs, perhaps due to a problem in folding of the EML1 portion of the protein (Richards et al. 2015). Indeed, the EML1-ABL1 breakpoint falls within the C-terminal β-propeller of EML1, meaning the structure would be considerably unstable (Richards et al. 2014). Despite the disruption in EML protein structure, this fusion gene has potent transforming activity due to the constitutive activation of the tyrosine kinase with transient expression of EML1-ABL1 causing Ba/F3 interleukin independent growth. This was dependent on EML-mediated oligomerisation as a mutant lacking the coiled-coil remained interleukin dependent (De Keersmaecker et al. 2005). Furthermore, only the EML1-ABL1 with the coiled-coil was tyrosine phosphorylated. Kinase inhibition is often effective in treating these fusion proteins due to the constitutive activity. Taking this into account, EML1-ABL1 showed sensitivity to imatinib (a selective ABL1 inhibitor) with a decrease in phosphorylation and an increase in apoptosis (De Keersmaecker et al. 2005). This research sheds hope on new treatments for T-ALL patients.

More recently, EML1 mutations have been identified in the rare brain disorder, classical subcortical band heterotopia, part of the type I lissencephaly spectrum (Kielar et al. 2014). This disorder is characterised by aberrantly located neurons within the white matter (Figure 1.8). Mutations in the platelet-activating factor acetylhydrolase IB subunit alpha (PAFAH1B1) and TUBA1A genes have already been identified in these disorders, highlighting the crucial role of the MT cytoskeleton in normal brain function. The EML1 mutation was discovered in heterotopic cortex (HeCo) mice. These mice were used as animal models to study subcortical band heterotophia as they present bilateral masses of heterotopic neurons in the white matter, a similar phenotype to the human disorder. Surprisingly, HeCo neurons could migrate normally in a wild-type environment and cell distribution was considered normal (Kielar et al. 2014). However, at both early and late stage corticogenesis actively dividing cells were abnormally positioned in the HeCo brains, thought to be due to altered cell death (Kielar et al. 2014). A microarray assay was carried out to determine the genes responsible for this disorder. Interestingly, EML1 transcripts were 2.5 fold more abundant in HeCo then wild-type brains, with full length transcripts reduced 96-fold (Kielar et al. 2014). Using RT-PCR, HeCo mice showed abnormal EML1 transcripts corresponding to the skipping of exon 21 and 22. Both of these abnormal transcripts would induce a frameshift mutation with a premature stop codon in exon 23 leading to either loss of 84 or 117 C-terminal amino acids replaced by 19-20 unrelated amino acids (Kielar et al. 2014). This lack of full length EML1 transcripts was also confirmed by in situ hybridisation (Kielar et al. 2014). Localisation of transiently transfected EML1 in both Vero and COS7 cells also showed punctate staining of EML1 along the MTs in interphase and in the region of the spindle during mitosis. From this it was postulated that EML1 was responsible for the finely tuned mechanisms regulating spindle orientation.

Human EML1 maps to chromosome 14q32 which has been linked to lissencephaly, but no patients with specific mutations in EML1 had been identified. In contrast, screening studies of two families with subcortical heterotophia revealed EML1 point mutations. Affected children showed similar MRI patterns with giant bilateral periventricular and ribbon-like subcortical heterotopia with polymicrogyria and agenesis of the corpus callosum (Kielar et al. 2014). In family 1 the mutation was a 481 C to T mutation changing an arginine to a stop codon from the mother and a 769

A to G mutation changing threonine 243 to alanine from the father, whereas in family 2 the mutation was a homozygous 673 T to C mutation (Kielar et al. 2014). Interestingly, both mutations fell within the HELP domain. A T243A EML1 mutant, T being a conserved residue of the HELP domain across various EMLs, ablated MT association of EML1 and thus the disorder may be caused by lack of EML1 association to the MTs (Kielar et al. 2014).

1.5.2.2 EML2 and EML3 – The least characterised members of the EML family

EML2 shares 57% sequence identity with sea urchin EMAP (Eichenmuller et al. 2002). EML2 is expressed in a variety of normal tissues but is also abundant across a range of cancer types including cervical, chronic myelogenous leukemia, lymphoblastic leukemia, colorectal adenocarcinoma, lung carcinoma and melanoma (Eichenmuller et al. 2002). Northern blot analysis also detected a smaller isoform in promyelocytic leukemia and Burkitts lymphoma, making it highly likely that EML2 exists as alternative splice variants (Eichenmuller et al. 2002). EML2 sediments with the MT pellet from HeLa cells and by immunofluorescence microscopy is seen along the length of the MT. Also, EML2 is greatly enriched at the mitotic spindle apparatus during mitosis, indicating that this protein may play a role in regulating MT dynamics during both interphase and mitosis (Eichenmuller et al. 2002). A His-tagged EML2 purified protein was used to analyse the effect of this protein on MT dynamics using video-enhanced differential interference contrast light microscopy (VE-DIC) microscopy revealing that (i) nucleation was dependent on EML2 concentration, (ii) MTs were dramatically shorter in the presence of EML2 and (iii) EML2 reduced the elongation rate at the plus end whilst increasing the catastrophe frequency (plus end catastrophes every 140s with EML2 compared to 300s with tubulin alone) (Eichenmuller et al. 2002). A proposed model is that EML2 destabilises MTs by association of EML2 with the tubulin subunits in adjoining protofilaments. Another suggestion is that EML2 induces a conformational change in the tubulin dimer which no longer favours the extended protofilament sheet associated with growing MTs (Eichenmuller et al. 2002).

EML3 was identified as a MT-binding protein in a purified preparation of microtubule binding proteins that localise to the nucleus in interphase (Tegha-Dunghu et al. 2008).

Antibodies against EML3 were generated using two specific peptides which identified a band at 95 kDa (Tegha-Dunghu et al. 2008). Using this antibody it was found that EML3 localised to MTs throughout interphase and all stages of mitosis. Some protein was also detectable in the nucleus during interphase, consistent with the purification approach (Tegha-Dunghu et al. 2008). In order to verify the function of the conserved HELP domain a EML3 NTD fragment was generated lacking this region, this protein still localised to the nucleus but was found to lack the ability to bind MTs (Tegha-Dunghu et al. 2008). Further to this, the EML3 NTD with the HELP domain intact only localised to the MTs during interphase but not during mitosis (Tegha-Dunghu et al. 2008). Time lapse imaging of stably expressing EGFP-histone 2B cells from which EML3 had been depleted allowed scoring of a range of phenotypes. EML3 depletion caused an increase in the mitotic index, apoptotic index and shape index (nuclei defect) as well as an overall reduction in proliferation (Tegha-Dunghu et al. 2008). EML3 depletion also caused cells to accumulate in mitosis for a few hours with chromosomes that were poorly aligned, indicating that the SAC might be activated in these cells (Tegha-Dunghu et al. 2008). It was also postulated that EML3 depletion caused inefficient bipolar MT attachment delaying the alignment of chromosomes in metaphase (Tegha-Dunghu et al. 2008).

EML3 has been shown to be a strong binding partner for LC8, a small adaptor protein that also acts as a dynein light chain. LC8 is essential for survival, with LC8 depletion causing severe pleiotrophic phenotypes and embryonic lethality (Rapali et al. 2011). This eukaryotic hub protein is thought to have key roles in protein dimerization and play a key role is a range of cellular processes such as apoptosis, DNA repair, transcriptional regulation and cancer development (Rapali et al. 2011). EML3 has a perfect LC8 binding motif (K/R) XTQT at residues 83-87 (RGTQT) within the N-terminal domain, the exact role of this interaction is currently unknown but it has been postulated that LC8 supports EML3 trimerisation (Rapali et al. 2011).
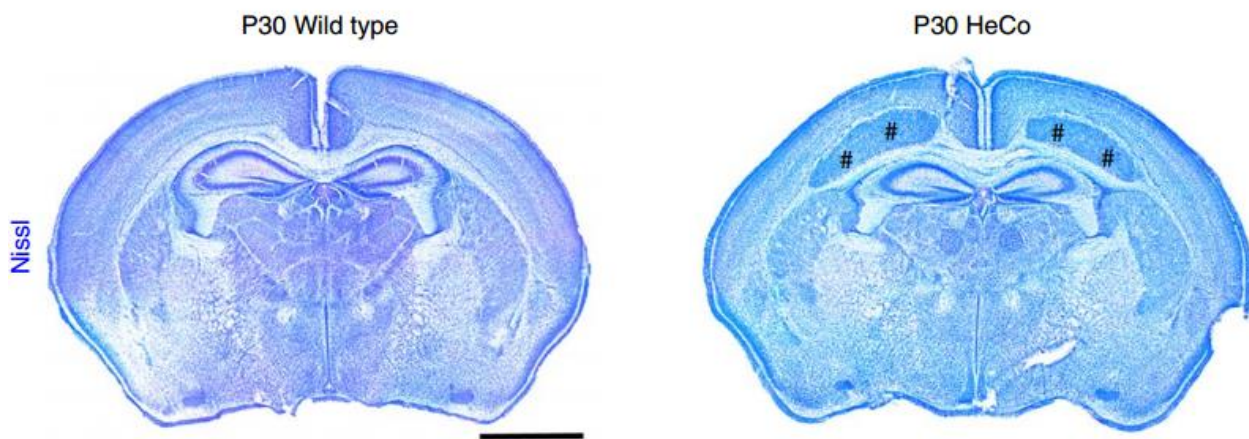
Figure 1.8 EML1 mutations lead to classical subcortical band heterotopia, part of the type I lissencephaly spectrum

Nissl stained brain slices highlight the development of classical subcortical band heterotopia (labelled with #) in P30 HeCo mice, caused by mutations in EML1. Scale bar: 2 mm. Taken from Kielar et al. 2014.

Lastly, EML3 has been shown to associate with 14-3-3 proteins as identified by LC-MS/MS of 14-3-3-sepharose of proliferating cells (Pozuelo Rubio et al. 2004, Jin et al. 2004).14-3-3 proteins are highly conserved, abundantly expressed eukaryotic proteins that, much like LC8, regulate many cellular processes including signal transduction, apoptosis and cell cycle control, with over 200 signaling proteins already identified (Pozuelo Rubio et al. 2004).

1.5.2.3 EML4 and EML4-ALK Fusions in NSCLC

EML4 was first identified in 1978 following the isolation of MT associated proteins in HeLa cells. The unnamed 120,000 Da component (now known to be EML4) bound to and cosedimented with tubulin (Bulinski & Borisy 1979). EML4, then called Ropp120, was subsequently identified as a cytoplasmic protein of 120 kDa (Heidebrecht et al. 2000). This protein shared 57% homology with EMAP and was renamed EML4 by Pollmann and colleagues in 2006. *In situ* hybridisation in mice has shown EML4 is highly expressed in the embryo, in the central nervous system and peripheral nervous system as well as the liver, thymus, intestines, eye, kidneys, salivary glands and paws, but in adults is mainly restricted to the cortex, olfactory bulb, hippocampus and cerebellum (Houtman et al. 2007).

EML4 comprises of 981 amino acids with a theoretical weight of 108.9 kDa, although EML4 can exist as different isoforms with differential splicing of exons 2, 5, 6 and 8. Initial studies showed EML4 could cosediment with *in vitro* polymerised tubulin whilst immunofluorescent microscopy revealed that EML4 had a microtubule localisation in interphase. Of two antibodies developed, one showed no spindle association in mitosis, but the other one did (Pollmann et al. 2006). In mitosis EML4 is phosphorylated on serine and threonine residues. Hence, one antibody may detect hyperphosphorylated EML4, which remains on the spindle, and the other may only detect unphosphorylated EML4, which remains off the spindle (Pollmann et al. 2006). HeLa cells transiently transfected with full-length EML4 showed strong localisation to the MT network in interphase as did the EML4 (1-249) N-terminal domain construct; however no specific localisation was visible with the C-terminal TAPE or HELP domains only (Pollmann et al. 2006). This led to the suggestion that the basic character

of the NTD (pI = 9.28) contributed to MT association as the rest of the protein was acidic (pI = 5.45). Conversely, Chen et al. 2015 showed that the HELP domain and part of the TAPE domain mediate MT binding with the NTD containing the CC and basic region only able to bind when endogenous EML4 was present. This not only contradicts previous localisation data but is confusing in terms of the EML protein structure in which the HELP domain is inaccessible, as it forms part of the hydrophobic core, and is therefore unlikely to bind MTs (Richards et al. 2014). Furthermore the CC and basic region of the N-terminus are available and have been shown *in vivo* and *in vitro* to be the regions required for MT binding (Richards et al. 2014). The TAPE domain is important for the interaction with soluble tubulin and constructs disrupting this domain, such as the 1-478 used in Chen et al. 2015, are likely to form unstable proteins. Transiently expressed GFP-EML4 in Cos7 and HeLa cells localises to MTs in interphase but can only be seen on the spindle in cells expressing a low amount of protein (Houtman et al. 2007). Conversely, Chen et al. (2015) describe EML4 as showing obvious localisation to the spindle throughout all stages of mitosis. The key dfference between Chen et al. (2015) and Pollmann et al. (2006) is highlighted in table 1.2.

In terms of function, overexpression of EML4 has been noted to have no effect on the cell (Pollmann et al. 2006). On the other hand, EML4 has been indicated as a MT stabiliser by both groups with depletion significantly altering the MT network and overexpression leading to resistance in nocodazole induced depolymerisation (Pollmann et al. 2006, Houtman et al. 2007). Furthermore, expression led to MTs with a circular appearance thought to be caused by MT elongation and bundling (Houtman et al. 2007). EML4 depletion caused an increase in apoptosis after 48 hours, indicating that EML4 is crucial for cell survival (Pollmann et al. 2006, Chen et al. 2015). Depletion of EML4 in HeLa cells expressing GFP-H2B showed a significant defect in chromosome alignment compared to controls. This is similar to EML3 depletion and is likely due to improper MT/kinetochore attachments. Furthermore, EML4 has been shown to regulate NUDC, a nuclear migration protein necessary for the correct formation of mitotic spindles, chromosome separation and cytokinesis. NUDC localisation at the spindle significantly decreased in the absence of EML4 (Chen et al. 2015). Hence, EML4 may contribute to trafficking of spindle-associated functions as well as directly regulating MT dynamics.

Pollmann et al. 2006	Chen et al. 2015
Only phosphorylated EML4 localises to spindle MTs	EML4 accumulated at the MTOC during prophase and localized to the mitotic spindle during metaphase
EML4 localisation to MTs is not dependent on the HELP domain but another region within the NTD	The HELP domain and adjacent partial WD40 repeats are required for the localization of EML4
EML4 overexpression does not have an obvious phenotype	Not mentioned
EML4 RNAi alters the interphase MT network and increases the apoptotic index	EML4 knockdown delayed proper chromosome alignment and induced the SAC

Table 1.2 Key differences in EML4 localisation and function between Pollmann et al. 2006 and Chen et al 2015.

EML4 was also found as an oncogenic fusion protein with ALK in non-small cell lung cancer (NSCLC). Lung cancer remains the leading causes of cancer deaths in Western Europe with NSCLC accounting for 80% of all lung cancer cases (Soda et al. 2007). EML4-ALK positive NSCLC patients have distinct clinical features including young age of onset, absence of smoking history and adenocarcinoma histology (Katayama et al. 2012). ALK was first identified as a fusion protein of neucleoposmin (NPM) in anaplastic large cell lymphoma, whereas the EML4-ALK fusion was first identified in 2007 from a lung adenocarcinoma specimen (Soda et al. 2007). EML4 and ALK map to the short arm of chromosome 2 (2p21 and 2p23 respectively) but have opposite orientations making it likely that an internal inversion generates the fusion (Soda et al. 2007). In the first EML4-ALK fusion identified, intron 13 of EML4 was disrupted 3.6 kb downstream of exon 13 and is inverted to connect to a position 296 bp upstream of exon 21 of ALK (Soda et al. 2007). This results in the fusion gene having the EML4 NTD and the kinase domain of ALK which causes constitutive activity of the tyrosine kinase. Indeed, the ability to trimerise due to the presence of the EML4 CC activates ALK presumably by promoting autophosphorylation (Choi et al. 2010).

However, EML4-ALK fusions exist as a range of different variants, due to diversity at the breakpoint region of EML4 (Figure 1.9). In total 7 variants have been identified, some as different isoforms giving variant 1, variant 2, variant 3 a/b, variant 4 a/b, variant 5 a/b, variant 6 and variant 7. Variant 1 (33%), variant 2 (10%) and variant 3 a/b (29%) are the most frequent fusions and have different sensitivities to ALK inhibitors (Heuckmann et al. 2012). In terms of localisation, when transiently expressed variant 1 and 2 localise in the cytoplasm, whereas variant 3a is distributed throughout the cytoplasm and nucleus (Heuckmann et al. 2012). In terms of structure, the breakpoint of variant 1 falls within the N-terminal β-propeller whilst that of variant 2 falls within the C-terminal β-propeller; as a result these two variants are considered unstable as they contain only a partial TAPE domain (Richards et al. 2014). Variants 3a/b and variant 5 exhibit much greater stability as they do not lack any part of the TAPE domain (Richards et al. 2014). Subcutaneous injection of cells expressing EML4-ALK into 3T3 nude mice led to formation of tumours, irrespective of the variant, demonstrating the transformation potential of each fusion protein. Following EML4-ALK protein identification, the ALK inhibitor, Crizotonib, was developed specifically for

EML4-ALK positive NSCLC patients. Initially, this drug worked efficiently with significant tumour shrinkage but the benefits are relatively short lived with the mean progression-free survival being 10 months (Katayama et al. 2012).

Following identification of the EML4-ALK variant 1 as the oncogenic fusion from a 28 year old man without a history of smoking with lung adenocarcinoma, this patient was given 250 mg crizotonib orally, twice a day and after a week his symptoms improved markedly, however by 5 months the tumour abruptly began to re-grow resulting in rapid expansion of the pleural effusion and the development of tumours in both lungs (Choi et al. 2010). Re-evaluation confirmed mutations in the ALK kinase domain following treatment, with a cysteine to tyrosine mutation at amino acid 1156 and a leucine to methionine at amino acid 1196 (Choi et al. 2010). This mechanism of resistance was supported by finding 22% of mutations within the ALK kinase domain, either as missense mutations or amino acid insertions (Katayama et al. 2012). In terms of ALK's structure all mutations occurred within the ATP-binding pocket of ALK, preventing appropriate inhibitor binding (Katayama et al. 2012). The individual variants also affect the efficacy of this drug with total ALK expression levels greatly reduced, in cells expressing variant 2 exposed to crizotonib but no effect seen in variant 3a (Heuckmann et al. 2012).

Similarly, some EML4-ALK fusions have been shown to respond to Hsp90 inhibitors, depending on the variant expressed. Using the Hsp90 inhibitor Ganetespib, EML4-ALK degradation was seen with both variants 1 and 2, but not 3a or 5a. Similarly, patient derived H3122 cells which naturally express variant 1 also showed sensitivity to ganetespib (Richards et al. 2014). Thus, it was predicted that the intrinsic stability of the variant impacts their dependency on the chaperone protein Hsp90 and Hsp90 inhibitor sensitivity (Heuckmann et al. 2012). As a result more work needs to be done to understand the role of the variants and design new treatments to overcome the generation of resistant mutations.
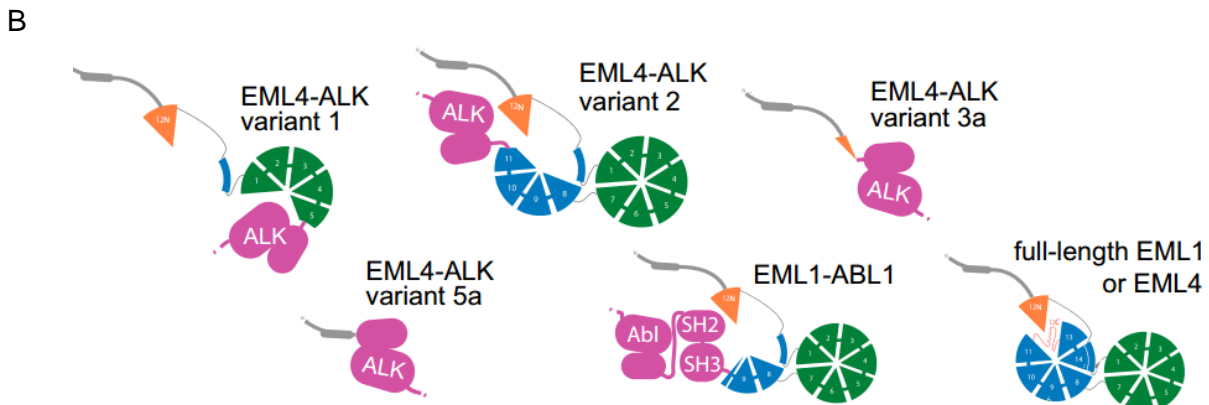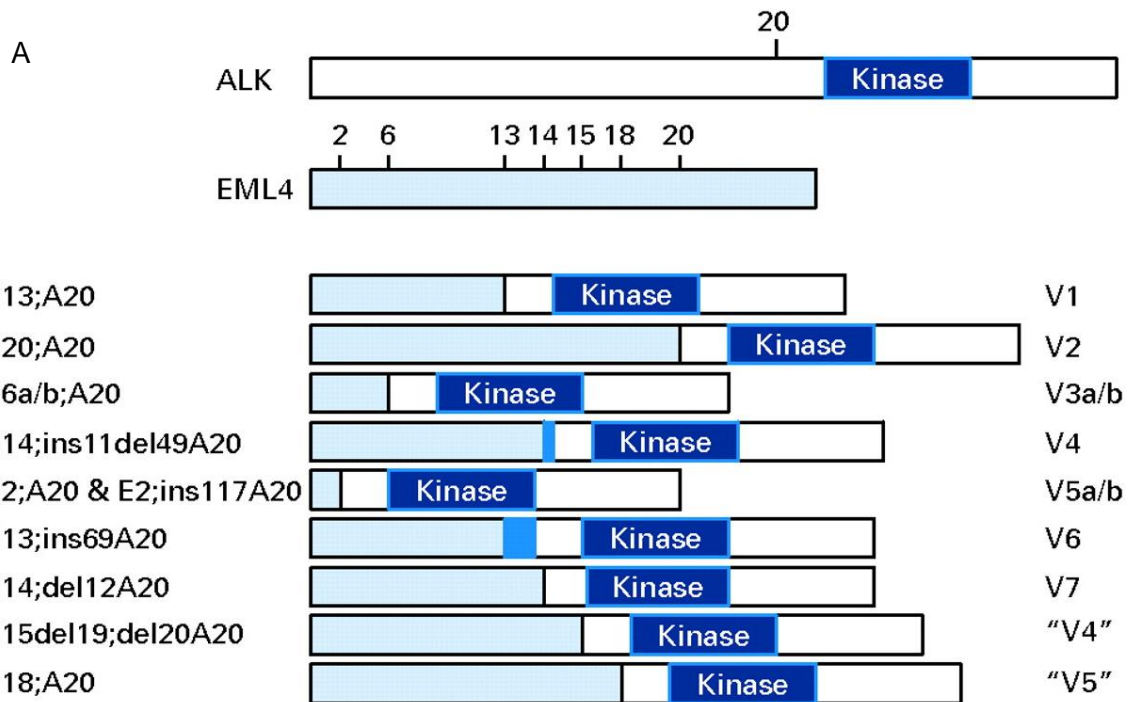
Figure 1.9 EML4-ALK fusions proteins exist as different variants in NSCLC

A) EML4-ALK is an oncogenic fusion protein generated by a fusion between EML4 and the tyrosine kinase ALK. Recent studies have shown these fusions can exist as different variants. Taken from Horn & Pao 2009. **B)** All the variants contain part of the EML4 NTD and either none or part of the highly structured TAPE domain together with the kinase domain of ALK resulting in proteins with potentially different characteristics and resistance to therapies. EML1-ABL1 the fusion in T-cell acute lymphoblastic leukaemia is also shown along with full length EML4 for comparison. Taken from Richards et al. 2014.

1.5.2.4 EML5 and EML6

EML5 and EML6 are the two largest members of the EML family and naturally exist with three intact HELP and TAPE domains but without additional NTD regions (O'Connor et al. 2004, Richards et al. 2014). EML6 has not yet been characterised. EML5 exists as two splice variants EML5a (130 kDa) and EML5b (150 kDa) (O'Connor et al. 2004). EML5b is mainly expressed throughout the brain including the cerebellum, hippocampus, cortex and olfactory bulb as early as E13 and E17 with Purkinje neurons of the cerebellum having the highest expression (O'Connor et al. 2004). Due to expression of EML5 during development it has been postulated that EML5 is involved in processes underlying the large scale cytoskeletal rearrangements during neuronal development.

1.6 The Nek Family of Protein Kinases

In this section I will discuss the family of human Nek (NIMA-related) kinases and their roles in centrosome organisation and mitotic spindle formation with particular focus around the Nek9, Nek6 and Nek7 mitotic cascade. However, I will also briefly discuss the Neks involved in other cellular mechanisms, such as the DNA damage response and ciliogenesis to highlight their diverse functions.

1.6.1 The never-in-mitosis A (NIMA) Protein

In 1983, Ron Morris and associates carried out a genetic screen for cell division cycle mutants and identified the never-in-mitosis A (NIMA) protein of *Aspergillus nidulans* (Morris 1975). Additional analysis revealed *nimA* overexpression caused premature entry into mitosis whilst loss of function mutations caused G2 arrest (Osmani et al. 1991). NIMA must also be degraded to enable mitotic exit to take place (Pu & Osmani 1995). Hence in *Aspergillus*, NIMA is essential for mitotic entry and must be degraded for mitotic exit. Structurally similar kinases to NIMA have also been isolated from many other lower eukaryotes, including *Neurospora crassa* (nim-1), *Schizosaccharomyces pombe* (Fin1)*, Saccharomyces cerevisiae* (Kin3/NPK1)*, Trypanosoma brucei* (nrkA

and nrkB) and *Chlamydomonas* (Fa2p and Cnk)*.* The first NIMA homologue identified was the *nim-1* gene in another filamentous fungi *Neurospora crassa,* which shares 75% identity to NIMA within the catalytic domain (Pu et al. 1995). Although their C terminal extensions are much less similar, both contain nuclear localisation motifs and PEST sequences, involved in protein degradation. Identification of Fin1 in *Schizosaccharomyces pombe,* allowed analysis of its expression through the cell cycle, revealing an obvious peak during mitosis (Krien et al. 1998). Overexpression of Fin1 protein in fission yeast cells caused chromatin to condensate prematurely, however, recent studies have shown that this is merely an artefact on the nuclear envelope. (Krien et al. 1998). Meanwhile, temperature sensitive mutants resulted in elongated cells and blocked spindle formation at 37˚C with one of the two spindle pole bodies failing to nucleate MTs (Grallert & Hagan 2002). A related protein kinase, NPK1, is present in *Saccharomyces cerevisiae.* This shares 64% similarity with NIMA, within the protein kinase domain (Schweitzer & Philippsen 1992). Taken together, these data indicate that NIMA-related kinases are a common feature of the cell cycle across different fungal species.

Interestingly, *Aspergillus nidulans* expresses only a single NIMA-related gene, whereas in humans eleven genes are expressed encoding Nek1 to Nek11 (Figure 1.10). The roles of the Nek kinases include cilia organization (Nek1, Nek4 and Nek8), prolactin signaling (Nek3), DNA damage response (Nek1, Nek10 and Nek11) and mitosis (Nek2, Nek5, Nek6, Nek7 and Nek9). All members of the family, with the exception of Nek10, contain a catalytic domain at the N-terminus, which shares 40-50% amino acid homology with NIMA. The catalytic domains of the eleven Nek's contain a series of serine and threonine residues within the activation loop that are available for autophosphorylation. The C-terminal regions are more divergent in length, sequence and organization, although most Neks have an oligomerization motif that facilitates autophosphorylation and thus activation of the kinase. Nek6 and Nek7 are unusual as they lack a C-terminal domain, having only short N-terminal extensions before their highly similar catalytic domains.

The Nek kinase family has a diverse range of functions, some of which have not yet been discovered (Table 1.3). In the following sections, I will discuss the individual roles of these kinases with particular focus on the functions and interactions of the mitotic Neks.

1.6.2 Nek Proteins and Centrosome Organisation

During mitosis cells rely on the formation of the mitotic spindle to correctly segregate the duplicated chromosomes into two identical daughter cells. In order to form a mitotic spindle, MTs are nucleated from the primary MTOC; for fungi this is the spindle pole body and in higher organisms this is the centrosome (Fry 2002). The centrosome is a complex structure consisting of two cylindrical centrioles, each composed of nine short triplets of stabilised MTs organised in a barrel. These are then surrounded by an extensive lattice of fibrous and globular proteins which forms the pericentriolar material (PCM).

During the cell cycle the centrosomes replicate with each centriole giving rise to the growth of a new centriole. This begins in S-phase and is completed by late G2 phase. The PCM then becomes enlarged through 'maturation' and the parental centrioles become detached in a process known as centrosome disjunction. The two pairs of duplicated centrioles can then separate to either end of the cell to assemble the mitotic spindle (Faragher & Fry 2003). These events are regulated in large part through phosphorylation and here I discuss the role of Nek2 and Nek5 in controlling centrosome splitting.

1.6.2.1 *Nek2 – The Closest Human Relative to NIMA*

Nek2 is the most closely related kinase by protein sequence to NIMA of *Aspergillus nidulans*, sharing 44% amino acid homology within the catalytic domain (Fry et al. 1995). Nek2 is a 445 amino acid protein (48 kDa) consisting of an N-terminal kinase domain and a C-terminal regulatory domain that has the ability to heterodimerise. Nek2 localises to the proximal ends of centrosomes in interphase and this is independent of the MTs (Fry et al. 1998, Fletcher et al. 2005, Faragher & Fry 2003). Initial overexpression studies using a myc-tagged Nek2 wild type construct shed light on the functionality of the kinase, with 45% of transfected cells showing prematurely split centrosomes (Fry et al. 1998). When the experiment was repeated with a catalytically inactive construct premature centrosome splitting did not occur demonstrating that this is a response to increased Nek2 kinase activity (Fry et al. 1998).
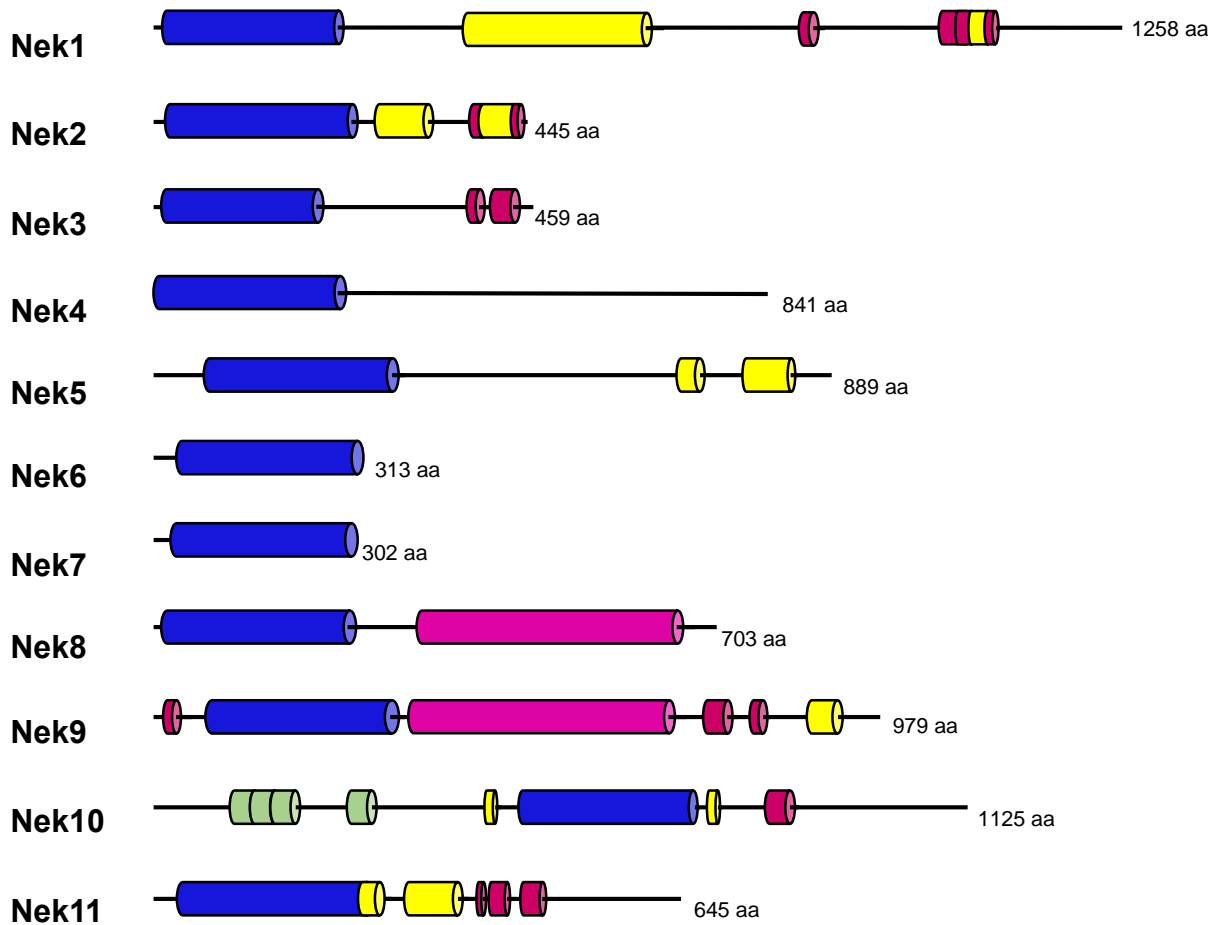
Figure 1.10 The human Nek kinase family

Schematic representation of the human Nek protein kinase family. The amino acid length is indicated on the right. The specific domains highlighted include; coiled-coil domains (yellow), the kinase domain (blue) and RCC1-like domains (pink). Note Nek6 and Nek7 are the shortest in length and most closely conserved of the family. Taken from Fry et al. 2012.

Nek	Localization	Activation	Function
Nek1	Cytoplasm, nucleus? centrosomes, cilia, sites of DNA damage	Genotoxic insults	Ciliogenesis/ DDR
Nek2	Centrosomes	S, G2/M phases	Mitosis
Nek3	Cytoplasmic	Prolactin receptor	Prolactin signaling
Nek4	Basal bodies	?	Ciliogenesis/ DDR
Nek5	Centrosomes	?	Mitosis
Nek6	Mitotic spindle	Nek9	Mitosis
Nek7	Mitotic spindle (weakly)	Nek9	Mitosis
Nek8	Nucleus, centrosomes and cilia	Serum starvation	Ciliogenesis/ DDR
Nek9	Mainly cytoplasmic, nuclear and spindle poles	Mitosis (CDK1 and PLK1)	Mitosis
Nek10	?	UV, G2/M	DDR
Nek11	Nucleus, nucleolar and spindle MTs	S, G2/M phase and genotoxic insults	DDR

Table 1.3 Characteristics of the Nek kinase family

Summary of Nek kinase localisation, activation and function based on current literature with the mitotic kinases highlighted in light grey. Adapted from Fry et al. 2012.

A similar phenotype was observed in the *Dictyostelium discoideum* model system, whereby overexpression of Nek2 showed aberrations in centrosome number and morphology (Gräf 2002). This indicates that centrosome organisation is regulated by Nek2 kinase activity. Further to this, RNAi depletion of Nek2 showed abnormal mitosis including duplicated centrosomes that failed to separate, further supporting the hypothesis that Nek2 is also required for maintaining the integrity of the centrosome (Prigent et al. 2005).

Human Nek2 exists as three splice variants: Nek2A, Nek2B and Nek2C (Wu et al. 2007). Nek2A and Nek2C differ only in a short internal sequence and show similar kinase activity and centrosome localization (Wu et al. 2007). However, the splice variants provide an unusual mechanism to modulate Nek2 function via localization to either the nucleus or the cytoplasm. Nek2A is evenly distributed within both the nuclei and cytoplasm, Nek2B is mainly cytoplasmic and Nek2C is mainly nuclear (Wu et al. 2007). Nek2A (48 kDa) and Nek2B (44 kDa) differ in their C-terminus and exhibit distinct patterns of expression during the cell cycle (Fletcher et al. 2005). Nek2A localises to the centrosomes in interphase but localisation disappears at the onset of mitosis as a result of degradation by the anaphase-promoting complex/cyclosome (APC/C) (Faragher & Fry 2003). Nek2A is recognized by the APC/C through a KEN (Lys-Glu-Asn) box and a C-terminal methionine-arginine dipeptide (MR)-tail; this 'tail' mediates a direct interaction with the APC/C core subunits promoting Nek2A degradation in early mitosis (Hayes et al. 2006). Nek2A is also capable of forming a complex with the catalytic subunit of protein phosphatase 1 (PP1) and C-Nap1 (discussed further below). Nek2A regulates both proteins via phosphorylation as well as undergoing autophosphorylation. Meanwhile, PP1 can regulate Nek2A and C-Nap1 via dephosphorylation. This means the balance of activities within this complex regulates the phosphorylation/dephosphorylation state of Nek2 substrates to regulate centrosome integrity. Bearing this in mind, Nek2A overexpression may cause premature centriole splitting because it saturates PP1 which is then incapable of regulating C-Nap1 and Nek2A through dephosphorylation. Nek2B lacks the C-terminal degradation sequence and continues to be present on the centrosomes during mitosis and only begins to decline upon re-entry into the next G1 phase (Fry 2002). Overexpression of Nek2B does not induce centrosome splitting suggesting

different substrates but downregulation of Nek2B results in mitotic delay and this isoform is also key to embryo cleavage (Fletcher et al. 2005, Uto & Sagata 2000).

As already mentioned, Nek2 is known to act upstream of other centrosomal proteins and form part of a pathway crucial for centrosome disjunction. Arguable the most important of these is C-Nap1 (centrosomal Nek2-associated protein 1), a large (281 kDa) low abundance, coiled-coil protein identified from a yeast two-hybrid screen using Nek2 as the bait (Fry et al. 1998). C-Nap1 also localises to the proximal end of centrioles, via its C-terminal domain which can be phosphorylated by Nek2 (Hardy et al. 2014). Depletion studies show the dependence of the two proteins for one another, with depletion of C-Nap1 resulting in a significant reduction in centrosomal Nek2 and depletion of Nek2 leading to excessive recruitment of C-Nap1. Other key substrates of Nek2 involved in this pathway are rootletin and β-catenin. Rootletin interacts with C-Nap1 and stably links the two centrioles like a tether and is also required for the recruitment of Nek2 (Hardy et al. 2014, Bahe et al. 2005). Similarly, β-catenin also acts as a centrosomal linker protein and can be phosphorylated by Nek2. Overexpression of Nek2 causes β-catenin to relocate from the cytoplasm to the nucleus, which is a hallmark characteristic of cells undergoing epithelial to mesenchymal transition (Neal et al. 2014). As a result the current centrosome disjunction model is that hyperphosphorylation of C-Nap1, rootletin and β-catenin by Nek2 triggers a loss in interaction between the proximal ends of the centrosomes. Upon loss of interaction and association with rootletin the integrity of the centriolar linker is broken which allows the centrosomes to establish opposing poles via motor driven transport by MT-based motors such as Eg5 (Hardy et al. 2014). However, there are certainly many other proteins involved in this complex process including Cep68, Cep215 and Centlein (Graser et al. 2007, Fang et al. 2014).

Nek2 is potentially important in cancer progression. Studies have shown Nek2 protein is elevated in a range of human tumours including cervical, ovarian, breast, prostate, and leukaemia (Hayward et al. 2004). In prostate cancer cells, depletion of Nek2 reduced cell proliferation and suppressed tumorigenicity (Zeng et al. 2015). Similarly, in colorectal cancers all three Nek2 isoforms were shown to be elevated and Nek2 expression directly correlated with the tumour stage. In the animal model *Drosophila melanogaster,* overexpression of Nek2 led to an increase in the number of centrosomes, alterations in the size and shape of different tissues and altered cell

migration (Das et al. 2013). Furthermore, high Nek2 expression is associated with drug resistance, for example to bortezomib, a proteasome inhibitor for the treatment of multiple myeloma and mantel cell lymphoma (Meng et al. 2014). Nek2 expression is also linked to shortened disease free survival (Neal et al. 2014). These findings highlight the Nek2 kinase as a potential target for chemotherapeutic agents. Likewise, Nek2's structure is not characteristic of many human kinases as it adopts a tyrosine down inactive conformation, making it a good target for selecting specific inhibitors (Richards et al. 2009). To date there are no clinically used Nek2 inhibitors, although research into identifying new compounds is underway (Innocenti et al. 2014). One compound, propynamide 16, has been identified which irreversibly inhibits cellular Nek2 without affecting the mitotic kinases, Cdk1, Aurora B, or Plk1 but data with this compound is currently limited (Henise & Taunton 2011).

Another approach to targeting Nek2 overexpression in cancer is to inhibit Nek2 interacting partners. Highly expressed in cancer 1 (Hec1) is a protein involved in kinetochore structure and spindle checkpoint activation. It is a known target of Nek2 and is phosphorylated on Ser165 during M phase (Hu et al. 2014). A novel small molecule INH1 is able to bind Hec1 and ablate Nek2 binding. As a result, there is a reduction in Hec1 phosphorylation which leads to mitotic defects and cell death (Hu et al. 2014).

1.6.2.2 Nek5 – A New Regulator of Centrosome Organisation

Nek5 is one of the least characterised members of the Nek kinase family, although recent research has highlighted the crucial role it plays during the cell cycle. Like Nek2, Nek5 localises to the proximal ends of the centrioles and also colocalises with basal bodies (Prosser et al. 2015). During mitosis Nek5 is detectable at spindle poles but displays reduced staining during metaphase and anaphase (Prosser et al. 2015). Depletion of Nek5 and expression of a kinase-dead mutant resulted in premature centrosome separation, but the degree of separation was more modest than that seen upon Nek2 overexpression. Furthermore, overexpression of Nek5 had no effect on centrosome positioning (Prosser et al. 2015). Interestingly, the localisation of Nek2 and C-Nap1 to centrosomes was reduced in Nek5 depleted cells while rootletin

increased two-fold. This suggests cooperative functions of the two kinases in centrosome linked organisation (Prosser et al. 2015). It is hypothesised that the absence of Nek5 hinders the recruitment of Nek2 to the centrosomes which results in reduced C-Nap1 phosphorylation and inappropriate retention of centrosome linker proteins (Prosser et al. 2015). These results provide a first insight into the function of Nek5 although specific substrates of the kinase have not yet been identified.

1.6.3 Nek Proteins in Mitotic Spindle Formation

At the onset of mitosis, the MT network quickly reorganises to form the mitotic spindle. These MTs are more numerous, shorter and less stable then in interphase. Spindle MTs capture the chromosomes by interacting with the kinetochores and then depolymerise to exert enough force to separate the chromosomes to either ends of the cell. However, the mechanisms that regulate these changes in microtubules dynamics are not fully understood but is likely to involve a combination of post translational modifications of MTs, MTOCs and MAPs (Hammond et al. 2008). One set of key regulators are the Nek kinase family. In this section, I discuss the role of Nek9, Nek6 and Nek7 and their identified substrates in mitotic spindle assembly.

1.6.3.1 Nek9 – The Upstream Kinase

Nek9 (also known as Nercc1) was first identified through its interaction with Nek6, when a FLAG-Nek6 construct was transfected into Hek293 cells and immunoprecipitated to identify binding partners (Roig et al. 2002). Initially, Nek9 was termed p120 as it was 120 kDa protein, however is was soon identified as a Nek kinase due to the typical features of a serine/ threonine kinase and the close similarity to other Nek kinases.

The Nek9 protein starts with an N-terminal kinase domain followed by a nuclear localisation signal (NLS) (Roig et al. 2002). This is followed by an RCC1-like domain, which contains seven consecutive RCC1 repeats and is predicted to form a β-propeller, and a coiled-coil at residues 891-940 (Roig et al. 2002). The RCC1 domain acts in an autoinhibitory manner through directly binding to the Nek9 kinase domain

(Roig et al. 2005). Although Nek9 protein levels remain constant during the cell cycle, Nek9 activation occurs during mitosis, much like NIMA. This activation is dependent on Cdk1 and Plk1. Firstly, Nek9 is phosphorylated on Ser869 by Cdk1 enabling it to interact with Plk1 which recognises the phospho-Ser869 via its polo-box. Plk1 then activates Nek9 through phosphorylation of Thr210 in the catalytic domain activation loop (Bertran et al. 2011).

Localisation data showed that both recombinant and endogenous Nek9 were distributed diffusely throughout the cytoplasm during interphase and mitosis. However, using a pT210 antibody active Nek9 was localised to the centrosomes in early mitosis; only upon separation in prophase were centrosomes stained (Roig et al. 2005). The staining then increased three-fold in metaphase but then decreased during anaphase. During telophase and cytokinesis the staining at centrosomes dwindled with active Nek9 moving to the midbody, whilst in interphase staining disappeared completely (Roig et al. 2005).

From a functional perspective, immunodepletion of Nek9 from *Xenopus laevis* egg extracts revealed that lack of Nek9 interferes with bipolar spindle formation and causes misalignment of chromosomes; importantly these phenotypes could be rescued by addition of Nek9 (Roig et al. 2005). Further to this, microinjection of anti-Nek9 IgGs into prophase PtK2 (male rat-kangaroo epithelial kidney) and CF-PAC1 (pancreatic carcinoma) cells caused similar mitotic abnormalities including prometaphase arrest and defective chromosome orientation and segregation (Roig et al. 2002). Nek9 depletion in Caki2 kidney carcinoma and U1242 glioblastoma cells also led to multinucleation, reduced cell proliferation and cytokinesis failure (Kaneta & Ullrich 2013). Taken together this reveals that Nek9 is involved in spindle assembly as well as chromosome attachment, alignment at the spindle midzone and segregation (Roig et al. 2002). It has also been suggested that Nek9 depletion may somehow compromise the spindle assembly checkpoint (SAC) (Kaneta & Ullrich 2013).

Work has also gone into identifying potential Nek9 substrates. One potential substrate is the Ran-GTPase. The Ran cycle is involved in mitotic spindle assembly, playing essential roles in chromatin driven MT assembly. The RCC1 domain of Nek9 is a potential guanine-nucleotide exchange factor for the small G protein Ran. Binding of Ran to Nek9 can occur through both the RCC1 domain and the catalytic domains and

there is evidence that Nek9 depletion interferes with Ran-GTPase function (Roig et al. 2005). However the significance of this remains unclear.

As previously mentioned active Nek9 localises to the centrosomes in early mitosis and this may result from an interaction with γ-tubulin or its partners (Roig et al. 2005). In mouse oocytes γ-tubulin is normally localized to the spindle poles. However, Nek9 depletion caused γ-tubulin to no longer accumulate at the spindle poles (Yang et al. 2012). Further to this, studies have shown that Nek9 interacts with and phosphorylates NEDD1, which recruits γ-tubulin to centrosomes (Kaneta & Ullrich 2013).

Similarly, Nek9 binds to LC8 which acts as a negative regulator of Nek6 binding (Regué et al. 2011). LC8, as previously mentioned, is a cytoplasmic, ubiquitous, essential and extremely conserved protein that interacts with a vast range of proteins and protein complexes. Nek9 binds LC8 via a (K/R) XTQT motif present at the C terminus of Nek9. This interaction is regulated by the activation state of Nek9, as autophosphorylation of Ser944 results in perturbation of the complex (Gallego et al. 2013). This indicates that LC8 binding to Nek9 prevents its association with Nek6 and Nek7 and that only when Nek9 is phosphorylated on Ser944 and LC8 binding is perturbed can Nek9 bind and activate Nek6 and Nek7 (Gallego et al. 2013).

Since Nek9 plays such a crucial role in spindle assembly this makes it a good target for cancer chemotherapy. Nek9 is upregulated in a vast range of cancers including breast, kidney, colorectal, testicular, melanoma, glioma and neuroendocrine (Uhlén et al. 2005, Berglund et al. 2008, Uhlen et al. 2010). More recently Nek9 overexpression has been identified in patients with lung adenocarcinomas, whereby excessive proliferation is concordant with reduced p53 expression and amplified Nek9 (Kurioka et al. 2014). Hence, Nek9 may be a useful target against p53-deficient lung cancers. However, currently there are no specific Nek9 inhibitors available for cancer treatment.

1.6.3.2 Nek6 and Nek7 – Components of a Mitotic Signalling Cascade

Nek6 and Nek7 are the smallest and most closely conserved Nek kinases. They consist almost entirely of a catalytic domain which shares 86% homology together with a short 30-40 amino acid N-terminal extension. They were first discovered using the

dBEST database to search for novel murine NIMA-related cDNAs with the predicted Nek6 and Nek7 sequences containing the 12 conserved regions which are hallmarks of eukaryotic protein kinases (Kandli et al. 2000). Northern blot analysis of RNA samples from various murine tissues revealed that both kinases were expressed within the ovaries and brain whilst Nek6 levels were also high within the intestine and placenta and Nek7 was high within the kidneys (Kandli et al. 2000).

Nek6 and Nek7 form part of a signalling cascade, functioning downstream of Nek9 (Figure 1.11). However, despite interaction with Nek9, Nek6 and Nek7 are unable to interact directly with one another (O'Regan & Fry 2009). Both Nek6 and Nek7 activation occurs through release of an autoinhibitory tyrosine motif: Tyr97 for Nek7 and Tyr108 for Nek6. The side chain of this inhibitory tyrosine sits between the β4 and αC helix into the active site; this then allows the aromatic ring of the Tyr to form a hydrogen bond with the DLG motif (Richards et al. 2009). Only upon re-orientation of this residue from a 'tyrosine-down' to a 'tyrosine-up' can the αC helix move into the active conformation and allow the kinase to be activated (Richards et al. 2009).

In interphase Nek6 is diffusely distributed through the cytoplasm and the nucleus, but in mitosis Nek6 weakly localises on the mitotic spindle in metaphase, central spindle in anaphase and midbody in cytokinesis (O'Regan & Fry 2009). Importantly, Nek6 shows an increased abundance and activity of the kinase in mitosis as a result of activity by upstream Nek9, with coexpression of Nek6 with active Nek9 resulted in a 20-25 fold activation of Nek6 kinase activity and phosphorylation of Ser206 (Belham et al. 2003). Nek6 is also phosphorylated during mitosis as detected by a doublet on a SDS-PAGE gel. Using liquid chromatography and mass spectrometry, Thr202, Ser37 and Ser206 were all phosphorylated in the more rapidly migrating band (Belham et al. 2003).

In order to understand the mitotic function of Nek6, catalytically inactive (K75M) mutants were expressed in cells (O'Regan & Fry 2009, Yin et al. 2003). These 'kinase dead' constructs induced apoptosis in 40-70% of cells and resulted in a slower proliferation rate. Flow cytometry experiments demonstrated that a lack of Nek6 activity caused cells to accumulate in G2/M phase (Yin et al. 2003). While immunofluorescent microscopy revealed cells expressing inactive Nek6 were delayed in mitosis (O'Regan & Fry 2009). Kinase dead Nek6 also caused cells to have fragile

spindles with less focussed spindle poles, a reduction in overall microtubule intensity and abnormal chromosome condensation and alignment; similar defects were seen upon disruption of Nek9 activity (O'Regan & Fry 2009, Roig et al. 2002). It was also noted that Nek6 depletion caused an increase in multinucleated cells due to cytokinesis defects (Yin et al. 2003). Intriguingly these results imply that Nek7 is incapable of replacing the function of Nek6, meaning although these kinases are structurally very similar, they perform independent functions (O'Regan & Fry 2009). Presumably, inactivation of Nek6 prevented cells being able to exit mitosis due to activation of the spindle assembly checkpoint (O'Regan & Fry 2009).

More recently a number of Nek6 substrates have been identified that offer further insight into the Nek9/Nek6 pathway. One important substrate is Eg5 which can specifically co-precipitate with Nek6 and Nek9. Eg5, also known as kinesin-5 and Kif11, is a plus-end directed kinesin of the BimC family. It is necessary for centrosome separation, spindle pole formation and poleward translocation of microtubules. Inhibition or depletion of Eg5 results in mitotic arrest and monopolar microtubule structures (Rapley et al. 2008). Nek6 is able to bind to the C-terminal tail of Eg5 via residues 762-1057 and can phosphorylate both the head and tail of the kinesin (Rapley et al. 2008). It was proposed that Eg5 exists as two populations: a phosphorylated fraction at the spindle poles and an unphosphorylated population within the cytoplasm. It was also proposed that Nek6 phosphorylation enabled normal Eg5 function and spindle bipolarity (Rapley et al. 2008).

Another important substrate of Nek6 is Hsp72, a member of the family of heat shock proteins (HSPs). This was identified following both a Nek6 KESTREL assay and a coprecipitation assay. HSPs are a family of chaperones that use ATP hydrolysis to assist the folding of polypeptides and maintaining proteins in unstable conformations (O'Regan et al. 2015). Overexpression of Hsp70 proteins in cancer has been linked to poor prognosis and drug resistance and are therefore considered a good potential therapeutic target (O'Regan et al. 2015). One member of the family, specifically Hsp72, is thought to associate with Nek6. Hsp72 relies on phosphorylation on Thr66 by Nek6 to localise to the mitotic spindle and this phosphorylation is crucial for the assembly of a robust mitotic spindle (O'Regan et al. 2015). Intriguingly, the interaction with Hsp72 depends on the N-terminal extension of Nek6 explaining why Hsp72 does not interact with Nek7 (O'Regan et al. 2015). Hsp72 is also able to interact with two

crucial K-fibre stabilising proteins; transforming acidic coiled coil protein 3 (TACC3) and ch-TOG, which in turn require Hsp72 for recruitment to the spindle and as a result these are also indirectly dependent on Nek6 activity (O'Regan et al. 2015).

Lastly, a large scale proteomic screen indicated a strong association between Nek6 and EML3 (Figure 1.12). This screen chose 407 bait proteins selected on their implied disease association (Ewing et al. 2007). Nek6 was used as a bait and 42 prey proteins were identified that included Nek9, EML2, EML3 and EML4 (Ewing et al. 2007). As previously discussed, EMLs are a family of MAPs that play a role in regulating MT dynamics. In humans there are six EML proteins and although none have been characterised in much detail, EML3 was found to have a key role in correct metaphase chromosome alignment (Tegha-Dunghu et al. 2008). Intriguingly, these results are similar to the consequences of Nek6 and Nek9 depletion which also cause M phase arrest and misaligned chromosomes. Furthermore, like Nek9, EML3 is predicted to bind to LC8. Taken together, it is likely EML proteins play a role in the Nek9/Nek6 mitotic cascade pathway and this is the focus of my research project.

As discussed, Nek6 is crucial in mitotic progression making it a potential target for cancer treatment. Nek6 expression is frequently increased in cancers, notably of the lung, liver and stomach (Uhlén et al. 2005, Uhlen et al. 2010, Berglund et al. 2008). Nek6 transcription, protein and kinase activity have all been shown to be elevated in a range of cancer tissues, whilst depletion of Nek6 in MDA-MB-231 cells caused reduced growth rate (Yin et al. 2003). Further to this Nek6 depletion or expression of a kinase dead mutant resulted in apoptosis and suppression of cancer cell transformation indicating that elevated Nek6 is key for tumour survival and would indeed be a useful target for cancer chemotherapy (Nassirpour et al. 2010). To date, only early studies with the isogranulatimide compound have been shown to reduce Nek6 kinase activity (Moraes et al. 2015).
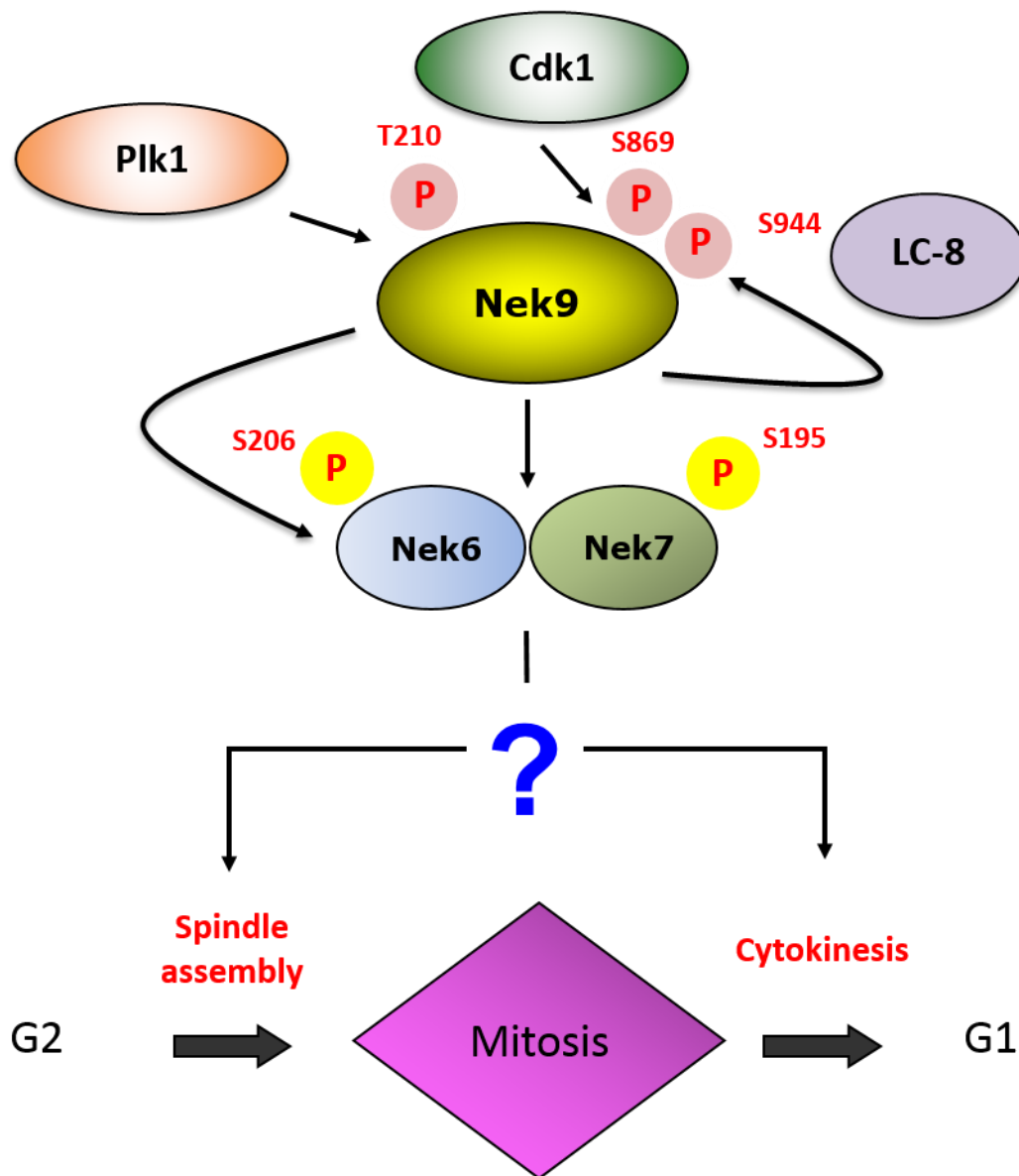
Figure 1.11 The Nek9 signalling cascade

Upon the onset of mitosis, Nek9 forms part of a signalling cascade crucial for mitotic progression. Cdk1 phosphorylated Nek9 at S869 to enable recruitment of Plk1. Plk1 then phosphorylates Nek9 at T210 on its activation loop causing activation. Nek9 can then autophosphorylate at S944 thus releasing LC8 and enabling interaction with Nek6 and Nek7. Nek6 and Nek7 then to maintain a robust spindle and ensure complete cytokinesis during mitosis. Data taken from the Avruch, Roig, Motro, Fry and Bayliss labs.
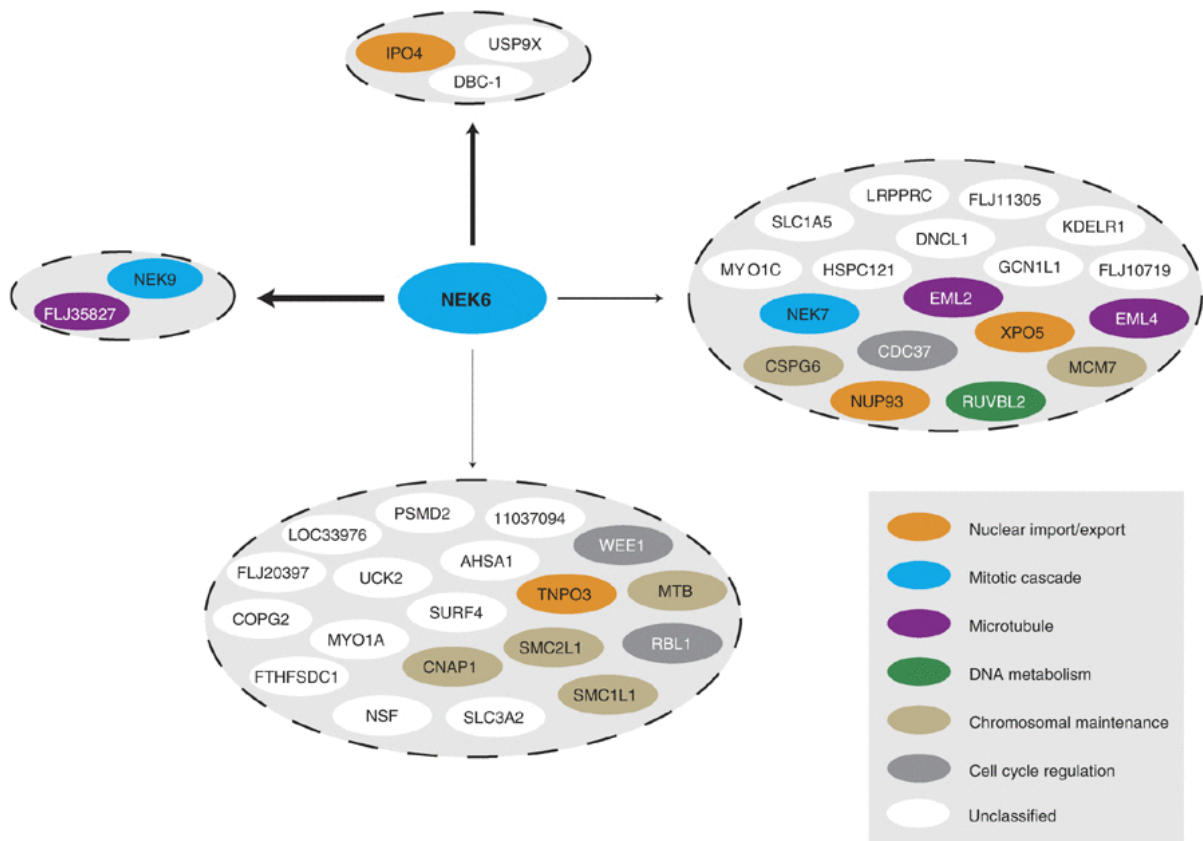
Figure 1.12 Proteomic identification of the interaction between Nek6 and EML3

Large-scale study of protein-protein interactions using Nek6 as a bait protein, the thickness of the arrow indicates the confidence of interaction. Nek6 strongly interacts with Nek9 (already well characterised) and FLJ35827 (purple) which we now know is EML3. Nek6 can also interact with Nek7 (blue), EML2 and EML4 (purple). Taken from Ewing et al. 2007.

Nek7 is distributed throughout the cytoplasm during interphase and during mitosis can be detected at spindle poles where it remains throughout mitosis (O'Regan & Fry 2009). Some groups have also found Nek7 to localise to the centrosomes (Kim et al. 2011). In terms of Nek7 function, depletion of Nek7 or expression of kinase dead mutants shows very similar phenotypes to loss of Nek6 function including apoptosis, fragile spindles, less focussed spindle poles, a reduction in overall microtubule intensity and abnormal chromosome condensation and alignment (O'Regan & Fry 2009). Nek7 has also been reported to regulate centrosome duplication (Kim et al. 2011). It localises, more obviously then Nek6, to the centrosome and Nek7 depletion causes reduced γ-tubulin levels and reduced centriole numbers (Prosser et al. 2015). It was also noted that Nek7 depletion caused an obvious reduction in the accumulation of other PCM proteins (Kim et al. 2011).

The key regulator of Nek7 is Nek9, whereby phosphorylation of Ser195 by Nek9 results in a 20-25% increase in kinase activity (Belham et al. 2003). In terms of structure, Nek7 exists in an autoinhibitory conformation, whereby the aromatic side chain of Tyr97 protrudes into the active site, forming a hydrogen bond with Leu180 of the DLG motif. Addition of the Nek9 CTD relieves Nek7 autoinhibition, however this alone is not sufficient to completely release the kinase (Haq et al. 2015). Nek9 forms homo-oligomers through its CC domain and although the CC is not required for binding to Nek7 it is important for the activation (Haq et al. 2015). The proposed model of interaction is that Nek9 self-association brings Nek7 protomers together as back-to-back dimers which releases Nek7 autoinhibition through a set of specific interactions which in turn switches the conformation of Tyr97 (Haq et al. 2015).

Whilst genuine substrates of Nek7 remain to be identified, both Nek6 and Nek7 have been shown to phosphorylate MT preparations *in vitro* (O'Regan & Fry 2009). Moreover, Nek7 has been shown to regulate MT dynamics in interphase (Cohen et al. 2013). MT dynamics were monitored using cells expressing GFP-EB3 (Cohen et al. 2013). Nek7 depletion caused a reduction in the mean growth speed of MTs by 14% and there was a significant difference in catastrophe with the duration of catastrophe events being shortened in the absence of Nek7 (Cohen et al. 2013). Mouse embryonic fibroblasts taken from Nek7 knockout animals, confirmed the Nek7 depletion phenotypes showing frequent cytokinesis failure and aneuploidy (Cohen et al. 2013).

However, what is still not clear is whether Nek7 is directly influencing MT dynamics or acting through a MAP, such as a member of the EML family.

More recently, Nek7 has been identified as a major component of the NLRP3 infammasome. Inflammasomes are intracellular protein complexes that drive activation of inflammatory caspases. Four inflammasomes involving NLRP1, NLRP3, NLRC4 and AIM2 have been described, which then recruit the common adaptor protein ASC. ASC then activates caspase-1, resulting in the secretion of mature IL-1β and IL-18 proteins (He et al. 2016). Recent studies have shown that mutations in Nek7 impaired NLRP3 inflammasome activation and that Nek7 binding to NLRP3 via the LRR domain promotes inflammasome assembly. Therefore, Nek7 is a key component of the NLRP3 inflammasome, thought to work downstream of the initial potassium efflux, to promote NLRP3 oligomerisation and activation (He et al. 2016; Shi et al. 2015; Schmid-Burgk et al. 2015).

Nek7 is overexpressed in renal, glioma and liver tumours, while Nek7 depletion in MDA-MB-468 and HeLa cells resulted in a reduced proliferation rate (Yin et al. 2003, O'Regan & Fry 2009). A recent study has revealed that Nek7 expression is directly correlated to poor prognosis with increased Nek7 levels causing shorter overall survival time with patients suffering from gall-bladder carcinoma (Wang et al. 2013). As for Nek6, only early drug discovery studies have taken place to identify Nek7 inhibitors. One such study identified GSK-3 Inhibitor XIII as a Nek7 inhibitor, as it decreased kinase activity by more than 50% (Moraes et al. 2015). Taken together, these studies reveal the Nek9-Nek7-Nek6 cascade as essential for mitotic progression and a potential target for new anti-cancer therapy.

1.6.4 Linking Neks to Ciliogenesis and the DNA Damage Response

These sections have mainly focussed on the roles of the Nek kinases in regulating centrosomes and mitosis. However, other members of the family may have cellular functions that are not directly involved in mitotic spindle assembly. Moreover, some of these Neks have been linked to human disease most notably an autosomal recessive form of polycystic kidney disease.

Firstly, Nek1 and Nek8 have been linked to an autosomal recessive form of polycystic kidney disease (PKD). Mutations in the mouse models (*kat/kat2*) for this disease map to the Nek1 gene (Upadhya et al. 2000). Mutations in human Nek1 have been identified in patients with autosomal recessive short rib polydactyl syndrome Majewski (Thiel et al. 2011). Localisation studies have shown that Nek1 localises to centrosomes and to the basal bodies that contribute to cilia formation. The absence of Nek1 causes a reduction in cilia number and changes to cilia morphology *in vivo* (Mahjoub 2005, Thiel et al. 2011). Similarly, Nek8 is also involved in PKD progression specifically the human juvenile cystic kidney disease, nephronophthisis. Nek8, also termed NPHP9, localises to centrosome in dividing cells and the proximal region of the primary cilium in ciliated cells (Mahjoub 2005). Induction of ciliogenesis upon cell cycle exit is accompanied by both the activation (dependent upon phosphorylation within the catalytic domain) and proteasomal degradation of Nek8 (Zalli et al. 2012). Hence both Nek1 and Nek8 and loss of function mutations leads to PKD progression. An intriguingly hypothesis is that both kinases somehow link cilia, centrosomes and cell cycle regulation.

Secondly, some of the Nek kinases have been shown to play a role in the DNA damage response. Nek10 is required for the activation of ERK1/2 signalling upon UV irradiation (Moniz & Stambolic 2011). Nek10 interacts with Raf-1 which in turn mediates MEK1 activation to cause G2/M arrest. This pathway is crucial in order to maintain the G2/M checkpoint following UV irradiation (Moniz & Stambolic 2011). Likewise, Nek11 has been shown to play a role in the DNA damage response. Nek11 is most closely related to Nek1, Nek3 and Nek4 and consists of an N-terminal kinase domain which shares 33% amino acid identity to NIMA. Nek11 exists as four splice variants named S, L, C and D, and their localisation is predominantly cytoplasmic but can undergo nucleocytoplasmic shuttling (Sabir et al. 2015). Nek11 is cell-cycle regulated with expression increasing from S phase and peaking at G2/M, not dissimilar to other Nek family members and NIMA (Noguchi et al. 2002). The activity of Nek11 increases in response to genotoxic stress and it's activity is inhibited when cells are treated with caffeine (Noguchi et al. 2002). More recent studies have shown that not only does Nek11 depletion reduce cell viability but also prevents G2/M arrest induced by genotoxic agents. It also promotes p53-dependent apoptosis both in the presence and absence of DNA damage and in HCT116 colorectal cancer cells (Sabir et al.

2015). Taken together, these data prove that Nek11 is a downstream kinase in the pathway activated upon response to DNA damage. Moreover, an interaction between Nek11 and another member of the family, Nek2A was reported. Nek11 co-localised with Nek2A at nucleoli and Nek11 could immunoprecipitate with active Nek2A (Noguchi et al. 2004). The model proposed from these data was that phosphorylation of Nek11 by Nek2A releases an autoinhibitory conformation of Nek11 resulting in activation. This is not dissimilar to what is seen with Nek6 and Nek7 being activated by Nek9 (Noguchi et al. 2004). In conclusion, not only are Nek kinases crucial for proper mitosis and mitotic progression, but they play a wider role in terms of cilia, centrosomes and the cell cycle.

1.7 Aims and Objectives

The overall aims of my project is to understand how EML proteins are regulated through the cell cycle. In order to do this there are four specific aims as follows:

1) How do EML proteins interact with MTs and is this mediated through tubulin E-hooks?

- Generate fluorescently labelled U2OS stable cell lines.
- Determine the localisation and dynamics of EML proteins during interphase using immunofluorescence and live cell imaging techniques such as FRAP analysis.
- Determine the effect of MT poisons on EML localisation and dynamic behaviour.
- Use purified EML proteins and MT seeds to determine whether EMLs associate with MTs via tubulin E-hooks.
- Use immunoprecipitation to assess whether EML proteins can oligomerise

2) Where does EML3 localise during mitosis and is it essential for mitotic spindle organisation and cell division?

- Use the stable cell lines to assess mitotic localisation using immunofluorescence microscopy and live cell imaging.
- Determine the importance of EML3 in maintaining the interphase network using siRNA-mediated depletion and immunofluorescence.
- Determine the importance of EML3 in mitotic progression using siRNA-mediated depletion and immunofluorescence microscopy to quantify abnormalities in cell morphology, microtubule organisation and chromosome segregation.

3) Are EML proteins physiological substrates of the mitotic Nek6 and Nek7 kinases and is their phosphorylation essential for mitotic progression?

- Confirm the interaction between Nek6 and EML3 using *in vitro* kinase assays and immunoprecipitation experiments.
- Analyse the effect of activated Nek6/Nek7 and depleted Nek6/Nek7 on EML3 localisation in interphase and mitosis.
- Map specific Nek6 phosphorylation sites using mass spectrometry and generate multi-site EML3 mutants.

4) How do EML fusion proteins drive properties associated with human cancer?

- Verify whether the EML4 NTD undergoes phosphorylation during mitosis.
- Analyse whether active Nek7 and a selection of EML4-ALK variants can induce protrusions like wild-type EML4 and active Nek9 using immunofluorescence.
- Determine whether EML4-ALK induced protrusions are reliant on Nek7 expression using transient transfections, Nek7 siRNA-mediated depletion and immunofluorescence.

CHAPTER 2   MATERIALS AND METHODS

2.1 Materials

2.1.1 Reagents and chemicals

All chemicals were of analytical grade or higher and supplied by the following companies: Sigma (Poole, UK), Roche (Lewis, UK) or as otherwise stated in the table below.

Reagent	Supplier
Precision Plus Protein Dual Colour Standards	BioRad (Hemel Hempstead, UK)
G418 sulfate Hoechst 33258	Calbiochem (Nottingham, UK)
Bovine serum albumin EDTA, EGTA, KCL, $MgCl_2$, $MnCl_2$, NaCl, Na_2HPO_4 Ethanol Glycerol Methanol Tween-20	Fisher Scientific (Loughborough, UK)
PMSF (phenylmethylsulfonyl fluoride)	Fluka (Gillingham, UK)
Super RX X-ray film	Fuji (Tokyo, Japan)
Nitrocellulose Transfer Membrane (0.45 μm)	GE Healthcare (Amersham, UK)

Dulbecco's Modified Eagle Medium (DMEM) GlutaMAX supplement Fetal Bovine Serum Lipofectamine 2000 reagent NuPAGE Bis-Tris Precast gels (10-15 well) NuPAGE MES SDS running buffer (20x) NuPAGE Transfer Buffer (20x) Oligofectamine reagent Opti-MEM, reduced serum medium Penicillin/Streptomycin RNase A Trypsin-EDTA (0.05%)	Invitrogen Life Sciences (Paisley, UK)
Hepes SDS	Melford (Suffolk, UK)
ECL Western Blotting Reagent	Pierce (Rockford, USA)
Skimmed Milk Powder	Premiere Beverages (Stafford, UK)

2.1.2 Radioisotopes

Isotope	Specific activity	Supplier
$[\gamma\text{-}^{32}P]$-ATP	111 TBq/mmol	Perkin Elmer

2.1.3 Vectors

Most of the constructs used were previously designed and made by members of the Fry lab (Flag-Nek6, Flag-Nek6 Y198A, Flag-Nek7 and Flag-Nek7 Y97A) or collaborating labs; Bayliss Lab (all YFP-EML constructs) and Straube Lab (mCherry-EB3). The vectors used for these constructs are outlined below, vector maps available in the appendix.

Vector	Application	Supplier	Antibiotic resistance
pFLAG-CMV-2	Eukaryotic expression vector	Sigma-Aldrich	Kan/Neo
pcDNA3	Eukaryotic expression vector	Invitrogen	Amp/Neo
pcDNA3.1	Eukaryotic expression vector	Invitrogen	Amp/Neo
pLEICS-12	Eukaryotic expression vector	PROTEX (University of Leicester, UK)	Amp/Neo

2.1.4 Antibodies

2.1.4.1 Primary antibodies

Primary antibodies were diluted into 3% w/v BSA in PBS for immunofluorescence microscopy (IF), PBS supplemented with 0.1% v/v Tween-20 and 5% v/w non-fat milk powder for Western Blotting (WB) and into lysis buffer with protein beads for immunoprecipitation (IP) (unless otherwise stated).

Primary antibodies (species)	Dilution (concentration)	Supplier (catalogue number)
Anti-GFP (rabbit)	1:1000 WB (0.5 µg/ml) 1:500 IF (1 µg/ml)	Abcam (ab6556)
Anti-GFP (mouse)	1:500 WB/IP	Sigma-Aldrich (G6539)
Anti-α-tubulin (mouse) (detects unmodified α-tubulin)	1:2000 IF (0.3 µg/ml) 1:1000 WB (0.6 µg/ml)	Sigma-Aldrich (T5168)
Anti-γ-tubulin (rabbit)	1:500 IF	Sigma-Aldrich (T3559)
Anti-GAPDH (rabbit)	1:500 WB	Cell Signaling Technology (2118)

Anti-Nek6 (rabbit)	1:1000 WB in TBS [0.1% w/v Tween-20 and 5% w/v milk powder]	Rabbit serum (in house antibody)
Anti-Nek7 (goat)	1:250 WB in TBS [0.1% Tween-20 and 5% w/v milk powder]	Aviva Systems Biology (OAEB01009)
Anti-FLAG M2 (mouse)	1:1000 WB (0.5 µg/ml) 1:500 IP (1 µg/ml)	Sigma-Aldrich (F3165)
Anti-FLAG (Rabbit)	1:1000 IF	Sigma-Aldrich (F7425)

2.1.4.2 Secondary antibodies

Secondary antibodies	Dilution (concentration)	Supplier
Goat anti-mouse horseradish peroxidase conjugate	1:1000 WB	Sigma Aldrich
Goat anti-rabbit horseradish peroxidase conjugate		
Rabbit anti-goat horseradish peroxidase conjugate		
Goat anti-mouse Alexa 488	1:200 IF (10 µg/ml)	Molecular Probes – Life Technologies
Goat anti-mouse Alexa 594		
Goat anti-rabbit Alexa 488		
Goat anti-rabbit Alexa 594		

2.1.5 Drugs

The following stock solutions were prepared in ddH$_2$O unless otherwise stated.

Drug	Stock concentration	Final concentration	Supplier
G418	100 mg/ml	1 mg/ml	Calbiochem
Nocodazole	0.5 mg/ml in DMSO	50 ng/ml	Sigma-Aldrich
Taxol	10 mM in DMSO	10 µM	Sigma-Aldrich

2.1.6 Small interfering RNA oligonucleotides

Two EML3 RNAi oligonucleotides were used throughout the experiments as both were equally successful at knocking down EML3. Conversely, two oligonucleotides for both Nek6 and Nek7 were used initially but Nek6 siRNA 6.9 and Nek7 siRNA 7.13 were the most effective at depleting endogenous protein so were used exclusively for the remainder of experiments. Knockdown of GAPDH was used as a control to ensure effects were specific.

siRNA Oligoneucleotide name	Target Sequence (5' to 3')	Supplier
EML3 siRNA 3.1	UGGCGCCAAAGAGACCUAUGGGAUU	Invitrogen
EML3 siRNA 3.2	CCAUGACAACGUGAUCUACAUCUAU	Invitrogen
Nek6 siRNA 6.6	UCUCGCAGAUGAUCAAGUA	Thermo Scientific
Nek6 siRNA 6.9	GAAGAUAGGCCGAGGACAG	Thermo Scientific
Nek7 siRNA 7.13	GGAUAUGGGCUAUAAUACA	Thermo Scientific
Nek7 siRNA 7.14	GAAAAUUGGUCGCGGACAA	Thermo Scientific
GAPDH siRNA	Sequence unavailable	Ambion

2.2 Mammalian cell culture

2.2.1 Cell maintenance

U2OS cells were cultured in Dulbecco's Modified Eagles media (DMEM) with GlutaMAX™ supplemented with 10% v/v heat-inactivated foetal bovine serum (FBS) and 1% v/v penicillin/streptomycin (100 ug/ml). U2OS cells stably expressing YFP-EML constructs, mCherry-EB3 and YFP only were also supplemented with 1 mg/ml G418 sulphate. Cells were then maintained in a humidified environment of 37°C and

5% CO_2 until they reached a confluency of around 80%. To passage cells the growth media was aspirated from the plate and cells were washed with 1x phosphate buffered saline (PBS) (137 mM NaCl, 8.1 mM Na_2HPO_4, 2.7 mM KCL and 1.4 mM KH_2PO_4 at pH 7.4). Cells were then disassociated from the plate using 2 ml 0.05% trypsin/EDTA and seeded into appropriate plates in fresh, pre-warmed media at the required density.

2.2.2 Cell storage and recovery

In order to store the cells long term they were cryopreserved in liquid nitrogen. Once cells were confluent for storage they were washed in 1x PBS and detached using 2 ml 0.05% trypsin-EDTA (as outlined in section 2.2.1), cells were then resuspended in pre-warmed culture medium. The cells were pelleted using centrifugation for 5 minutes at 1100 rpm at room temperature. The remaining supernatant was aspirated and the pellet of cells was resuspended in 1 ml FBS supplemented with 10% v/v DMSO and transferred to a cryotube. The cryotubes were placed in -20°C for a few hours before being transferred to -80°C overnight and then into liquid nitrogen to be stored indefinitely.

To recover these cells, the cryotube was removed from liquid nitrogen and allowed to thaw rapidly in a water bath at 37°C for approximately 2 minutes, cells were then washed in pre-warmed media and pelleted via centrifugation (1,100 rpm for 5 minutes). The supernatant was removed and the cells were resuspended in fresh media and seeded onto culture plates.

2.2.3 Transient transfection

Due to the lack of effective EML antibodies, recombinant YFP-EML proteins were expressed in mammalian cells using transient transfection of cultured mammalian cells. Transient transfections were carried out using Lipofectamine 2000, a lipid based transfection reagent. Cells were seeded 24 hours before transfection so that they reached 70-80% confluency at the time of transfection.

Before transfection took place, cells were washed in 1x PBS and the media was changed to Opti-MEM^{TM} media and returned to the incubator. Plasmid DNA and lipofectamine were mixed according to the construct used (typically 1 ug of DNA to every 4µl lipofectamine) in OptiMEM^{TM} reduced serum medium, according to the manufacturer's instructions. The transfection mixture was then added drop by drop onto the seeded cells, which were then returned to the incubator for 4 hours. After the 4 hour incubation the media was replaced with pre-warmed complete fresh media and the cells were returned to the incubator for a further 24 hours until required.

2.2.4 Generation of stable cell lines

Stable cell lines were generated using DNA vectors containing genes that conferred neomycin resistance. These were transfected into U2OS cells seeded into 10 cm plates. The YFP-EML, YFP and mCherry-EB3 stable cell lines were developed following FuGENE HD mediated transfections, as this method is less cytotoxic compared to lipofectamine.

For FuGENE HD transfections, plasmid DNA and FuGENE were mixed at a ratio of typically 1 ug of DNA to every 3 ul FuGENE in Opti-MEM^{TM}, according to the manufacturer's instructions. This mixture was then added to the cells drop by drop and incubated at 37°C, 5% CO_2 for 24 hours. After this time the growth media was replaced with pre-warmed growth media containing 1 mg/ml G418, to select for the successfully transfected cells. Cells were allowed to proliferate in selection media until foci containing 50-100 cells could be detected, this usually took 4-5 weeks. The foci were then pooled together to generate a mixed stable cell population and passaged as normal. Stable expression of the recombinant protein was then determined using SDS-PAGE and Western blotting of whole cell lysates and indirect immunofluorescence microscopy of fixed cells (techniques outlined in 2.3.1 and 2.4.1).

A mixed population of stable cell lines was used rather than a clonal cell line so that different expression levels could be examined. However, there are pros and cons for each approach. Firstly, you are unable to control the genome integration site because integration is random, as a result clonal selection gives you a cell population comprised of cells that all have the same location of integration. One problem with this is that the integrated location might cause serious off-target effects, which in a clonal

population would give you a whole cell population perhaps giving you false results caused by an off-target gene rather than the gene of interest. Another argument against a mixed population is the ability of the population to change because of, for example, differences in cell growth. However studies have shown clonal recombinant cell lines also have a high degree of heterogeneity due to phenotypic drift (Barnes et al. 2006). For these reasons it was decided a mixed population would be more beneficial for the experiments in this project.

2.2.5 RNA interference

U2OS cells were seeded in growth media containing 10% FBS but no antibiotics 24 hours prior to RNAi treatment in order to reach 30% confluency at the time of transfection. Before the experiment, the cell culture hood was cleaned with RNaseZap to remove any unwanted RNAse. 100 nM of siRNA oligonucleotide and Oligofectamine™ transfection reagent were mixed in Opti-MEM™ according to the manufacturer's instructions. The seeded cells were then washed and left in DMEM media before the transfection mixture was added drop by drop. Cells were then returned to the incubator for 4 hours and then DMEM containing 30% FBS was added. Cells were then incubated for 48-72 hours before being processed as required.

2.2.6 Cell synchronisation

Cells were cultured in the appropriate complete growth medium to a confluency of 70-80%. M-phase arrested cells were obtained by treating with 50 ng/ml nocodazole for 16 h. After this time mitotic cells were rounded and could therefore be collected by gently pipetting off the rounded cells and were pelleted via centrifugation ready for lysis.

2.3 Protein analysis

2.3.1 Preparation of whole cell lysates

Whole cell lysates were prepared for SDS-PAGE or immunoprecipitation using either; RIPA lysis buffer (50 mM Tris-HCl (pH 8.0), 150 mM NaCl, 0.5 % v/v Nonidet P-40, 1% w/v Sodium dodecyl sulfate (SDS), 0.5% w/v sodium deoxycholate,) or NEB lysis buffer (50 mM HEPES-KOH (pH 7.4), 5 mM $MnCl_2$, 10 mM $MgCl_2$, 5 mM EGTA (ethylene glycol tetraacetic acid), 2 mM EDTA (Ethylenediaminetetraacetic acid), 100 mM NaCl, 5 mM KCl, 0.1 % v/v Nonidet P-40). Both buffers were supplemented with 5 mM NaF, 1 mM phenylmethylsulfonyl fluoride (PMSF), 5 mM β-glycerophosphate, 1 x protease inhibitor cocktail ((PIC) which includes: AEBSF, aprotinin, bestatin hydrochloride, E-64, leupeptin hemisulfate salt, pepstatin A) and 30 µg/ml RNase A and 30 µg/ml DNase 1 before use.

For the cell lysis, cells were washed with 1 x PBS and an appropriate volume of ice-cold lysis buffer was added directly to the plate. A cell scraper was then used to collect the cell into an Eppendorf tube and left to incubate on ice for 30 minutes. Samples were then passed multiple times through a 27G needle before centrifugation (10 minutes, 4°C, 13,000 rpm) to separate the insoluble material. The supernatant was then transferred to a fresh Eppendorf and either snap frozen and stored at -80°C or for SDS-PAGE analysis samples mixed with an appropriate amount of sample buffer (63 mM Tris-HCl (pH 6.8), 2% w/v SDS, 10% v/v glycerol, 5% v/v β-mercaptoethanol, 0.01% bromophenol blue) and denatured at 95°C for 5 minutes. For immunoprecipitation a small sample was taken prior to snap freezing as the input.

2.3.2 Kinase assays

Briefly, 5 mg of substrate was incubated with 100 ng of kinase and 1 µCi radioactive γ-^{32}P-ATP in 40 µl kinase buffer (50 mM Hepes-KOH (pH 7.4), 50 mM $MnCl_2$, 50 mM β-glycerophosphate, 50 mM NaF, 4 µM non-radioactive ATP, 1 mM DTT). Samples were incubated for 30 minutes at 30°C with agitation before the reaction was stopped by the addition of 40 µl sample buffer. The samples were then analysed by SDS-PAGE, Coomassie Blue staining and autoradiography.

2.3.3 Immunoprecipitation

Immunoprecipitation was carried out on whole cell lysates using either the mouse GFP monoclonal or the M2 Flag monoclonal antibody bound to Protein G Agarose beads. Firstly, 80 μl of packed Protein G beads (per sample) were washed 3 times in 1 x PBS and resuspended in RIPA or NEB buffer. Cell lysates were then incubated with 30 μl washed bead slurry for 30 minutes rotating at 4°C to preclear the lysates of any proteins which may non-specifically bind to the beads. Meanwhile the remaining beads were incubated on ice with the required antibody to allow the bead-antibody complexes to form. Following pre-clearing, samples were centrifuged (5,000 rpm for 2 minutes) to pellet the beads and the supernatant was added to the antibody / bead solution; samples were rotated overnight at 4°C. The beads were then washed 3 times in NEB buffer and finally resuspended in sample buffer ready for SDS-PAGE analysis.

2.3.4 SDS-PAGE

Protein samples were resolved using SDS-polyacrylamide gel electrophoresis (PAGE) using 4-12% gradient NuPAGE Bis-Tris pre-cast gels. Protein samples were loaded on the gel and separated at 200 V for 35 minutes using 1 x MES buffer in the XCellSureLock Mini-Cell. Precision Plus Protein Dual Colour Standards were used as the molecular weight markers.

2.3.5 Western blotting

The NuPAGE XCell II Blot module was used for Western blotting according to the manufacturer's instructions. Proteins were transferred to nitrocellulose membrane to allow for immunodetection. Briefly, the gel was placed onto a piece of pre-soaked 3MM Whatmann chromatography paper before nitrocellulose was placed on top of the gel and then another pre-soaked piece of paper. This 'sandwich' was then placed between wet blotting pads and loaded into the XCell II Blot module. The inner chamber was then filled with NuPAGE transfer buffer whilst the outside was filled with dH_2O and this was left to transfer for 1 hour at 30 V.

Once transfer was complete, membranes were stained with Ponceau stain (1% ponceau, 5% acetic acid) to ensure the proteins had transferred efficiently. The membrane was then blocked in 5% w/v non-fat milk powder in 1x PBST or 1 x TBST for 30 minutes with agitation to prevent non-specific antibody binding. The pre-blocked membrane was then incubated with the primary antibody at a suitable dilution in 5% non-fat milk powder in 1 x PBST for 1- 2 hours at room temperature with agitation. Following antibody incubation, the membrane was washed 3 times for 10 minutes each with 1 x PBST to remove excess antibody, before incubation with the secondary horseradish peroxidase conjugated antibody diluted in PBST at room temperature for 1 hour with agitation. The membrane was then washed a further 3 times to discard unbound secondary antibody and developed using an enhanced chemiluminescence (ECL) Western blotting detection kit according to the manufactures instructions. Protein bands were then visualised by exposing the membrane to X-ray film for appropriate times and developing using an X-ray film processor.

2.3.6 Stripping nitrocellulose membranes

If a membrane was to be reanalysed, the membrane was stripped of the previous antibodies using a stripping solution composed of 5% v/v Acetic Acid. The membrane was immersed in the stripping solution for 15 minutes at room temperature with agitation and then thoroughly washed in dH_2O. Membranes were then reblocked and analysed as in 2.3.5.

2.3.7 Staining of protein gels

To directly visualise proteins for kinase assays or phosphosite analysis, SDS-PAGE gels were stained using Coomassie Blue solution (40% v/v IMS, 10% acetic acid and 0.25% w/v Brilliant Blue R). Gels were incubated with the solution for 1 hour at room temperature before the Coomassie Blue solution was removed and replaced with destain solution (7.5% v/v acetic acid, 25% IMS). The gel was repeatedly washed until the protein bands could be easily distinguished and suitable to scan. For mass spectrometry / phosphosite analysis the bands were cut directly out of the gel. For

kinase assays, gels were dried onto Whatman 3 MM chromatography paper using a vacuum for at least 2 hours at 80°C. Radiolabelled proteins could then be visualized by autoradiography.

2.4 Microscopy

2.4.1 Indirect immunofluorescence

Acid etched coverslips were prepared by treating with 1 M HCL for 30 minutes followed by 100% ethanol for another 30 minutes, wash in dH_2O and then baked for 4 hours at 250°C. Cells were then grown on acid-etched coverslips and once cells were ready for fixing, they were washed in 1 x PBS and fixed in ice-cold methanol for at least 30 minutes at -20°C. Methanol was used as it fixes cells very quickly, gives a clear background to images and paraformaldehyde fixation can remove weak interactions such as MT plus-tip tracking proteins. Cells were then rehydrated by three five minute washes in 1 X PBS and then blocked using 1% w/v BSA in PBS for 10 minutes at room temperature. Primary antibody solutions were made up in 3% w/v BSA in PBS and incubated for 30 minutes to 2 hours (depending on antibody). Following this incubation, the coverslips were washed three times for five minutes with 1 X PBS and then incubated with the secondary antibodies (including Hoechst 1:1000 for DNA visualization), again in 3% BSA-PBS for 30 minutes to 1 hour. Following the secondary antibody incubation, the coverslips were washed for a final three times for 5 minutes with 1 X PBS, before being inverted onto a labelled coverslip using a small volume of mountant (80% glycerol, 3% n-propyl gallate in PBS). The coverslips were sealed using nail varnish and kept in the dark at 4°C.

Cells were visualized using the Leica TCS SP5 laser scanning confocal microscope (LSCM) fitted with a Leica DMI 6000B inverted microscope and a Plan Apo 63x oil objective (NA 1.4). Cells were located using either brightfield or via the Hoechst DNA fluorescence. For fixed imaging the following lasers were used: Diode 405 for DNA stain, Argon 488 laser (30%) for green staining and DPSS 561 for red staining. An area of interest was selected and a z stack set, usually of 0.4-0.6 µm steps. Individual stacks were used to give a maximum projection to give a single 3D image which was

saved as an individual TIF file or for quantification images were deconvolved using Huygens Essential software (version 4 64-bit, Scientific Volume Imaging). This program remove noise and reassigns out-of-focus light from the images using a theoretically calculated point spread function, using the classic maximum likelihood estimation deconvolution algorithm.

2.4.2 Cell scoring

Cells were scored to determine differences in, for example, multipolarity, as well as lagging and misaligned chromosomes following different treatments. Fixed images were used to randomly select broad regions of interest (ROIs) where cells within that region were scored accordingly. ROIs were chosen by blind scrolling systematically across the coverslip until enough cells had been counted.

2.4.3 Quantification of Colocalisation with microtubules

All images for quantification for a particular experiment were captured under identical conditions and processed uniformly. Briefly, TIF files were deconvolved using Huygens Essentials software to remove noise from the images. These deconvolved images were then opened in Volocity software where a Pearsons Correlation Coefficient was calculated to determine the percentage of signal A (e.g. YFP) linearly correlating to the amount of signal B (e.g. tubulin) within a 6 µm x 6 µm ROI near the cell periphery, as outlined below. This coefficient indicates the correlation between the two signals, giving R values between -1 and +1; +1 is positive correlation, -1 is negative correlation and 0 is no correlation.

Thresholded Statistics

Pearson's Correlation: 0.606   Overlap Coefficient (R): 0.918
Colocalization Coefficient (M1): 0.993   Overlap Coefficient (k1): 0.371
Colocalization Coefficient (M2): 0.969   Overlap Coefficient (k2): 2.274
Voxels over Threshold: 4501   Voxel Ratio Ch.1 / Ch.2: 0.941
Selected Voxels: 4501 (100.000%)

Global Statistics

Global Pearson's Correlation: 0.684   Total Voxels: 262144

Alternatively, TIF files were opened in Leica SP5 software to measure the overlap coefficient of two signals. A line was drawn across a distinct region of microtubules (near the cell periphery). The relative intensity of the two signals of interest was then saved as an excel file (e.g. YFP-EML and tubulin) to plot an overlap graph. This was used to determine whether a peak in tubulin signal correlates with a peak in EML signal.

2.4.4 Measuring cytoplasmic protrusion length

TIF files were opened in Leica SP5 software and cytoplasmic protrusion lengths measured from the edge of the nucleus to the furthest point of the cell membrane using the ruler tool, an example of this quantification is outlined below.
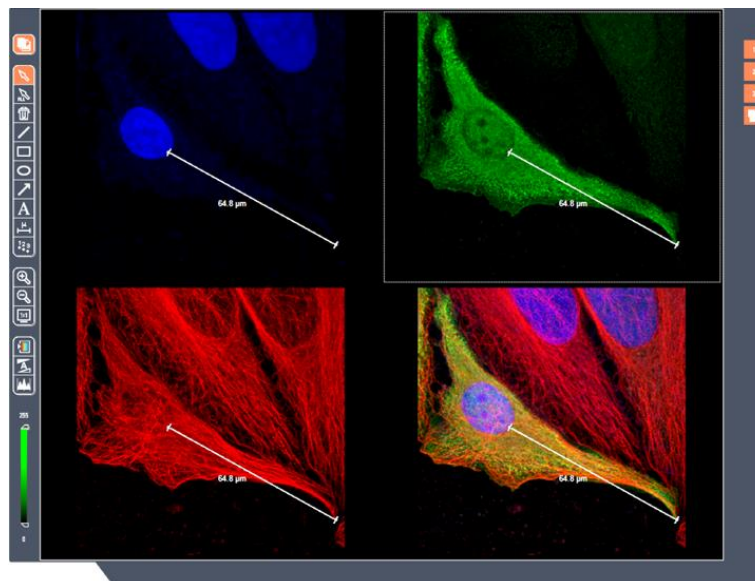
2.4.5 Tubulin intensity measurements

To quantify disruption to the MT network tubulin intensity plots were carried out. For this analysis, images were opened in Leica SP5 software. A line was then drawn near the periphery of the cell across a region of MTs, this revealed peaks in intensity where MTs were present and no defined peaks if the tubulin staining was diffuse throughout the cytoplasm.

2.4.6 Time-lapse imaging

For time-lapse imaging cells were seeded into glass bottom culture dishes in Opti-MEM™ media at least 12 hours before microscopy. Once on the microscope they were maintained in 5% CO_2 and 37°C using a temperature control system. An (ROI) was then selected. For MT network imaging, a single z section was chosen and imaging performed for 2 minutes with images being taken every second. For mitotic cells, a z stack was collected for each ROI (up to 5 ROIs imaged simultaneously) and with imaging collected every 12-15 minutes for 17 hours. Individual images were saved as TIF files and processed into a movie using ImageJ software.

2.4.7 Fluorescence recovery after photobleaching (FRAP)

FRAP studies were carried out on the Leica TCS SP5 LSCM on cells cultured as described for time-lapse imaging, A ROI of either 3 μm x 6 μm or 1 μm x 4 μm was selected depending on the experiment. These ROI were then bleached with 3 pulses at 100% argon 488 nm laser power. Three images were taken before the ROI was bleached and then images were taken for every 1 second for 2 minutes following bleaching. The intensity of each ROI was determined using Leica AF Software and saved as an Excel file. Using Excel, the corrected fluorescence intensity was calculated using the following equation:

$$\frac{\text{Intensity of ROI- Background fluorescence}}{\text{Fluorescence intensity of pre-bleach}}$$

These values were plotted to calculate the overall percentage recovery at 60 seconds and the half-life of recovery.

2.5 Statistical analysis

Results are presented as the mean of three independent experiments, unless otherwise stated. Error bars represent standard deviation of the mean or standard error of the mean. p values were calculated on Excel or GraphPad using a one-tailed unpaired Student's t-test assuming unequal variance.

2.6 Miscellaneous techniques

2.6.1 Protein purification

Protein purification was kindly carried out by Dr. Mark Richards. EML cDNAs were cloned from human cDNA (Clontech) and shorter constructs were made by PCR. YFP- and Flag-tagged constructs for expression in human cells were made by cloning EML constructs or full-length cDNAs in series with YFP- or Flag sequences and subcloning into pcDNA3 or pcDNA3.1-hygro. For production of EML proteins incorporating the TAPE domain, constructs were cloned into a modified version of pMAX (Lonza) providing a FLAG-tag and a pair of N-terminal Strep2-tags. HEK283F cells growing in suspension culture in Freestyle 293 media (Gibco) at a density of 1×10^6 cells/mL were transfected with these plasmids using 2 ug/mL polyethylenimine. Cells from ~1L cultures were harvested 2 days after transfection and lysed in tris-buffered saline (TBS). Proteins were purified from clarified lysate on Strep-tactin Sepharose columns and eluted with 3 mM desthiobiotin (IBA). Size exclusion chromatography in TBS supplemented with 2 mM dithiothreitol was carried out using a Superose 6 column (GE Healthcare) to remove co-purifying tubulin. EML N-terminal fragments were expressed as His-YFP-fusions in E. coli BL21 (de3) RIL cells (Agilent) induced with 0.6 mM isopropylthiogalactoside and purified from clarified cell lysate on Chelating Sepharose (GE Healthcare) . Tobacco-etch virus protease was used to remove the his-tag. The protease and his-tag were then removed by a second passage over Chelating Sepharose. Finally, gel filtration chromatography on Superdex 75 column (GE Healthcare) was used to separate aggregated protein away from the YFP-fusion protein sample.

2.6.2 Subtilisin digestion experiment

This experiment was carried out at the University of Warwick in the Laboratory of Dr. Anne Straube and adapted from: Straube, A. Microtubule Dynamics - Methods and Protocols. 1st ed. Springer, 2011.

Subtilisin is a serine protease which causes the digestion of the negatively charged C terminal tails of tubulin. Microtubule seeds were prepared using a mixture of tubulin (4mg/ml), including biotin labelled (0.5 µl), rhodamine labelled (0.2 µl) and unlabelled tubulin (2.5 µl), 1µl GMP CPP (10 mM) and 5 µl MRB80 (80 mM PIPES, 1 mM $MgCl_2$, 1 mM EGTA in H_2O, pH adjusted to 6.9 with KOH). This mixture was kept on ice for 40 minutes and then heated to 37°C for 20 minutes; after this time the microtubule seeds were stable enough to be kept in the dark at room temperature for a few weeks. The seeds were then treated with subtilisin (25 µg/ml) or left untreated and incubated for 20 minutes at 37°C. To terminate the digestion 2 mM PMSF was added and the reaction mix placed onto a 60% glycerol cushion and centrifuged for 5 minutes at 150,000 x g. The supernatant was then removed (containing the digested protein) and resuspended in MRB80 buffer.

A flow cell was then constructed using silanized cover glass. A thin channel of approximately 5 µl was produced using strips of double sided sticky tape approximately 4 mm apart. The resuspended supernatant/MRB80 mixture was pipetted into the chamber along with the reaction mix (2.4 µl Kappa casein, 0.4 µl glucose, 2 µl KCL and 0.4 µl oxidizing agent with 500 nM protein of interest. The flow cell was then imaged using an Olympus TIRF-3 system and images analysed using ImageJ software.

2.6.3 Mutagenesis reaction

Oligonucleotides were designed to introduce a number of mutations into the YFP-EML3 construct. They were designed so that the guanine-cysteine content was at least 50% and the annealing temperature (Tm) was between 70-80°C with a length of 30-35 nucleotides (properties checked using http://www.operon.com/). The forward and reverse primers contained the desired mutations in the middle of the sequence with 10-15 bases of correct sequence on both sides.

To generate multiple site YFP-EML3 mutants for expression into mammalian cells, appropriate PCR primers and vector containing target DNA were submitted to Protein Expression laboratory (PROTEX) at the University of Leicester where all the mutagenesis reactions were carried out. Sequencing was performed on the mutant plasmids using appropriate sequencing primers at the Protein Nucleic Acid Chemistry Laboratory (PNACL) at the University of Leicester. Sequencing data received from PNACL was translated using 4Peaks software and then aligned with the wild-type sequence using CLUSTALW2 (EMBL-EBI).

2.6.4 Bacterial transformation

Competent DH5α Escherichia coli cells were thawed on ice before 2 µl of ligation reaction was added. The two were gently mixed and then incubated on ice for 25 minutes before being heat shocked at 42°C for 45 seconds to induce plasmid DNA uptake. Following this they were incubated on ice for an additional 2 minutes, after which 450 µl of Luria Broth (LB) media (17 mM NaCl, 0.5% w/v yeast extract, 1% w/v tryptone, 10 mM Tris pH 7.5) was added to the cells and incubated for 1 hour at 37°C, 225 rpm. Following this incubation, 200 µl of the cell suspension was spread onto pre-warmed LB agar plates (LB plus 2% w/v agar) which contain the appropriate antibiotic for selection, either ampicillin (100 µg/ml) or kanamycin at (50 µg/ml). Once dry, plates were incubated for 16 hours at 37°C, after this time colonies were picked for plasmid preparation.

2.6.5 Isolation of plasmid DNA by maxiprep purification

A single transformation colony (as described in 2.5.5) was used to inoculate a 5 ml LB starter culture (plus antibiotic). This started culture was incubated for 8 hours at 37˚C, 225 rpm, after this time 1 ml was transferred to 100 ml fresh LB (plus antibiotic) which was again incubated for 16 hours at 37˚C, 225 rpm. Cells were collected by centrifugation at 6000x g for 15 minutes at 4˚C. Isolation of plasmid DNA was obtained using the QIAfilter Plasmid Maxi kit (QIAGEN) according to the manufacturer's instructions. One plasmid DNA was isolated it was made up to 1 µg/µl stocks and stored at -20˚C for use in transfections and stable cell line generation.

CHAPTER 3   CHARACTERISATION OF EML PROTEINS WITH MICROTUBULES IN INTERPHASE

3.1 Introduction

MAPs contribute to the dynamic turnover of MTs which are crucial for cell motility, cell morphogenesis, spindle formation and chromosome movements. Determining the localisation and behaviour of a specific MAP can provide crucial insights into its cellular roles during both interphase and mitosis. Originally it was assumed that all MAPs bind to and stabilise MTs, but more recently destabilisers such as katanin have been identified. Some of the more well characterised stabilising MAPs include; Tau, MAP4 and MAP2. MAP2 and Tau are found in neurons whereas MAP4 is present in neurons and a range of other tissues (Dehmelt & Halpain 2005). MAP2 is involved in neurite outgrowth and dendritic development, therefore making MAP2 a hallmark of neuronal differentiation. MAP4 is present in all neuronal tissues and is thought to be crucial for cytoskeletal reorganisation and regulation of MT-dependent transport along the neuron (Tokuraku et al. 2010).

In this chapter we begin to characterise the novel EMAP-like family of proteins, the EMLs. The exact function of the different members of the EML family of proteins has not yet been fully ascertained. The founding member of the EML family was the Echinoderm Microtubule Associated Protein (EMAP). EMAP was first isolated as a major non-tubulin component of spindle MT preparations from sea urchin eggs. In the study by Suprenant et al. (1993) tubulin from unfertilised sea urchin eggs was purified and a 77 kDa polypeptide (later termed EMAP) was found to readily coassemble. Localisation studies in interphase confirmed that EMAP colocalised with tubulin, whilst in mitosis EMAP was distributed throughout the spindle with astral regions stained much more strongly than the central spindle (Suprenant et al. 1993). In terms of microtubule dynamics, EMAP is a stabilising MT protein which is also required for MT assembly.

In terms of human EMLs, the exact functions have not yet been fully ascertained. EML1 has been indicated in mechanotransduction for sensory function and research from the Fry, Bayliss and Straube labs has shown EML1 to bind strongly to the MT network in interphase (R=0.886) when transiently transfected into HeLa cells. Moreover, truncated constructs indicated that the NTD of EML1 is critical for the association to the MT network and that the TAPE domain has the ability to bind soluble tubulin (Richards et al. 2014). The NTD also contains a trimerisation domain which is essential for the self-assembly of EML proteins and has been shown to be critical for MT binding. Research into EML2 (or ELP 70) indicated that this protein was a MT destabiliser and strongly associated to MTs in HeLa cells, in both interphase and mitosis (Eichenmuller et al. 2002). Likewise, EML3 was identified as a microtubule binding protein following a proteomics screen and immunofluorescence microscopy revealed that both endogenous and recombinant EML3 localised along the length of the MTs in interphase with no preference for one end (Tegha-Dunghu et al. 2008). However, there was no indication as to whether this protein was acting as a stabiliser or destabiliser. Lastly, GFP-EML4 colocalised clearly with β-tubulin in interphase and in some cases during mitosis and it was suggested that this protein was a MT stabiliser (Houtman et al. 2007). These results highlight the complexity of this family and infer that they may have very different effects on MT dynamics.

The following chapter will look further into the localisation, dynamic activity and specific affinity of the EML proteins for the MT network in interphase and start to explore the potential interactions of EML proteins with one another.

3.2 Results

3.2.1 Generation of YFP, YFP-EML1 and YFP-EML3 stable U2OS cell lines

At the start of this study there was no appropriate commercial antibodies available in order to characterise endogenous EML proteins. A significant amount of time and effort was put into testing commercial antibodies. However even by the end of the study, good commercial antibodies were only available for EML2 and EML4. As a result, tagged recombinant proteins were used for expression and analysis in cells. However, excessive overexpression of recombinant proteins can lead to altered properties which would not be seen with the endogenous protein. In order to combat this, U2OS cell lines were developed which stably expressed YFP-EML proteins. For this study, a mixed population of cells was used as not only does this overcome potential problems of using a single clonal population but it allows us to analyse the effects of varying expression levels. To generate these stable cell lines, U2OS cells were transfected with each of the following N-terminal tagged constructs: YFP-EML1, YFP-EML3 and YFP alone and treated with 1 mg/ml G418 as described in chapter 2.2.4.

To confirm the expression of recombinant protein in each stable cell line, cells were either lysed with RIPA buffer and analysed using SDS-PAGE and Western blotted with GFP antibodies (Figure 3.1A) or fixed in methanol and stained for immunofluorescence microscopy (Figure 3.1B). Western blot analysis confirmed expression and at the correct molecular weights for each protein, YFP-EML1 (119 kDa), YFP-EML3 (122 kDa) and YFP alone (27 kDa). Immunofluorescence also confirmed expression of YFP-tagged proteins in approximately 80% of cells. Immunofluorescence microscopy was also carried out to determine the localisation of YFP-EML1 and YFP-EML3 compared to that of YFP alone. Both YFP-EML1 and YFP-EML3 showed clear localisation to the MT network in interphase as indicated by

colocalisation with α-tubulin antibodies. This is in contrast to that of YFP, which was diffusely distributed between the cytoplasm and nucleus with no obvious MT localisation (Figure 3.2A). To support this, high magnification images were examined to visualise the distinct localisation of both YFP-EML1 and YFP-EML3 with the MT network (Figure 3.2B).

3.2.2 EML proteins localize and have different binding affinities for interphase MTs

We noted from images in Figure 3.2 that EML3 localization on MTs was more well-defined than that of EML1. We therefore postulated that EML proteins may possess differing affinities for the MT network. Dr Laura O'Regan had independently developed YFP-EML2 and YFP-EML4 U2OS stable cell lines in the Fry lab. U2OS cells stably expressing YFP only, YFP-EML1, YFP-EML2, YFP-EML3 and YFP-EML4 were lysed in RIPA buffer and analyzed via SDS-PAGE and Western blotted for GFP and α-tubulin in order to check relative expression levels (Figure 3.3A). The relative expression levels of each cell lines were relatively equal, with the exception of YFP-EML4, which appeared as a faint band. This could be due to problems in the initial transfection efficiency, the level of expression or the size of the protein affecting western blot detectability.

Despite this, these cell lines were then fixed in methanol and stained with GFP and α-tubulin antibodies for immunofluorescence microscopy as described in chapter 2.4.1. This revealed YFP-EML4 expression was present in a number of cells making them suitable for analysis. Images were taken under identical conditions on the Leica SP5 confocal microscope, deconvolved using Huygens essential deconvolution software and analyzed using volocity software and pearsons correlation coefficient as described in chapter 2.4.3. As a control it was decided to analyze YFP-ALK as this protein has been generated for other studies. The data revealed that YFP-EML2 (54.71 %) and YFP-EML3 (54.61 %) had a higher affinity for the interphase MT network then YFP-EML1 (39.80 %) and YFP-EML4 (43.33 %) (Figure 3.3C) and that this was statistically significant following an unpaired student T-test (Figure 3.3 D). This coincides with what can be seen by eye (Figure 3.3B).
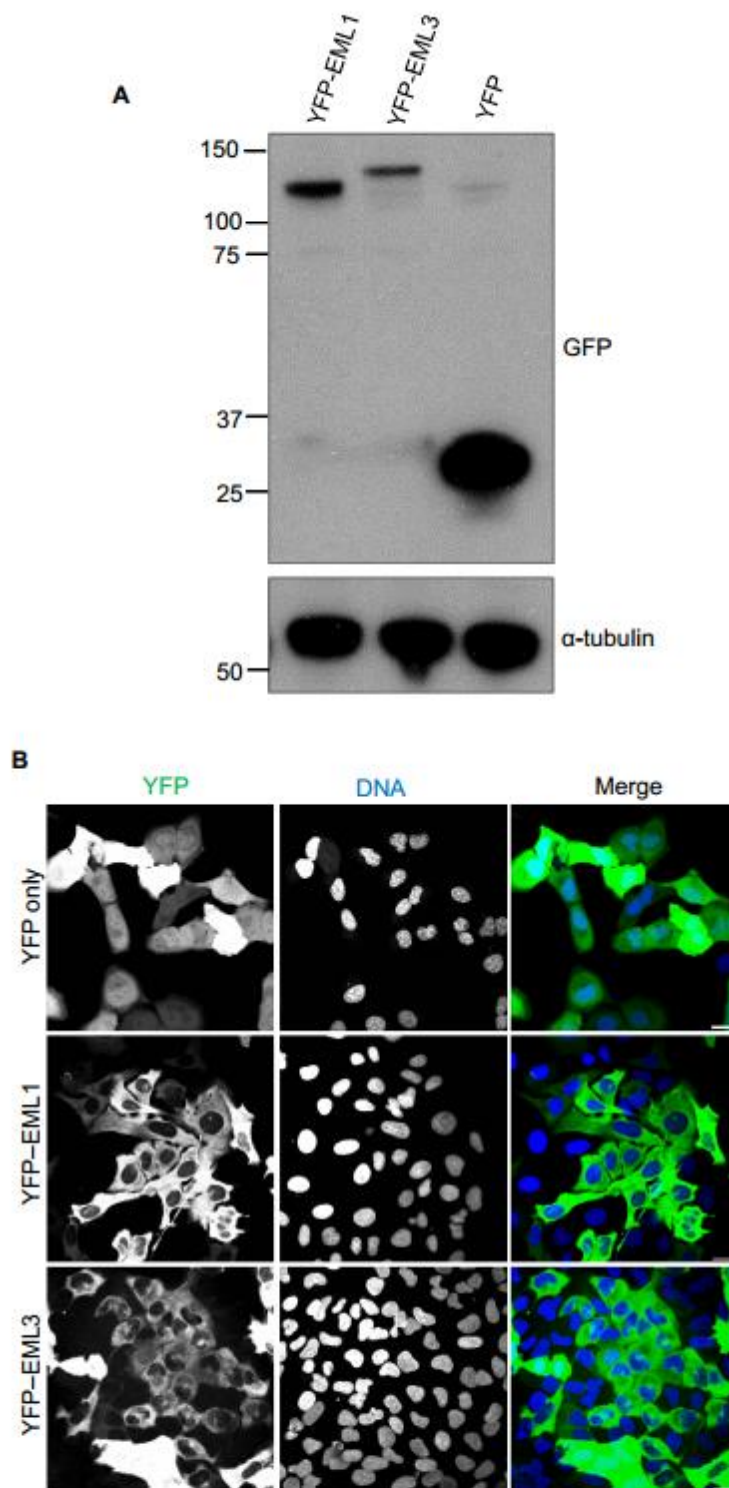
Figure 3.1: Generation of YFP, YFP-EML1 and YFP-EML3 stable U2OS cell lines

A. Cell lysates from U2OS cells stably expressing YFP only (27 kDa), YFP-EML1 (119 kDa) and YFP-EML3 (122 kDa) were western blotted with GFP and α-tubulin antibodies as indicated. Molecular weights (kDa) are indicated on the left. **B.** U2OS:YFP, U2OS:YFP-EML1 and U2OS:YFP-EML3 cells were fixed with methanol and immunostained using an α-GFP antibody (green) and Hoechst (blue) to visualise the DNA. Scale bars, 25 μm.
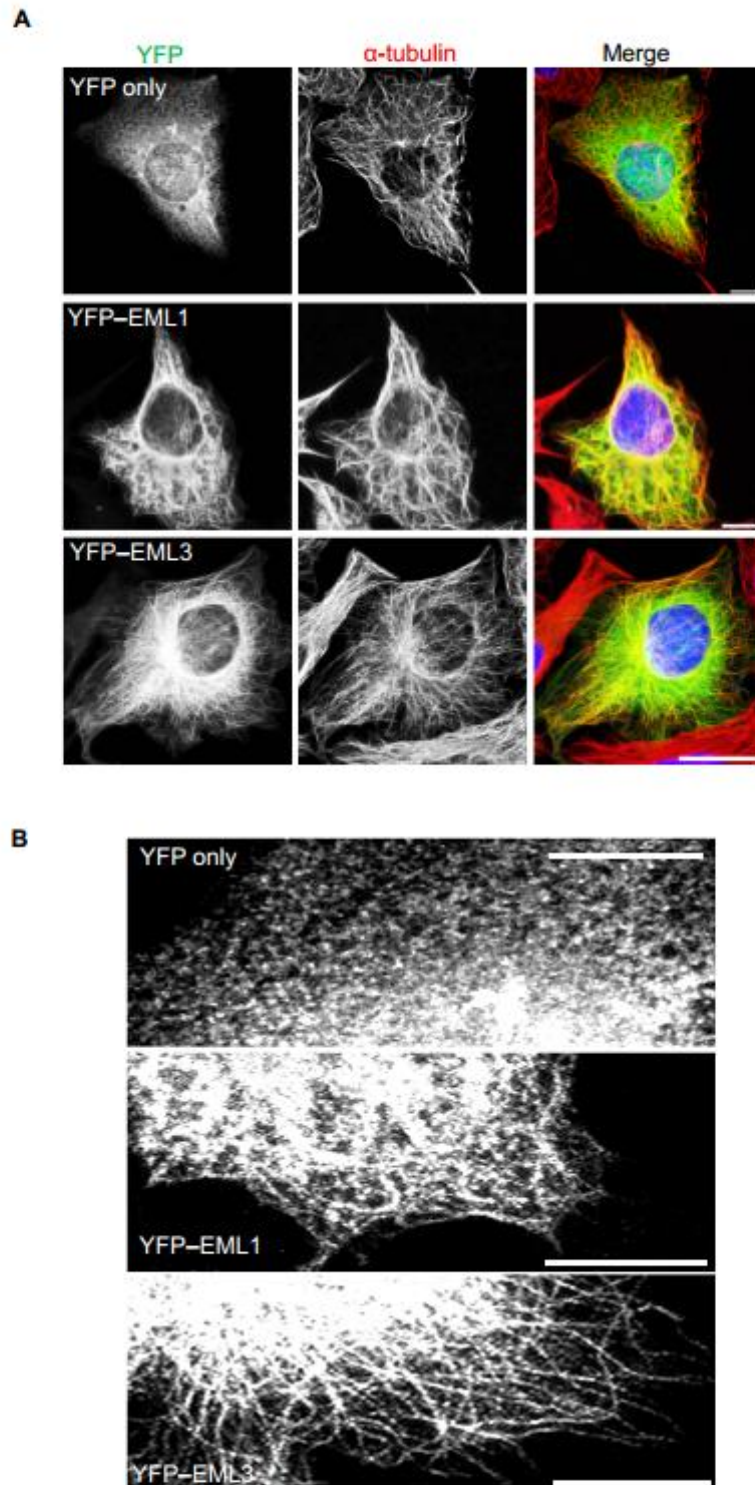
Figure 3.2: EML1 and EML3 proteins decorate the MT network in interphase

A. U2OS:YFP, U2OS:YFP-EML1 and U2OS:YFP-EML3 cells were fixed with methanol and immunostained with GFP (green) and α-tubulin (red) antibodies. Merged images include DNA stained with Hoechst (blue). Scale bars, 10 μm. **B.** High magnification of the YFP channel only. Scale bars, 5 μm.

C.

D.

Proteins	Significance
EML1 vs EML2	**
EML1 vs EML3	**
EML1 vs EML4	n/s
EML2 vs EML3	n/s
EML2 vs EML4	***
EML3 vs EML4	**
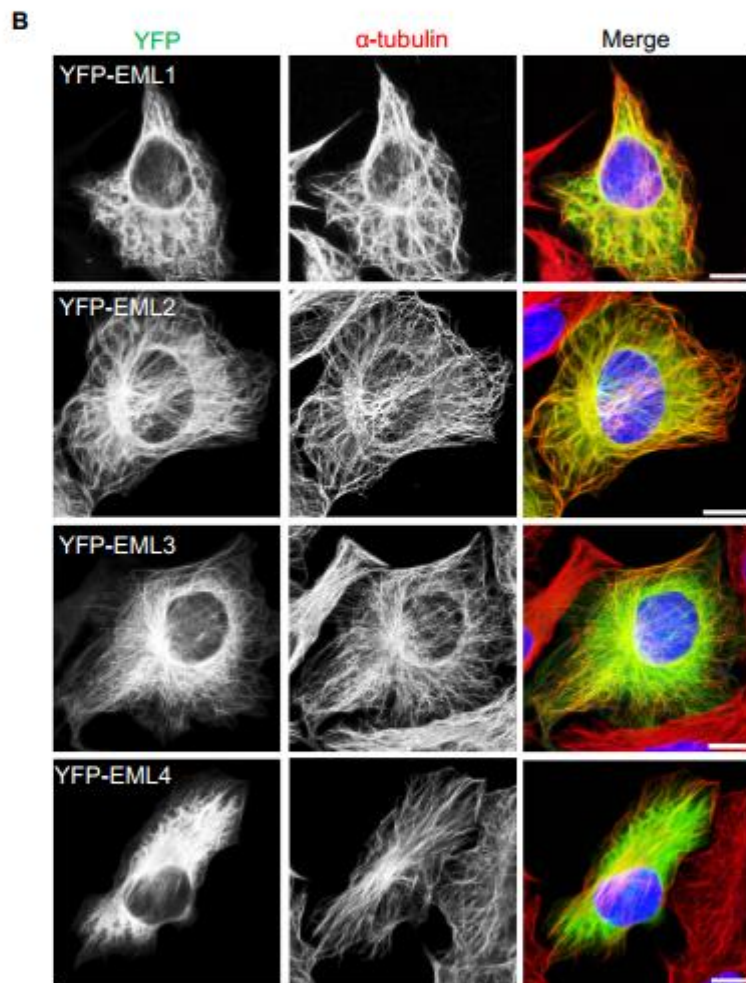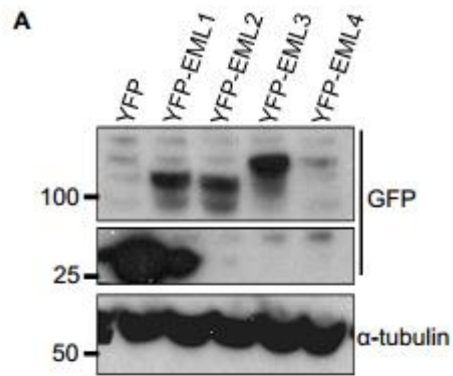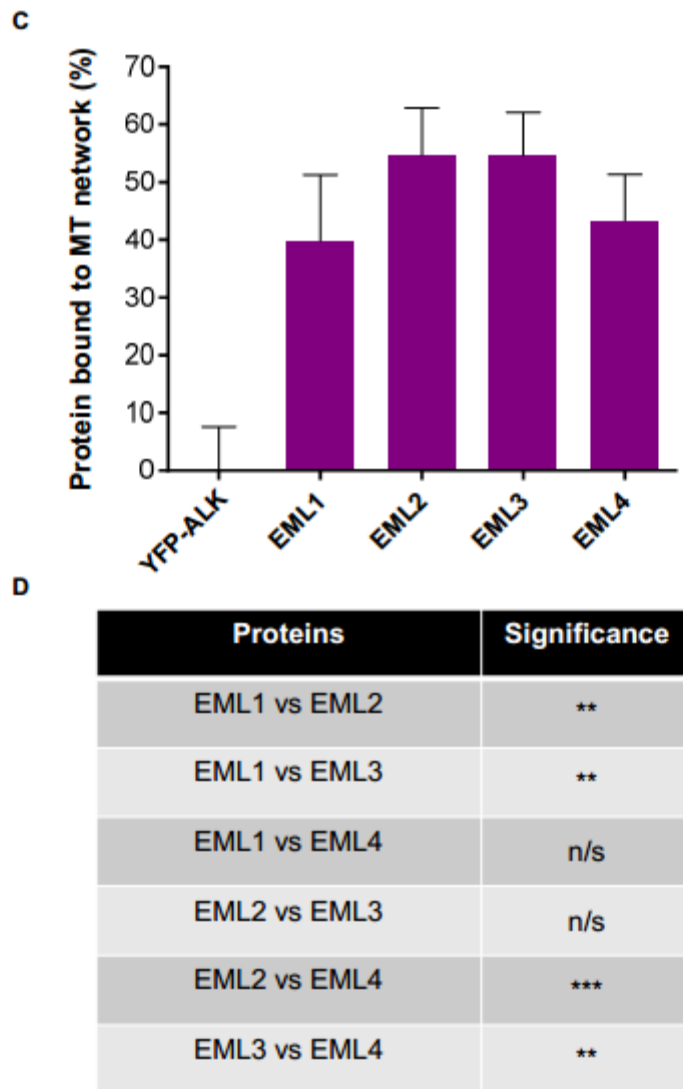
Figure 3.3: EML proteins have different affinities for MTs in interphase

A. Western blot analysis to show expression levels of the different proteins in stably expressing cells using a GFP antibody: YFP-EML1 (119 kDa), YFP-EML2 (117 kDa), YFP-EML3 (122.2 kDa), YFP-EML4 (135.9 kDa) and YFP (27 kDa); α-tubulin (55 kDa) used as a loading control. **B.** U2OS:YFP-EML stable cell lines were fixed with methanol and immunostained with GFP (green) and α-tubulin (red) antibodies. Merged images include DNA stained with Hoechst (blue). Scale bars, 10 μm. **C.** Histogram indicates the percentage of YFP-EML protein bound to the MTs in a specific ROI (4 μm x 4 μm). Data represent means (±SD) of measurements taken using Volocity software from 20 cells from one experiment. **D** Table of statistics from unpaired student T-tests (** $p < 0.01$, *** $p < 0.001$).

The reason for these differences has not yet been established but one could hypothesize that it reflects differences in the MT binding regions and may allow for functional differences between the different members of this family.

We then wanted to explore whether EML1 and EML3 localization was altered by microtubule poisons. The two drugs chosen for this were nocodazole and taxol. Nocodazole is a MT destabilizer which mimics the effects of the clinically available Vinca Alkaloids, common chemotherapeutic agents used for the treatment of ovarian and breast cancers (Gascoigne & Taylor 2009). Taxol is a microtubule stabilizer and in cancer therapy is administered to treat ovarian, breast and non-small cell lung cancer (NSCLC). YFP-EML1 and YFP-EML3 stable cell lines were treated with 50 ng/ml nocodazole or 10 nM taxol for 4 hours before being fixed and stained for immunofluorescence microscopy. Both YFP-EML1 and YFP-EML3 localization became cytoplasmic in the presence of nocodazole, as the MT network was no longer intact (Figure 3.4 A and B). Meanwhile, both YFP-EML1 and YFP-EML3 remained bound to the MTs following taxol treatment which caused overstabilisation and bundling of MTs (Figure 3.4 A and B). These results confirm the high affinity that the EML proteins have for MTs, even in the presence of taxol.

3.2.3 EMLs bind to MTs via tubulin E-hooks

Previous work in the lab had already identified the NTD of the EML proteins to be the region required for association to MTs; isolated NTD fragments were able to bind to the MTs whilst the TAPE domain alone remained diffusely distributed (Richards et al. 2015). To map the binding region more precisely truncated YFP-tagged EML1 NTD fragments were generated for transfections (Figure 3.5A) based on the predicted regions of binding for EML1 and EML3 found using the EXpasy pI calculator (shown in Figure 3.5B). The full EML1 NTD construct (1-174) (Figure 3.5C) showed the highest percentage of protein associated to the MTs, closely followed by the coiled coil motif (residues 23-78) (Figure 3.5D). This was somewhat surprising as the coiled coil motif had a low pI value, although this result could be due to trimerisation with endogenous EML1 protein. The other fragments were all able to associate to MTs to some degree according to the software analysis but none of the fragments showed clear localization by eye.
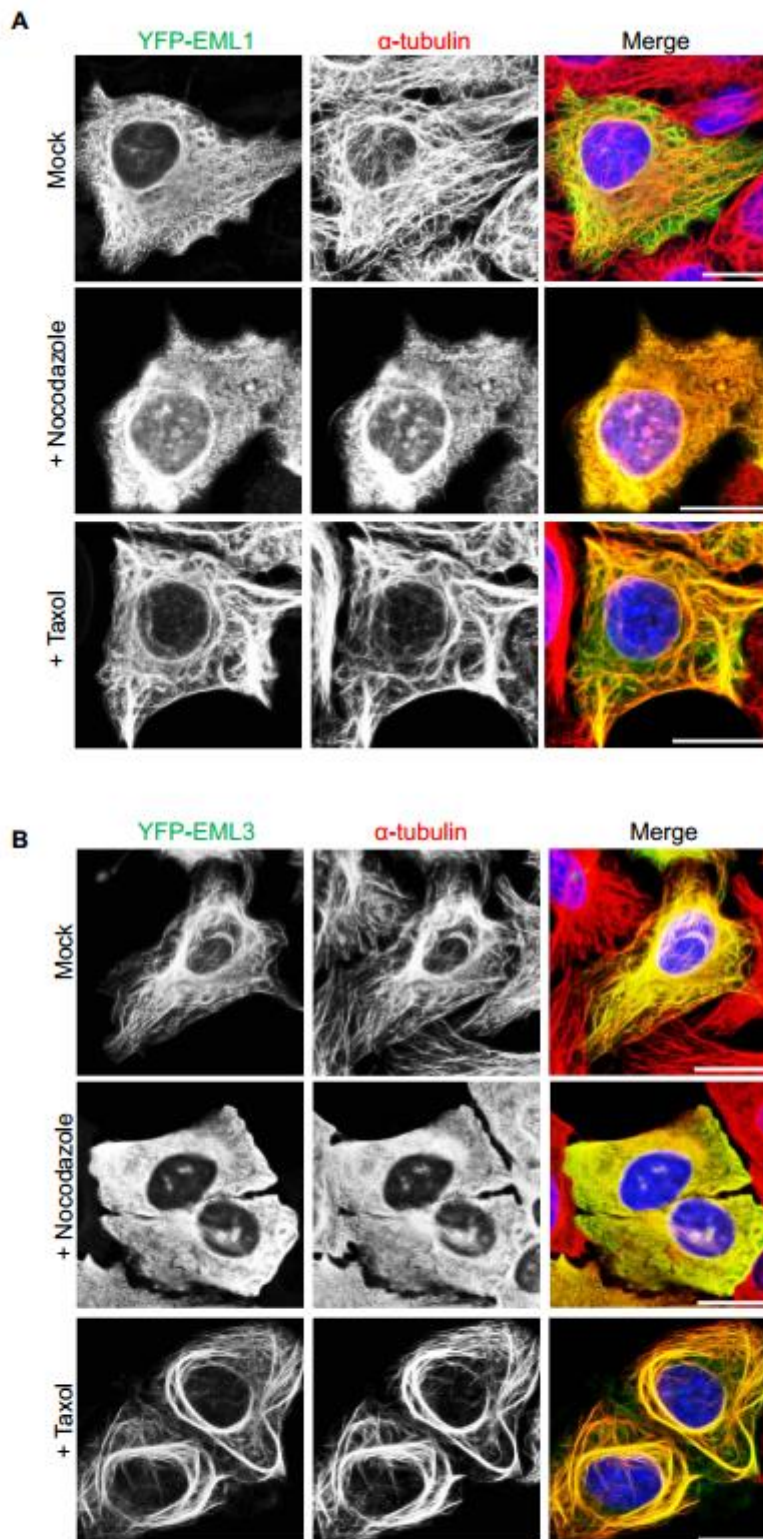
Figure 3.4: EML1 and EML3 are able to bind to stabilized MTs

Stable U2OS:YFP-EML1 **(A)** and U2OS:YFP-EML3 **(B)** were either mock treated or treated with 50 ng/ml nocodazole or 10 nM taxol for 4 hours, before being fixed with methanol and immunostained with GFP (green) and α-tubulin (red) antibodies. Merged images include DNA stained with Hoechst (blue). Scale bars, 20 μm.

A

YFP	α-tubulin	Merge

ALK

1-174

23-78 CC

74-174

74-125

100-150

125-174

B

EML1 NTD fragment	pI value
1-174	9.66
23-78 (CC domain)	4.21
74-125	12.71
74-174	12.60
100-150	12.54
125-174	12.39

C

```
MEDGFSSYSS LYDTSSLLQF CNDDSASAAS SMEVTDRIAS
LEQRVQMQED DIQLLKSALA DVVRRLNITE EQQAVLNRKG
PTKARPLMQT LPLRTTVNNG TVLPKKPTGS LPSPSGVRKE
TAVPATKSNI KRTSSSERVS PGGRRESNGD SRGNRNRTGS
TSSSSS
```

D

Figure 3.5: Mapping the MT binding region of EML1

A. U2OS cells were transiently transfected with YFP-EML1 NTD fragments and YFP-ALK, fixed with ice-cold methanol and immunostained GFP (green) and α-tubulin (red) antibodies. Merged images include DNA stained with Hoechst (blue). Images were deconvolved using Huygens essential software. Scale bars, 10 µm. **B.** Endmemo PI software (http://www.endmemo.com/bio/proie.php) was used to calculate the pI value of the YFP-EML1 NTD fragments to predict the binding region. **C.** Amino acid sequence of the EML1 NTD **D.** Volocity software was used to calculate the percentage of YFP-EML protein directly localised to tubulin. Data shown represent the mean (±SD) of 20 individual cells from one experiment.

It can also be argued that both the coiled-coil motif and basic region before the TAPE domain are required for maximal binding.

Our hypothesis was that E-hooks are negatively charged (α-tubulin pI is 4.94) and thus only proteins with positive charged regions would be able to associate. As a result by calculating the most positively charged region within the NTD we thought we would be able to predict the MT binding region and develop the correct constructs (Figure 3.5C). Using the EXpasy pI calculator we looked at the pI values of the full length protein, NTD and TAPE domain (Figure 3.6C). The NTDs of EML1 and EML3 were positively charged consistent with the hypothesis that EMLs may bind to the negatively charged C-terminal tails of tubulin, termed E-hooks, via electrostatic interactions. To test this, purified GFP-EML1 NTD protein, generated by the Bayliss lab, was incubated with fluorescently labeled MT seeds that had been pre-treated with and without subtilisin, a protease with the ability to digest E-hooks (Figure 3.6 A and B). By TIRF microscopy, a clear reduction in GFP-EML1-NTD association to the MT seeds was observed following subtilisin treatment (p<0.0001) (Figure 3.6D). This experiment strongly supports the hypothesis that EML proteins bind to MTs through an electrostatic interaction with the tubulin E-hooks.

3.2.4 EML proteins interact in a dynamic manner to MTs

We next wanted to investigate the dynamics of EML protein association with the MT network. For this purpose time lapse imaging was used to visualise the proteins and determine whether any distinct movements could be seen. YFP-EML3 stable cell lines were analysed by confocal microscopy in comparison with a mCherry-EB3 stable cell line which we generated as a control cell line. EB3 is a plus end binding protein that plays a role in microtubule growth and cell migration. When imaged MT plus end 'flares' were visible with mCherry-EB3 representing the growing end of an individual MT. In contrast, YFP-EML3 decorated the entire MT network, with EML3 showing a stronger association consistent with previous data (Figure 3.7A). Following the generation of kymographs (Figure 3.7B), YFP-EML3 showed no clear directional movement along the MTs, especially when compared to EB3 which showed very obvious plus tip tracking. These data are similar to that of Eichenmuller et al. 2002, who reported that EML2 did not preferentially bind to MT ends.
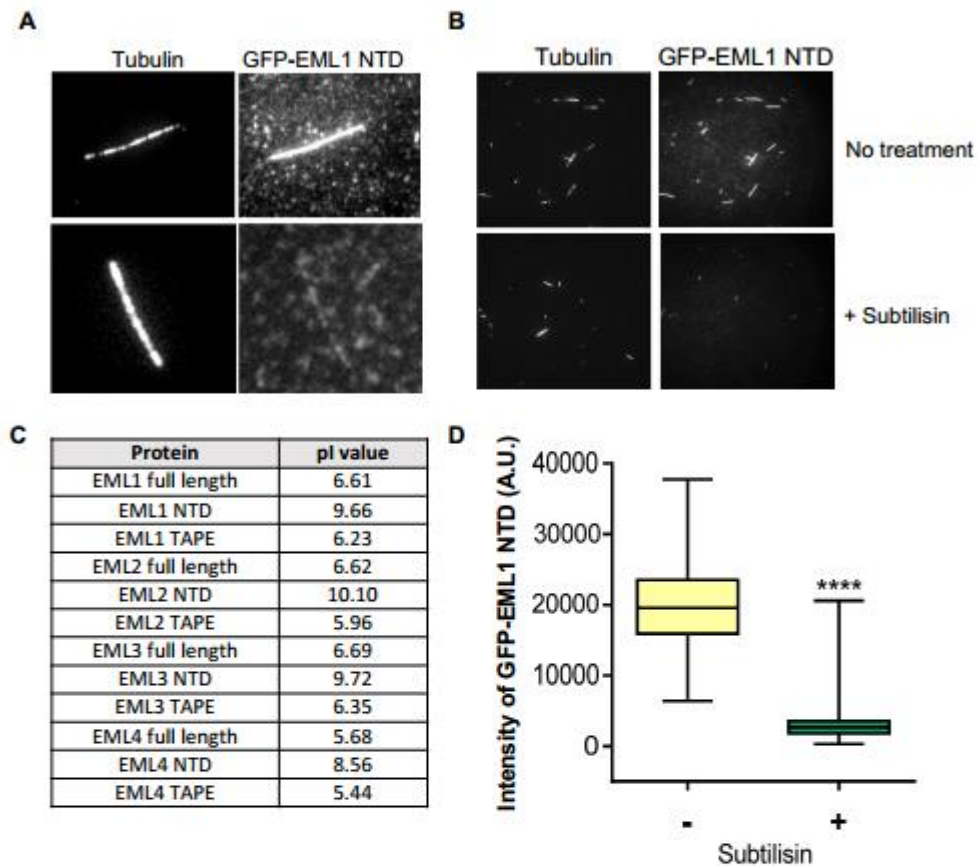
Figure 3.6: MT binding of the EML1-NTD is lost upon subtilisin treatment

High **(A**) and low magnification (**B)** images of the microtubule seeds with and without subtilisin treatment. MT seeds made using rhodamine labelled tubulin and were treated with 25 ug/ml subtilisin or left untreated as indicated. **C** pI values of the EML proteins including values for the full length proteins, NTD and TAPE domains only. **D.** Box and whiskers plot of GFP-EML1 intensity with and without subtilisin treatment (n>200). Quantification was carried out using ImageJ intensity software (p<0.0001).

Fluorescence recovery after photobleaching (FRAP) was then carried out, as described in chapter 2.4.6. Briefly, the YFP is photodestroyed and then the rate and amount of YFP-EML repopulation into the bleached area is measured. This will ascertain whether, despite the lack of obvious movement, these proteins were able to interact in a dynamic manner with the MT network. Using U2OS transiently transfected with YFP-EML1, YFP-EML2, YFP-EML3 or YFP-EML4 (Figure 3.8A), FRAP analysis revealed that each protein recovered to at least 60% (EML4 highest recovery > EML1 > EML3 > EML2 lowest recovery) within one minute and the half-lives were all under 10 seconds (EML1 fastest recovery > EML4 > EML3 > EML2 slowest recovery) (Figure 3.8B and C). This indicates that all four of the EML proteins exhibit a highly dynamic association with MTs.

We were also interested to determine whether the NTD fragment was able to recover rapidly or whether this recovery was somehow dependent on the TAPE domain and the interaction with soluble tubulin, mediated through this region. U2OS cells transiently transfected with full length YFP-EML3 and YFP-EML3 NTD were subject to FRAP analysis carried out as before (Figure 3.9) The EML3 NTD neatly decorates the MT network in interphase in a similar manner to the EML3 WT protein (Figure 3.9A). However, FRAP analysis revealed that the NTD had a much faster recovery (half-life of less than 1.5 seconds) compared to the WT protein (7 seconds) and the percentage recovery at 60 seconds was also higher (82% for WT, 97% for NTD) (Figure 3.9B and 3.9C). This shows that in the experiments using EML3 WT protein there is an immobile fraction remaining on the MTs hence the lower percentage of recovery then the NTD alone. This suggests that the TAPE domain is somehow 'anchoring' a small population of the EML protein onto the MTs whereas in the NTD alone the whole population is free to move and recover on the MTs. Furthermore, the sheer rate of the EML3 NTD recovery suggests the protein is recovering via simple on-off exchange, rather than sliding along MTs. This makes EML proteins similar to MCAK which reaches the plus-tips via diffusion along the length of the MTs, an interaction mediated via the tubulin E-hooks (Helenius et al. 2006).
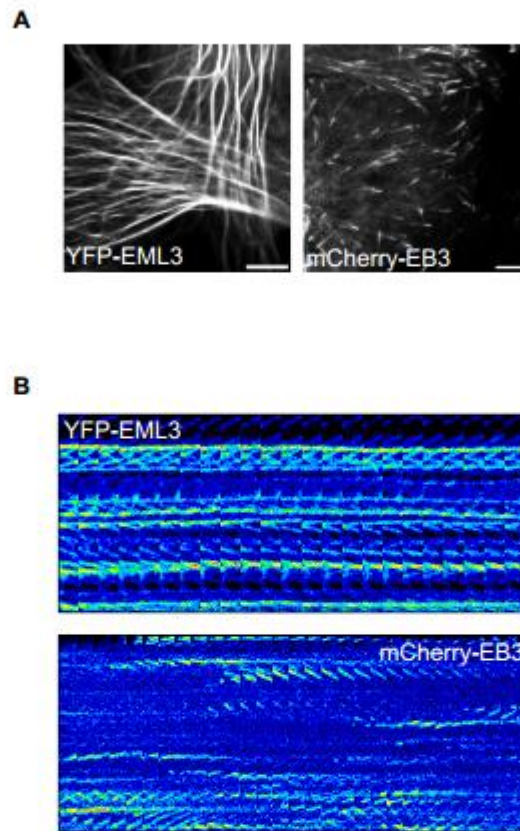
Figure 3.7: EML3 localizes along the length of the MTs

A. Time lapse imaging of YFP-EML3 and mCherry-EB3 stably expressing U2OS cells. Cells were imaged every second for 2 minutes using either the Argon 488 or DPSS 561 laser. Scale bars, 7.5 μm.
B. Representative kymographs of YFP-EML3 and mCherry-EB3 stably expressing U2OS cells, generated using ImageJ.
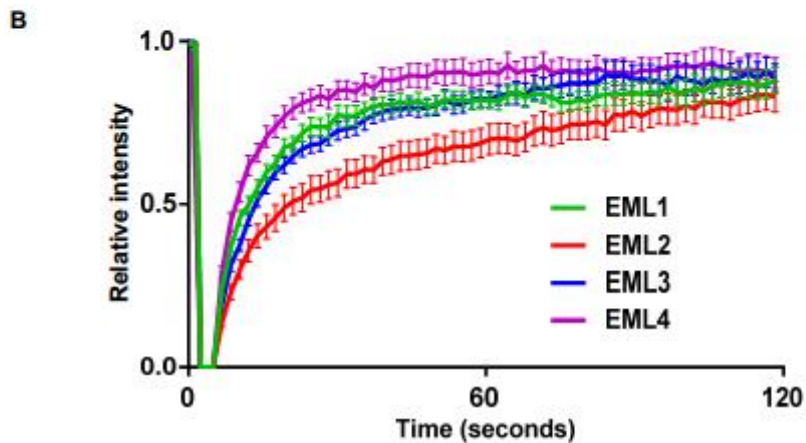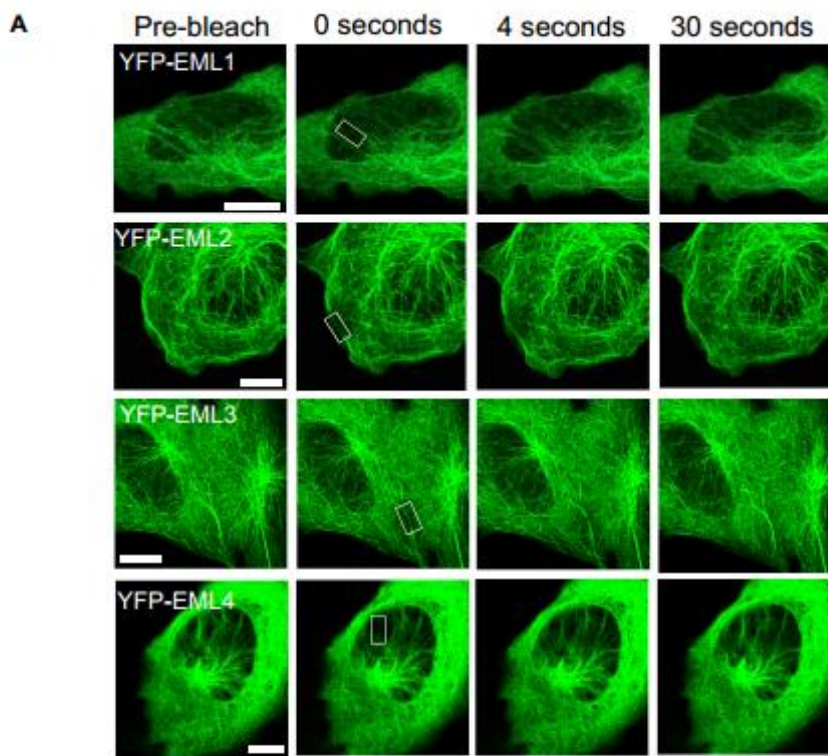
Figure 3.8: EML proteins interact in a dynamic manner with the MT network

A. U2OS cells were transfected with either YFP-EML1, YFP-EML2, YFP-EML3 or YFP-EML4 for 24 hours prior to imaging. Region of photobleaching highlighted in the white box at 0 seconds for each treatment. Scale bars, 10 μm. **B.** Graph shows mean fluorescence recovery after photobleaching (FRAP) after 2 minutes, error bars represents ±SEM. **C.** Data shown represent the mean percentage recovery (±SEM) after 60 seconds and half-life (± SEM) for each EML protein.

A

Pre-bleach   0 seconds   4 seconds   30 seconds

EML3 NTD

B
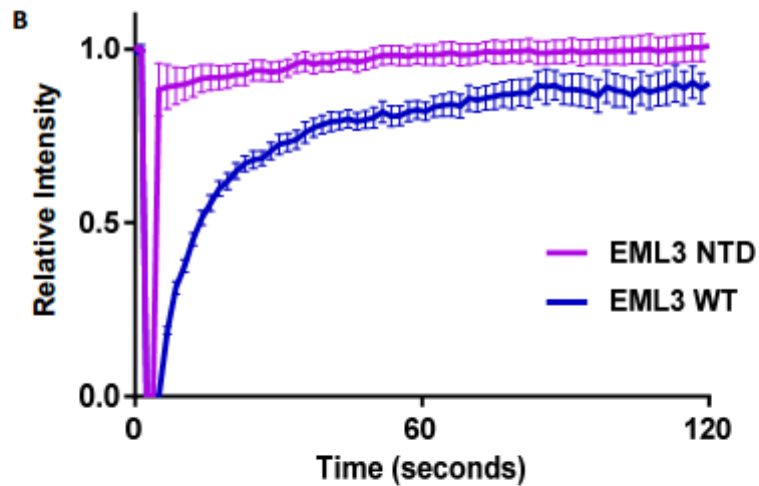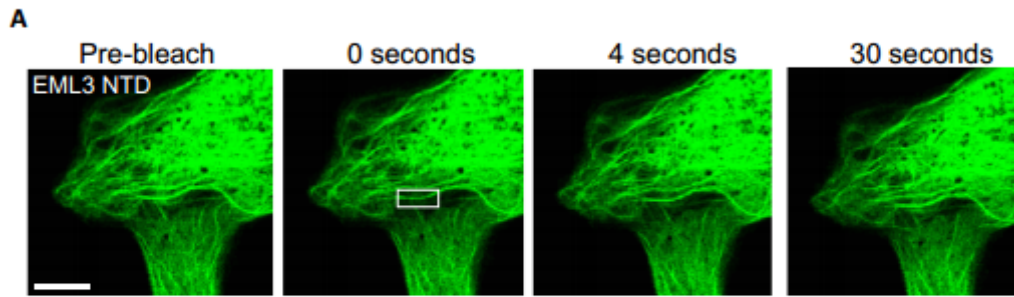
Protein	Percentage recovery (±SEM)	Half life of recovery (seconds) (±SEM)	Cells analysed
EML3 WT	82.01 ± 2.92	7.44 ± 0.54	20
EML3 NTD	97.8 ± 2.85	<1.5 ± 0.60	13

Figure 3.9: EML3 NTD shows different dynamics to the WT protein

A. U2OS cells were transfected with YFP-EML3 NTD for 24 hours prior to imaging. Region of photobleaching highlighted in the white box at 0 seconds for each treatment. Scale bars, 10 µm **B.** Graph shows mean fluorescence recovery after photobleaching (FRAP) vs EML3 WT, error bars represent ± SEM. **C.** Data shown represent the mean percentage recovery (± SEM) after 60 seconds and half-life (± SEM).

A

EML3 WT + Taxol

B

C

Protein	Percentage recovery (± SEM)	Half life of recovery (seconds) (± SEM)	Cells analysed
EML3	80.77 ± 2.92	6.73 ± 0.53	20
EML3 + Taxol	49.58 ± 10.11	9 ± 1.62	15
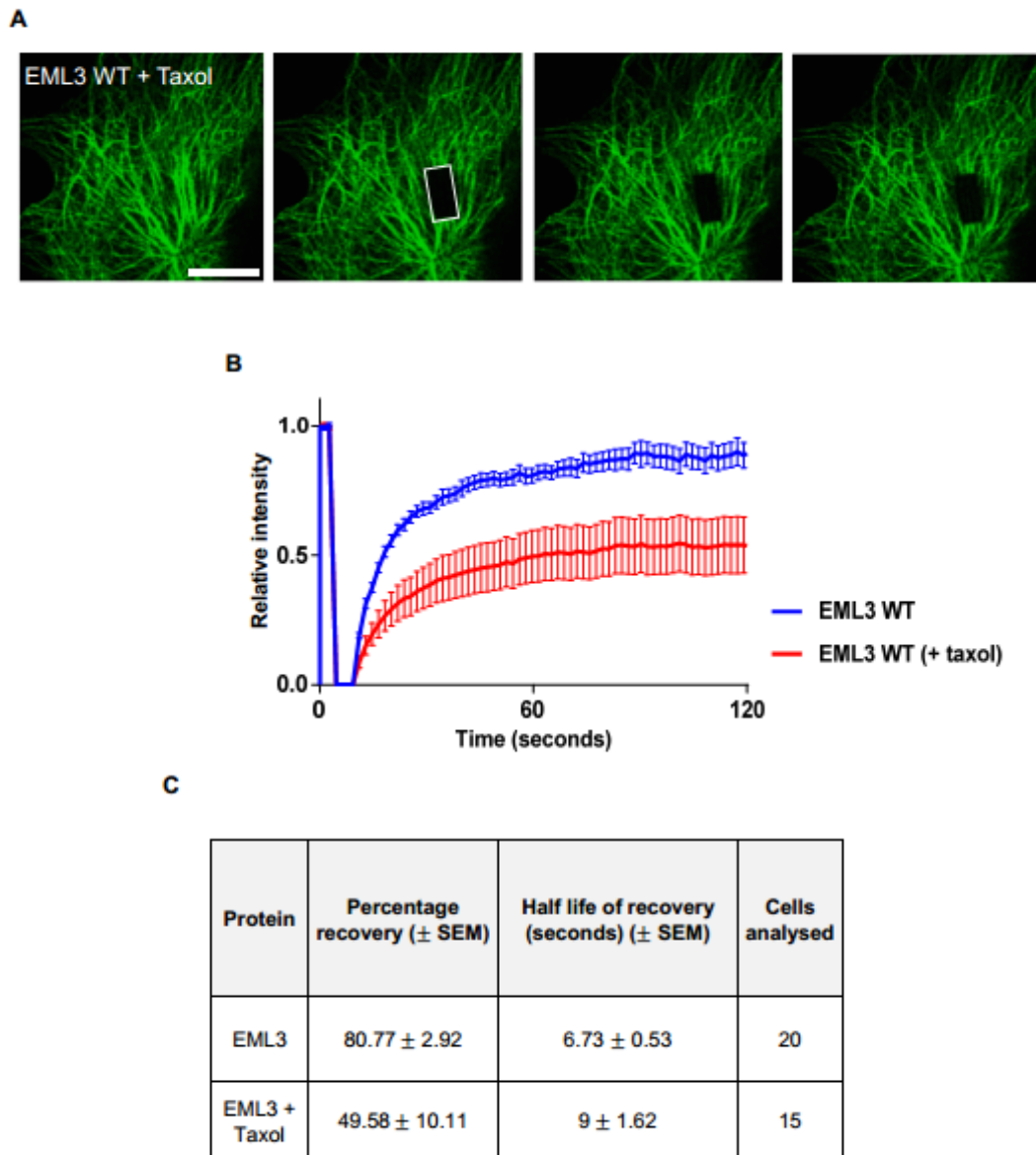
Figure 3.10: EML3 recovery is reduced on stabilized MTs

A. U2OS:YFP-EML3 cells were Taxol treated 4 hours prior to imaging. The region subjected to photobleaching is highlighted in the white box at 0 seconds. Error bars represents ± SEM. Scale bars, 10 μm. **B.** Graph shows mean fluorescence recovery after photobleaching (FRAP) for each treatment. **C.** Data shown represent the mean percentage recovery (± SEM) after 60 seconds and half-life (± SEM).

We then asked whether EML proteins would recover to the same degree on stabilised MTs. In order to test this YFP-EML3 stable cell were treated with taxol for 4 hours prior to FRAP analysis. YFP-EML3 was unable to recover as well on stabilised MTs with the percentage recovery after 60 seconds decreasing from 80% to less than 50% on stabilised MTs and the half-life increasing from 6 seconds to 9 seconds on stabilised MTs (Figure 3.10 A-C). The reasons for this are currently not clear but it could be that MT stabilisation reduces the cytoplasmic pool of EML3 and thus there is less protein left to replace the bleached population. Another possibility is that EML proteins preferentially move on and off dynamic MTs, therefore when the MTs are stabilised by Taxol, the EML proteins are unable to recover as effectively. Similarly, taxol treatment may alter the levels of PTMs, which may consequently alter the dynamics of the MAPs associated, for example KifC preferentially binds to detyrosinated MTs (Dunn et al. 2008).

3.2.5 EML3 localization is independent of EML1, EML2 and EML4

To determine whether localization of one member of the EML family was dependent on other members of the family we first examined how EMLs might interact with one another. EML1 to EML4 contain a coiled-coil motif that is proposed to allow oligomerization. Structural studies undertaken in the Bayliss lab revealed that the coiled-coil promotes trimerisation (Richards et al. 2015). However it was unclear whether EMLs could heterotrimerise or homotrimerise. To test this we transiently co-transfected U2OS cells with a combination of Flag and YFP tagged full length EML proteins. These cells were then lysed after 24 hours and immunoprecipitated with the Flag M2 antibody. The interaction of YFP-EML1 with Flag-EML1, Flag-EML2 and Flag-EML4 indicated that EML1 is able to homotrimerise and heterotrimerise with EML2 and EML4 (Figure 3.11A). We therefore repeated the experiment using YFP-EML3 as the 'bait' protein. This revealed that EML3 was able to interact strongly with itself but only very weakly with EML1, EML2 or EML4 (Figure 3.11B, data used in Richards et al. 2015). This indicates EML3 is an isolated member of the family and prefers to homotrimerise.
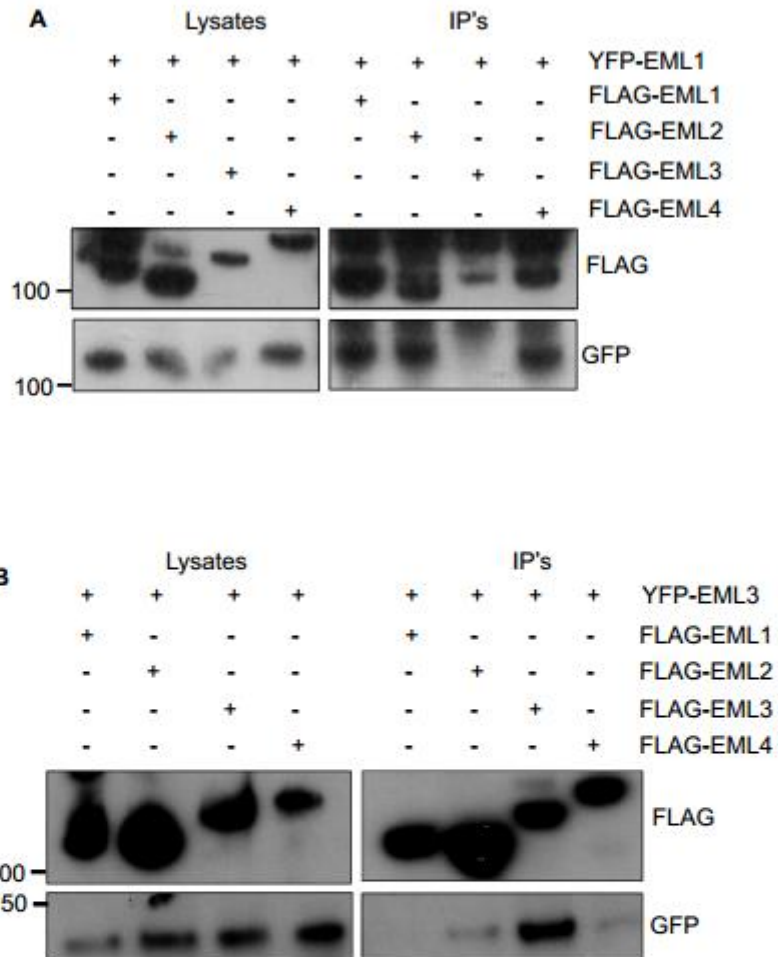
Figure 3.11: EML proteins preferentially homo-oligomerise

A. Hek293 cells were transiently transfected with YFP-EML1 and either Flag-EML1, Flag-EML2, Flag-EML3 or Flag-EML4 for 24 hours before cells were lysed. Lysates (Inputs) were subjected to immunoprecipitation with the Flag M2 antibody. Samples were resolved by SDS-PAGE and analysed by Western blot with the antibodies indicated. **B.** Hek293 cells were treated as in A, except that YFP-EML1 was substituted for YFP-EML3.
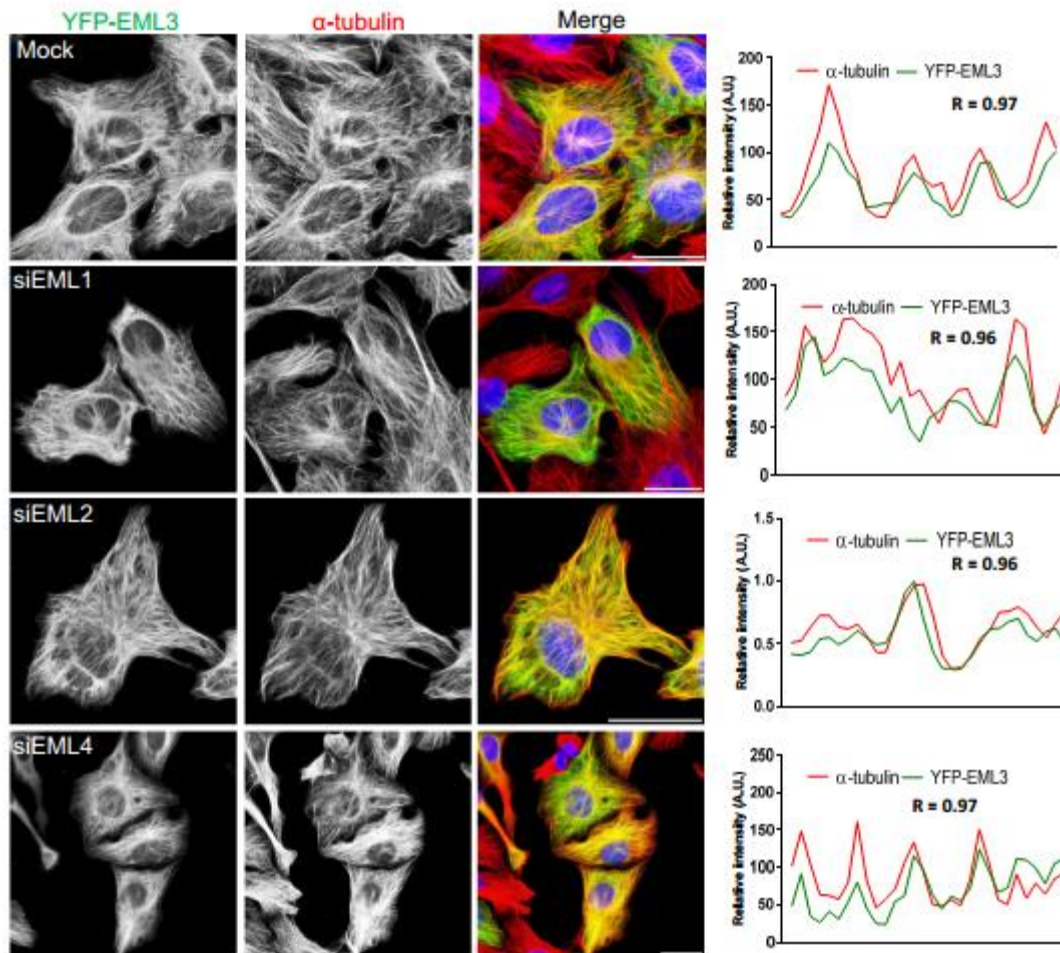
Figure 3.12: EML3 localization in interphase is not affected by depletion of EML1, EML2 or EML4
U2OS:YFP-EML3 cells were transfected with siRNAs against EML1, EML2 and EML4 for 48 hours prior to methanol fixation. Cells were immunostained with GFP (green) and α-tubulin (red) antibodies. Merged images include DNA stained with Hoechst (blue). Overlap coefficient measurements (R) were then determined for the images presented by line profiles crossing multiple MTs and measuring the YFP and α-tubulin signal. Scale bars, 25 µm.

To examine whether the localization of EML3 was also independent of the other members of the EML family, we decided to deplete the other EMLs and monitor EML3 localization. To do this we depleted EML1, EML2 and EML4 for 48 hours from the U2OS:YFP-EML3 stable cell line and fixed and stained the cells for immunofluorescence microscopy. Using confocal microscopy we took images using identical settings and calculated overlap coefficients as described in chapter 2.4.3 (Figure 3.12). From the images and the overlap coefficients it was clear that EML3 localization during interphase is not altered upon removal of the other EMLs. Taken together this data argues that EML3 association with MTs is independent of other EMLs.

3.3 Discussion

From the generation of stable cell lines we have been able to shed light on the behaviour of EML proteins in interphase. YFP-EML1 and YFP-EML3 show very clear localisation to the microtubule network in interphase and this interaction is not perturbed and potentially increased in the presence of taxol, which is interesting in terms of cancer chemotherapy. Bearing this in mind it would be worthwhile examining whether EML proteins alter the sensitivity of the MT network to MT poisons such as the taxanes. This is a problem already associated with overexpression of MAP4 which decreases microtubule binding and sensitivity to Vinca alkaloids, which promotes microtubule depolymerization (Zhang et al. 1999).

From our results EML proteins show statistically significant differences in their affinity for MTs with EML1 and EML4 binding to MTs at a lower affinity then EML2 and EML3 (Figure 3.3). Currently it is unknown as to why there are these differences, although this presumably relates to the sequence of the MT binding region. The consequence of this is unclear but could be related to the functionality of these proteins, for example XMAP215 binds MTs directly with relatively low affinity to allow for cycles of binding and release and to allow for rapid diffusion along the MT lattice (Al-Bassam & Chang 2011). Also, EML family members have been indicated as both stabilising and destabilising; EML2 has been reported to destabilise MTs, whilst EML4 was shown to stabilize MTs by forming circular MTs and reducing sensitivity to nocodazole treatment

(Eichenmuller et al. 2002, Houtman et al. 2007). This indicates that this family of proteins are potentially diverse in terms of their influence on MT dynamics.

All four members of the family interact in a dynamic manner with MTs and recover rapidly following photobleaching. This indicated that EML proteins move on and off MTs via simple exchange, in a similar manner to MCAK, which reaches the plus-tips via diffusion along the length of the MTs (Helenius et al. 2006). Moreover, the EML3 WT protein was unable to recover to the same extent as the NTD alone which indicates a population of the EML3 WT protein is remaining bound to MTs, thus preventing 100% recovery. This is likely to be mediated through the TAPE domain as the NTD alone did not possess the same phenotype and showed a much higher level of recovery. This indicates a novel characteristic of the TAPE domain whereby it 'anchors' a population of the EML3 protein to the MTs.

It has been identified that both the coiled-coil and the basic region before the TAPE domain contribute to MT association (Richards et al. 2015). Unfortunately, in this study we were unable to further validate the exact residues of the EML protein necessary for MT interaction. However, we have identified that EML proteins probably bind to MTs via the negatively charged tubulin E-hooks present on the surface of MTs. Our data suggests that it is residues within the NTD which interact with the MTs and these residues interact with E-hooks via an electrostatic interaction. This is interesting, as the precursor protein EMAP does not use E-hooks to interact with MTs as shown in a similar subtilisin digestion experiment (Hamill et al. 1998).

Previously it was thought that EML proteins might associate with MTs due to the interaction of the EML TAPE domain with soluble tubulin. However, we demonstrate that the NTD alone not only binds to the MT network but exhibits increased dynamicity than the full length protein. This indicates that the TAPE domain is somehow slowing the dynamic recovery of these proteins rather than enabling it. The last key finding for this section was that EML3 acts relatively independently of the other EML proteins, as shown via immunoprecipitation interaction studies and RNAi depletion of the other EMLs within the YFP-EML3 stable cell line. EML3 is preferentially a homotrimer which does not rely on other members of the family for it's localization and association to interphase MTs, meaning functional studies can be carried out without the complication of other EML protein interactions perhaps skewing the results.

Conversely, EML1 showed strong interaction with both EML2 and EML4 which would make it difficult to determine individual phenotypes and specific interactions for these proteins.

CHAPTER 4 THE ROLE OF EML3 IN INTERPHASE AND MITOSIS

4.1 Introduction

The MTs in interphase maintain the structure of the cell and are required for intracellular transport, however it is in mitosis where the MTs become crucial for the development of the mitotic spindle and the survival of the cell. At the onset of mitosis there is a universal shift in the architecture within the cell, the MT network disintegrates and then reassociates to form a bipolar mitotic spindle. After nuclear envelope breakdown (prometaphase), the chromosomes direct MT assembly to ensure interaction with the kinetochores. During anaphase, the MTs rapidly depolymerise exerting enough force to 'pull' the sister chromatids to the two distinct poles of the cell. In animal cells, there are 3 distinct subclasses of MTs which make up the mitotic spindle; astral MTs, interpolar MTs and the kinetochore fibres (K fibres). Any problems during cell division can cause chromosome instability and aneuploidy, which is a hallmark of cancer. This suggests that alterations in MT dynamics and problems in MT assembly could be key events in tumorigenesis and tumour progression.

MAPs are important regulators of MT dynamicity in both interphase and mitosis making them desirably targets for cancer chemotherapy. In this section we use a depletion approach to explore the role of one of the novel EML family members, EML3, in maintaining interphase MTs and regulating spindle formation in mitosis. EML3 itself is a novel member of the EML family and not much is known about its function. However, initial studies carried out by the Gruss lab began to shed light on the importance of this protein in mitotic progression. They first identified FLJ46843 (EML3) as part of a proteomics screen and antibodies were generated using two specific peptides (Tegha-Dunghu et al. 2008). In this study it was found that endogenous EML3 localised to the MTs throughout all the mitotic stages and some protein was detectable

in the nucleus during interphase, thought to be due to protein shuttling from the cytoplasm to the nucleus (Tegha-Dunghu et al. 2008). EML3 siRNA and time lapse imaging of stably expressing EGFP-histone 2B cells allowed scoring of a range of phenotypes, and the data showed that EML3 depletion caused an increase in the mitotic index, apoptotic index and shape index (nuclei defect) but an overall reduction in proliferation (Tegha-Dunghu et al. 2008). Also, it was noted that EML3 depletion caused cells to accumulate in mitosis for a few hours whereby chromosomes were less well aligned, indicating that the SAC might be activated in these cells (Tegha-Dunghu et al. 2008). It was also postulated that EML3 depletion caused inefficient bipolar MT attachment which delays the alignment of chromosomes in metaphase (Tegha-Dunghu et al. 2008).

4.2 Results

4.2.1 EML3 depletion disrupts the integrity of the MT network in interphase

To explore the role of EML3 in interphase MTs, EML3 depletion was carried out using two specific siRNAs named siRNA3.1 and siRNA3.2 (sequences given in Chapter 2.1.6). The efficiency of these oligos was determined using the YFP-EML3 stable cell lines due to the lack of EML3 antibodies to detect endogenous protein. U2OS:YFP-EML3 cells were transfected with 100 nM siRNA oligonucleotide and Oligofectamine reagent as described in chapter 2.2.5. GAPDH siRNAs were used as a control. Cells were lysed and analysed by Western blot with GFP and GAPDH antibodies (Figure 4.1A). Both EML3, as well as GAPDH oligos, were shown to be highly effective at depleting their respective target proteins from the stable cell line. Next, U2OS cells were seeded and transfected for 48 hours with either siRNA3.1 or siRNA3.2 to deplete the endogenous protein; cells were then fixed and analysed by immunofluorescent microscopy.
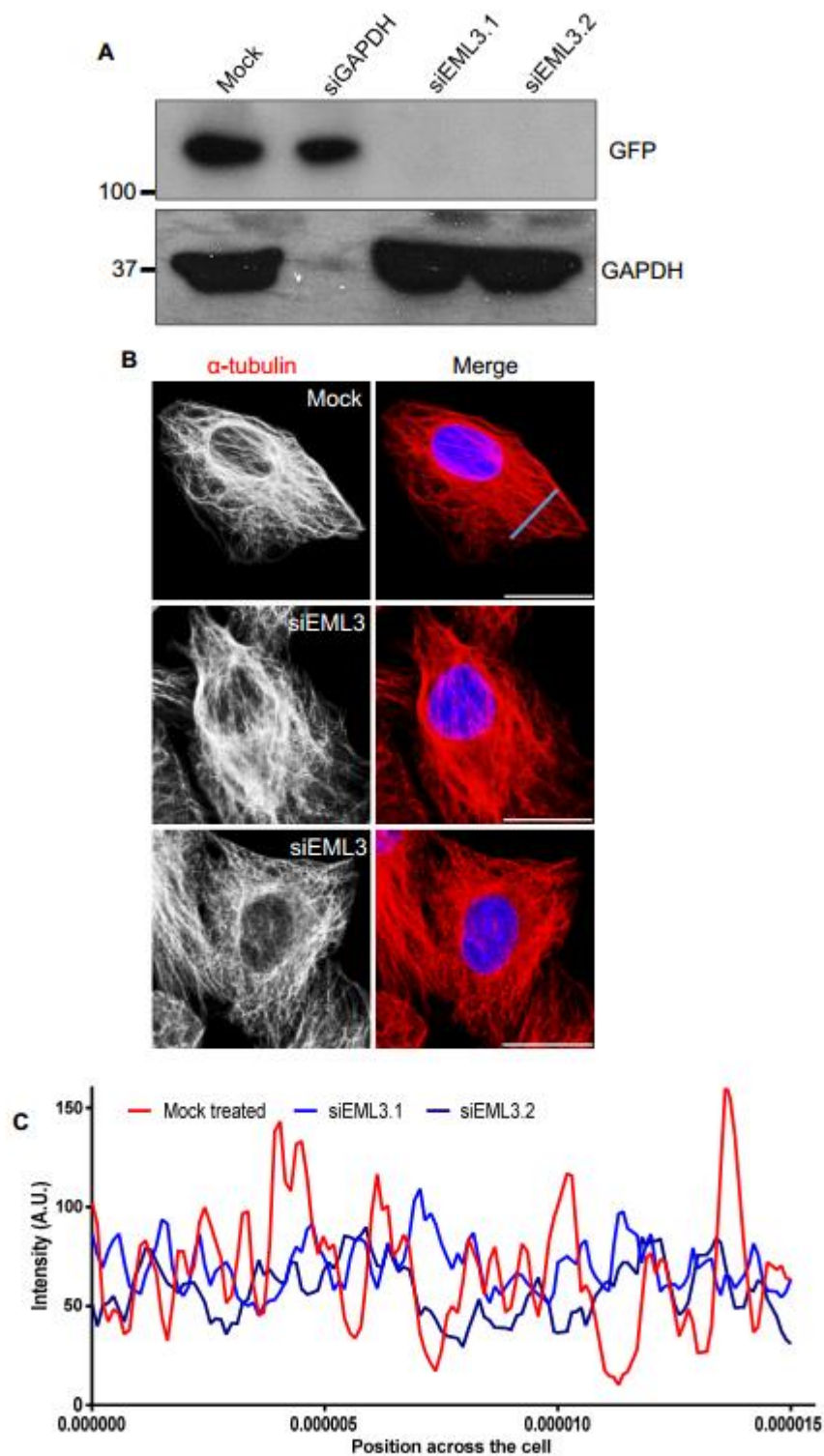
Figure 4.1: EML3 RNAi alters the integrity of the MT network in interphase

A. U2OS:YFP-EML3 cells were transfected with two independent siRNAs against EML3 (siRNA3.1 and siRNA 3.2), lysed 48 hours post transfection and analysed via western blot analysis with antibodies and molecular weights (kDa) indicated **B.** U2OS cells were transfected with siRNAs against EML3 (siRNA3.1 and siRNA 3.2) for 48 hours, fixed in methanol and immunostained with α-tubulin (red) antibodies. Merged images include DNA stained with Hoechst (blue). Scale bars, 10 μm. Blue line represents where the line was drawn for quantification. **C.** Intensity plot of the mock and EML3 siRNA treated cells. Peaks represent defined MTs, units represent the position across the cell determined by the ROI.
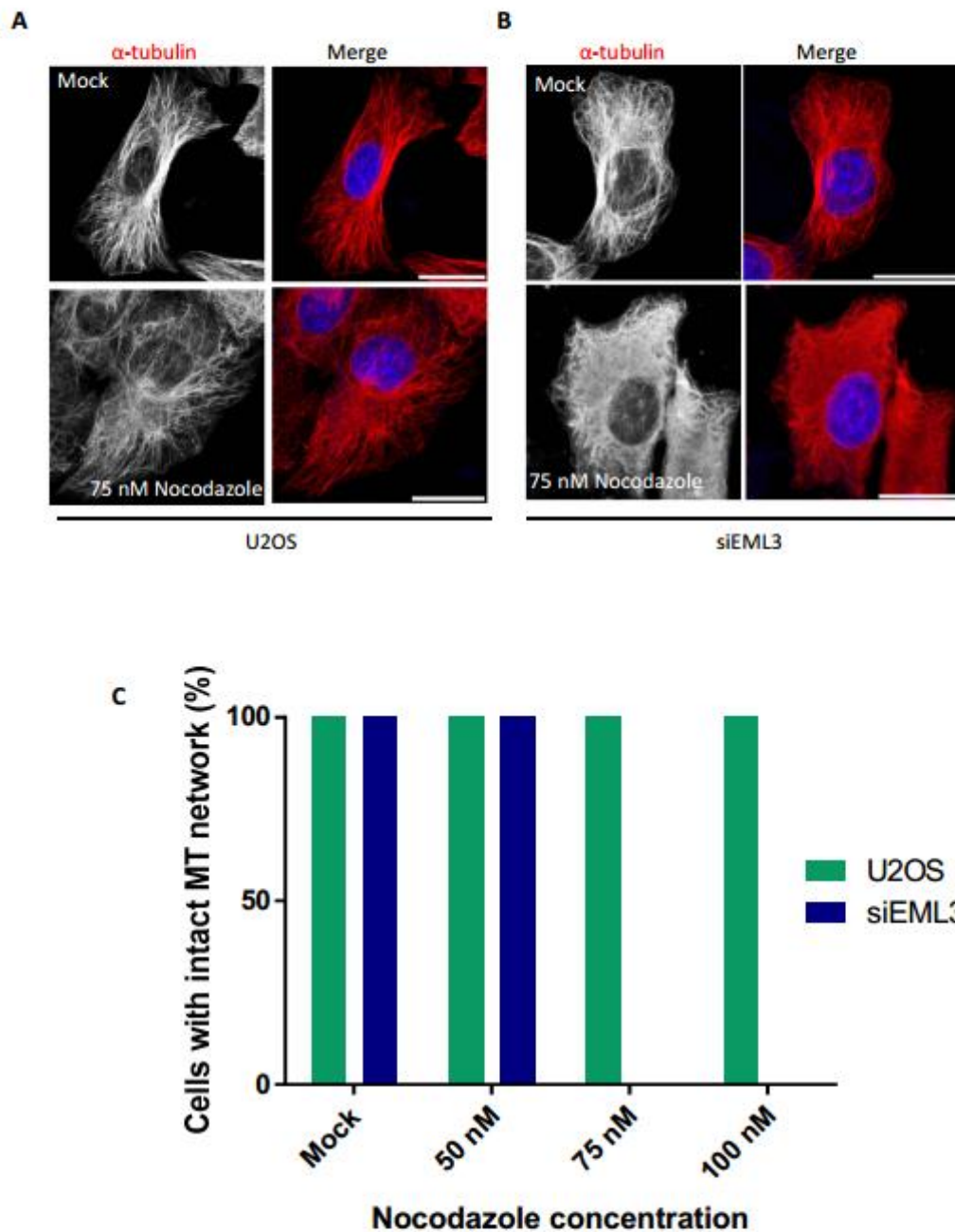
Figure 4.2: EML3 depletion increases microtubule sensitivity to nocodazole
A. U2OS cells were either mock transfected or transfected with siRNAs against EML3 for 48 hours. Cells were then either untreated or treated with 75 nM of nocodazole for 30 minutes, before being fixed in methanol immunostained with α-tubulin (red) antibodies. Merged images include DNA stained with Hoechst (blue). Scale bars, 10 µm. **B.** Mock or EML3 depleted cells treated with nocodazole at the dose indicated above, were scored as to whether the MT network was intact or not (n = 100). Experiment only repeated one due to time constraints.

Confocal microscopy revealed that the EML3 depleted U2OS cells had an unusual MT network in interphase with the network appearing less robust than that of control cells (Figure 4.1B). To quantify this change we used a tubulin intensity plot; for this analysis, images were opened in Leica SP5 software. A line was then drawn near the periphery of the cell across a region of MTs (as indicated by the blue line in Figure 4.1B). This revealed peaks in intensity where MTs were present and no defined peaks if the tubulin staining was diffuse throughout the cytoplasm. This analysis was carried out for the control cells, the siRNA3.1 and siRNA3.2 treated cells. In the control cells the average intensity was lower but there was much more defined MTs with higher intensity peaks whereas in EML3 depleted cells there was no clear MT peaks but a higher average intensity (Figure 4.1C). This shows that in the absence of EML3 MTs are less well defined, indicating that EML3 is a potential MT stabiliser.

To confirm this hypothesis we decided to test whether EML3 depleted cells showed a reduced sensitivity to nocodazole. U2OS cells were seeded and either mock transfected or transfected with siRNA3.2 to deplete the endogenous protein for 48 hours. Cells were treated with increasing doses of nocodazole (0 nM, 50 nM, 75 nM, 100 nM) for 30 minutes before being fixed and stained to visualise the MT network (Figure 4.2 A and B). From confocal microscopy analysis it was clear that the MT network in siEML3 depleted cells had a much lower tolerance to nocodazole treatment. At 75 nM and 100 nM, 100% of U2OS cells possessed an intact MT network whereas none of the EML3 depleted cells had a clear MT network (Figure 4.2 C). It should be noted that this experiment was only carried out once due to time constraints, but the data does support the idea that EML3 is a MT stabiliser and that without it the MT network is more unstable.

4.2.2 EML3 depletion perturbs chromosome segregation in mitosis

Following demonstration of interphase depletion phenotypes, we wanted to confirm the effect of EML3 depletion on mitosis. Tegha-Dunghu et al. 2008 had reported that EML depletion caused an increase in the mitotic index, apoptotic index and nuclei shape index, as well as misaligned chromosomes.

Firstly, we used time-lapse imaging to look at how EML3 depleted U2OS cells behaved during mitosis progression. Using the bright field microscopy we analysed both mock and siEML3.1 depleted cells for a period of 17 hours and noted an increase in the number of EML3-depleted cells in mitosis (Figure 4.3), consistent with the findings from Tegha-Dunghu et al. 2008. Next, U2OS cells were depleted using either siEML3.1 or siEML3.2, or mock treated as a control. Cells were then fixed and stained for α-tubulin. Using confocal microscopy, we scored the number of cells in mitosis out of a total of 100 cells to calculate the mitotic index for each cell population. EML3 depletion caused a small increase in the mitotic index (Figure 4.3B).

Next, using confocal microscopy, siEML3.1 and siEML3.2 depleted fixed cells were imaged at different stages of mitosis. Normally, in metaphase, chromosomes align neatly along the metaphase plate, a phenomenon mediated via the interaction with spindle MTs. However, our data show that in an EML3 depleted environment the chromosomes are more dispersed (Figure 4.4A). Quantification revealed that EML3 depletion causes misalignment of chromosomes in over 40% of metaphase cells (52% siEML3.1 and 41% siEML3.2), compared to only 18% in mock treated cells (Figure 4.4B). We next assessed cells in anaphase. During anaphase, depolymerisation of the MTs should exert sufficient force to pull sister chromatids apart. EML3 depletion caused chromosomes to lag in anaphase cells with chromosomes visible at what was once the metaphase plate (Figure 4.5A). Scoring showed lagging chromosomes present in 9% of mock depleted cells but 39% and 30% in siEML3.1 and siEML3.2 depleted cells, respectively (Figure 4.5B). It is likely that the lagging chromosomes seen in anaphase are a result of either improper attachment of MTs to chromosomes or abnormal MT dynamics. Either way it confirmed that EML3 is crucial for accurate chromosome segregation during mitotic progression.
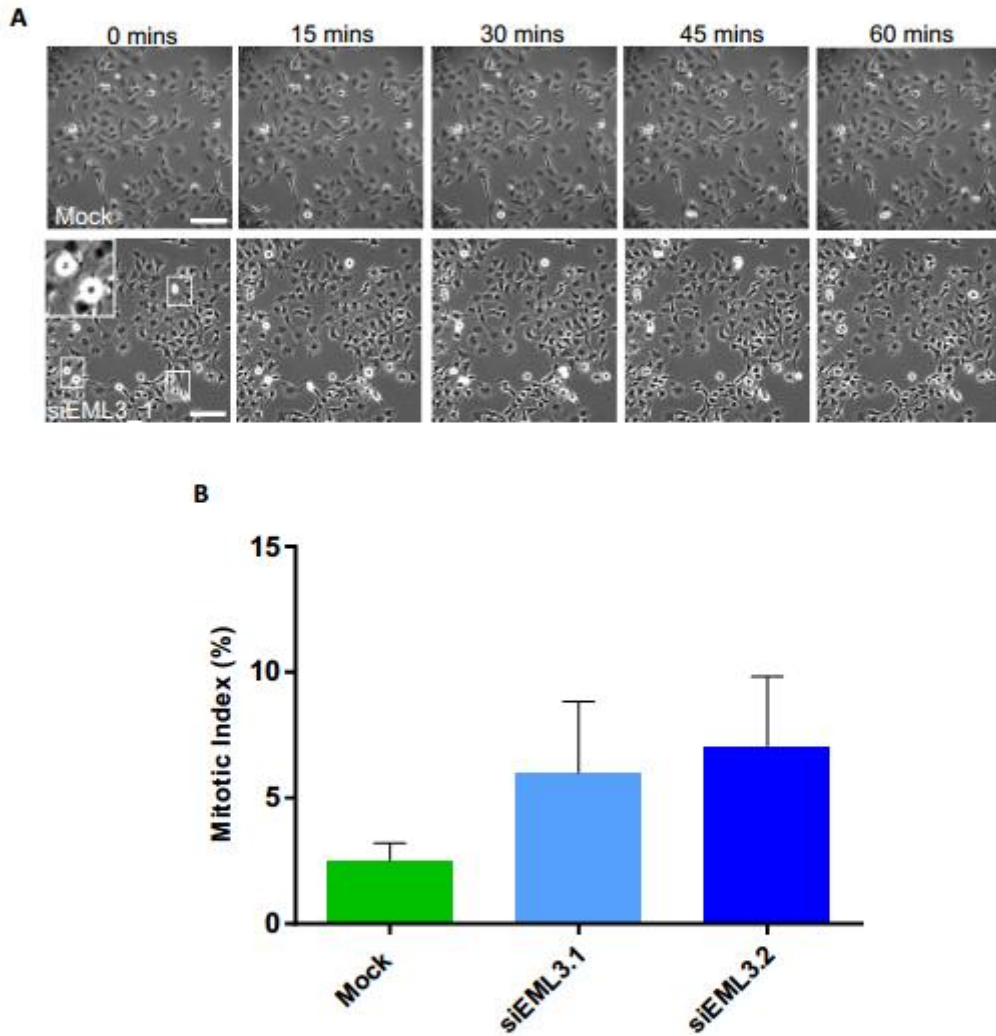
Figure 4.3: EML3 RNAi causes a marginal increase in the mitotic index

 A. U2OS cells were either mock transfected or transfected with siRNA3.1 and siRNA 3.2 for 48 hours and imaged overnight using brightfield microscop, 5 fields of view. Scale bars 100 µm. **B.** Mitotic index counts were taken of fixed U2OS that had been either mock transfected or transfected with siRNA3.1 and siRNA 3.2 for 48 hours. Data represent means ($\pm$SD) of measurements from 100 cells (n=3).
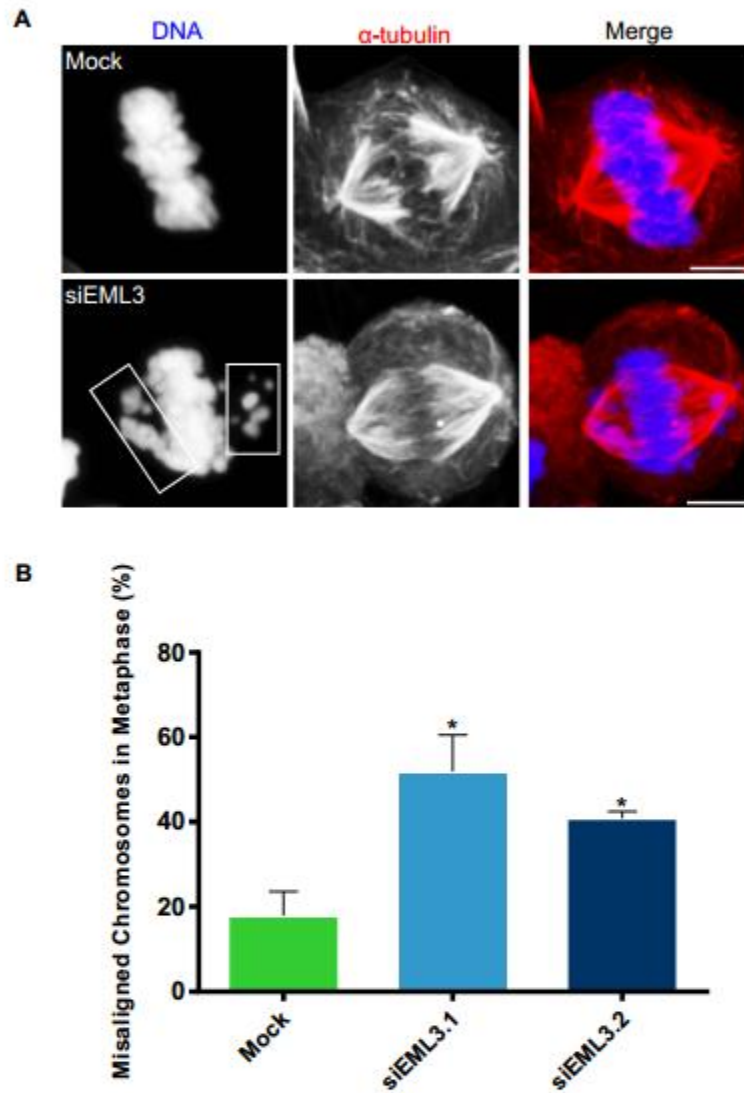
Figure 4.4: Depletion of EML3 causes unaligned chromosomes in metaphase

A. U2OS cells were either mock transfected or transfected with siRNA3.1 and siRNA 3.2 for 48 hours, fixed in methanol and immunostained with α-tubulin (red) antibodies. Merged images include DNA stained with Hoechst (blue). Boxes indicate misaligned chromosomes. Scale bars, 5 μm. **B.** Histogram indicates increase in unaligned chromosomes in the absence of EML3 (p<0.05). Data represent means (±SD) of measurements from 100 metaphase cell (n=3).
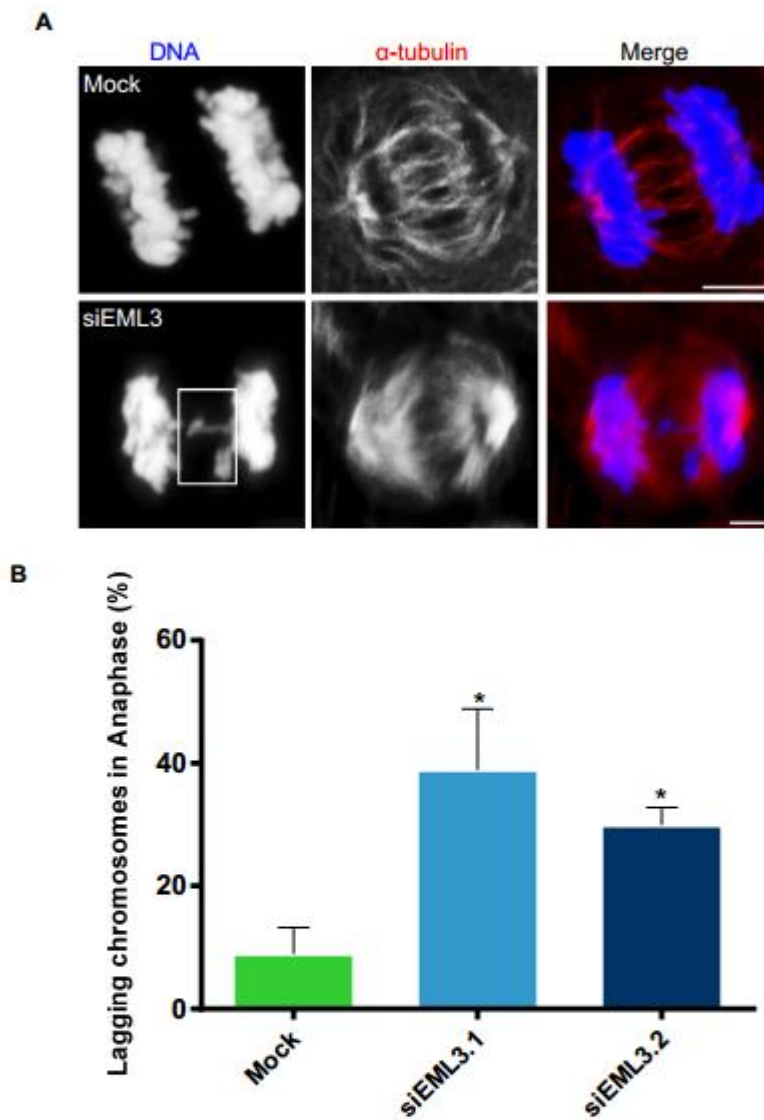
Figure 4.5: Depletion of EML3 causes lagging chromosomes in anaphase

A. U2OS cells were either mock transfected or transfected with siRNA3.1 and siRNA 3.2 for 48 hours, fixed in methanol and immunostained with α-tubulin (red) antibodies. Merged images include DNA stained with Hoechst (blue). Boxes indicate lagging chromosomes. Scale bars, 5 μm. **B.** Histogram indicates the percentage of cells treated as indicated with a bipolar spindle. (p<0.05). Data represents means (±SD) of measurements from 100 anaphase cells (n=3).

.
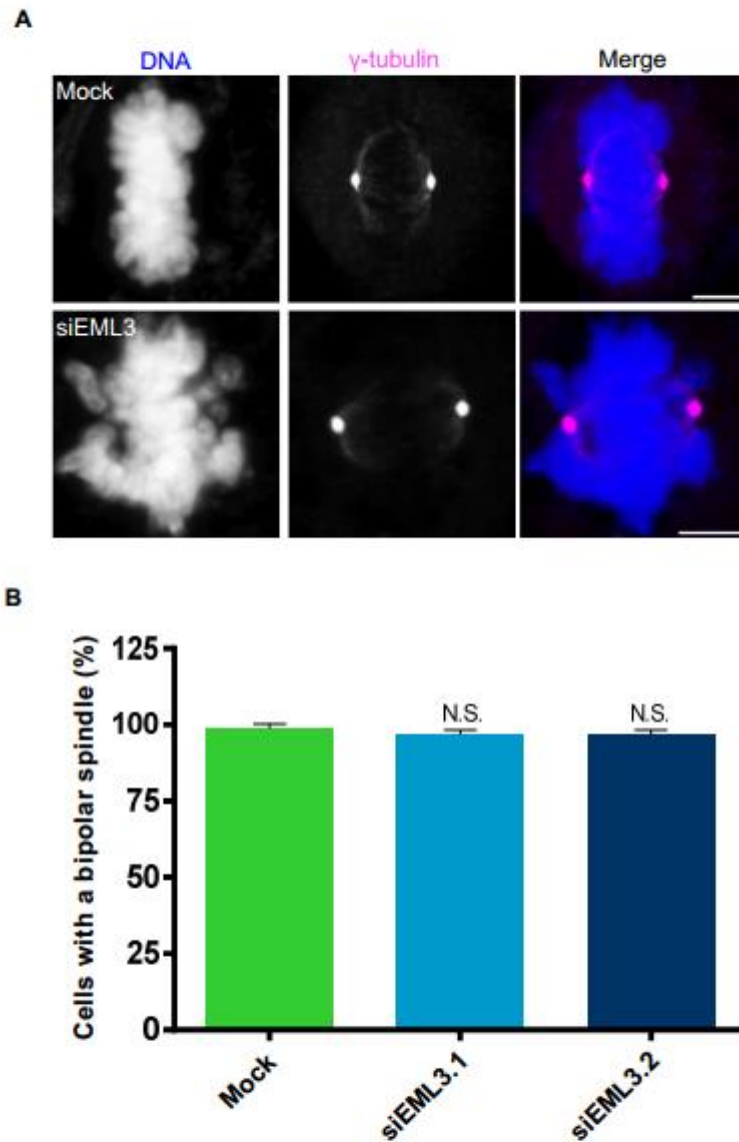
Figure 4.6: Depletion of EML3 does not increase multipolarity in mitosis

A. U2OS cells were either mock transfected or transfected with siRNA3.1 and siRNA 3.2 for 48 hours, fixed in methanol and immunostained with γ-tubulin (pink) antibodies. Merged images include DNA stained with Hoechst (blue). Scale bars, 5 μm. **B.** Histogram indicates the percentage of metaphase cells with a bipolar spindle. Data represent means (±SD) of measurements from 100 metaphase cells (n=3).

4.2.3 EML3 depletion does not induce mitotic spindle multipolarity

Lastly, we wanted to explore whether EML3 depletion affected centrosome number or could cause multipolarity during mitosis. U2OS cells were depleted using either siEML3.1 or siEML3.2 or mock treated, fixed and stained for γ-tubulin to detect and count the number of centrosomes. Despite the clear misalignment of chromosomes following EML3 depletion the cells possessed a bipolar spindle with two clear centrosomes (Figure 4.6A). This was confirmed by quantifying the frequency of cells with bipolar spindles in metaphase indicating that multipolarity is not the reason for misaligned chromosomes during metaphase (Figure 4.6B).

4.3 Discussion

In this chapter we have explored the role of EML3 in interphase and mitosis using siRNA-mediated depletion. The first key finding was the potential role of EML3 in maintaining the integrity of the MT network in interphase. From immunofluorescence microscopy analysis there was an obvious disruption in the structure of the MT network in the absence of EML3. This was further supported by the MT intensity analysis whereby there were no obvious MT peaks in the siEML3 treated cells compared to mock treated U2OS. Moreover, EML3 depleted cells increased the sensitivity of the MT network to nocodazole with a loss of MT network at 75-100 nM of nocodazole. Mock treated U2OS cells still retained an intact network at these doses. Taken together, these results strongly suggest that EML3 is a MT stabilising MAP and joins the family of stabilising MAPs which include MAP1, MAP2, MAP4 and Tau (Dehmelt & Halpain 2005). The precursor protein EMAP has been shown to stabilise MTs and regulate MT assembly, as has EML4 whereby cells expressing GFP-EML4 were able to evade the MT depolymerisation effects seen in control cells treated with 10 µM nocodazole (Suprenant et al. 1993, Houtman et al. 2007). Conversely, EML2 has been shown to reduce nucleation and increase catastrophe rates, which are key characteristics of a destabilising MAP (Eichenmuller et al. 2002). Curiously then, it appears that the EML proteins may have opposite modes of action and that although they are part of the same family they have different effects on MTs. One could hypothesise that they are working in combination to keep a basal stability or perhaps

they work in competition with one another to modulate MT stability under different conditions.

The next set of experiments aimed to confirm the role of EML3 in mitosis. Firstly we set out to identify whether EML3 increased the mitotic index. Observations of live cell imaging suggested this was the case but quantification via scoring of fixed cells showed the apparent increase to be relatively small and not significant. This opposes the data from Tegha-Dunghu who shows a significant increase in the mitotic index following EML3 depletion. Arguable our result could be due to the relatively small sample size (n=100) and perhaps by extending this screen a more substantial increase would be observed. To confirm the specific mitotic defects in the absence of EML3, we focussed on metaphase and anaphase cells. Normally, in metaphase, chromosomes align neatly along the metaphase plate and then during anaphase sister chromatids are separated. Both of these events are regulated by the activities of the mitotic microtubules. Our data shows that in an EML3 depleted environment the chromosomes are more dispersed, perhaps due to problems in correct spindle formation or a change in MT dynamics. Further to this chromosome misalignment was not due to multipolarity with EML3 depleted cells still possessing a bipolar spindle. This misalignment may delay anaphase, explaining the reason for the slight increase in the mitotic index; cells arrest in metaphase to await suitable chromosomes capture, potentially following activation of the SAC. Likewise EML3 depletion caused a remarkable increase in the number of lagging chromosomes in anaphase, which arguable could be due to the misaligned chromosomes in metaphase and the cell continuing through the cell cycle without the correct chromosomes capture. This is possible as the cancer derived U2OS cells are likely to have weakened SAC machinery.

Taken together, the data confirms that EML3 plays a role in chromosome congression and segregation. As EML3 is a MT stabilising protein we can speculate that EML3 is required on spindle MTs for them to remain stable enough to capture the chromosomes effectively. Without EML3 the spindle MTs remain too dynamic resulting in inadequate time for chromosomes to be captured. This is the most likely explanation as the actual structure and robustness of the spindle appears unchanged in both control and siEML3 depleted cells. Another possible explanation is that EML3

somehow interacts with the kinetochores themselves and that without EML3 this interaction is disrupted or weakened in some way.

In terms of disease, misaligned and lagging chromosomes are mechanisms that in foetal development can cause serious conditions such as Downs syndrome and Pataus syndrome. In cancer this facilitates aneuploidy and chromosome instability. It is therefore interesting that EML3 depletion acts as a potential tumour suppressor. However, no EML3 mutations or deletions have been described to date.   This highlights the question as to whether EML3 is involved in cancer progression or whether EML3 expression could be used as a biomarker for predicting the response of a tumour to MT poisons such as the taxanes or vinca alkaloids.

CHAPTER 5   LOCALISATION OF EML3 IN MITOSIS IS REGULATED BY MITOTIC NEKS

5.1 Introduction

During the different stages of mitosis the structure and roles of the mitotic spindle changes, which is reflected in the dynamics of the MTs themselves. During prophase there's a loss of the long, stable MTs typical of interphase, with MTs becoming more numerous, shorter and less stable, in metaphase the MT arrange the chromosomes along the metaphase plate and lastly, during anaphase there is depolymerisation to exert enough force to pull the chromosomes apart. MT dynamics both in interphase and mitosis are regulated by MAPs and we postulate that the EML family is one of these key regulators. EMAP was first isolated from dividing sea urchin eggs, *Strongylocentrotus prupuratus*, as the most abundant non-tubulin spindle-associated protein. It was subsequently confirmed to locate to spindle MTs during mitosis (Suprenant et al. 1993). In humans the EMAP-like proteins have also been shown to localise to spindle MTs. Endogenous EML2 , recombinant YFP-EML3 and GFP-EML4 localise to the mitotic spindle apparatus (Eichenmuller et al. 2002, Tegha-Dunghu et al. 2008, Houtman et al. 2007, Pollmann et al. 2006).

Interestingly, EMAP is phosphorylated during mitosis by the kinase p34^{cdc2}. Phosphorylation was observed in both meiotic sea urchin eggs and during the first embryonic mitotic cell division (Brisch et al. 1996). As the embryo enters mitosis EMAP phosphorylation increases and as the embryo exits mitosis, phosphorylation decreases. Moreover, this paper suggested that the EMAP protein acts as a scaffold for the p34^{cdc2} kinase to associate with the MTs and directly modify them (Brisch et al. 1996). This is not unusual for MAPs, for example EMAP115 strongly associates with interphase MTs but is not required for mitotic spindle formation and is therefore phosphorylated on the onset of mitosis to lose MT association (Masson & Kreis 1995). Whilst XMAP215 phosphorylation during mitosis, by CDK1, reduces its ability to promote MT elongation (Gard & Kirschner 1987). This led us to consider whether human EML proteins were also regulated by kinases in a cell cycle dependent manner. This hypothesis was fuelled by the proteomic analysis carried out by Ewing et al. (2007). This study took 50 bait proteins, one of which was Nek6, to look for potential interaction partners. Strikingly, this study revealed a strong interaction between Nek6 and EML3 with the same confidence level as interactions between Nek6 and Nek9. Based on this result, we began to investigate whether EML3 is regulated by Nek6 and whether they might regulate EML3 localisation.

Nek6 is one of the smallest member of the NIMA-related kinase family which together regulate; ciliogenesis, DNA damage response, prolactin signalling and mitosis. Nek6 localises to microtubule based structures during mitosis and is considered to be a mitotic kinase as this is when its kinase activity is highest (O'Regan & Fry 2009). Lack of Nek6 results in G2/M arrest, whereby cells appear trapped in metaphase (Yin et al. 2003, O'Regan & Fry 2009). Nek6 is regulated by the upstream kinase Nek9, which also regulates Nek7. Nek6 already has well characterised substrates including; Eg5 and Hsp72. In terms of the latter phosphorylation by Nek6 is crucial for Hsp72 localisation to the mitotic spindle. (Rapley et al. 2008, O'Regan et al. 2015).

5.2 Results

5.2.1 EML1 and EML3 show reduced association with MTs in mitosis

In this section we look at the localisation of YFP-EML1 and YFP-EML3 in both transiently and stably expressing U2OS cells. As mentioned above, EML2, EML3 and EML4 have all been shown to localise to the MT network in interphase and show some localisation to the spindle in mitosis. As EML1 localisation has not yet been characterised, this acted as the starting point for this work. Firstly, we transiently transfected U2OS cells for 24 hours with an YFP-EML1 full length construct, and processed for indirect immunofluorescence as described in 2.4.1. Confocal microscopy revealed that YFP-EML1 localised to the MT network in interphase and that there was localisation to the spindle in some mitotic cells (Figure 5.1). However, when the same analysis was carried out with U2OS:YFP-EML1 stable cell lines, YFP-EML1 localised strongly to interphase MTs but not to any of the MT structures during mitosis (Figure 5.2). The U2OS:YFP-EML1 stable cells were then analysed via time-lapse live cell imaging (Figure 5.3). This revealed that the EML1 protein did not localise to the spindle MTs during mitosis, despite being clearly detectable on interphase MTs. This supports fixed imaging data, confirming that it is not an artefact of fixation. We hypothesis that the reason YFP-EML1 is detected on the spindle in metaphase upon transient expression and not stable expression is because of the increased amount of protein expressed upon transient expression. Taken together, we propose that EML1 localises strongly to MTs in interphase but is less well associated with MTs during mitosis from the onset of prophase and until cytokinesis.

A similar set of experiments were performed to determine the localisation of EML3 during mitosis. Firstly, we transiently transfected U2OS cells with YFP-EML3 for 24 hours, before cells were fixed and stained with α-tubulin and GFP antibodies. Confocal microscopy revealed that YFP-EML3 localised strongly to the interphase MTs but there was no obvious localisation to the mitotic spindle from prophase to anaphase, before YFP-EML3 protein started to reassociate with MTs from cytokinesis (Figure 5.4). This was surprising and contradicted the data published in Tegha-Dunghu et al. (2008), in which both transient and endogenous EML3 was clearly

localised to the spindle in metaphase. Consequently, the experiment was repeated with a Flag-EML3 construct; U2OS cells were transiently transfected for 24 hours with a Flag-EML3 construct, cells were then fixed in ice-cold methanol and stained with α-tubulin and Flag antibodies. Confocal microscopy revealed that transiently expressed Flag-EML3 was also unable to localise to the spindle during metaphase (Figure 5.5). Next, we used the U2OS:YFP-EML3 stable cells to determine if this would make a difference to the localisation observed. U2OS:YFP-EML3 cells were fixed with ice-cold methanol and stained with α-tubulin and GFP antibodies. Imaging showed that YFP-EML3 localised neatly to the interphase MT network but that localisation to the MTs was lost upon the onset of mitosis. During prophase and metaphase only diffuse/cytoplasmic staining for YFP-EML3 could be seen, but as the cells enters anaphase a more distinct MT pattern could be visualised. However, during cytokinesis the YFP-EML3 localised very strongly to the MTs (Figure 5.6).

These changes in YFP-EML3 localisation during the cell cycle were confirmed by time-lapse live cell imaging. These movies show clear YFP-EML3 localisation in both interphase (0 mins) and cytokinesis (228 mins) but no distinct localisation of YFP-EML3 to MTs could be seen from prophase to telophase (Figure 5.7). This indicates that EML3 localisation is more complex than initially thought and that during mitosis it is not obviously associated to the MT spindle.

Due to the potential interactions between EML proteins we wanted to ensure that the localisation of EML3 was working independently and not being hindered by the expression of other EMLs. To do this we depleted EML1, EML2 and EML4 using two different siRNA's from the YFP-EML3 stable cell line for 48 hours before cells were fixed and stained. Images were captured to visualize the YFP-EML3 localization in mitosis. From this, it was clear that depletion of EML1, EML2 or EML4 has no obvious effect on YFP-EML3 localization (Figure 5.8).
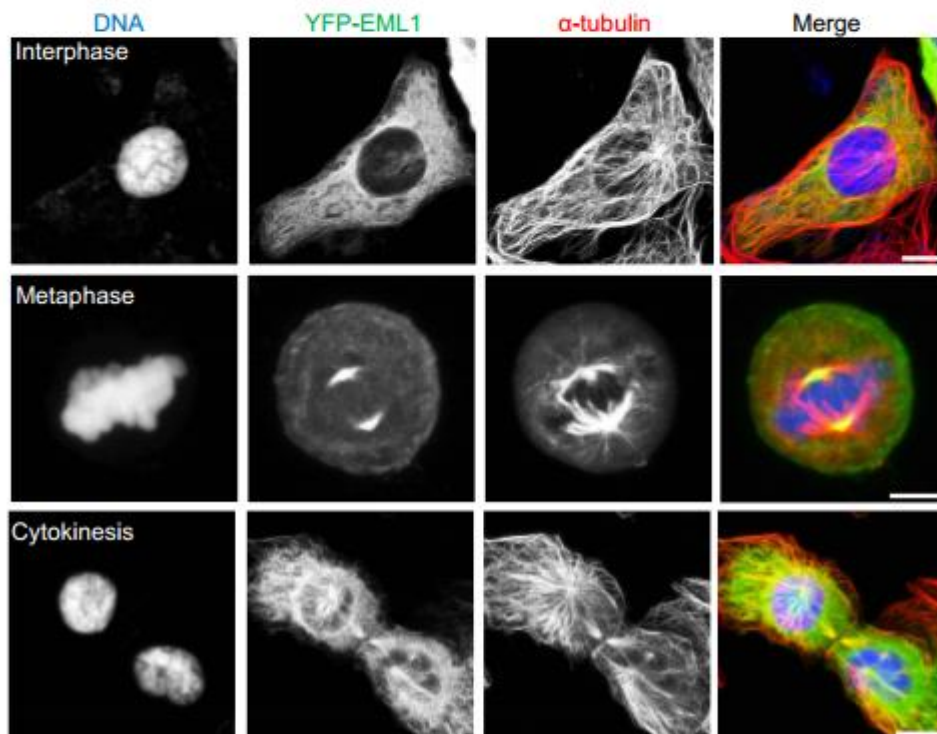
Figure 5.1: Recombinant EML1 localises to the mitotic spindle following transient expression
U2OS cells were transiently transfected with YFP-EML1 for 24 hours, fixed with ice-cold methanol and immunostained with GFP (green) and α-tubulin (red) antibodies. Merged images include DNA stained with Hoechst (blue). Images were captured from different stage of mitosis as indicated. Scale bar in metaphase, 5 µm, other stages 10 µm.
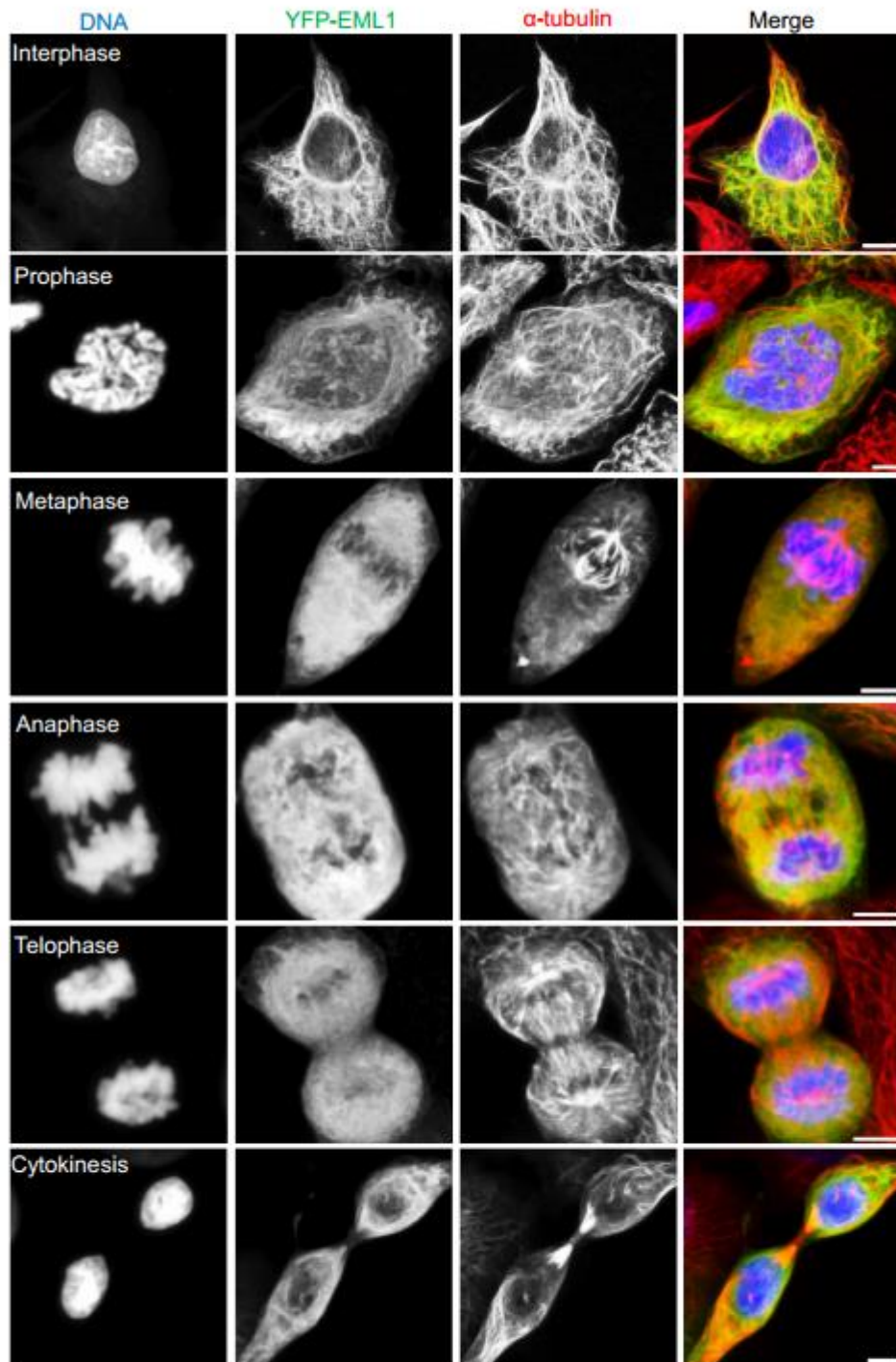
Figure 5.2: Recombinant EML1 does not localise to the mitotic spindle upon stable expression
U2OS:YFP-EML1 cells were fixed with ice-cold methanol and immunostained with GFP (green) and α-tubulin (red) antibodies. Merged images include DNA stained with Hoechst (blue). Images were captured from different stage of mitosis as indicated. Scale bars interphase, 10 μm, other stages, 5 μm.
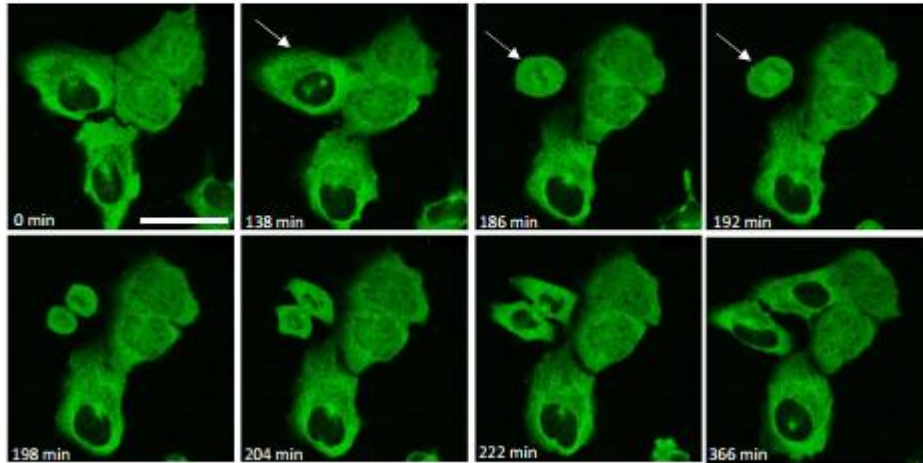
Figure 5.3: Time-lapse imaging shows YFP-EML1 does not localise to the spindle during mitosis

U2OS:YFP-EML1 cells imaged using confocal microscopy. Image captured every 15 minutes for 17 hours. The arrow indicates a cell that progresses through mitosis during this period. Scale bars, 25 μm.
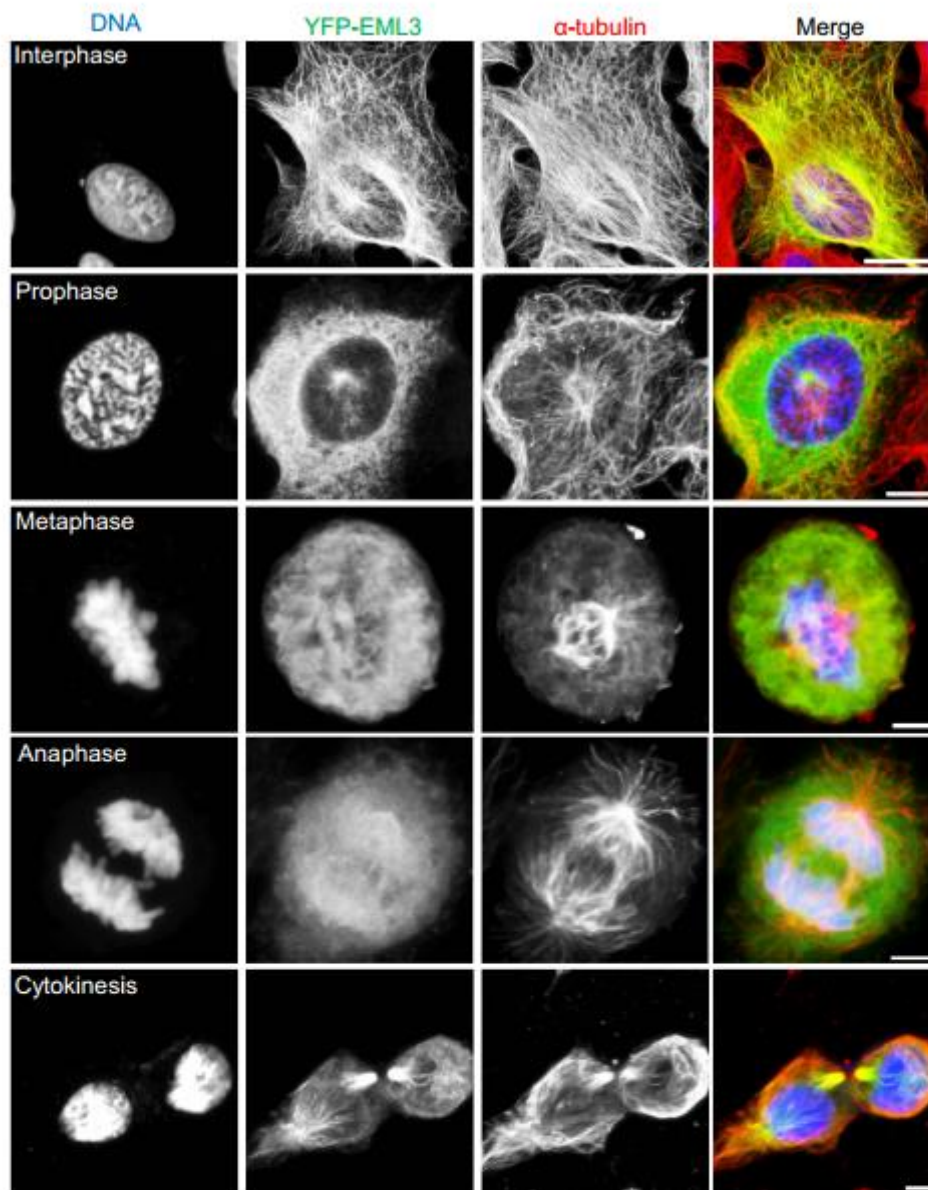
Figure 5.4: Recombinant EML3 does not localise to the mitotic spindle following transient expression

U2OS cells were transiently transfected with YFP-EML3 for 24 hours, fixed with ice-cold methanol and immunostained with GFP (green) and α-tubulin (red) antibodies. Merged images include DNA stained with Hoechst (blue). Images were captured from different stage of mitosis as indicated. Scale bars, 5 μm, interphase, 25 μm.
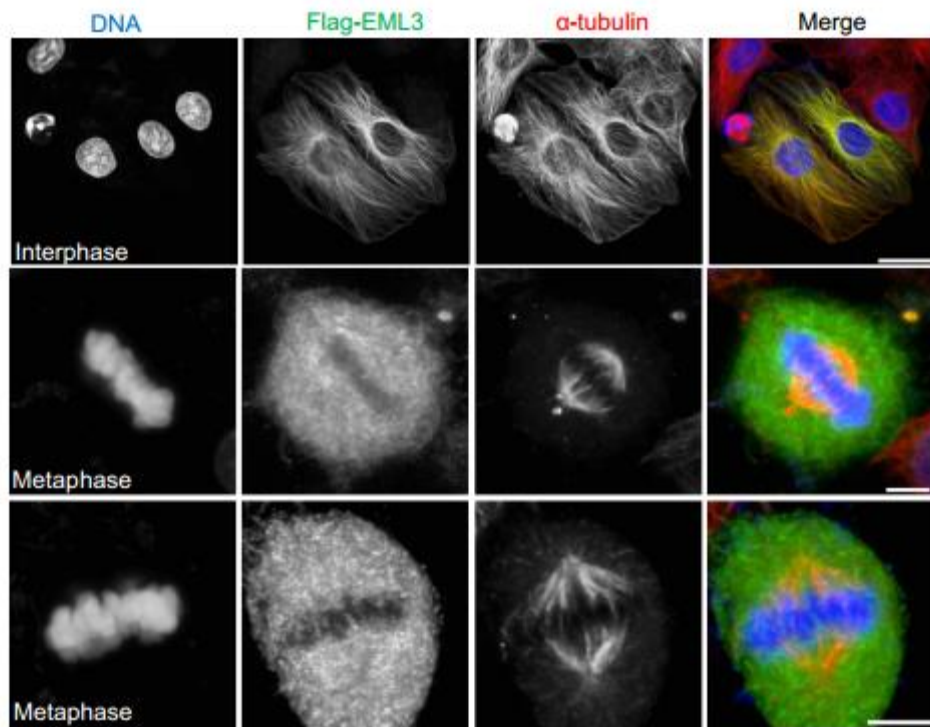
Figure 5.5: Recombinant Flag tagged EML3 does not localise to the mitotic spindle following transient expression

U2OS cells were transiently transfected with Flag-EML3 for 24 hours, fixed with ice-cold methanol and immunostained with Flag (green) and α-tubulin (red) antibodies. Merged images include DNA stained with Hoechst (blue). Images were captured from different stage of mitosis as indicated. Scale bars, 5 μm, interphase, 25 μm.
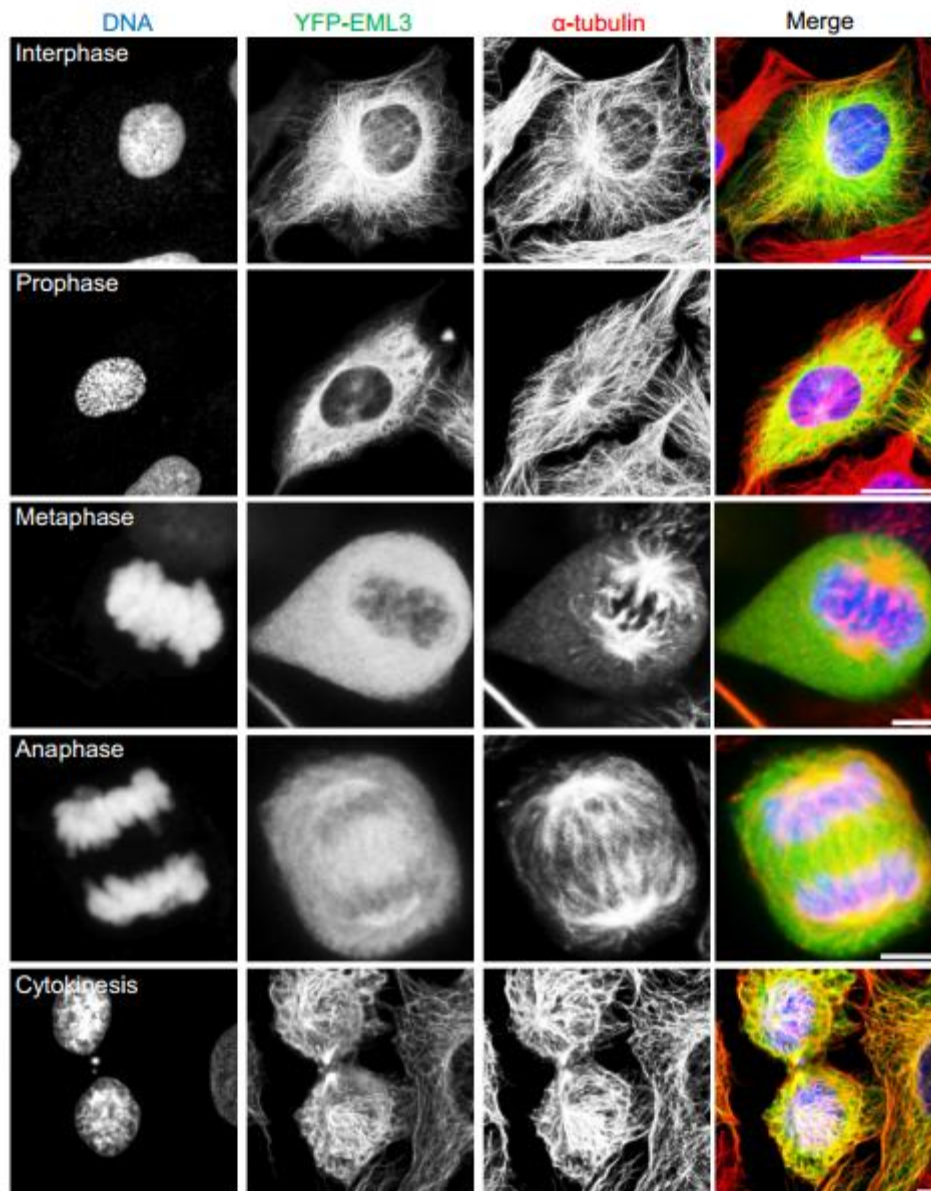
Figure 5.6: Recombinant EML3 does not localise to the mitotic spindle upon stable expression.
U2OS:YFP-EML3 cells were fixed with ice-cold methanol and immunostained with GFP (green) and α-tubulin (red) antibodies. Merged images include DNA stained with Hoechst (blue). Images were captured from different stage of mitosis as indicated. Scale bars, 5 μm, interphase, 25 μm.
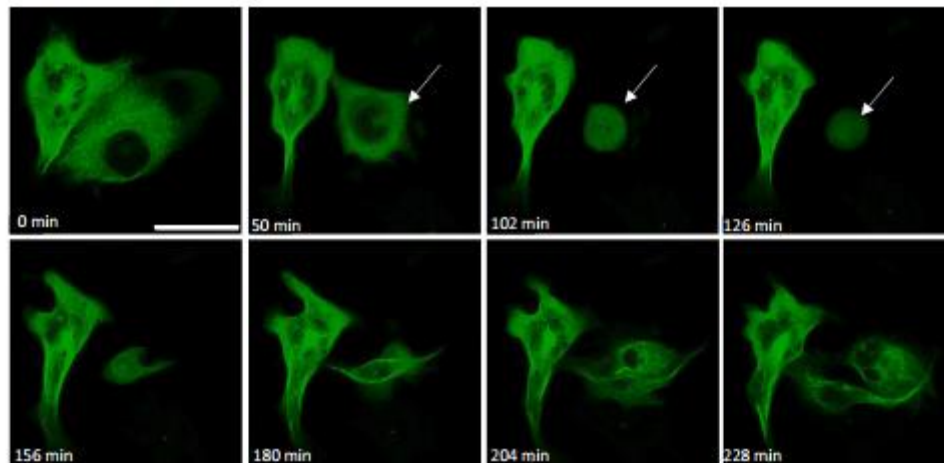
Figure 5.7: Time-lapse imaging shows YFP-EML3 does not localise to the spindle during mitosis
U2OS:YFP-EML3 cells imaged using confocal microscopy. Image captured every 15 minutes for 17 hours. The arrow indicates a cell that progresses through mitosis during this period. Scale bars, 25 µm.
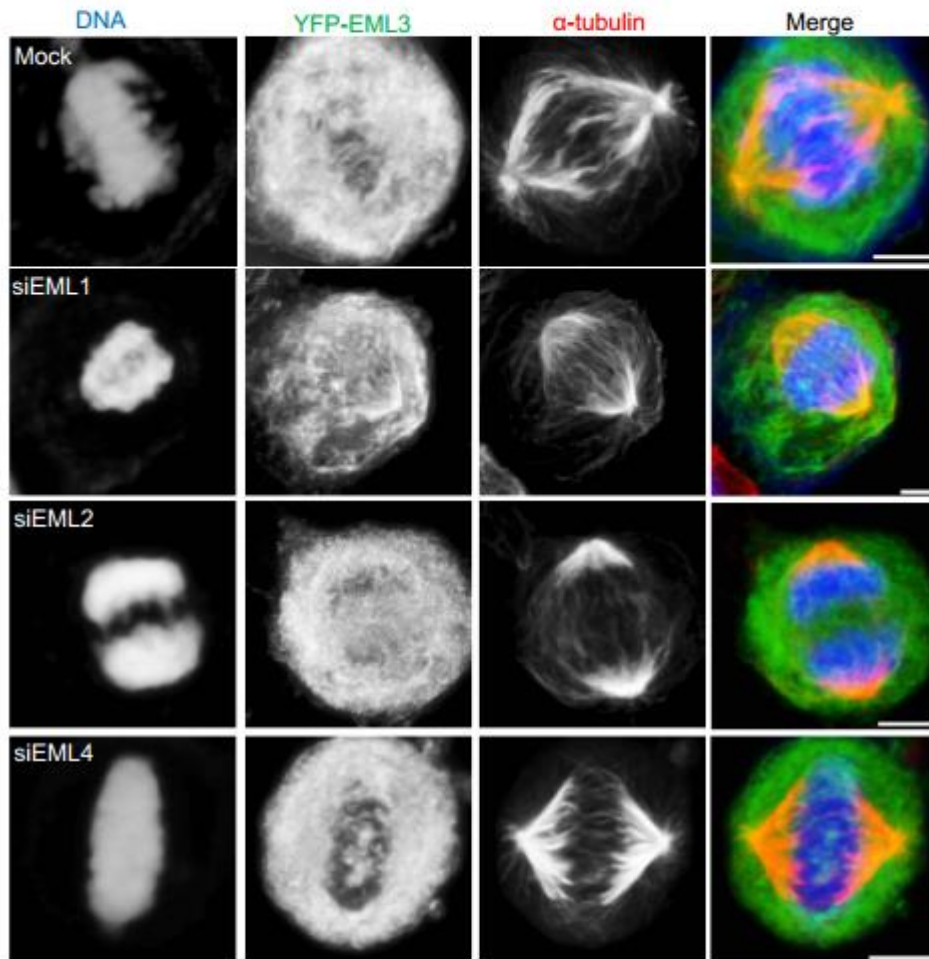
Figure 5.8: EML3 localisation during mitosis is not dependent on EML1, EML2 or EML4

U2OS:YFP-EML3 cells were transfected with siRNAs against EML1, EML2 and EML4 for 48 hours prior to staining with GFP (green) and α-tubulin (red) antibodies. Merged images include DNA stained with Hoechst (blue). Images were captured from different stage of mitosis. Scale bars, 5 µm.

5.2.2 EML3 interacts with Nek6 in mitosis

As indicated, a strong interaction had been detected between EML3 and Nek6 (Ewing et al. 2007). We wanted to test how these proteins interact and whether Nek6 was phosphorylating the EML3 protein. To begin, an *in vitro* kinase assay was performed using GFP-EML3 (kindly provided by Dr Mark Richards) and commercial Nek6 kinase as described in chapter 2.3.2, β-casein was used as a model substrate. This assay revealed a number of interesting findings: firstly EML3 was clearly phosphorylated in the sample containing Nek6, however, there was also phosphorylation of EML3 in the sample without Nek6 (Figure 5.9A). Secondly, although Nek6 is known to autophosphorylate, there was increased Nek6 autophosphorylation when the EML3 was present (Figure 5.9A). As expected β-casein was heavily phosphorylated by Nek6. Having demonstrated phosphorylation of EML3 protein in the presence of Nek6 we sought to identify the phosphorylated residues. For this experiment we performed kinase assays with purified Nek6 and GFP-EML3 protein in the absence of radiolabelled ATP. Following SDS-PAGE and Coomassie Blue staining the GFP-EML3 band was cut out of the gel for phosphosite analysis and digested using either trypsin only or trypsin and Glu C before analysis by mass spectrometry. The first experiment (trypsin only) highlighted a number of Nek6 phosphorylation sites throughout the EML3 protein, with the majority within the EML NTD (Figure 5.9B). The second experiment (trypsin and Glu C) identified additional residues, some of which were present in the first analysis (Figure 5.9B). Two consecutive phosphorylated residues identified S156 and S157, were of particular interest as they are the first two serines of a serine rich patch containing 6 consecutive serine residues. The overall coverage of the combined experiments was 83% indicating that the majority of potential phosphorylation sites had been detected in one of the experiments (Figure 5.9B).

In order to understand why EML3 was phosphorylated in the absence of Nek6 the remainder of the purified EML3 protein preparation was analysed by SDS-PAGE and Coomassie blue stain. This revealed a number of additional bands which were analysed by mass spectrometry following an in gel trypsin digest. The four bands that migrated at 70 kDa, 55 kDa, 37 kDa and 25 kDa were identified as Hsp70, α/β tubulin,

Nek6 and 14-3-3 epsilon respectively. This potentially explains why the EML3 protein preparation was phosphorylated in the absence of added kinase as Nek6 was already present in the protein sample (Figure 5.9C). Also interesting is the presence of Hsp70, another interacting partner of Nek6 (O'Regan et al. 2015) and 14-3-3 a diverse signalling protein. Less surprising is the presence of tubulin known to exhibit a strong interaction with EML3.

Co-immunoprecipitation of the endogenous EML3 and Nek6 proteins was demonstrated by Dr Laura O'Regan using the EML3 antibody generated by the Gruss lab and an in-house Nek6 antibody (Figure 5.10A). This showed that EML3 and Nek6 have an enhanced interaction in synchronous cells arrested in M-phase and an almost undetectable interaction in cells synchronised in S-phase (Figure 5.10A). This indicates that the EML3/Nek6 interaction is enhanced during mitosis, coinciding with the changes observed in EML3 association with MTs. Next we used constructs expressing truncated fragments (Figure 5.10B) to establish which region of the EML3 protein the Nek6 was interacting with. U2OS cells were transiently transfected with YFP only, YFP-EML3 TAPE or YFP-EML3 NTD along with Flag-Nek6 for 24 hours before cell lysis. Lysates were immunoprecipitated using a GFP antibody and western blotted for GFP and Flag. This experiment identified the Nek6 binding region within the EML3 TAPE domain, which was surprising as it was thought Nek6 might target the serine rich EML3 NTD. As a result we hypothesise that although Nek6 directly binds to the EML3 TAPE domain it is still able to phosphorylate the serine rich patches of the EML3 NTD (Figure 5.10C).
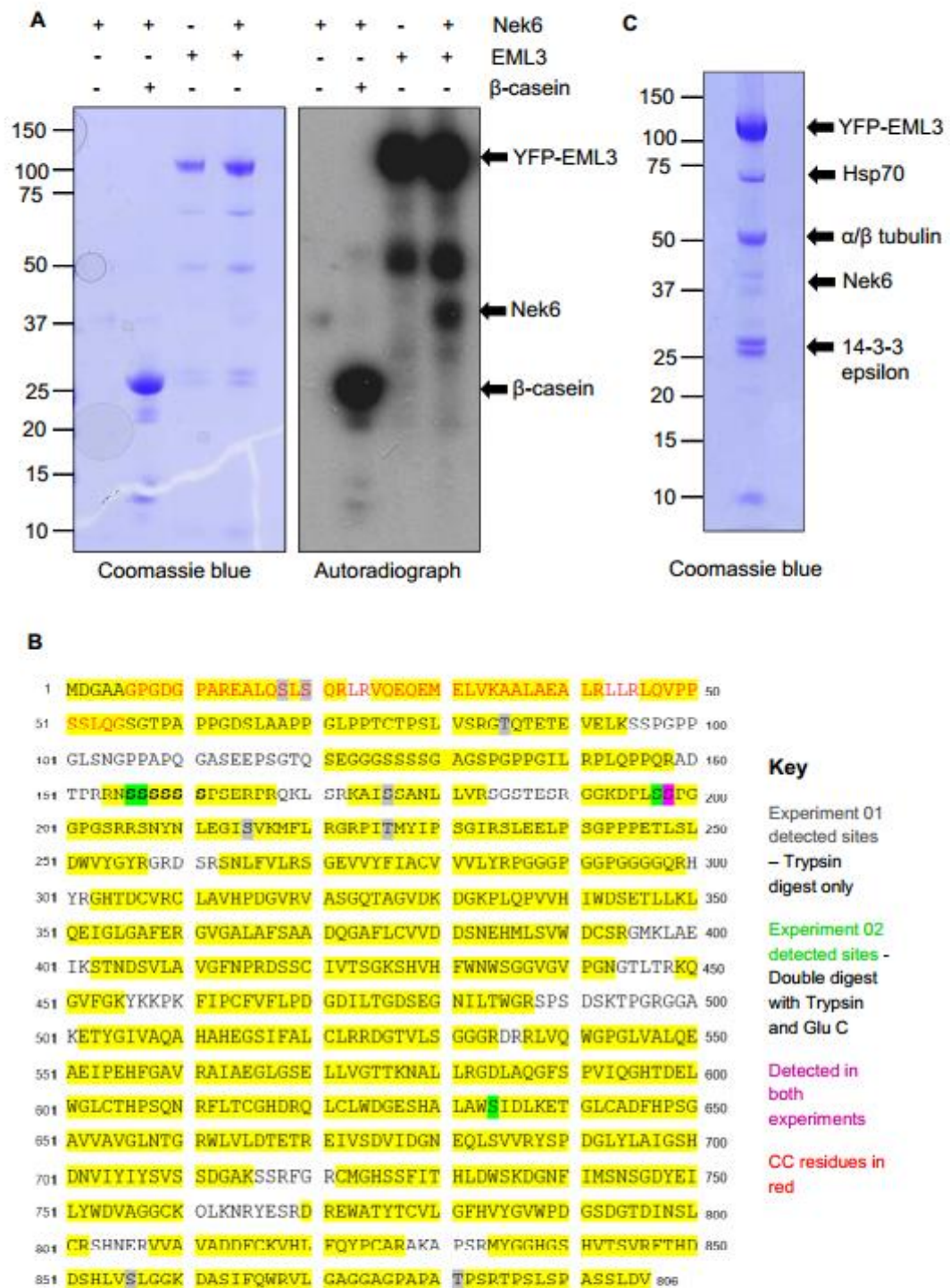
Figure 5.9: *In vitro* phosphorylation of EML3 by Nek6

A. Purified YFP-EML3 protein or β-casein were used as substrates in a kinase assay with and without commercial Nek6 kinase or β-casein. Kinase assays were analysed by SDS-PAGE and coomassie blue staining (left) and autoradiography (right). **B.** Phosphomapping reveals sites in EML3 phosphorylated by Nek6. Purified EML3 phosphorylation *in vitro* by Nek6 were analysed for phosphomapping by mass spectrometry. Two separate digests were carried out as shown combined protein coverage is shown in yellow. Serine rich regions are indicated in bold. **C.** Mass spectrometry identified the additional bands within the YFP-EML3 purified protein to be Hsp70, α/β tubulin, Nek6 and 14-3-3 epsilon protein as indicated.
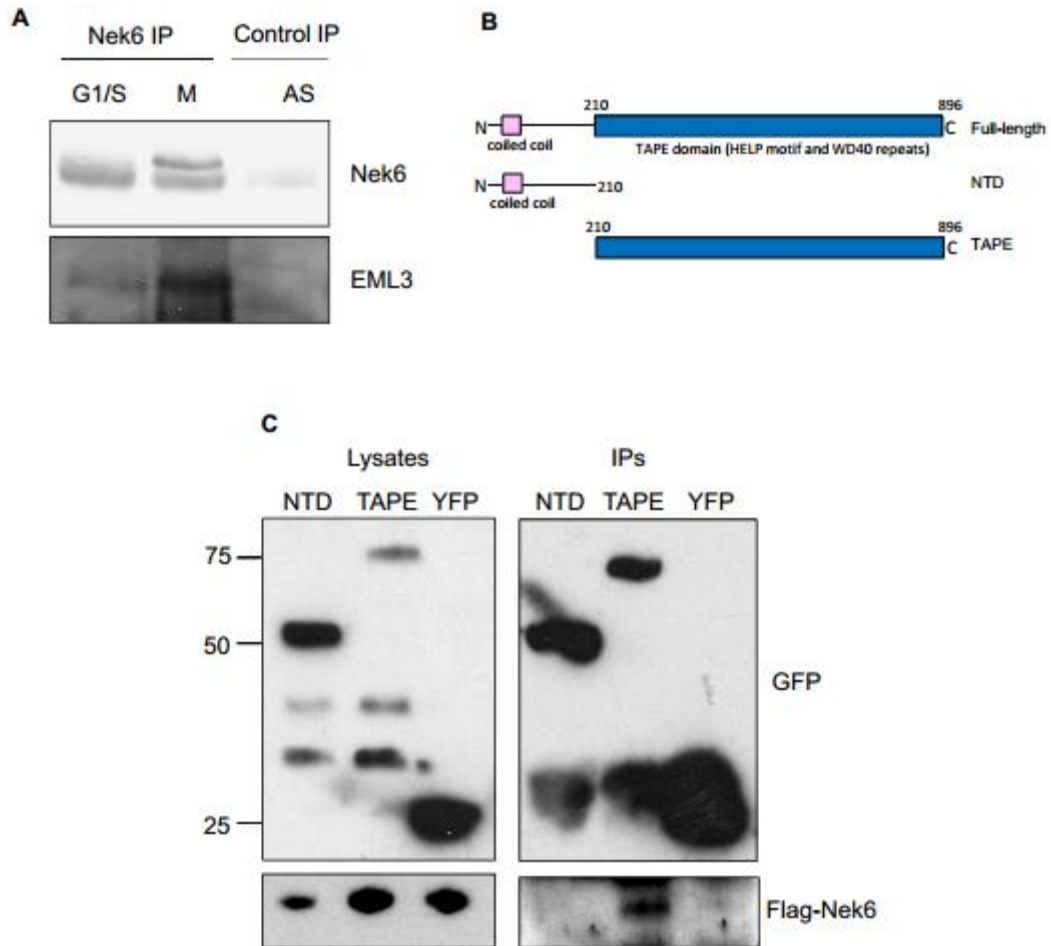
Figure 5.10: Nek6 interacts with the TAPE domain of EML3 and the interaction is enhanced during mitosis

A. Control (rabbit IgGs) or Nek6 immunoprecipitates prepared from asynchronous (AS), G1/S arrested or M-phase arrested cells were western blotted with antibodies indicated (data from Dr Laura O'Regan).

B. Schematic representation of the EML3 constructs used in (C). Numbers indicate amino acid residues

C. U2OS cells were transiently co-transfected with YFP only or YFP-EML3 NTD or TAPE fragments and Flag-Nek6 for 24 hours. Cells were lysed and subjected to immunoprecipitation with GFP antibodies. Samples were resolved by SDS-PAGE and analysed by Western blot with the antibodies and molecular weights (kDa) are shown on the left.

5.2.3 EML3 association with MTs is dependent upon Nek6 but not Nek7 kinase activity

Once we confirmed an interaction between EML3 and Nek6 we hypothesised that Nek6 activation in mitosis released EML3 from the MTs. Because of the close similarity between Nek6 and Nek7, Nek7 was also used in these experiments. To test the hypothesis we first observed the consequences of constitutive activation of Nek6 and Nek7 on EML3 protein localisation in interphase. Both Nek6 and Nek7 activation occurs through release of an autoinhibitory conformation involving a tyrosine residue: Tyr97 for Nek7 and Tyr108 for Nek6. Mutants of these residues to alanine was shown to generate constitutively active mutants (Richards et al. 2009).

U2OS:YFP-EML3 cells were therefore transfected with either Flag-Nek7 WT or the active mutant Flag-Nek7 Y97A for 24 hours before being processed for indirect immunofluorescence as described in chapter 2.4.1. Imaging showed that EML3 localisation to the MT network in interphase was not affected by the presence of WT or active Nek7 (Figure 5.11). In a similar manner, U2OS:YFP-EML3 cells were transiently transfected with either Flag-Nek6 WT or the active mutant Flag-Nek6 Y108A. Imaging showed that EML3 localisation to the MT network in interphase was normal in cells co-expressing Nek6 WT and EML3. However, in cells co-expressing EML3 and Nek6 Y108A, EML3 localisation became diffusely cytoplasmic with no MT network staining visible (Figure 5.13A). Quantification showed a significant decrease in the number of cells showing EML3 localisation from 85.66% in the mock treated cells to 50.33% in cells co-expressing the activated Nek6 (Figure 5.13B). This showed that premature activation of Nek6 in interphase caused EML3 to disassociate from MT's.

RNAi depletion of Nek6 and Nek7 was then optimised with GAPDH as a control. U2OS cells were transfected with 100 nM siRNA oligonucleotide and Oligofectamine for 48 hours as outlined in chapter 2.2.5, then lysed ahead of SDS-PAGE and Western blot analysis to confirm efficiency of depletion (Figure 5.12A). U2OS:YFP-EML3 cells were first depleted of Nek7 for 48 hours before being fixed and stained with GFP and α-tubulin antibodies. Despite the mitotic defects seen when Nek7 is depleted (abnormal spindle shape and multipolarity) YFP-EML3 was not detected on spindle MTs in the absence of Nek7.
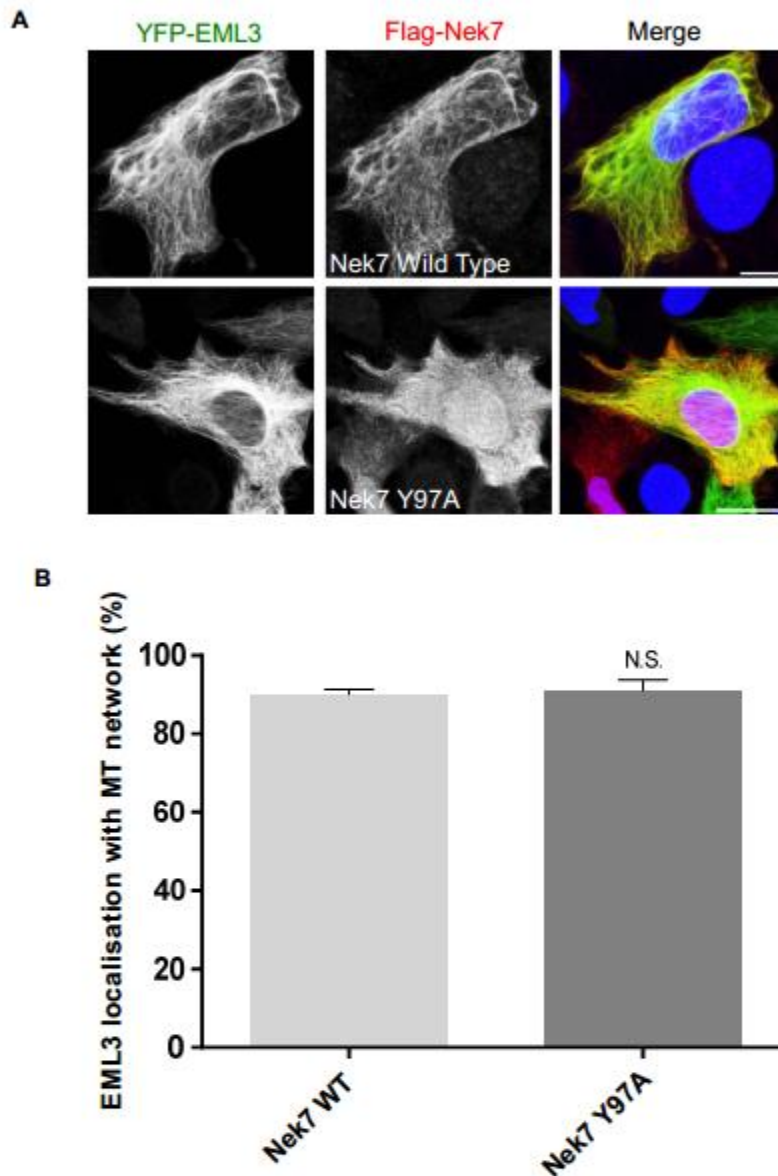
Figure 5.11: Nek7 activation does not alter localization of EML3 in interphase

A. U2OS:YFP-EML3 cells were transfected with either Flag-Nek7 wild-type or Flag-Nek7 Y97A, a constitutively active mutant. Cells were fixed in ice-cold methanol and immunostained with GFP (green) and α-FLAG (red) antibodies. Merged images include DNA stained with Hoechst (blue). Scale bars, 10 μm. **B**. Cells were scored for colocalisation of EML3 with the MT network. Data represents means ($\pm$SD) of measurements from 300 co-transfected cells, n =3.
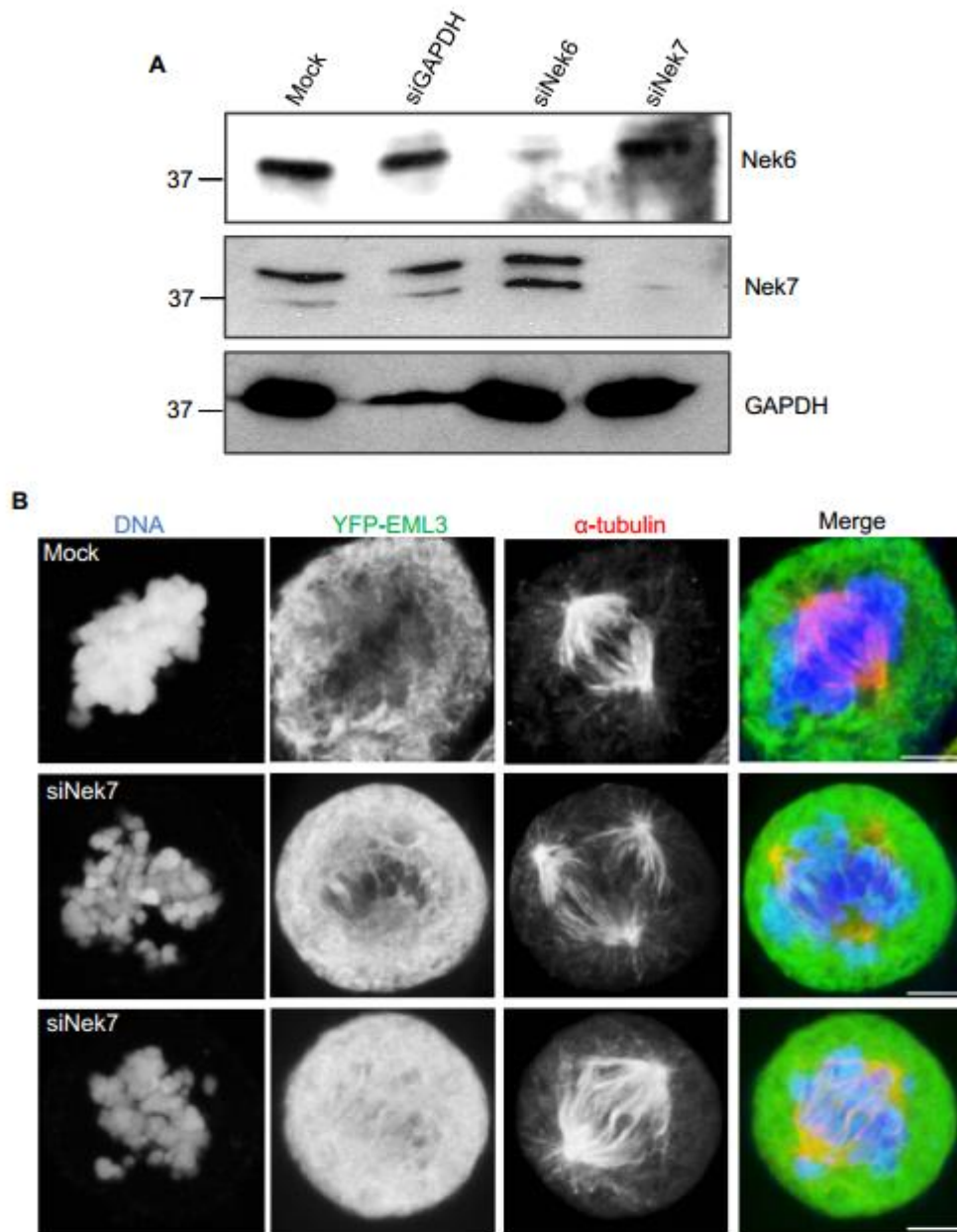
Figure 5.12: Nek7 depletion does not alter localization of EML3 in mitosis

A. U2OS:YFP-EML3 cells were either mock transfected or transfected with siRNAs as indicated. Cells were lysed 48 hours post transfection and analysed via western blot analysis with antibodies as indicated. Molecular weights (kDa) are shown on the left. **B.** U2OS:YFP-EML3 cells were treated with either mock or Nek7 siRNAs for 48 hours, fixed in methanol and immunostained with GFP (green) and α-tubulin (red) antibodies. Merged images of metaphase cells include DNA stained with Hoechst (blue). Scale bars, 5 µm.
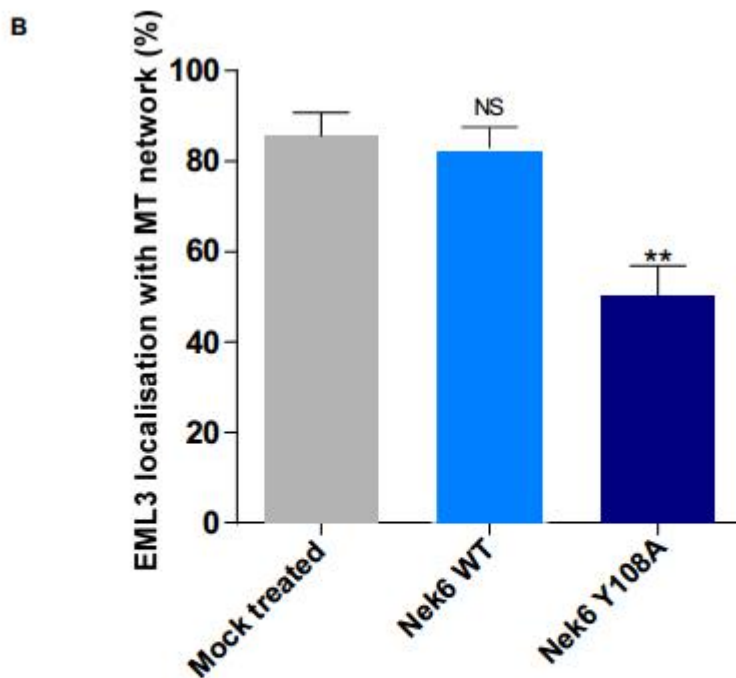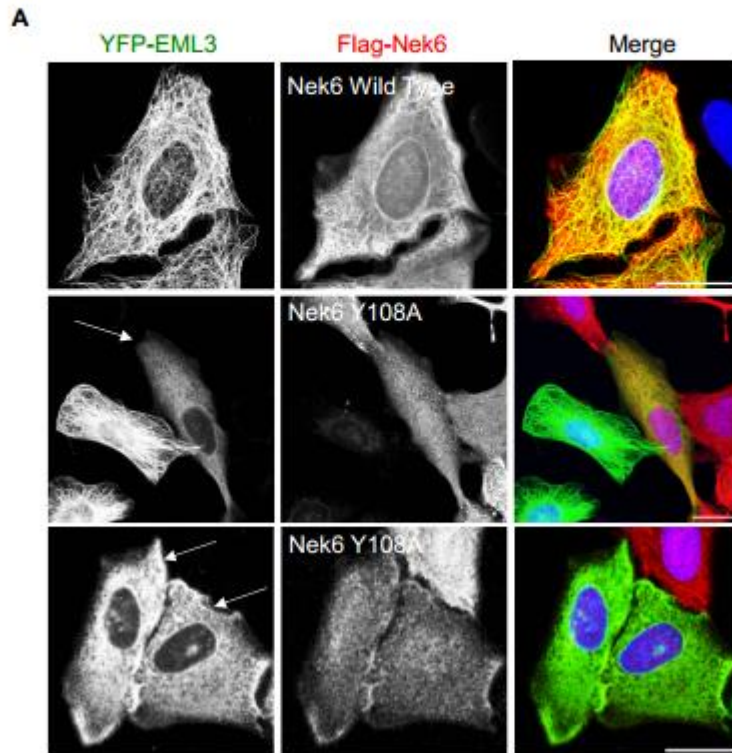
Figure 5.13: Activated Nek6 causes disassociation of EML3 from the microtubules

A. U2OS:YFP-EML3 cells were transfected with either Flag-Nek6 wild-type or Flag-Nek6 Y108A, a constitutively active mutant. Cells were fixed in ice-cold methano and immunostained with GFP (green) and α-FLAG (red) antibodies. Merged images include DNA stained with Hoechst (blue). Loss of EML3 localisation indicated by the white arrows. Scale bars, 25 μm. Cells were scored for colocalisation of EML3 with the MT network. **B**. Data represents means ($\pm$SD) of measurements from 300 co-transfected cells ($p < 0.01$), n =3.
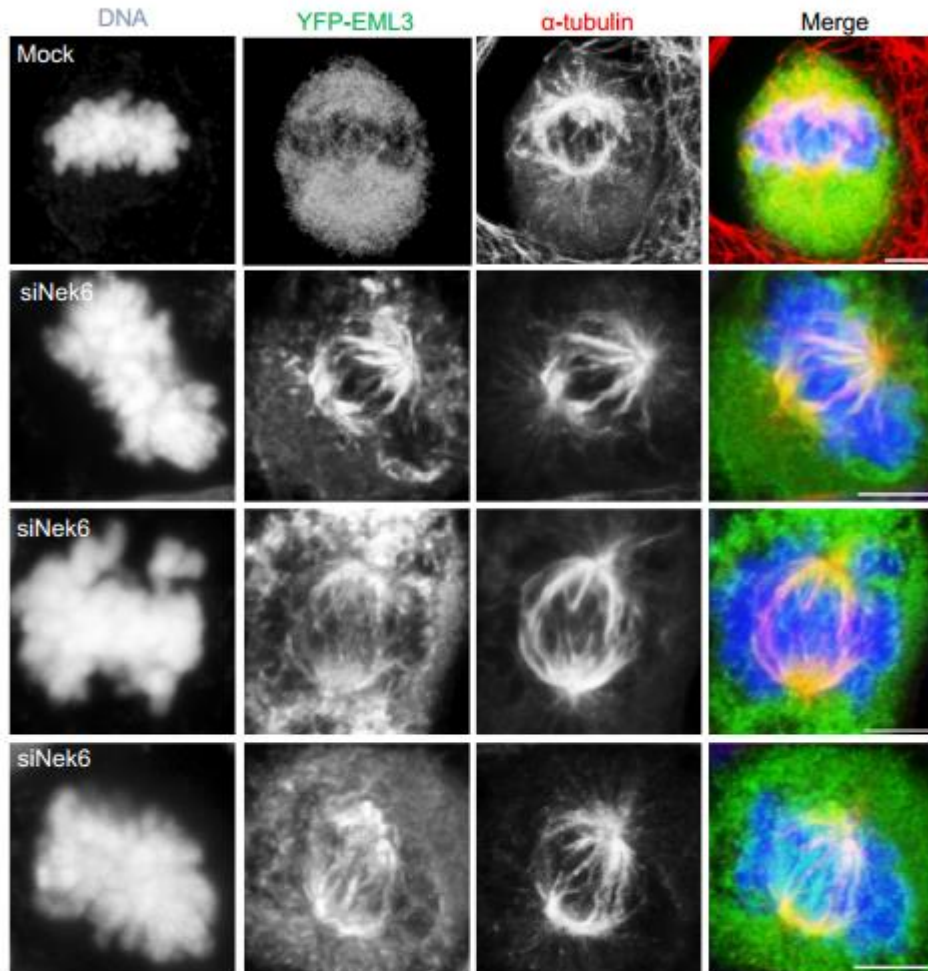
Figure 5.14: Nek6 depletion causes EML3 to localize to the mitotic spindle

U2OS:YFP-EML3 cells were treated with either mock or Nek6 siRNAs for 48 hours, fixed in methanol and immunostained with GFP (green) and α-tubulin (red) antibodies. Merged images of metaphase cells include DNA stained with Hoechst (blue). Scale bars, 5 µm.
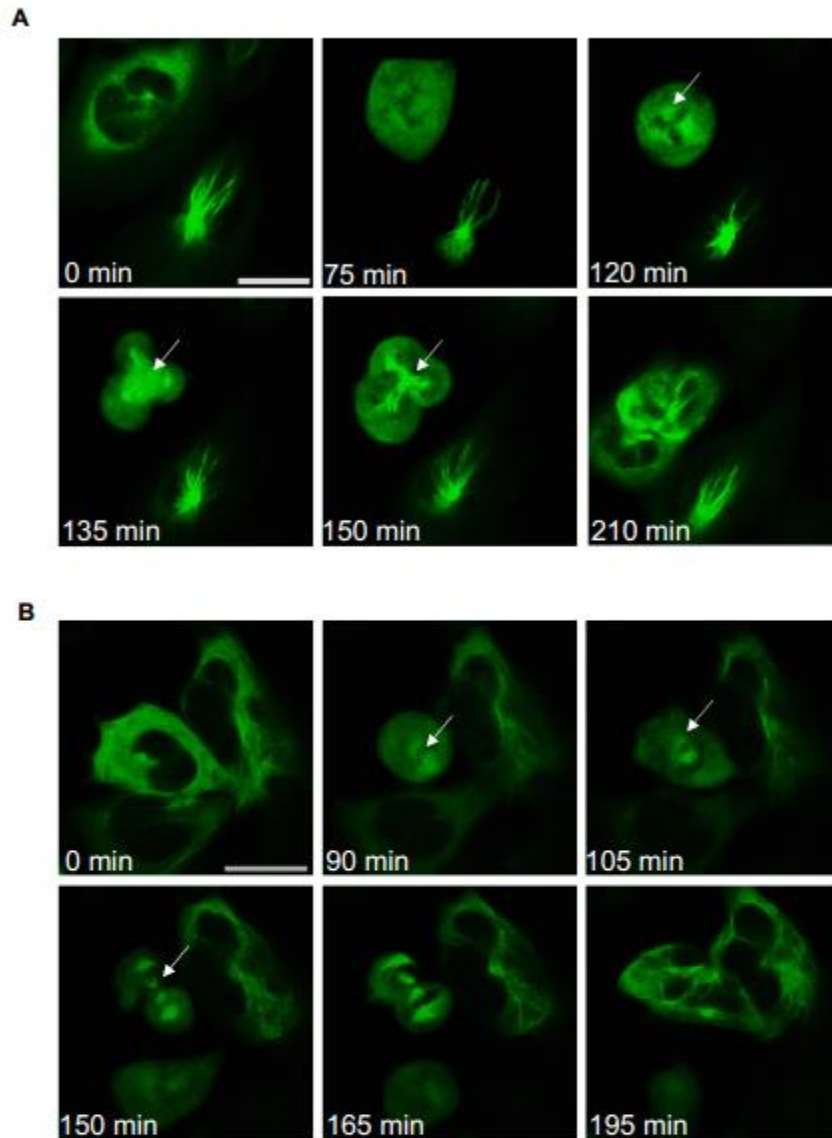
Figure 5.15: Time-lapse imaging reveals retention of EML3 on mitotic spindles in Nek6 depleted cells.

A and B. U2OS:YFP-EML3 cells were transfected with Nek6 siRNAs for 48 hours prior to imaging. Images were captured using confocal microscopy; image capture occurred every 12 minutes for 17 hours. White arrow indicate EML3 accumulation at the predicated site of the mitotic spindle. Scale bars, 25 μm.

U2OS:YFP-EML3 cells were then depleted of Nek6 for 48 hours before being fixed and stained with GFP and α-tubulin antibodies. Imaging revealed that YFP-EML3 now localised to the spindle MTs in Nek6 depleted cells (Figure 5.14). To confirm this result we depleted Nek6 for 48 hours from the U2OS:YFP-EML3 cells and performed live cell imaging. This indicated the presence of YFP-EML3 on what is likely to be the MT spindle (Figure 5.15). Together this data provides persuasive evidence that EML3 localisation to MTs is regulated by Nek6 and that phosphorylation by activated Nek6 in mitosis leads to displacement of EML3 from spindle MTs.

5.2.4   EML3 mutants alter the MT binding affinities

Following identification of a number of Nek6 phosphosites in the EML3 NTD, we decided to generate mutants of two serine rich patches within the EML3 NTD: S126-129 and S156-161, one of which contained two of the serines identified as Nek6 phosphorylation sites (S156 and S157). Mutagenesis was performed by the in house PROTEX facility and constructs were sequenced to confirm incorporation of the mutant residues. All serines < aspartic acid in the patches were mutated to create: S126-129D and S156-161D constructs (Figure 5.16A). Interaction with the negatively charged tubulin E-hooks is likely to be perturbed by introducing negatively charged aspartic acid residues if this region is important for MT association. Furthermore mutation of serine to aspartic acid essentially creates a phosphomimetic mutant protein which no longer relies on Nek6 phosphorylation. Before we assessed localisation, we wanted to confirm that these mutants retained functions similar to the wild-type protein and did not merely result in misfolded protein. For this purpose we tested their ability to interact with soluble tubulin a function associated with the TAPE domain (Richards et al. 2014). Specifically, we transiently transfected YFP-EML3 full-length, NTD and TAPE domain along with YFP only and the two YFP-EML3 mutants (S126-129D and S156-161D) for 24 hours, cold-treated by incubating the cells on ice for 60 minutes, immunoprecipitated and analysed by Western blot. Both the NTD and YFP were unable to bind tubulin (although weak binding was detected potentially due to the 'sticky' nature of the protein), whilst the TAPE domain and both mutants showed a strong interaction with soluble tubulin indicating that these proteins still retain functions associated with the wild-type protein (Figure 5.16B).

We then investigated the localisation of the mutants and wild–type protein. U2OS cells were transiently transfected for 24 hours before being stained with GFP and α-tubulin antibodies. Confocal microscopy revealed that the YFP-EML3 WT protein showed clear overlap with the MTs giving an overlap coefficient of 0.8 $\pm$ 0.04, which was expected, unlike the S126-129D mutant which showed a reduced association and overlap coefficient of 0.61 $\pm$ 0.074 (Figure 5.17). Strikingly, the S156-161D mutant showed an even more reduced overlap with MTs, giving an R value of only 0.32 $\pm$ 0.099 (Figure 5.17). This indicates that mutations of these serine residues reduces MT association. We therefore generated another mutant S156-161A, six serine residues were changed to a hydrophobic alanine residue. Transfection of U2OS cells and analysis by immunofluorescent microscopy revealed that the S156-161A mutant showed enhanced MT binding compared to WT protein R = 0.87 $\pm$ 0.044 (Figure 5.17). To test whether the S156-161A mutant would remain on MTs during mitosis, we transiently transfected U2OS cells with the YFP-EML3 S156-161A mutant for time-lapse live cell imaging. However, none of the cells imaged progressed through mitosis with many undergoing apoptosis only a few hours into imaging (Figure 5.18A). However, the MTs in cells expressing the S156-161A mutant were longer than in WT cells with MTs often bundled. Moreover, small circular rings of EML3 protein were observed detached from the MT network which are potentially MT rings (Figure 5.18 A and B).
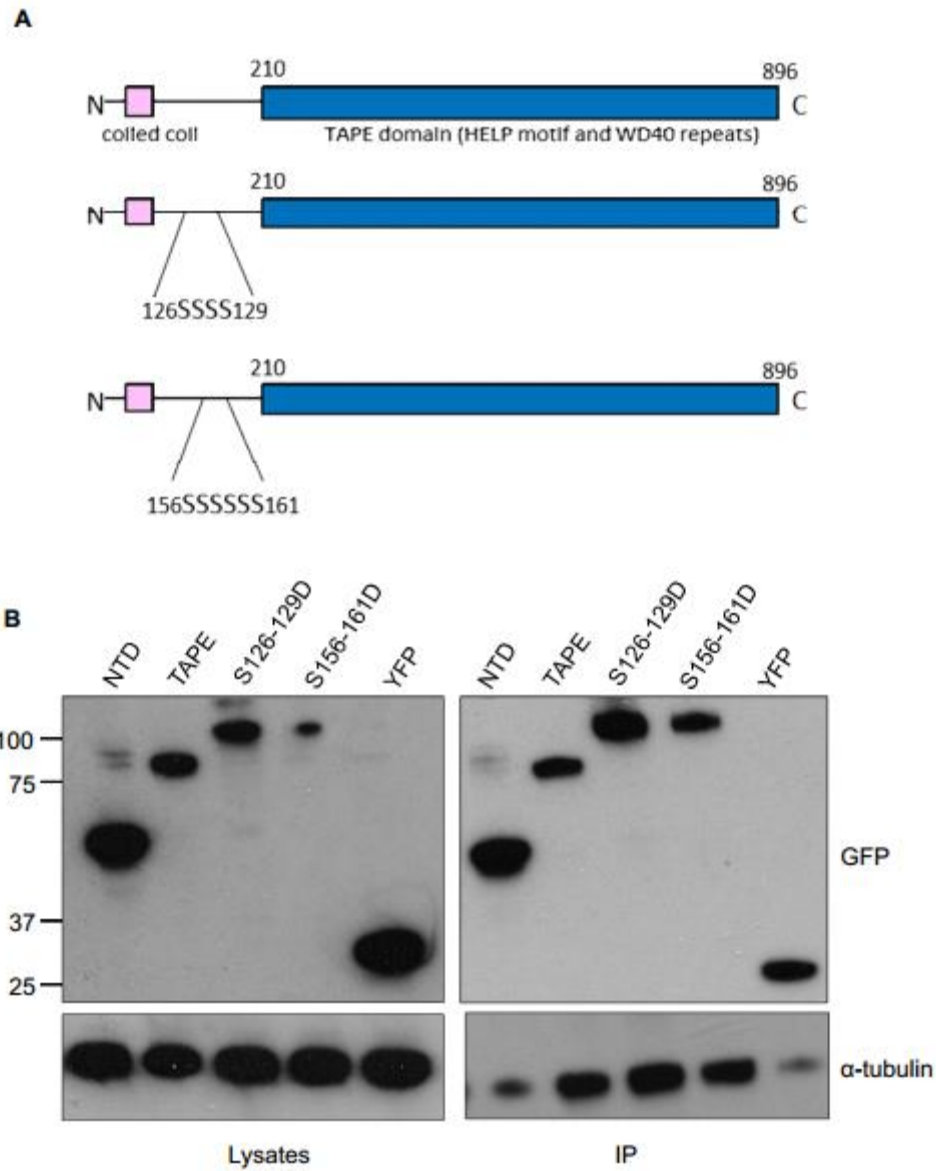
Figure 5.16: EML3 mutants can still bind soluble tubulin

A. Schematic diagram to show the YFP-EML3 S126-129D and the S156-161D mutants compared to the wild-type protein**. B.** U2OS cells were transiently transfected with YFP-EML3 mutants 24 hours before cells were cold treated, lysed and subjected to immunoprecipitation GFP antibodies. Samples were resolved by SDS-PAGE and analysed by Western blot with the antibodies indicated. Molecular weights (kDa) are shown on the left.
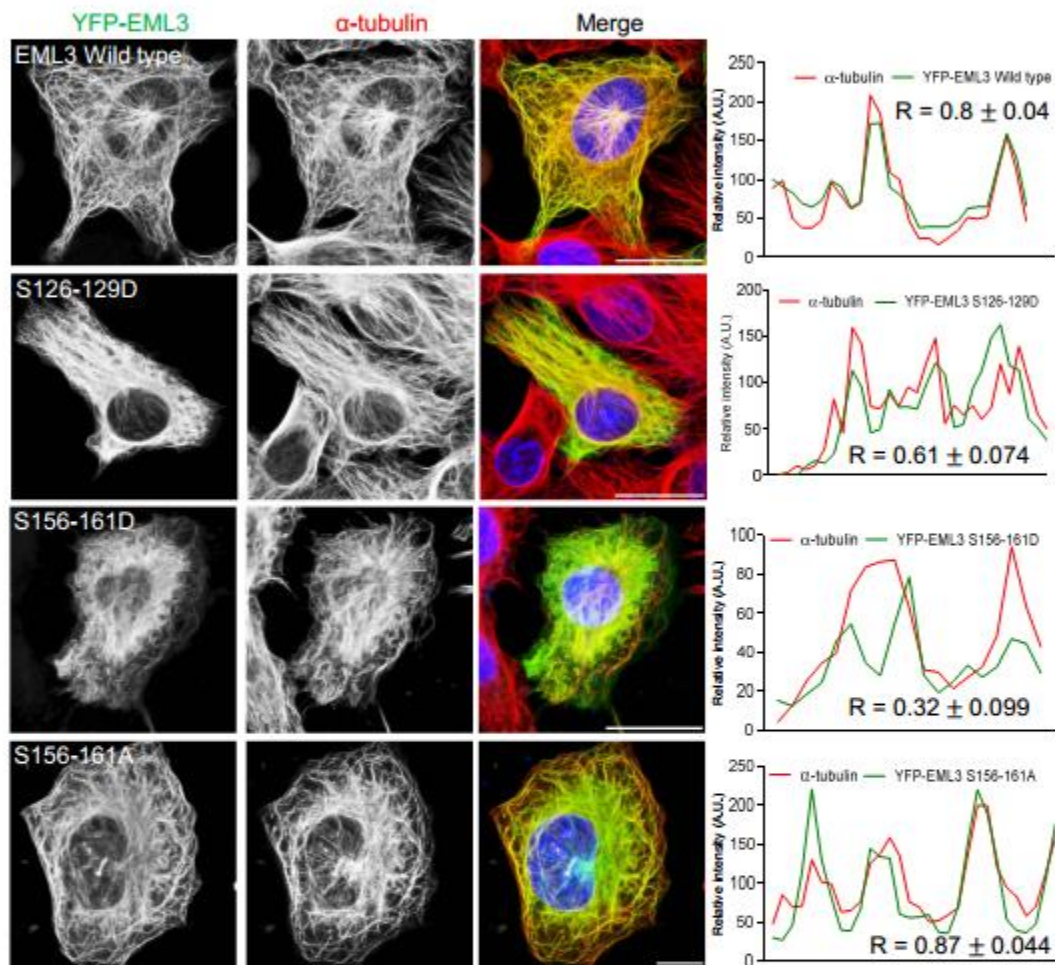
Figure 5.17: EML3 mutants exhibit altered affinity with the MT network in interphase

U2OS cells were transiently transfected with YFP-EML3 constructs as indicated for 24 hours and immunostained with α-tubulin (red) and α-GFP (green) antibodies. Images were analysed so that overlap coefficient values could be determined. R values represent mean from 20 transfected cells. Scale bars, 25 μm.
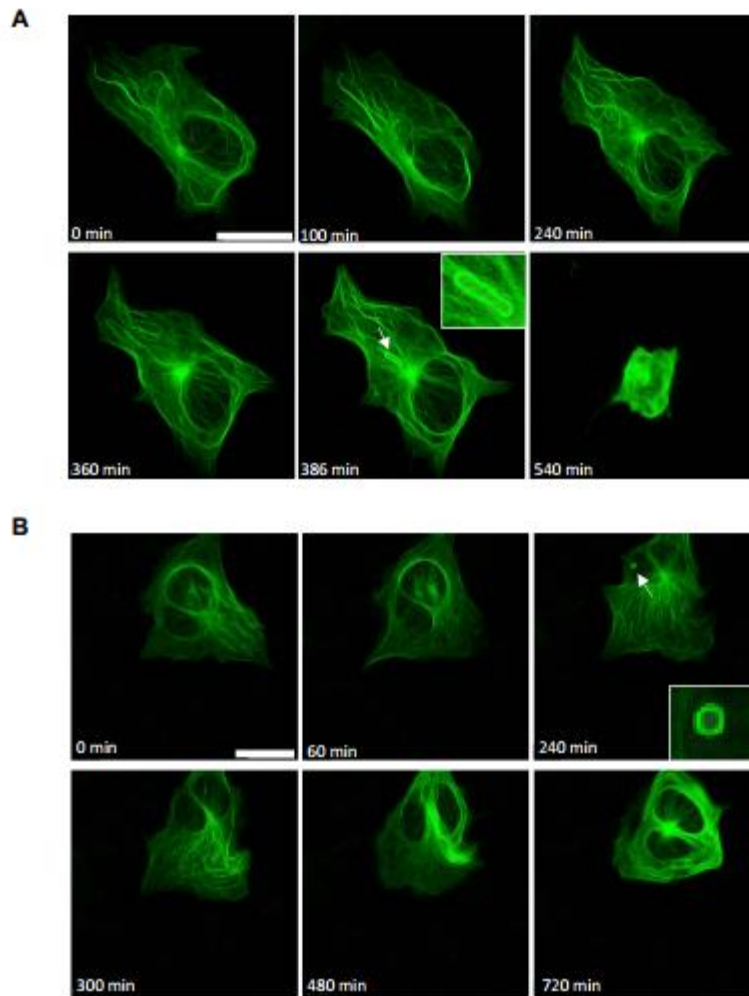
Figure 5.18: Time-lapse imaging reveals the YFP-EML3 S156-161A mutant forms transient ring like structures

A and B. U2OS cells transiently transfected with the YFP-EML3 S156-161A mutant images were imaged 24 hours post transfection using confocal microscopy. Images were captured every 12 minutes for 17 hours. 'Transient Ring structures' are highlighted by the white arrows. Scale bars, 25 μm.

5.3 Discussion

In this section we explore the functional consequences of the interaction between EML3 and the mitotic kinase Nek6. Localisation studies revealed an interesting change in the association of EML3 with MTs as the cell progresses through mitosis. EML3 decorates the MT network neatly in interphase but as the cell enters prophase this localisation becomes less apparent with a more diffuse appearance throughout the cytoplasm. This is maintained in metaphase and only when the cell enters late anaphase does EML3 show a distinct localisation to the MTs. There is particularly strong association of EML3 with MTs during cytokinesis. These phenotypes have been observed in both fixed and time-lapse imaging and a similar phenotype was observed for EML1.

This was surprising and contradicts the findings described in Tegha-Dunghu et al. (2008), in which EML3 was shown to localise to the MTs at all times of the cell cycle. This was reported with both transient transfections of EML3 and an antibody to detect endogenous EML3. However, on close analysis of the microscopy images in this paper YFP-EML3 localisation is not always as clear as they suggest. The YFP-EML3 appears overexpressed in the cells and can be seen throughout the cytoplasm in the prophase and anaphase images. Importantly, specificity of the metaphase signal for the endogenous EML3 was not confirmed in this study by RNAi.

In previous chapters, EML3 has been shown to be a highly dynamic protein. Moreover, the dynamicity of MTs themselves changes upon entry into mitosis. We propose that only a small amount of EML3 is required to be associated with MTs during spindle formation and that EML3 localisation is regulated in a manner that reflects changes in MT stability. Our data implies that EML3 is a MT stabiliser, hence reduced association would coincide with the fact MTs are less stable in prophase and metaphase. Its enhanced localisation to MTs in late mitosis is consistent with the increased stability of MTs in interphase and cytokinesis that is required to establish the central spindle that drives abscission. The fact that RNAi depletion of EML3 causes mitotic defects including misaligned and lagging chromosomes suggests a small amount is required for the right balance of MT dynamics. However, there is always the possibility that these mitotic defects are independent of MTs and work through another mechanism.

Following the interesting changes observed in cellular localisation of EML3 during mitosis we postulated that Nek6 might be responsible for regulating the association of EML3 with MTs. Indeed, Nek6 kinase activity increases during mitosis when the affinity of EML3 for MTs is reduced (Belham et al. 2003). Intriguingly, the phenotypes described upon depletion of EML3 are highly reminiscent of those observed upon Nek6 and Nek9 depletion, which also cause M phase arrest and misaligned chromosomes (Tegha-Dunghu et al. 2008, Kaneta & Ullrich, 2013, O'Regan & Fry 2009). This indicates that these proteins may operate within the same pathway. We demonstrate that endogenous EML3 and Nek6 proteins could immunoprecipitate and that this interaction was enhanced during mitosis. We then showed that Nek6 is able to bind to EML3 via its TAPE domain but is able to phosphorylate residues that reside mainly within the NTD. What's more, expression of the constitutively active Nek6 mutant caused YFP-EML3 to disassociate from the MTs in interphase, whilst active Nek7 had no effect on EML3 localisation. In addition, Nek6 depletion in the U2OS:YFP-EML3 cells caused the YFP-EML3 protein to load onto the spindle during mitosis, most notably metaphase. These data taken together imply that phosphorylation of EML3 by Nek6 causes EML3 to have reduced ability to associate with MTs and confirms that Nek6 is a key regulator of EML3. Phosphorylation of MAPs for regulation is not unusual. Firstly, the neuronal MAP doublecortin (DCX) is phosphorylated on residue Ser-47 by protein kinase A (PKA), Ser-332 by c-Jun N-terminal kinases (JNKs) and Ser-297 by Cdk5. These phosphorylation events are crucial for the displacement of this protein from the microtubules (Toriyama et al. 2012, Teruyuki et al. 2004, Jin et al. 2010). Similarly, phosphorylation of CLIP-170 on Ser312 by Plk1 during mitosis diminishes CLIP-170 binding to the MT ends and lattice (Kakeno et al. 2014). Lastly, the EML precursor protein EMAP undergoes phosphorylation events during mitosis by the p34^{cdc2} kinase (Brisch et al. 1996).

Interestingly, Nek6 autophosphorylation appeared to increase in the presence of EML3. Although this needs repeating, it is possible that EML proteins can act as a scaffold for the Nek kinases, perhaps facilitating dimerization and autophosphorylation in a similar manner to Nek9 (O'Regan & Fry 2009). Alternatively, EML3 might promote the phosphorylation of MTs by Nek6, especially as Nek6 has been shown previously to phosphorylate MTs *in vitro* and can localise to MT structures (O'Regan & Fry 2009).This means rather than being a linear relationship, these proteins may exhibit

feedback mechanisms with EML3 able to regulate Nek6 activity as well as vice versa (Figure 7.1). This idea is similar to that of EMAP and p34^{cdc2} whereby EMAP was proposed as a scaffold for the kinase to access and phosphorylate the MTs as well as itself being a substrate (Brisch et al. 1996). It is also possible that Nek6 removes EML3 so that it can access the MTs itself as it has been shown to localise to the mitotic spindle in metaphase, central spindle in anaphase and midbody in cytokinesis (O'Regan & Fry 2009). Related to this, EML3 is predicted to bind to LC8, a key regulator of Nek9, indicating that EML3 could also play other roles in mitotic Nek kinase control (Regué et al. 2011, Rapali et al. 2011).

As mentioned, Nek6 was able to phosphorylate residues within the NTD of EML3. The two key residues of interest were identified, S156 and S157, that are part of a serine rich patch from residues 156-161. This patch was chosen to generate a multi-site serine to aspartic acid mutant S156-161D. Another serine rich patch earlier within the NTD was also mutated to generate S126-129D. The S126-129D mutant proved to have a relatively minor effect on MT localisation compared to that of wild-type EML3. However YFP-EML3 S156-161D showed a reduction in MT localisation. Conversely, the S156-161A mutant bound to the MT network more tightly than the wild-type protein while in live cell imaging was observed to form circular bundles similar to what was noted for EML4 overexpression (Houtman et al. 2007).

There are two possibilities why these mutants behaved in this way. Firstly, by introducing aspartic acid residues in place of serines, this patch changes from being polar and allowing an electrostatic interaction with the negatively charged tubulin E-hooks, to being negatively charged and thus repelling the E-hooks. This would explain why the S156-161D mutant showed limited MT association. The S126-129D mutant still showed reasonable localisation to MTs despite the introduction of this negative patch, suggesting this region is less involved in MT binding. Secondly, the S156-161D mutant has two residues identified as Nek6 phosphorylation sites, S156 and S157. Therefore, by mutating these to D156 and D157, these residues now mimic phosphorylated residues and the protein behaves in the same manner as EML3 would in mitosis. Conversely, the S156-161A mutant showed increased localisation to MTs in interphase causing what appeared to be MT stabilisation and apoptosis. In this mutant the serine residues have been mutated to alanine such that the original polar

amino acids are now hydrophobic. The hydrophobic group may enhance MT binding and hence associate more strongly to the MTs.

On the other hand, although Nek6 activity is known to increase upon mitotic entry, it is plausible that there is a low level of Nek6 activity during interphase that could lead to basal phosphorylation of EML3. This mutant may therefore show increased association with MTs because it evades the basal level of Nek6 activity in interphase. Furthermore, if this mutant can no longer be phosphorylated as the cell enters mitosis, this may cause sufficient alterations in MT dynamics that cause the cells to enter apoptosis. This also supports the idea that only a very specific amount of EML3 protein is needed on the spindle during mitosis, with too much causing overstabalisation and apoptosis, and too little causes chromosomes to misalign and failure to separate properly.

Lastly, it was interesting that the purified EML3 protein preparation contained other proteins that presumably strongly associated with EML3 in cycling cells. It was not surprising that tubulin was present as EML3 has a strong affinity for both soluble tubulin and the MT network (Richards et al. 2015). Also, based on the data presented here, showing an interaction between EML3 and Nek6, it was reassuring that this kinase was also present. Intriguingly, although there is no evidence that EML3 interacts with Hsp70, this protein has recently been identified as a Nek6 interaction partner (O'Regan et al. 2015). Hsp70 proteins are a family of chaperones that use ATP hydrolysis to assist the folding of polypeptides and maintaining proteins in unstable conformations (Mayer & Bukau 2005). Hsp72 associates with Nek6 and relies on phosphorylation at Thr66 by Nek6 to localise to the mitotic spindle (O'Regan et al. 2015). It could be that Hsp70 was present in the preparation because of its interaction with Nek6 or could it be that EML3 interacts with Hsp70 directly. In this regard it will be interesting to test whether inhibition of Hsp70 alters the stability of EML3, its interaction with Nek6 or its association with MTs. The other coprecipitating protein identified was 14-3-3 epsilon, a small abundant acidic protein present as dimers (Roberts et al. 1997). 14-3-3 dimers bind phosphorylated epitopes on other proteins and are thought to stabilize the modification (Su et al. 2009). Therefore it will be important to test whether the interaction of these proteins with EML3 depend on EML3 phosphorylation and if so, what role they play in regulating the phosphorylation of the protein.

Overall, we have confirmed the interaction of EML3 and the mitotic kinase Nek6 and show that this leads to phosphorylation of EML3 on multiple residues including S156 and S157. We also show that introduction of negative charge causes the NTD to lose interaction with the MTs, potentially through repelling the E-hooks. This can explain the loss of EML3 we find at the mitotic spindle. During late mitosis EML3 may well be required for MT stabilisation and at the central spindle and completion of cell division.

CHAPTER 6   NEK7 INTERACTS WITH EML4-ALK NSCLC VARIANTS

6.1 Introduction

In the previous chapter we discussed how Nek6 regulates EML3 localisation. However, we had also observed cell-cycle dependent changes in EML1 localisation and therefore wished to investigate other potential EML/Nek interactions. The first evidence for EML/Nek interactions came from the proteomics interaction study discussed earlier, in which Nek6 was found to not only associate with EML3 but also with EML2 and EML4. Nek9 and Nek7 were also identified in the screen, hinting towards a wider association between the two protein families. In support of this mass spectrometry analysis of Nek9 immunoprecipitates in our lab identified EML4 as a binding partner (Barone and Fry unpublished studies). Here we have therefore explored the relationship between EML4 with Nek9 and its downstream partners, Nek6 and Nek7.

Importantly EML proteins are indicated in cancer biology and inherited disorders. EML4 can form a fusion protein with anaplastic lymphoma kinase (ALK) with the oncogenic fusion protein present in 5% of non-small cell lung cancer patients. Similarly, EML1 has been shown to form an oncogenic fusion protein with Ableson 1 (ABL1) in T-cell acute lymphoblastic leukaemia, while a point mutation in EML1 leads to the severe brain disorder, neuronal heterotopia (De Keersmaecker 2005, Kielar et al. 2014). Following identification of the EML4-ALK fusion gene patients harbouring the translocation were treated with the ALK inhibitor, Crizotonib. This was highly

effective in inhibiting cancer progression in these patients. Ultimately though these patients soon began to show resistance to crizotonib, mainly as a result of secondary mutations in the kinase portion of the fusion protein (Soda et al. 2007, Katayama et al. 2012). The specific breakpoint in the EML4 gene can vary leading to fusion proteins with different amounts of the EML4 protein. At least 9 individual variants have been identified which all contain different regions of the EML4 proteins (variants outlined in Figure 1.8). All of the variants contain at least part of the EML4 NTD, although they differ in how much if any of the TAPE domain they possess (Richards et al. 2014). All variants have the TD motif which promotes oligomerisation presumably inducing activation of the ALK kinase. This also allows interaction with endogenous EML proteins. However the differing lengths of the variants means that they are likely to exhibit differential regulation and localisation to the MT network.

For this study we have concentrated on V1, V3a and V5. V1 has all of the EML4 NTD as well as part of the TAPE domain. However, it does not localise strongly to the MT network, potentially due to the presence of a truncated TAPE domain that disrupts its folding (Richards et al. 2015). As a consequence, V3a is able to localise to the MTs as it has the full NTD including the basic region between the TD and TAPE domain, but none of the TAPE domain. V5 has only a very small section of the EML4 NTD that encompasses the TD but lacks both the basic MT binding region and the TAPE domain. It is unable to localise to the MTs in interphase (Richards et al. 2015). In this section we present preliminary analysis of the association between Nek9 and Nek7 with EML4 and the EML4-ALK variants.

6.2 Results

6.2.1 EML4 can interact with the mitotic kinase Nek9 and may be phosphorylated during mitosis

Following the interaction identified between Nek9 and EML4 by mass spectrometry we started to investigate the interaction of these proteins further. Firstly, immunoprecipitation experiments were carried out to confirm the interaction between Nek9 and EML4. Cell were transfected with myc-Nek9 and YFP-EML4 or YFP only for 24 hours before lysis and immunoprecipitated with myc antibodies. Western blot of the immunoprecipitate confirmed that the two proteins are able to interact with myc-Nek9 precipitating strongly with YFP-EML4 but not YFP only (Figure 6.1A, data kindly provided by Dr Giancarlo Barone).

From this data we have confirmed an initial interaction between Nek9 and EML4 and from this we wanted to further characterise the pathway and introduce the EML4-ALK variants to incorporate a cancerous aspect to this research. We then investigated whether EML4 might be phosphorylated during mitosis when Nek9 is activated. To do this U2OS cells were transiently transfected with a construct expressing YFP-EML4 NTD for 24 hours. After this time cells were either untreated or synchronised as outlined in chapter 2.2.6. This revealed an upshifted population of YFP-EML4 NTD in the synchronised sample, suggesting that the protein had become phosphorylated and thus migrated more slowly during SDS-PAGE (Figure 6.1B). We speculate that, it may be Nek9, Nek6 or Nek7 that is responsible for this phosphorylation of EML4, based on our data showing phosphorylation of EML3 by Nek6.
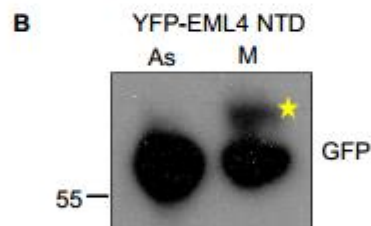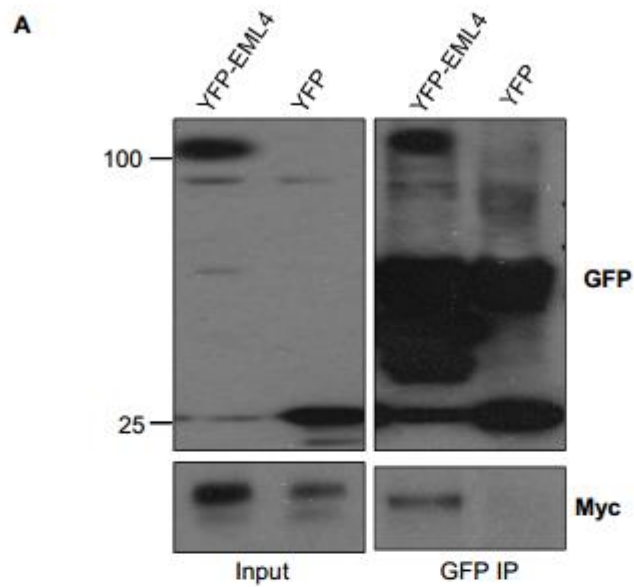
Figure 6.1: EML4 can interact with Nek9 and is phosphorylated during mitosis
A.U2OS cells were co-transfected with myc-Nek9 and YFP-EML4 for 24 hours before cells were lysed and subjected to immunoprecipitation GFP antibodies. Samples were resolved by SDS-PAGE and analysed by Western blot with the antibodies indicated. Molecular weights (kDa) are shown on the left. (Data from Dr Giancarlo Barone). **B.** Cell lysates from asynchronous and nocodazole synchronized (M) U2OS cells transiently expressing YFP-EML4 NTD were western blotted with GFP antibodies. Yellow star represents phosphorylated EML4 NTD population.

6.2.2 Expression of EML4 or activated Nek7 causes altered cell morphology

When we investigated YFP-EML4 localisation, following transient expression in U2OS cells, we found that it is not only localised to MTs but the MTs became elongated and either the cell formed cytoplasmic protrusions or exhibited bundled MTs similar to that seen with taxol treatment (Figure 6.2A). Furthermore, altered cell morphology and cytoplasmic protrusions were observed following the generation of U2OS:YFP-EML4 stable cell lines (O'Regan and Fry unpublished studies). Taken together these data suggest that like EML3, EML4 is a MT stabilising protein, as proposed by Houtman et al. (2007). However, what was particularly interesting was that a similar phenotype was observed following induced expression of constitutively active Nek9 (Barone and Fry unpublished data).

As both EML4 and activated Nek9 overexpression caused altered cell morphology and an increased length in cytoplasmic protrusions, we wanted to identify whether a similar phenotype would be observed upon expression of activated Nek7. U2OS cells were transfected with either wild-type Nek7 or Nek7 Y97A (a constitutively active mutant) for 48 hours before being fixed and stained with Flag and α-tubulin antibodies (Figure 6.2B). Images were then captured using confocal microscopy. The presence of cytoplasmic 'protrusions' were determined by measuring the distance from the edge of the nucleus to the furthest point of the cell membrane. In mock cells the average distance was 41.5 µm, however both wild-type Nek7 and Nek7 Y97A caused a statistically significant increase ($p < 0.0001$) in the average protrusion length to 53.7 µm and 72.2 µm respectively (Figure 6.2C). This reveals that Nek7 like EML4 and Nek9 can alter cell morphology and induce the formation of cytoplasmic protrusions.
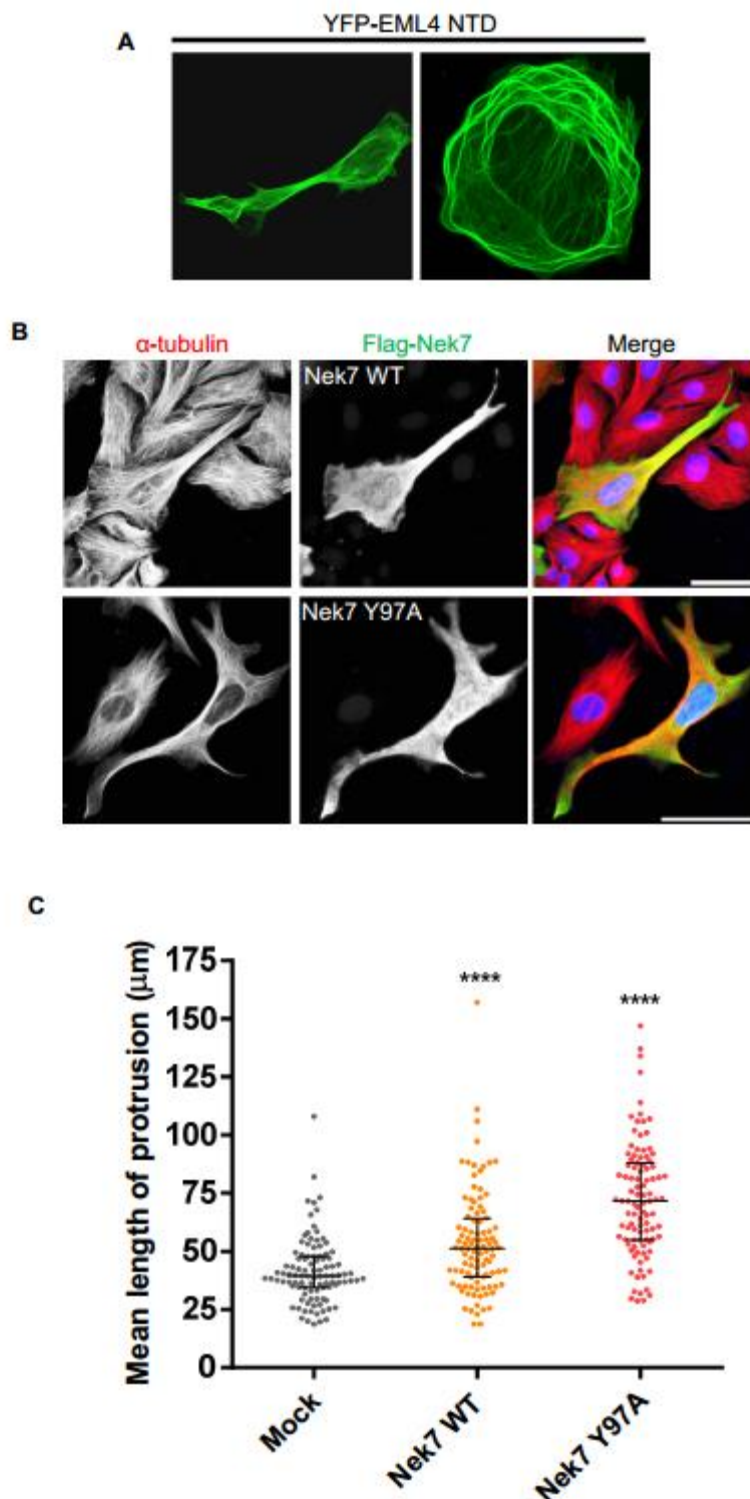
Figure 6.2: EML4 expression or Nek7 activation causes altered interphase cell morphology

A. U2OS cells transiently transfected with the YFP-EML4 NTD were imaged 24 hours post transfection using confocal microscopy. Scale bars 25 µm. **B.** U2OS cells transiently transfected with Flag-Nek7 wild-type or Flag-Nek7 Y97A, a constitutively active mutant. Cells were immunostained with FLAG (green) and α-tubulin (red) antibodies. Merged images include DNA stained with Hoechst (blue). Scale bars, 50 µm. **C.** Dot plot shows protrusion length following expression of Nek7 constructs; measurements were taken from the nuclei to the furthest point of the cell membrane as outlined in chapter 2.4.4). The middle horizontal lines shows the mean and the higher and lower lines represent the upper and lower quartiles respectively. Data represent measurements from 100 cells. (p<0.0001).

6.2.3 EML4-ALK variants alter cell morphology in a Nek7 dependent manner

From the previous data and other work carried out within the Fry lab, it was becoming clear that EML4 was regulated in some way by the Nek9/Nek7 pathway. As a result we decided to focus on analysing the consequence of expression of EML4-ALK V1, V3a and V5 proteins (variants structure outlined in figure 1.8). To confirm expression YFP-EML4-ALK V1, YFP-EML4-ALK V3a and YFP-EML4-ALK V5 were transfected into U2OS cells for 24 hours before cells were lysed and analysed by Western blot analysis using GFP antibodies. This revealed that all three EML4-ALK variants were expressed at the correct size (Figure 6.3A). Cells were then transfected with the EML4-ALK variants for 24 hours before being stained with α-tubulin and GFP antibodies (Figure 6.3B). Immunofluorescence microscopy revealed that these variants also caused changes in cell morphology with an increase in cytoplasmic protrusion length, despite the fact that none of these variants localised obviously to the MT network in this experiment. Quantification showed that all three variants caused an increase in average protrusion length from 30.5 µm in the control sample to 63.5 µm (V1), 71.7 µm (V3a) and 72.3 µm (V5). We then tested whether these EML4-ALK induced protrusions were Nek7 dependent. U2OS cells were transiently transfected as above and then treated for 48 hours with Nek7 siRNAs. Cells were fixed and stained with α-tubulin and GFP antibodies to measure cell morphology (Figure 6.4A). The data confirmed that all three variants induced these protrusions after 24 hours but that these protrusions significantly reduced upon depletion of Nek7. These results indicate that Nek7 is somehow regulating consequences of EML4 and EML4-ALK variant proteins on the cell morphology.
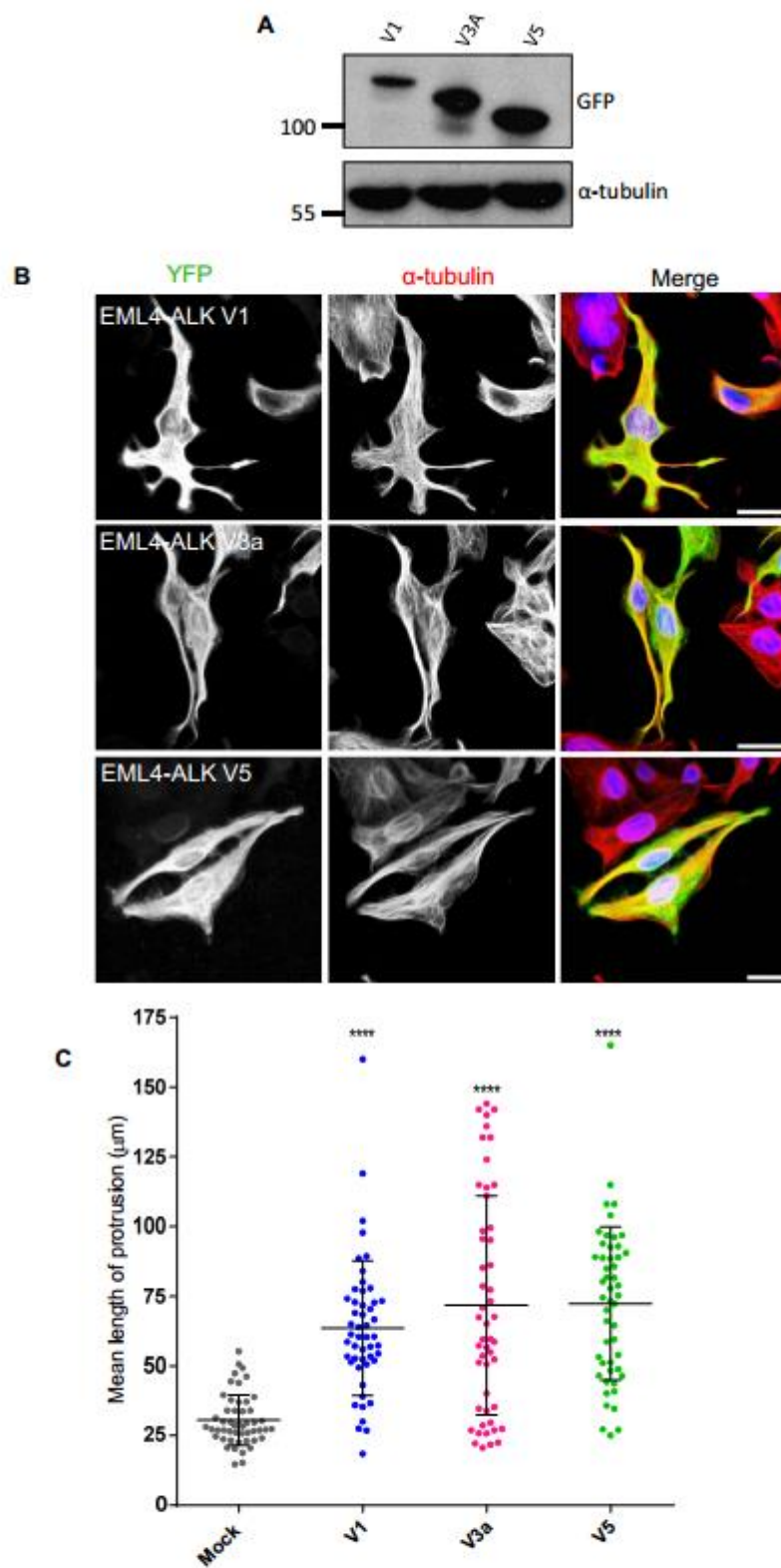
Figure 6.3: EML4-ALK variants causes altered interphase cell morphology

A. Cell lysates from U2OS cells transiently expressing EML4-ALK variants; 1, 3a and 5 were western blotted with GFP and α-tubulin antibodies as indicated. Molecular weights (kDa) are indicated on the left. **B.** Cells transfected as in (A) were immunostained with GFP (green) and α-tubulin (red) antibodies. Merged images include DNA stained with Hoechst (blue). Scale bars, 25 µm **C.** Dot plot shows protrusion length following expression of different EML4-ALK constructs; measurements were taken from the nuclei to the furthest point of the cell membrane. The middle horizontal lines shows the mean and the higher and lower lines represent the upper and lower quartiles respectively. Data represent measurements from 100 cells. (p<0.0001).
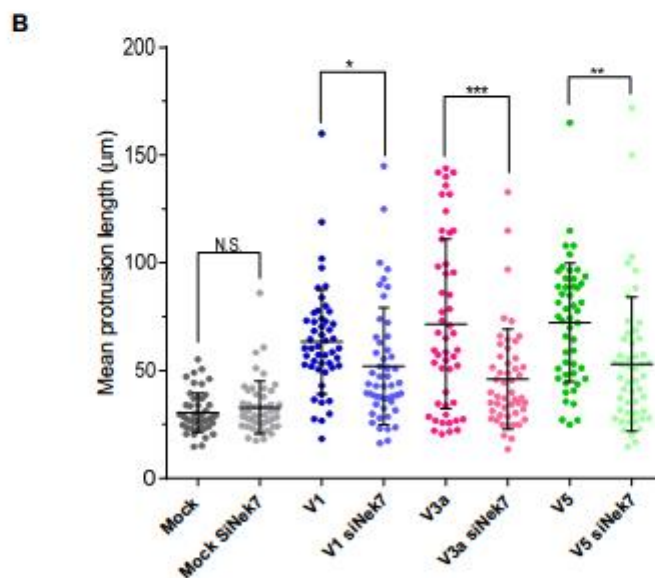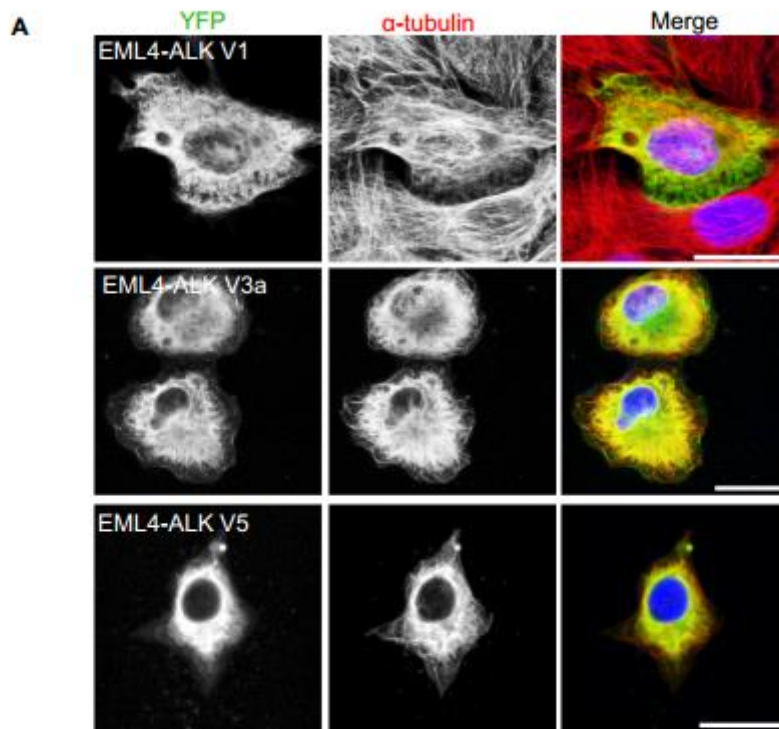
Figure 6.4: EML4-ALK induced morphology changes are dependent upon Nek7

A. U2OS cells were transiently transfected with different YFP-EML4-ALK variants for 24 hours, transfected with Nek7 siRNA for a further 48 hours then immunostained with GFP (green) and α-tubulin (red) antibodies. Merged images include DNA stained with Hoechst (blue). Scale bars, 25 μm. **B.** Dot plot shows protrusion length following depletion of Nek7 in EML4-ALK expressing cells; measurements were taken from the nuclei to the furthest point of the cell membrane. The middle horizontal lines shows the mean and the higher and lower lines represent the upper and lower quartiles respectively. Data represent measurements from 100 cells. (n = 100, V1 p<0.05, V3a p<0.001, V5 p<0.01).

6.3 Discussion

In this chapter we have identified another EML/Nek interaction pathway involving Nek9, Nek7 and EML4. Our observations supported the proposal that EML4 is a MT stabilising protein (Houtman et al. 2007). We obtained evidence that the NTD of EML4 becomes phosphorylated during mitosis, which parallels the phosphorylation of EML3 and phosphosites identified mainly throughout the NTD (see chapter 5.2.3). We propose that the phosphorylation of EML4 is catalysed via Nek9 or its downstream kinase Nek7. This fits the identification of Nek9 in an EML4 mass spectrometry screen. Further to this we confirmed via direct immunoprecipitation that these proteins can interact with one another. We therefore propose that EML4 is regulated by the interaction with Nek7 and Nek9.

Next, we hypothesised that the altered cell morphology, which forms cytoplasmic protrusions, was likely due to altered MT stability as growing MTs are important to coordinate cell shape changes and directed migration during epithelial remodelling. As shown in previous studies and in this study, EML4 is likely to be a MT stabiliser (Houtman et al. 2007). Therefore, if EML4 (or the EML4-ALK variants) is unregulated it stabilises the MTs which become bundled and much longer. These eventually push against the cell membrane, resulting in the formation of protrusions. This a similar phenotype reported by Whipple et al. (2011), whereby mammary epithelial cell lines produce long and dynamic protrusions of the plasma membrane when detached. In this study the protrusions were enriched in detyrosinated tubulin, a modified version of tubulin that promotes MT stability. Video microscopy revealed that these protrusions promoted cell-cell attachment, and inhibiting microtubule-based protrusions correlated with reduced extracellular matrix attachment (Whipple et al 2011). Furthermore, studies with EB1 have highlighted the ability of MAPs to influence protrusion formation and dynamics. EB1 depletion disrupts MT organization in cell extensions, decreases the extensions of flat membrane protrusions (called lamellipodia) and results in loss of opposed protruding and retracting cell edges (Gierke et al. 2012, Schober et al. 2009). EB1 depletion also causes a reduction in the migratory capacity of the cells thought to be due to regulation of both lamellipodial and fingerlike protrusions called (filopodia) (Schober et al. 2009).

In terms of Nek regulation, active Nek9 and Nek7 also stimulated the cytoplasmic protrusion phenotype. From our results it is possible to speculate that active Nek9 and Nek7 maintain the association between EML4 and the MTs, therefore when active Nek9 and Nek7 are expressed EML4 induced MT stabilisation occurs. Alternatively, Nek7 and Nek9 depletion would cause a loss of EML4 association to the MTs, which would destabilise them. This would also explain the reduced MT mean growth speed when Nek7 is depleted (Cohen et al. 2013). Then again, Nek7 may bind EML4 as a means to interact with the MTs themselves. This idea supports the findings that both Nek6 and Nek7 can phosphorylate MT preparations in vitro and that Nek7 regulates MT dynamics in cells (O'Regan & Fry 2009, Cohen et al. 2013).

Likewise, we hypothesised that if Nek9 and Nek7 could regulate EML4, then perhaps these kinases could regulate the EML4-ALK oncogenic fusion proteins prevalent in NSCLC patients. How these variants are involved in cancer progression is not fully understood. The TD domain almost certainly leads to constitutive activation of ALK by facilitating autophosphorylation. However, it is possible the different amounts of NTD present give the fusion proteins different properties. As the NTD contributes to MT binding and is the site of phosphorylation, one would expect it to have distinct effects on the MT network. For this work we concentrated on V1, V3a and V5 as they are structurally quite similar, variants outlined in figure 1.8. As already discussed, V1 has the majority of the EML4 NTD but does not localise strongly to the MT network due to a truncated TAPE domain. Similarly, V5 comprises only a very small section of the EML4 NTD and lacks the basic MT binding region and does not localise to MTs. Conversely, variant V3a is able to localise well to the MTs as it has the full NTD including the basic region between the TD and TAPE domain with no TAPE domain (Richards et al. 2015).

However, evidence for MT dependent protrusions is sparse and arguably these phenotypes could be a result of changes in the actin cytoskeleton, rather than the MT network. Actin is a globular multi-functional protein that forms microfilaments and has many roles including muscle contraction, cell motility, cell division and cytokinesis, vesicle and organelle movement and cell signaling. In order for a cell to migrate it must first become polarized, then at the cell front, actin assembly drives the extension of lamellipodia and filopodia (Le Clainche et al. 2008). Actin is, in part, regulated by myosins, which directly influence actin organization and cell morphology. Myosins are

a family of ATP-dependent motor proteins that play a role in muscle contraction and other actin-based motility processes. For example, the myosin isoform myosin10 is highly expressed in metastatic prostate cancer and knockdown of this isoform has been shown to ablated filopodia and decreased cell migration speed (Makowska et al. 2015). Whereas knockdown of myosin 2B causes bipolar shaped cells which are more elongated than normal (Swailes et al. 2006). Furthermore, many of the phenotypes observed with EB1 depletion, as discussed above, are thought to be mediated by the actin cytoskeleton rather than the MT network (Schober et al. 2009).

 In this chapter, we show that all three variants are able to induce altered cell morphology with clear cytoplasmic protrusions. This was surprising as two of the variants do not localise to the MT network. However, all variants contain the TD domains and could therefore trimerise with endogenous EML4 or other EML proteins in order to affect the MTs. Conversely, there is always a possibility that they are stimulating protrusion formation via another unknown mechanism. Either way, one could speculate the protrusions can increase the migratory capacity of the cell and would account for the invasiveness of tumours expressing the EML4-ALK variants. Additionally, we have convincing data that shows the protrusions induced by the expression of the EML-ALK variants are regulated by the Nek7 kinase. Remarkably, all three variants were influenced by the absence of Nek7. However, the strongest effect of Nek7 depletion was seen with V3a, the variant previously shown to localise to the MT network in interphase. Again, this supports the hypothesis that active Nek9 and Nek7 maintain the association between EML4 / EML4-ALK variants and the MTs and is an interesting interaction for future studies and new cancer therapies.

In conclusion, EML4 was confirmed to be a MT stabilising protein. Transient expression caused elongated MTs resulting in protrusions and rings, a result of MT stabilisation and bundling. Similar consequences were also seen in the U2OS:YFP-EML4 stable cell lines and coincides with the phenotype observed in cells expressing the constitutively active Nek7 or Nek9 mutants. We propose that the protrusions are formed from stabilised MTs due to the presence of EML4 which in turn is regulated by phosphorylation of the Nek9 and Nek7 kinases.

CHAPTER 7   DISCUSSION

7.1 How do EMLs interact with MTs?

EML proteins are a novel class of MAPs, whose mode of interaction with MTs has not been fully characterised. From this study, we have confirmed that EMLs decorate the lengths of the MTs, a localisation pattern not dissimilar to Tau protein in neurons (Harada et al. 1994). However, we have also shown that each member of the family has a different affinity for MTs, with EML2 and EML3 possessing stronger association than EML1 and EML4. This is likely due to differences within the MT binding region and could result in functional differences between the proteins. Likewise, we have identified that EML proteins exist as homo and hetero oligomers with EML1 interacting strongly with itself but also able to interact with EML2 and EML4, whilst EML3 can only strongly interact with itself. This is interesting as it means that EML1, EML2 and EML4 could work in conjunction with one another, whilst EML3 is more likely operating independently.

When we compared the dynamic behaviour of EML3 to EB3 in live cells, there was no obvious directional movement of EML3 along the MTs where EB3 showed typical plus-end tip tracking movement. Despite the lack of obvious movement at the population level of EML proteins, they are nevertheless highly dynamic. FRAP analysis revealed that all four members of the family investigated showed rapid and near complete recovery onto MTs following photobleaching. At this stage, our data would suggests that EML proteins move on and off via simple exchange, this is similar to MCAK, which reaches the plus-tips via diffusion along the length of the MTs (Helenius et al. 2006). Moreover, the EML3 WT protein was unable to recover to the same extent as the NTD alone which indicates a population of the EML3 WT protein is remaining bound to MTs, thus preventing 100% recovery. This is likely to be mediated through the TAPE domain as the NTD alone did not possess the same phenotype and showed a much higher level of recovery. This indicates a novel characteristic of the TAPE domain whereby it 'anchors' a population of the EML3 protein to the MTs.

Previous studies from our lab and others have shown that the NTD of the EML family is required for MT association (Pollmann et al. 2006, Richards et al. 2015). In this study, we confirmed that isolated NTD fragments of EML3 localised strongly to the MT

network in interphase and exhibited faster dynamics than the full length protein. Structural-functional studies on EML1 revealed that the isolated N-terminal region of YFP-EML1 (aa 1-174) strongly associated to the MT network and that the interaction was mediated by both the TD (23-78) and the basic region between the TD and TAPE domain (Richards et al. 2015). Due to the involvement of the TD in this interaction, it could be that only EML trimers have the ability to associate with the MT network. My studies on EML1 revealed that there did not appear to be a specific motif required for MT localisation but that the whole region is required for maximal binding. This suggests that MT association occurs across a relatively extended region.

Microtubules themselves carry a highly negative charge on their surface due to the presence of multiple glutamic acid residues within the C-terminal tails of α and β tubulin. These glutamate rich tails have been referred to as 'E-hooks' and can provide a key interaction surface for basic patches within MAPs and microtubule-associated motor proteins (Janke & Chloë Bulinski 2011). Within this study, we determined that the NTDs of EMLs are extremely basic, with pI values of >11 for EML1 and EML3. Importantly, a subtilisin digestion experiment of purified MTs prevented binding of the EML1 NTD protein *in vitro*. As subtilisin is known to remove the tubulin E-hooks, we propose that the mechanism of interaction is via electrostatic interactions which occur between the basic NTD of EML proteins and the acidic E-hooks present on the surface of microtubules. This is particularly interesting as Hamill et al. 1998 reported that EMAP, the EML protein found in sea urchins, does not utilise the tubulin E-hooks for MT association. However, in support of our findings, we found that introduction of negative charge to the EML3-NTD reduced its affinity for microtubules. Later on, we discuss evidence that shows that Nek6 is responsible for the altered localization of EML3 in mitosis through introduction of negative charge by phosphorylation. Other proteins also utilise the tubulin E-hooks for MT association, including the destabilising MAPs, MCAK and Dam1. MCAK relies on electrostatic interactions with tubulin E-hooks for binding and for fast diffusion of the protein along the MT (Helenius et al. 2006). Similarly, Dam1, the budding yeast kinetochore complex, can form a ring complex around the MTs whereby it's flexible extensions interact with the E-hooks of tubulin to mediate binding; this ring complex can then diffuse along the microtubules (Gardner & Odde 2008, Ramey et al. 2011). Hence, one could hypothesis that EML

proteins use a similar mechanism of diffusion to move along MTs, a mechanism enabled by the tubulin E-hooks.

Lastly, it has been identified that EML3 can bind soluble tubulin via its TAPE domain. This is not unusual for a MAP, as shown by XMAP215 which binds to soluble tubulin dimers with high affinity via its TOG domains, thus promoting MT rescue and supressing catastrophe (Al-Bassam & Chang 2011, Al-Bassam et al. 2010). In terms of EML3, the purpose of this interaction is currently unknown but there are a number of possibilities. Firstly, it could be that the stabilising capacity of EML3 is determined by the addition of tubulin subunits into the MT and that EML3 is therefore responsible for the addition of subunits and consequently MT growth, much like XMAP215. However, if this is the case it is not clear why EML3 localises equally well along the length of MTs. Secondly, it could be that EML3 requires tubulin binding before it can associate with the MTs. Lastly, it may bind soluble tubulin to promote further interactions for example recruiting kinases, such as Nek6, to MTs.

7.2 Is EML3 a MT stabiliser?

This study has provided evidence that in interphase cells EML3 acts as a MT stabiliser. The MT network in EML3 depleted cells showed a greater sensitivity to nocodazole treatment than mock depleted cells. This supports the hypothesis that EML3 contributes somehow to the stabilisation of the MT network, working against the destabilising activities of nocodazole. Further to this, without EML3 the MT network becomes arguable less well defined with individual MTs appearing fragile and less robust. If EML3 has a similar role in mitosis, then one could argue that the mitotic defects identified in EML3 depleted cells could also be a result of unstable MTs. In other words, a certain level of EML3 is required for MT stability during chromosome alignment in metaphase. This is similar to results with the other EML family member, EML4, which is also reported to be a MT stabilising protein. For EML4, overexpression causes bundled MTs and resistance to nocodazole treatment in interphase, whilst depletion disturbs chromosome congression in mitotic cells (Pollmann et al. 2006, Chen et al. 2015).

There are already a number of well characterised MT stabilising proteins including; MAP2, MAP4, Tau, ch-TOG and EB1. Each family of stabilising MAPs may carry out their function differently; MAP2, MAP4 and tau bind to the outer surface of the MTs and stabilize microtubules by favoring polymerization and accelerating growth (Dehmelt & Halpain 2005). XMAP215 proteins, which includes ch-TOG, are tip trackers which contain multiple tubulin-binding TOG domains. They promotes incorporation of tubulin into the growing plus ends or structurally stabilise polymerised tubulin at the plus end ensuring the MT remains in a growth phase (Widlund et al. 2011). EB proteins can recognize growing microtubule plus and minus ends, and they can recruit a range of different factors including APC, dynein, XMAP215 and p150Glued (Vitre et al. 2008). One could argue that EMLs are similar to XMAP215 proteins as both have separable domains for both microtubule binding and soluble tubulin binding. Indeed, the majority of stabilising MAPs discussed here are predominantly associated with the plus-tips, whereas EML3 is associated with the MT lengths and therefore may act through a different mechanism of stabilisation. In order to examine how EML3 operates as a stabilising MAP, *in vitro* assays with purified proteins could be used to measure growth and shrinkage rates. Alternatively, growth and shrinkage rates could be measured in EML3 depleted cells expressing a fluorescent marker of MT tips such as EB3.

7.3 Is EML3 required during mitosis?

In terms of mitosis, it has been shown that EML3 siRNA causes unaligned chromosomes in metaphase (Tegha-Dunghu et al. 2008). Our studies also revealed that depletion of EML3 caused an increase in unaligned chromosomes in metaphase and also lagging chromosomes in anaphase, indicating that although EML3 may not be strongly bound to mitotic MTs a specific amount is required for correct mitosis.Taken together it is apparent that EML3 depletion may activate the SAC, currently there are two models for how the spindle assembly checkpoint is turned off following the attachment of chromosomes. The first is the `attachment model', whereby saturation of kinetochores by spindle microtubules switches off the checkpoint. Secondly is the `tension model', in which the proper tension exerted by

the bipolar microtubules is required to silence the SAC (Zhou et al. 2002). In terms of EML3, we propose EML3 is a stabilizing protein and thus able to regulate MT dynamics in both interphase and mitosis. Therefore, upon EML3 depletion there is a loss in this MT regulation resulting in either a lack of bipolar attachment or a lack of tension which results in SAC activation. Another possibility is that EML3 activates the SAC through another mechanism such as through its ability to recruit crucial kinetochore proteins such as CENP-E or BUBR1. Without all the required proteins the kinetochore-microtubule interface is compromised and could alter MT-kinetochore attachments thus resulting in SAC activation. This wouldn't be surprising as EML4 has recently been shown to regulated NUDC localisation, a protein required for chromosome alignment and for the recruitment of Plk1 and CENP-E to the kinetochore (Chen et al. 2015, Nishino et al. 2006).

This study also provided further evidence for a role of EML3 in mitosis. Human EML3 is a 95kDa protein, identified during a screen for nuclear proteins that bound to MTs in mitosis (Tegha-Dunghu et al. 2008). The study by Tegha-Dunghu and colleagues showed EML3 to be localised strongly to the MTs throughout all mitotic stages but was mainly nuclear during interphase. In contrast, our results showed that EML3 localised prominently to MTs in interphase with no detectable localisation within the nucleus. There was a reduced affinity for mitotic MTs from prophase to anaphase, before EML3 reassociated to MTs during telophase and cytokinesis. Despite this reduced association of EML3 with MTs in mitosis, EML3 depletion interfered with the correct alignment of chromosomes during metaphase and chromosome separation in anaphase. This indicates that a small fraction of EML3 likely remains on spindles to ensure the right level of MT dynamics for proper mitosis to occur. We therefore propose that the affinity of EML3 for MTs is reduced in mitosis but that there is not total loss of protein from the spindle.

There could be a number of reasons why EML3 was shown to localise strongly to spindle MTs in metaphase cells in the study by Tegha-Dunghu et al. (2008); Firstly, different cell types could give different results due to differences in expression of MAPs, regulators and tubulin isoforms. Our studies were done using U2OS cells whereas their study used HeLa cells, if one cell type has reduced Nek6 levels, a

regulator of EML3 identified in this study, then EML3 would associate more strongly to the mitotic spindle in mitosis. Alternatively, if MAPs are expressed which out compete EML3 then this could reduce binding. Secondly, lack of specific EML3 antibodies meant that we have relied upon analysis of recombinant EML3 and we have not been able to address endogenous EML3 localization in U2OS cells. However, loss of YFP-EML3 from the mitotic spindle was observed by both fixed and time-lapse imaging indicating that this is unlikely to be an artefact of cell fixation or epitope masking. Similar results were also observed in fixed U2OS cells with Flag-EML3. Tegha-Dunhgu and colleagues reported localization of YFP-EML3 at the mitotic spindle in HeLa cells. This argues against a different behaviour between the endogenous and recombinant proteins. Furthermore, Tegha-Dunghu and colleagues developed their own antibody, but on close inspection the western blot used to validate this antibody has a number of additional bands, one of which is around 55kDa, the same molecular weight as tubulin. On the other hand, Tegha-Dunghu and colleagues did observe a change in localization of the MT-binding N-terminal fragment of EML3, which localised to interphase MTs but not mitotic MTs. This fits well with our proposed model that EML3 exhibits altered affinity for MTs in mitosis due to phosphorylation within the NTD. Nevertheless, the fact that we also observed mitotic chromosome attachment defects upon EML3 depletion argues that a small amount of EML3 may remain associated with and regulate MTs in mitosis (Tegha-Dunghu et al., 2008).

7.4 Is EML3 regulated by Nek6?

In this study we have identified an interesting property of EML3, whereby its affinity for MTs changes in accordance with the stage of the cell cycle. This raises the question of how EML3 is regulated and which proteins are responsible for this regulation. Our starting point came from the large scale protein-protein interaction screen carried out by Ewing and colleagues, which found a strong association between the mitotic serine/threonine kinase Nek6 and EML3 (Ewing et al. 2007). Furthermore the mitotic consequences of EML3 depletion are highly similar to depletion of Nek6 and Nek9 depletion, with M phase arrest and misaligned chromosomes observed in all cases (O'Regan & Fry 2009, Tegha-Dunghu et al. 2008, Roig et al. 2005). Similarly, it is not unusual for MAPs to be regulated by kinases, for example the neuronal MAP

doublecortin (DCX) is phosphorylated on residue Ser-47 by protein kinase A (PKA), Ser-332 by c-Jun N-terminal kinases (JNKs) and Ser-297 by Cdk5. These phosphorylation events are crucial for the displacement of this protein from the microtubules (Toriyama et al. 2012, Teruyuki et al. 2004, Jin et al. 2010). Whilst, phosphorylation of CLIP-170 on Ser312 by Plk1 during mitosis diminishes CLIP-170 binding to the MT ends and lattice (Kakeno et al. 2014).

In this study we show Nek6 to be a major regulator of EML3 localisation. First, we confirmed that these proteins interact in cells and identified that the interaction between the proteins is significantly enhanced in mitosis. Evidence that there is a function behind the interaction came from demonstration that untimely activation of Nek6 in interphase led to loss of EML3 from MTs, while depletion of Nek6 in mitosis led to increased accumulation of EML3 on spindle MTs in mitosis. We already know that EML3 associates with MTs via an electrostatic interaction between the basic region of the EML3 NTD and the E-hooks of tubulin.
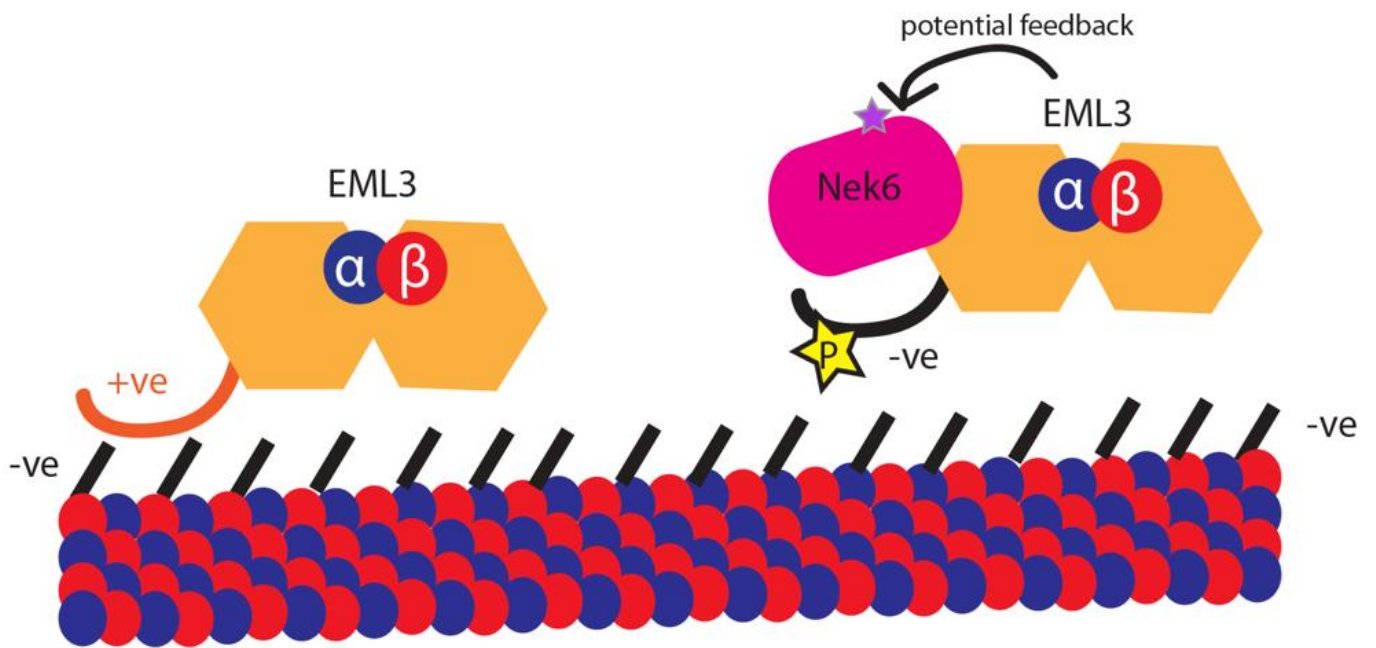
Figure 7.1: The interaction between EML3 and MTs

EML3 strongly associates to the MT network in interphase but this association is reduced at the onset of mitosis. EML3 associates to MTs via its positively charged NTD which enables an electrostatic interaction with the negatively charged tubulin E-hooks. Phosphorylation of residues within the NTD by Nek6 reduces the net charge of the NTD causing EML3 to lose MT association at the onset of mitosis.

This led us to propose that activation of Nek6 upon mitotic entry leads to phosphorylation of EML3 thereby reducing its affinity for MTs by blocking key electrostatic interactions (Outlined in Figure 7.1). We hypothesise that this contributes to the altered MT stability that is observed in mitotic cells, which is necessary for accurate chromosome congression and segregation.

Incorporating this newly identified pathway with what is already known about Nek6 leads to the following model: Nek6 is activated by the upstream kinase Nek9 at the onset of mitosis, Nek6 activation then causes the majority of EML3 to disassociate from the mitotic MTs helping to remodel the MTs during spindle assembly, then as the level of Nek6 kinase activity decreases at the end of mitosis, EML3 is presumably dephosphorylated enabling it to reassociate with the MT network. Interestingly, we identified that Nek6 interacts with EML3 via the TAPE domain, despite the majority of phosphorylation occurring on residues within the NTD. Similar experiments carried out with the closely related kinase Nek7 had no effect on EML3 localisation, so we predict this is a specific interaction between Nek6 and EML3. However, based on other results there is possibly an interaction between Nek7 and EML4 and so it would be interesting to extend this study to the other EML family members and mitotic Nek kinases to gain further understanding of how these two families interact.

Nek6 was able to phosphorylate multiple residues in EML3 mainly throughout the NTD. Two residues in particular were of interest to us, namely S156 and S157, as these are the first two serines of a six serine patch which falls between residues 156-161. These results led us to generate a multi-site serine to aspartic acid mutant S156-161D in the full-length EML3 protein. For comparison, another serine rich patch earlier within the NTD was also mutated to generate S126-129D. Expression of these two mutant proteins in cells revealed that the S126-129D mutant showed relatively similar MT localisation to that of wild-type EML3. However, the YFP-EML3 S156-161D mutant showed an obvious reduction in MT localisation. There are two possible explanations for this: firstly, by introducing aspartic acid residues in place of serines, this patch changes from being polar, to being negatively charged thus repelling interaction with the tubulin E hooks on the surface of the MTs. Secondly, the S156-161D mutant has two residues identified as Nek6 phosphorylation sites, S156 and S157. Therefore, by mutating these to D156 and D157, these residues now mimic phosphorylated EML3,

which equally blocks MT association. The S126-129D mutant still showed reasonable localisation to MTs, this region is less likely to be involved in MT binding.

According to our model, failure to phosphorylate EML3 should lead to EML3 retaining an abnormally high affinity for microtubules in mitosis and this could disturb spindle assembly and chromosome congression. To test this, we generated an YFP-tagged EML3-S156-161A mutant. This bound strongly to the interphase microtubule network, even more tightly than the wild-type protein. Unfortunately, neither fixed nor time-lapse imaging was able to detect mitotic cells expressing this protein, despite high transfection efficiencies. This could suggest that for some reason this mutant blocked mitotic entry or promoted apoptosis. Indeed, the formation of highly elongated and bundled MTs was observed in cells expressing this mutant. Unusual, short-lived circles of the EML3 mutant protein were also frequently observed that most likely represent bundled microtubule rings, similar to those noted upon EML4 overexpression (Houtman et al. 2007). With respect to regulation by Nek6 it is likely that there is a low level of Nek6 activity during interphase that could lead to basal phosphorylation of EML3. This mutant will not be subject to basal phosphorylation potentially explaining the increased association with MTs.

To extend these experiments, it would be necessary to make more restricted S156/157D mutants, as these were the two specific sites identified in the Nek6 phosphosite analysis screen. This would distinguish whether the phenotypes observed with the current mutants are due to specific mutations of these two sites or due to disrupting the larger patch of serines. In conclusion, our results support the following pathway: Nek6 binds to the highly structured TAPE domain of EML3, Nek6 then phosphorylates the EML3 protein on specific sites, mainly within the NTD, including two key residues; S156 and S157. This phosphorylation causes the majority of EML3 to disassociate from MTs on the onset of mitosis. However, as the cell exits mitosis, the kinase activity of Nek6 decreases allowing EML3 dephosphorylation and its reassociation to the newly established interphase MT network. An overview of the cellular roles of EML3 from this study are outlined in Figure 7.2.
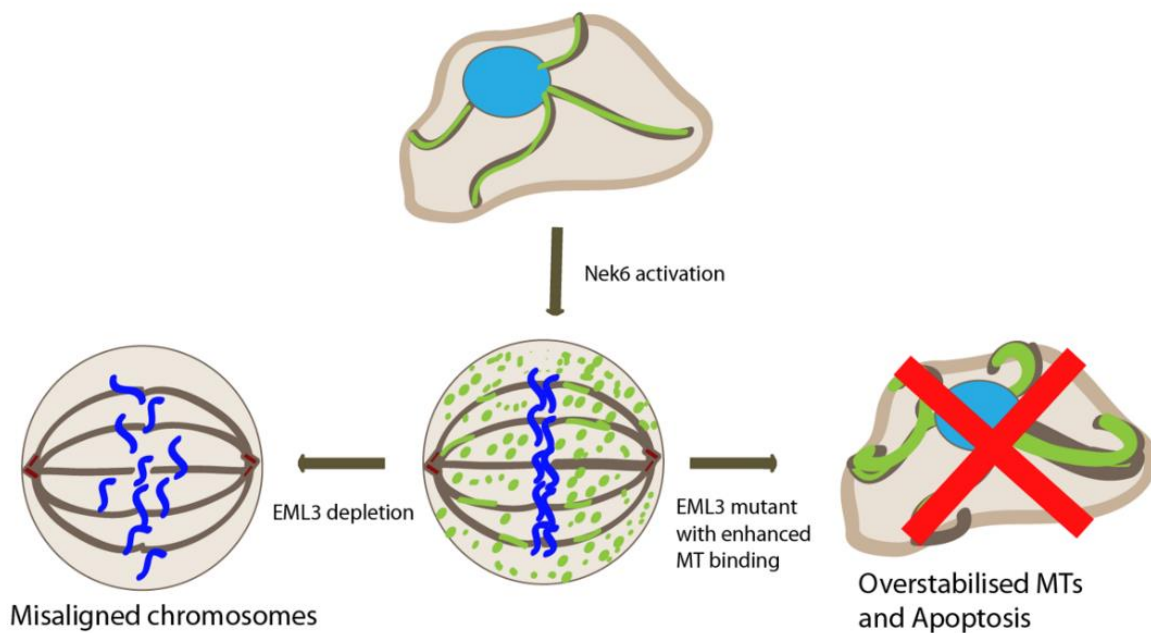
**Figure 7.2: The cellular roles of EML3**

EML3 localises to the MTs in interphase whereby it stabilises the MT network. At the onset of mitosis Nek6 phosphorylation causes a reduced affinity of EML3 for mitotic MTs. Complete loss of EML3 causes misaligned chromosomes in metaphase whilst a phosphonull EML3 mutant with enhanced MT association causes bundled MTs and eventually leads to apoptosis.

The above pathway describes the interaction between Nek6 and EML3 as linear, with Nek6 upstream of EML3. However, results from this study and others within the lab have raised the possibility of Nek6 being regulated by EML3. This suggests that these proteins may be able to exhibit feedback mechanisms with EML3 able to regulate Nek6 activity as well as vice versa. It is possible that EML proteins can act as a scaffold for the Nek kinases, perhaps facilitating dimerization and autophosphorylation in a similar manner to Nek9 (O'Regan & Fry 2009). Scaffolding proteins either facilitate flow of activation from one kinase to the next in a signaling cascade or hold the protein kinase in a state that promotes interaction with other partners. It is not unusual for kinase pathways to rely on scaffolding proteins; for example the mitogen-activated protein kinase (MAPK) pathway relies on scaffolding proteins, Ste5 in yeast and the kinase suppressor of Ras (KSR) in mammals, for efficient signal transduction (Good et al. 2011, Dhanasekaran et al. 2007). Equally, EML3 might recruit Nek6 to the MTs for direct phosphorylation of tubulin. Indeed, Nek6 has been shown to phosphorylate MTs *in vitro* and localise to MT structures (O'Regan & Fry 2009).This means that Nek6 may directly phosphorylate MTs to alter their dynamics in a similar manner to how EMAP is thought to act as a scaffold for the p34^{cdc2} kinase where it can directly phosphorylate MTs (Brisch et al. 1996). This could explain why the TAPE domain of EML3 can associate with soluble tubulin, to modulate the interaction with Nek6. It could also be that Nek6 removes EML3 from the spindle in order to access the MTs itself; this would explain why Nek6 has been shown to localise to the mitotic spindle in metaphase, central spindle in anaphase and midbody in cytokinesis (O'Regan & Fry 2009). It will therefore be very interesting to extend this study by ascertaining whether EML3 can regulate Nek6. This could be carried out by depleting EML3 and comparing Nek6 localisation and kinase activity during both interphase and mitosis in the presence and absence of EML3.

Nek6 itself has already been identified as a regulator of other proteins including Eg5 and Hsp72. In our study we have shown that Nek6 binds to the TAPE domain of EML3 but can phosphorylate residues, both within the NTD and at the extreme C-terminus. Similarly, Nek6 is able to bind to the C-terminal tail of Eg5 via residues 762-1057 and can phosphorylate both the head and tail of the kinesin (Rapley et al. 2008). This phosphorylation is essential to enable Eg5 localisation to centrosomes and spindle bipolarity (Rapley et al. 2008). Likewise, Hsp72 relies on phosphorylation by Nek6 to

localise to the mitotic spindle (O'Regan et al. 2015). Taken together, this indicates that Nek6 is likely to have multiple substrates in mitosis explaining the need for Nek6 activation for correct spindle assembly in mitosis. On the other hand, increased Nek6 expression has been linked to lung, liver and stomach cancers perhaps contributing to deregulated cell division (Uhlén et al. 2005, Uhlen et al. 2010, Berglund et al. 2008). As a result, Nek6 could be a useful target for future cancer treatment although more needs to be understood about its substrates to predict the likely consequences of Nek6 inhibitors.

7.5 Are there other potential interacting partners of EML3?

To date there is limited knowledge on EML3 partners, other than soluble and polymerised tubulin and Nek6. However, proteomics data has suggested LC8 as a potential partner (Regué et al. 2011). Whilst our mass spectrometry analysis has identified Hsp70 and 14-3-3 proteins.

LC8 is a protein essential for survival, with LC8 depletion causing severe pleiotropic phenotypes in cells and embryonic lethality in animals (Rapali et al. 2011). EML3 has a perfect LC8 binding motif, (K/R) XTQT, at residues 83-87 (RGTQT) within the N-terminal domain. Although the role of this interaction is unknown, it has been postulated that LC8 supports EML3 trimerisation or LC8 has the ability to oligomerise (Rapali et al. 2011). Interestingly, LC8 is a key regulator of Nek9, with LC8 acting as a competitive inhibitor of Nek6 and Nek7 binding. According to current models, autophosphorylation of Nek9 on Ser944 disturbs LC8 binding enabling it to then bind to Nek6 and Nek7 (Gallego et al. 2013). As a result, one could hypothesis that EML3 binds LC8 in order to allow Nek9 to bind and activate Nek6 and Nek7. This would support the notion that Nek6 and EML3 are part of a feedback pathway. In order to test this theory, experiments would need to be carried out to first confirm the interaction between EML3 and LC8 and then mutagenesis to look for the consequences of disrupting this binding.

Hsp70 proteins are a family of chaperones that use ATP hydrolysis to assist the folding of polypeptides and maintain proteins in unstable conformations (Mayer & Bukau 2005). It has been identified that Hsp72 is phosphorylated by Nek6 in mitosis to ensure the formation of a robust spindle (O'Regan et al. 2015). Therefore, it could be that Hsp70 was present in the EML3 preparation because of its strong interaction with Nek6. Alternatively, EML3 could interact directly with Hsp70. If the latter is the case, it could be that Hsp70 is required to maintain the stability of EML3 and it would be interesting to test whether inhibition of Hsp70 alters the stability of EML3, its interaction with Nek6 or its association with MTs.

14-3-3 family members are small abundant acidic proteins that bind phosphorylated epitopes on other proteins (Su et al. 2009, Roberts et al. 1997). Therefore it would be interesting to determine whether the interaction of 14-3-3ε with EML3 depends on EML3 phosphorylation by Nek6 and if so, what role this plays. For example, 14-3-3ε might preferentially bind to EML3 in mitosis and sequester EML3 away from MTs, thus providing an alternative explanation for why the phosphorylated protein is lost from mitotic spindles.

7.6 How does EML3 influence the activity of MT poisons?

Current cancer treatments tend to block a major process, such as nucleotide metabolism or division rather than targeting specific defective pathways. The anti-mitotic drugs used in the clinic are generally MT poisons that act to prevent the cancer cell from forming a spindle and dividing, these include the vinca alkaloids and the taxanes. However, these drugs have severe side effects due to the non-specific target of MTs and often patients show resistance through various mechanisms. One such mechanism is the expression level of MAPs; for example MAP4 expression correlates with decreased taxol sensitivity in ovarian cancer cell lines.

In this study we wanted to ascertain whether the association of EML proteins with MTs was affected by MT poisons as well as whether EML expression altered the sensitivity of MTs to these drugs. Both EML1 and EML3 associated with MTs in the presence of taxol to a similar extent as in cultured cells, meaning that taxol was not hindering MT

binding. However, FRAP analysis indicated that EML3 was unable to recover to the same level on taxol stabilised MTs. There could be a number of reasons for this. Firstly, taxol might somehow affect the movement of EML3 along the MTs. Secondly, the increased amount of polymerised tubulin in taxol-treated cells mean that all of the available EML3 protein might become associated with the MT network leaving no cytoplasmic EML3 to allow on-off recovery. Lastly, EML3 may need to associate with soluble tubulin in order to decorate the MT network and this would be hampered if there is no remaining soluble tubulin in the cell. Whatever the explanation, the effect of taxol on EML3 dynamics highlights the profound effect taxol can have on a range of proteins associated with the MTs. This could cause further detrimental effects on the cytoskeleton, by altering the finely tuned balance of MAPs. For example, if taxol is able to alter the distribution of EML3 within the cell it could alter the ability of EML3 to act as a tumour suppressor (discussed further in section 7.7). Long term drug exposure could also cause up regulation or down regulation of EML expression which in time could enable cells to become drug resistance. In conclusion, it is clear that more understanding of MT dynamics and MAP expression is required. Understanding the MAPs affected by a certain MT poison, how the drug interacts with MTs and whether MAPs become up-regulated or down-regulated could be valuable in terms of considering how to use the drugs in patients.

7.7 EML fusion proteins and cancer chemotherapy

Both EML1 and EML4 are able to form oncogenic fusion proteins being detected in T-cell acute lymphoblastic leukaemia and non-small cell lung cancer, respectively. From this, we suggest that EML proteins could be used as future cancer biomarkers. Biomarkers provide specific information about a cancer and allows for more precise treatment to be given to patients. They also allow monitoring of the disease during treatment and detection for recurrences after treatment. Current biomarkers used clinically already include: BRCA1 in breast and ovarian cancer (James et al. 2007), ALK in non-small cell lung cancer and anaplastic large cell lymphoma (Vincent et al. 2012) and prostate-specific antigen in prostate cancer (Velonas et al. 2013). In the case of BRCA1, a protein involved in repairing chromosome damage, clinicians can

examine genomic DNA extracted from a blood sample to measure the levels of BRCA1 or the presence of mutations. The majority of mutations are protein-truncating or missense mutations, both resulting in an ineffective BRCA1 protein (Balmana et al. 2011). For ALK translocations, fluorescence in situ hybridization (FISH) is regarded as the gold standard of detection (Kim et al. 2011). In terms of EML proteins, EML1 and EML4 are truncated in T-cell acute lymphoblastic leukaemia and non-small cell lung cancer respectively, meaning clinicians can look for truncated transcripts and determine the particular fusion variant expressed. This could be especially informative considering the different drug sensitivities of the EML4-ALK variants, with Hsp90 inhibitors being most effective, for example, against variants 1 and 2 (Richards et al. 2014).

Our studies show that depletion of EML3 causes misaligned chromosomes in metaphase and lagging chromosomes in anaphase. This leads to abnormal divisions which in turn can promote the "evolution" of a tumour (Green et al. 2005). We therefore suggest that wild-type EML3 could act as a tumour suppressor, regulating proper mitosis and preventing tumour formation. A similar situation exists for the well characterised tumour suppressor, Alternative Reading Frame (ARF), protein. Depletion of ARF causes mitotic defects including misaligned and lagging chromosomes and multipolar spindles, despite no obvious role in cell division (Britigan et al. 2014). Loss of ARF is linked to numerous cancers and homozygous deletions are found in glioblastoma. However, there is currently no evidence to show that EML3 is lost or mutated in any types of cancer. Nevertheless, it remains possible that there are copy number alterations or mutations in particular cancer subtypes that are yet to be discovered.

Another interesting finding was the fact that activated Nek7 or Nek9 expression or expression of EML4-ALK variants caused cells to form extended cytoplasmic protrusions. This phenotype is of particular interest because it could reflect altered adhesion or migratory capacity of the cells that in cancer could promote metastasis. During this process, the cancer cell detaches and migrates away from the primary tumor site invading neighboring tissue and in some cases enter the blood or lymphatic vessels. From here they can then exit the blood or lymphatic vessels at a distant organ and form secondary tumors (Yao et al. 2011). Additional experiments are being carried out within the lab to identify whether cells overexpressing activated Nek7 or Nek9 or

EML4-ALK variants have increased migratory capacity using migration and invasion assays. Western blot analysis is also being undertaken to identify whether the cells are undergoing an epithelial-mesenchymal transition (EMT). EMT is thought to be critical for the initial transformation from benign to invasive carcinoma whereby cells lose their cell polarity and cell-cell adhesion, and gain migratory properties. EMT is not fully characterized but is mainly associated with loss of E-cadherin, required for cell-cell adhesions, is regulated by transcription factors such as Snail1 (Snail), Snail2 (Slug), Twist, EF1/ZEB1, SIP1/ZEB2, and/or E47 (Yang & Weinberg 2008). It is therefore interesting that expression of the EML4-ALK variants could somehow stimulate EMT and increase the metastatic capacity of the tumor.

Furthermore, these data demonstrates a potential link between the Nek9/Nek7 pathway and EML4/ EML4-ALK regulation. As stated, cytoplasmic protrusions formed with activated Nek7 or Nek9, or EML4-ALK variant expression. These observations suggest a pathway whereby Nek9 activates Nek7 which in turn regulates EML4. Hence, Nek7 could regulate the association of EML4 with MTs is the same way that Nek6 regulates association of EML3 with MTs. Indeed, depletion of Nek7 caused a significant reduction in the ability of the EML4-ALK variants to form cytoplasmic protrusions. Currently, treatment of NSCLC patients with EML4-ALK expression involves the ALK inhibitor, Crizotonib, and the Hsp90 inhibitor, Ganetespib. However, patients treated with these drugs show varying responses, thought to be due to differences in variant expression (Heuckmann et al. 2012, Katayama et al. 2012). In terms of our study, the cytoplasmic protrusions induced by all three of the EML4-ALK variants tested were reduced upon Nek7 depletion. Thus, Nek7 inhibitors could have some benefit in treating EML4-ALK NSCLC in the future.

7.8 Concluding remarks

The first aim of this study was to provide new insights on the interaction of EML proteins with MTs. We have confirmed that EML proteins decorate the lengths of MTs with no detectable preference for MT ends. We have shown that the interaction with MTs is dynamic and mediated through the NTD, specifically through the TD and basic region before the TAPE domain. We have also demonstrated that EMLs likely

associate with MTs via tubulin E-hooks, which could allow for fast lateral diffusion of these proteins along MTs. Moreover, we have shown that EMLs preferentially form homo-oligomers but some, namely EML1, have the ability to interact with other members of the EML protein family. We also have evidence that EML protein have differing affinities for MTs, with EML2 and EML3 binding more strongly in interphase than EML1 and EML4.

The second aim was to characterize the roles of EML3 and test whether this protein is essential for maintenance of the interphase MT network and for mitotic progression. In this study, we present evidence that EML3 is a MT stabilizing protein, but unexpectedly found that the affinity of EML3 for MTs is reduced as the cell enters mitosis. However, a specific amount of EML3 must remain associated with mitotic MTs as depletion of EML3 causes a range of mitotic defects, including both misaligned chromosomes in metaphase and lagging chromosomes in anaphase.

The third aim was to study the regulation of EML3 by Nek6. Depletion of Nek6 caused EML3 to accumulate on the mitotic spindle in metaphase, whilst expression of active Nek6 caused loss of EML3 from the MT network in interphase. These phenotypes were not seen when similar experiments were carried out with Nek7. Further to this, we identified specific Nek6 phosphorylation sites within both the NTD and CTD of EML3, including both S156 and S157, the first two serines of a six serine sequence. When this serine patch was mutated to aspartic acid residues, localisation to the interphase network was greatly reduced, indicating that either these serines or the local charge are crucial for MT association. We therefore propose the following model: Nek6 is activated at the onset of mitosis by the upstream kinase Nek9. Nek6 then interacts with the TAPE domain of EML3 and phosphorylates specific residues, including S156 and S157 within the NTD. This causes EML3 to have a reduced affinity for mitotic MTs. As the cell enters cytokinesis the kinase activity of Nek6 decereases, allowing dephosphorylated EML3 to reassociate with the interphase MT network. Clearly, additional experiments need to be carried out to understand how EML3 stabilizes MTs in interphase and what exactly EML3 is doing during mitosis.

Lastly, we were able to identify additional interactions between members of the EML and Nek kinase families, namely Nek7 and EML4. Overexpression of EML4, Nek7 or Nek9 causes a change in cell morphology with the formation of cytoplasmic

protrusions, potentially resulting from changes in MT dynamics. This led us to hypothesis that these proteins form part of the same pathway. In this study we showed that a range of EML4-ALK fusion variants were also able to generate these protrusions and that this was dependent on Nek7 expression. It is possible that Nek7 phosphorylation of EML4-ALK mediates its localization to the MTs. This has particular importance as EML4-ALK fusions are found in 5% of NSCLC patients. Current NSCLC treatments cause a range of unpleasant side effects, are ineffective against all variants, and eventually patients develop drug resistance. Hence, a better understanding of the regulation of EML4-ALK fusion proteins raises the prospect of improved therapeutic options for these patients in the future.

CHAPTER 8   BIBLIOGRAPHY

Akhmanova, A & Steinmetz, M.O., 2008. Tracking the ends: a dynamic protein network controls the fate of microtubule tips. *Nature Reviews: Molecular Cell Biology*, **4,** 309-322.

Al-Bassam, J., Kim, H., Brouhard, G., Van Oijen, A., Harrison, S., Chang, F., 2010 CLASP promotes microtubule rescue by recruiting tubulin dimers to the microtubule. *Developmental Cell*, **19,** 245–258.

Al-Bassam, J. & Chang, F., 2011. Regulation of Microtubule Dynamics by TOG-domain proteins XMAP215/Dis1 and CLASP. *Trends in Cell Biology.* **21,** 604–614.

Alushin, G.M., Lander, G.C., Kellogg, E.H., Zhang, R., Baker, D., Nogales, E. 2014. High resolution microtubule structures reveal the structural transitions in αβ-tubulin upon GTP hydrolysis. *Cell*, **5,** 1117-1129.

Andersen, S.S.L., Buendia, B., Domfnguez, J.E., Sawyer, A., Kansenti, E.,1994. Effect on microtubule dynamics of XMAP230, a microtubule-associated protein present in Xenopus laevis eggs and dividing cells. *The Journal of Cell Biology*, **127,** 1289–1299.

Aoki, K. & Taketo, M.M., 2007. Adenomatous polyposis coli (APC): a multi-functional tumor suppressor gene. *Journal of Cell Science*, **120,** 3327–3335.

Bahe, S., Stierhof, Y.D., Wilkinson, C.J., Leiss, F., Nigg, E.A., 2005. Rootletin forms centriole-associated filaments and functions in centrosome cohesion. *Journal of Cell Biology*, **171,** 27–33.

Balmana, J., Diez, O., Rubio, I.T., Cardoso, F., 2011. BRCA in breast cancer: ESMO Clinical Practice Guidelines. *Annals of Oncology*, **22,** 31–34.

Barlan, K., Lu, W. & Gelfand, V.I., 2013. The microtubule-binding protein ensconsin is an essential cofactor of kinesin-1. *Current Biology*, **23,** 317–322.

Barnes, L.M., Moy, N. & Dickson, A.J., 2006. Phenotypic variation during clonal procedures: analysis of the growth behavior of clonal cell lines. *Biotechnology and Bioengineering*, **94,** 530-537.

Belham, C., Roig, J., Caldwell, J.A., Aoyama, Y., Kemp, B.E., Comb, M., Avruch, J., 2003. A mitotic cascade of NIMA family kinases: Nercc1/Nek9 activates the Nek6 and Nek7 kinases. *Journal of Biological Chemistry*, **278,** 34897–34909.

Berglund, L., Björling, E., Oksvold, P., Fagerberg, L., Asplund, A., Szigyarto, C.A.K., Persson, A., Ottosson, J., Wernérus, H., Nilsson, P., Sivertsson, A., Navani, S., Wester, K., Kampf, C., Hober, S., Pontén, F., Uhlén, M., 2008. A genecentric Human Protein Atlas for expression profiles based on antibodies. *Molecular & Cellular Proteomics : MCP*, **7,** 2019–2027.

Bertran, M.T., Sdelci, S., Regué, L., Avurch, J., Caelles, C., Roig, J., 2011. Nek9 is a Plk1-activated kinase that controls early centrosome separation through Nek6/7 and Eg5. *The EMBO journal*, **30,** 2634–2647.

Brisch, E., Daggett, M.A. & Suprenant, K.A., 1996. Cell cycle-dependent phosphorylation of the 77 kDa echinoderm microtubule-associated protein (EMAP) in vivo and association with the p34cdc2 kinase. *Journal of Cell Science*, **109,** 2885–2893.

Britigan, E.M.C., Wan, J., Zasadil, L.M., Ruan, S.D., Weaver, B.A., 2014. The ARF tumor suppressor prevents chromosomal instability and ensures mitotic checkpoint fidelity through regulation of Aurora B. *Molecular Biology of the Cell*, **25,** 2761–73.

Brouhard, G.J., Stear, J.H., Noetzel, T.L., Al-Bassam, J., Kinoshita, K., Harrison, S.C., Howard, J., Hymna, A.A., 2008. XMAP215 is a processive microtubule polymerase. *Cell*, **132,** 79-88.

Bulinski, J.C. & Borisy, G.G., 1979. Self-assembly of microtubules in extracts of cultured HeLa cells and the identification of HeLa microtubule-associated proteins. *Proceedings of the National Academy of Sciences of the United States of America*, **76,** 293–7.

Cassidy, L.D., Liau, S-S., Venkitaraman, A.R., 2014. Chromosome instability and carcinogenesis: insights from murine models of human pancreatic cancer associated with BRCA2 inactivation. *Molecular Oncology*, **8,** 161-168.

Chang, P. & Stearns, T., 2000. Delta-tubulin and epsilon-tubulin: two new human centrosomal tubulins reveal new aspects of centrosome structure and function. *Nature Cell Biology*, **2,** 30–35.

Chen, D., Ito, S., Yuan, H., Hyodo, T., Kadomatsu, K., Hamaguchi, M., Senga, T., 2015. EML4 promotes the loading of NUDC to the spindle for mitotic progression. *Cell cycle,* **14,**1529–39.

Choi, Y.L., Soda, M., Yamashita, Y., Ueno, T., Takashima, J., Nakajima, T., Yatabe, Y., Takeuchi, K., Hamada, T., 2010. EML4-ALK mutations in Lung Cancer that confer resistance to ALK inhibitors. *The New England Journal of Medicine, 363,* 16–21.

Chu, C.-W., Hou, F., Zhang, J., Phu, L., Loktev, A., Kirkpatrick, D.S., Jackson, P.K., Zhao, Y., Zou, H., 2011. A novel acetylation of β-tubulin by San modulates microtubule polymerization via down-regulating tubulin incorporation. *Molecular Biology of the Cell*, **22,** 448–56.

Cohen, S., Aizer, A., Shav-Tal, Y., Yanai, A., Motro, B., 2013. Nek7 kinase accelerates microtubule dynamic instability. *Biochimica et Biophysica Acta - Molecular Cell Research*, **1833,** 1104–1113.

Crown, J. & Michael, O., 2000. The taxanes: an update. *The Lancet*, **355,** 1176–1178.

Das, T.K., Dana, D., Paroly, S.S., Perumal, S.K., Singh, S., Jhun, H., Pendse, J., Cagan, R.L., Talele, T.T., Kumar, S., 2013. Centrosomal kinase Nek2 cooperates with oncogenic pathways to promote metastasis. *Oncogenesis*, **2,** 1-14.

Dehmelt, L. & Halpain, S., 2005. The MAP2/Tau family of microtubule-associated proteins. *Genome biology*, **6,** 204.

Dhanasekaran, D.N., Kashef, K., Lee, C.M., Xu, H., Reddy, E.P., 2007. Scaffold proteins of MAP-kinase modules. *Oncogene*, **26,** 3185–202.

Domnitz, S.B., Wagenbach, M., Decarreau, J., Wordeman, L., 2012. MCAK activity at microtubule tips regulates spindle microtubule length to promote robust kinetochore attachment. *The Journal of Cell Biology*, **197,** 231–237.

Duellberg, C., Trokter, M., Jha, R., Sen, I., Steinmetz, M.O., Surrey,T., 2014. Reconstitution of a hierarchical +TIP interaction network controlling microtubule end tracking of dynein. *Nature Cell Biology.* **16,** 804-811.

Dunn, S., Morrison, E.E., Liverpool, T.B., Molina-Paris, C., Cross, R.A., Alonso, M.C., Peckham, M., 2008. Differential trafficking of Kif5c on tyrosinated and detyrosinated microtubules in live cells. *Journal of Cell Science*, **121,** 1085–1095.

Eichenmuller, B., Everley, P., Palange, J., Lepley, D., Suprenant, K.A., 2002. The Human EMAP-like Protein-70 (ELP70) is a microtubule destabilizer that localizes to the mitotic apparatus. *Journal of Biological Chemistry*, **277,** 1301–1309.

Eudy, J.D., Ma-Edmonds, M., Yao, S.F., Talmadge, C.B., Kelley, P.M., Weston, M.D., Kimberling, W.J., Sumegi, J., 1997. Isolation of a novel human homologue of the gene coding for echinoderm microtubule-associated protein (EMAP) from the Usher syndrome type 1a locus at 14q32. *Genomics*, **43,** 104–106.

Ewing, R.M., Chu, P., Elisma, F., Li, H., Taylor, P., Climie, S., McBroom-Cerajewski, L., Robinson, M.D., O'Connor, L., Li, M., Taylor, R., Dharsee, M., Ho, Y., Heilbut, A., Moore, L., Zhang, S., Ornatsky, O., Bukhmann, Y.V., Ethier, M., Sheng, Y., Vasilescu, J., Abu-Farha, M., Lambert, J-P., Duewel, H.S., Stewart, I.I., Kuehl, B., Hogue, K., Colwill,K., Gladwish, K., Muskat, B., Kinach, R., Adams, S-L., Moran, M.F., Morin, G.B., Topaloglou, T., Figeys, D., 2007. Large-scale mapping of human protein-protein interactions by mass spectrometry. *Molecular Systems Biology*, **3,** 89.

Faire, K., Watermann-Storer, C.M., Gruber, D., Masson, D., Salmon, E.D., Bulinski, J.C., 1999. E-MAP-115 (ensconsin) associates dynamically with microtubules in vivo and is not a physiological modulator of microtubule dynamics. *Journal of Cell Science*, **112,** 4243–4255.

Fallet-Bianco, C., Laquerrière, A., Poirier, K., Razavi, F., Guimiot, F., Dias, P., Loeuillet, L., Lascelles, K., Beldjord, C., Carion, N., Toussaint, A., Revencu, N., Addor, M-C., Lhermitte, B., Gonzales, M., Martinovich, J., Bessieres, B., Marcy-Bonnière, M., Jossic, F., Marcorelles, P., Loget, P., Chelly, J., Bahi-Buisson, N., 2014. Mutations in tubulin genes are frequent causes of various foetal malformations of cortical development including microlissencephaly. *Acta Neuropathologica Communications*, **2,** 69.

Fang, G., Zhang, D., Yin, H., Zheng, L., Bi, X., Yuan, L., 2014. Centlein maintains centrosome cohesion by bridging an interaction between C-Nap1 and Cep68. *Journal of Cell Science*, **110,** 1631-1639.

Faragher, A.J. & Fry, A.M., 2003. Nek2A kinase stimulates centrosome disjunction and is required for formation of bipolar mitotic spindles. *Molecular Biology of the Cell,* **14,** 2876–2889.

Fletcher, L., Cerniglia, G.J., Yen, T.J., Muschel, R.J., 2005. Live cell imaging reveals distinct roles in cell cycle regulation for Nek2A and Nek2B. *Biochimica et Biophysica Acta*, **1744,** 89–92.

Fry, A.M., 2002. The Nek2 protein kinase: a novel regulator of centrosome structure. *Oncogene*, **21,** 6184–6194.

Fry, A.M., Mayor, T., Meraldi, P., Steirhof, Y.D., Tanaka, K., Nigg, E.A., 1998. C-Nap1, a novel centrosomal coiled-coil protein and candidate substrate of the cell cycle-regulated protein kinase Nek2. *Journal of Cell Biology*, **141,** 563–1574.

Fry, A.M., Meraldi, P. & Nigg, E.A., 1998. A centrosomal function for the human Nek2 protein kinase, a member of the NIMA family of cell cycle regulators. *EMBO Journal*, **17,** 470–481.

Fry, A.M., O'Regan, L., Sabir, S.R., Bayliss, R., 2012. Cell cycle regulation by the

NEK family of protein kinases. *Journal of Cell Science*, **125,** 4423–4433.

Fry, A.M., Schultz, S.J., Bartek, J., Nigg, E.A., et al., 1995. Substrate specificity and cell cycle regulation of the Nek2 protein kinase, a potential human homolog of the mitotic regulator NIMA of Aspergillus nidulans. *Journal of Biological Chemistry*, **270,** 12899–12905.

Gallaud, E., Caous, R., Pascal, A., Bazile, F., Gagnè, J.P., Huet, S., Poirier, G.G., Chrètien, D., Richar-Parpaillon, L., Giet, R., 2014. Ensconsin/map7 promotes microtubule growth and centrosome separation in Drosophila neural stem cells. *Journal of Cell Biology*, **204,** 1111–1121.

Gallego, P., Velazquez-Campoy, A., Regue, L., Roig, J., Rverter, D., 2013. Structural analysis of the regulation of the DYNLL/LC8 binding to Nek9 by phosphorylation. *Journal of Biological Chemistry*, **288,** 12283–12294.

Gard, D.L. & Kirschner, M.W., 1987. A microtubule-associated protein from Xenopus eggs that specifically promotes assembly at the plus-end. *Journal of Cell Biology*, **105,** 2203–2215.

Gardner, M.K. & Odde, D.J., 2008. Dam1 complexes go it alone on disassembling microtubules. *Nature Cell Biology*, **10,** 379–81.

Gascoigne, K.E. & Taylor, S.S., 2009. How do anti-mitotic drugs kill cancer cells? *Journal of Cell Science*, **122,** 2579–2585.

Ghosh, D.K., Dasgupta, D. & Guha, A., 2012. Models, regulations, and functions of microtubule severing by katanin. *ISRN Molecular Biology*, **2012,** 1–14.

Gierke, S., & Wittmann, T., 2012. B1-recruited microtubule +TIP complexes coordinate protrusion dynamics during 3D epithelial remodelling. *Current Biology*, **9,** 753-762.

Good, M.C., Zalatan, J.G. & Lim, W.A., 2011. Scaffold proteins: hubs for controlling the flow of cellular information. *Science,* **332,** 680–686.

Gräf, R., 2002. DdNek2, the first non-vertebrate homologue of human Nek2, is

involved in the formation of microtubule-organizing centers. *Journal of Cell Science*, **115,** 1919–1929.

Grallert, A. & Hagan, I.M., 2002. Schizosaccharomyces pombe NIMA-related kinase, Fin1, regulates spindle formation and an affinity of Polo for the SPB. *The EMBO Journal*, **21,** 3096–107.

Graser, S., Stierhof, Y-D. & Nigg, E.A., 2007. Cep68 and Cep215 (Cdk5rap2) are required for centrosome cohesion. *Journal of Cell Science*, **120,** 4321–4331.

Green, R.A., Wollman, R. & Kaplan, K.B., 2005. APC and EB1 function together in mitosis to regulate spindle dynamics and chromosome alignment. *Molecular Biology of the Cell*, **16,** 4609–4622.

Hamill, D.R., Howell, B., Cassimeris, L., Suprenant, K.A.,1998. Purification of a WD repeat protein, EMAP, that promotes microtubule dynamics through an inhibition of rescue. *The Journal of Biological Chemistry*, **273,** 9285–91.

Hammond, J.W., Cai, D. & Verhey, K.J., 2008. Tubulin modifications and their cellular functions. *Current Opinion in Cell Biology*, **20,** 71–76.

Haq, T., Richards, M.W., Burgess, S.G., Gallego, P., Yeoh, S., O'Regan, L., Reverter, D., Roig, J., Fry, A.M., Bayliss, R., 2015. Mechanistic basis of Nek7 activation through Nek9 binding and induced dimerization. *Nature Communications*, **6,** 1-12.

Harada, A., Oguchi, K., Okabe, S., Kuno, J., Terada, S., Ohshima, T., Sato-Yoshitake, R., Takei, Y., Noda, T., Hirokawa, N., 1994. Altered microtubule organization in small-calibre axons of mice lacking tau protein. *Nature*, **369,** 488–491.

Hardy, T., Lee, M., Hames, R.S., Prosser, S.L., Cheary, D-M., Samant, M.D., Schultz, F., Baxter, J.E., Rhee, K., Fry, A.M., 2014. Multisite phosphorylation of C-Nap1 releases it from Cep135 to trigger centrosome disjunction. *Journal of Cell Science*, **127,** 2493–2506.

Hartman, J.J., Mahr, J., McNally, K., Okawa, K., Iwamatsu, A., Thomas, S., Cheesman, S., Heuser, J., Vale, R.D., McNally, F.J., 1998. Katanin, a

microtubule-severing protein, is a novel AAA ATPase that targets to the centrosome using a WD40-containing subunit. *Cell*, **93,** 277–287.

Hayes, M.J., Kimata, Y., Wattam, S.L., Lindon, C., Mao, G., Yamano, H., Fry, A.M., 2006. Early mitotic degradation of Nek2A depends on Cdc20-independent interaction with the APC/C. *Nature Cell Biology*, **8,** 607–614.

Hayward, D.G., Clarke, R.B., Faragher, A.J., Pillai, M.R., Hagan, I.M., Fry, A.M., 2004. The centrosomal kinase Nek2 displays elevated levels of protein expression in human breast cancer. *Cancer Research*, **64,** 7370–7376.

Heidebrecht, H.J., Buck, F., Pollmann, M., Siebert, R., Parwaresch, R., 2000. Cloning and localization of C2orf2 (ropp120), a previously unknown WD repeat protein. *Genomics*, **68,** 348–50.

Helenius, J., Brouhard, G., Kalaidzidis, Y., Diez, S., Howard, J., 2006. The depolymerizing kinesin MCAK uses lattice diffusion to rapidly target microtubule ends. *Nature*, **441,** 115–119.

Henise, J.C. & Taunton, J., 2011. Irreversible Nek2 kinase inhibitors with cellular activity. *Journal of Medicinal Chemistry*, **54,** 4133–4146.

Heuckmann, J.M., Calke-Want, H., Malchers, F., Peifer, M., Sos, M.L., Koker, M., Meder, L., Lovly, C.M., Heukamp, L.C., Pao, W., Küppers, R., Thomas, R.K., 2012. Differential protein stability and ALK inhibitor sensitivity of EML4-ALK fusion variants. *Clinical cancer research : an official journal of the American Association for Cancer Research*, **18,** 4682–90.

He, Y., Zeng, M.Y., Yang, D., Motro, B., Núñez, G., 2016. NEK7 is an essential mediator of NLRP3 activation downstream of potassium efflux. *Nature*, **000,** 1–5.

Hirokawa, N. & Tanaka, Y., 2015. Kinesin superfamily proteins (KIFs): Various functions and their relevance for important phenomena in life and diseases. *Experimental Cell Research*, **334,** 16–25.

Horn, L. & Pao, W., 2009. EML4-ALK: Honing in on a new target in non-small-cell lung cancer. *Journal of Clinical Oncology*, **27,** 4232–4236.

Houtman, S.H., Rutteman, M., De Zeeuw, C.I., French, P.J., 2007. Echinoderm microtubule-associated protein like protein 4, a member of the echinoderm microtubule-associated protein family, stabilizes microtubules. *Neuroscience*, **144,** 1373–1382.

Hu, C.M., Zhu, J., Guo, X., Chen, W., Qiu, X., 2014. Novel small molecules disrupting Hec1/Nek2 interaction ablate tumor progression by triggering Nek2 degradation through a death-trap mechanism. *Oncogene*, **34,** 1–11.

Hueston, J.L., Herren, G.P., Cueva, J.G., Buechner, M., Lundquist, E.A., Goodman, M.B., Suprenant, K.A., 2008. The C. elegans EMAP-like protein, ELP-1 is required for touch sensation and associates with microtubules and adhesion complexes. *BMC developmental biology*, **8,** 110.

Hueston, J.L. & Suprenant, K.A, 2009. Loss of dystrophin and the microtubule-binding protein ELP-1 causes progressive paralysis and death of adult C. elegans. *Developmental Dynamics*, **238,** 1878–1886.

Hunter, A.W., Caplow, M., Coy, D.L., Hancock, W.O., Diez, S., Wordemann, L., Howard, J., 2003. The kinesin-related protein MCAK is a microtubule depolymerase that forms an ATP-hydrolyzing complex at microtubule ends. *Molecular Cell*, **11,** 445–457.

Innocenti, P., Cheung, K-M.J., Solanski, S., Mas-droux, C., Yeoh, S., Boxall, K., Westlake, M., Pickard, L., Hardy, T., Baxter, J.E., Aherne, G.W., Bayliss, R., Fry, A.M., 2014. Europe PMC Funders Group Design of potent and selective hybrid inhibitors of the mitotic kinase Nek2: SAR , structural biology and cellular activity. *Journal of Medical Chemistry,* **55,** 3228–3241.

Iqbal, K., Alonso, A.D.C., Chen, S., Chohan, M.O., El-Akkad, E., Gong, C-X., Khatoon, S., Li, B., Liu, F., Rahman, A., Tanimukai, H., Grundke-Iqbal, I., 2005. Tau pathology in Alzheimer disease and other tauopathies. *Biochimica et Biophysica Acta*, **1739,** 198–210.

James, C.R., Quinn, J.E., Mullan, P.B., Johnston, P.G., Harkin, D.P., 2007. BRCA1, a potential predictive biomarker in the treatment of breast cancer. *The Oncologist*, **12,** 142–50.

Janke, C., 2014. The tubulin code: Molecular components, readout mechanisms, and functions. *The Journal of Cell Biology*, **206,** 461–472.

Janke, C. & Chloë Bulinski, J., 2011. Post-translational regulation of the microtubule cytoskeleton: mechanisms and functions. *Nature Reviews Molecular Cell Biology*, **12,** 773–786.

Jin, J., Suzuki, H., Hirai, S., Mikoshiba, K., Ohshima, T., 2010. JNK phosphorylates Ser322 of doublecortin and regulates its function in neurite extension and neuronal migration. *Developmental Neurobiology*. **14,** 929-942.

Jin, N., Smith, F.D., Stark, C., Wells, C.D., Fawcett, J.P., Kulkarni, S., Metalnikov, P., O'Donnell, P., Taylor, P., Taylor, L., Zougman, A., Woodgett, J.R., Langeberg, L.K., 2004. Proteomic, functional, and domain-based analysis of in vivo 14-3-3 binding proteins involved in cytoskeletal regulation and cellular organization. *Current Biology*, **14,**1436–1450.

Johnson, G.V.W & Stoothoff, W.H., 2004. Tau phosphorylstion in neuronal cell function and dysfunction. *Journal of Cell Science*, **117,** 5721- 5729.

Jordan, M.A., Thrower, D. & Wilson, L., 1991. Mechanism of inhibition of cell proliferation by vinca alkaloids. *Cancer Research,* **51,** 2212-2222.

Jun Zhou, J., Joyce, Y., & Harish, J.C., 2002. Attachment and tension in the spindle assembly checkpoint. *Journal of Cell Science*, **115,** 3547-3555.

Kakeno, M., Matsuzama, K., Matsui, T., Akita, H., Sugiyama, I., Ishidate, F., Nakano, A., Takashima, S., Goto, H., Inagaki M., Kaibuchi, K., Watanabe, T., 2014. Plk1 phosphorylates CLIP-170 and regulates its binding to microtubules for chromosome alignment. *Cell Structure and Function*, **1,** 45-59.

Kandli, M., Feige, E., Chen, A., Kilfin, G., Motro, B., 2000. Isolation and characterization of two evolutionarily conserved murine kinases (Nek6 and nek7) related to the fungal mitotic regulator, NIMA. *Genomics*, **68,** 187–196.

Kaneta, Y. & Ullrich, A., 2013. NEK9 depletion induces catastrophic mitosis by

impairment of mitotic checkpoint control and spindle dynamics. *Biochemical and Biophysical Research Communications*, **442,** 139–146.

Katarzyna A. Makowska, K.A., Hughes, R.E., White, K.J., Wells, C.M., Peckham, M., 2015. Specific myosins control actin organization, cell morphology, and migration in prostrate cancer cells. *Cell Reports,* **13,** 2118-2125.

Katayama, R., Shaw, A.T., Khan, T.M., Mino-kenudson, M., Solomon, B.J., Halmos, B., Jessop, N.A., Wain, J.C., Tien, A., Benes, C., Drew, L., Saeh, J.C., Crosby, K., Lecia, V., Lafrate, A.J., Engelman, J.A., 2012. Mechanisms of acquired crizotinib resistance in ALK- rearranged lung cancers. *Science Translational Medicine*, **4,** 1–25.

Kaverina, I. & Straube, A., 2011. Regulation of cell migration by dynamic microtubules. *Seminars in Cell & Developmental Biology*, **22,** 968–74.

De Keersmaecker, K., Carlos Graux, C., D. Odero, M., Mentens, N., Somers, R., Maertens, J., Wlodarska, I., Vanderberghe, P., Hagemeijer, A., Maryen, P., Cools, J., 2005. Fusion of EML1 to ABL1 in T-cell acute lymphoblastic leukemia with cryptic t(9;14)(q34;q32). *Blood*, **105,** .4849–4852.

Kielar, M., Tuy, F.P.D., Bizzotto, S., Lebrand, C., Romero, D.J.R., Poirier, K., Oegema, R., Mancini, G.M., Bahi-Buisson, N., Olaso, R., Le Moing, A-G., Boutourlinsky, K., Boucher, D., Carpentier, W., Berquin, P., Deleuze, J-F., Belvindrah, R., Borrell, V., Welker, E., Chelly, J., Croquelois, A., Franice, F., 2014. Mutations in EML1 lead to ectopic progenitors and neuronal heterotopia in mouse and human. *Nature Neuroscience*, **17,** 923–933.

Kim, H., Yoo, S-B., Choe, J-Y., Paik, J.H., Xu, X., Nitta, H., Zhang, W., Grogan, T.M., Lee, C-T., Jheon, S., Chung, J-H., 2011. Detection of ALK gene rearrangement in non-small cell lung cancer. *Journal of Thoracic Oncology*, **6,** 1359–1366.

Kim, S., Kim, S. & Rhee, K., 2011. NEK7 is essential for centriole duplication and centrosomal accumulation of pericentriolar material proteins in interphase cells. *Journal of Cell Science*, **124,** 4126–4126.

Kinoshita, K., Habermann, B. & Hyman, A. A., 2002. XMAP215: A key component

of the dynamic microtubule cytoskeleton. *Trends in Cell Biology*, **12,** 267–273.

Kops, G.J.P.L. & Shah, J.G., 2012. Connecting up and clearing out: how kinetochore attachment silences the spindle assembly checkpoint. *Chromosoma*, **121,** 509–525.

Krien, M.J.E., Bugg, S.J., Palatsides, M., Asouline, G., Morimyo, M., O'Connell, M.J., 1998. A NIMA homologue promotes chromatin condensation in fission yeast. *Journal of Cell Science*, **111,** 967–76.

Krien, M.J.E., West, R. R., John, U.P., Koniaras, K., McIntosh, J.R., O'Connell, M.J., 2002. The fission yeast NIMA kinase Fin1p is required for spindle function and nuclear envelope integrity. The *EMBO Journal.* **21,** 1713–1722.

Kurioka, D., Takeshita, F., Tsuta, K., Sakamoto, H, Watanabe, S-I., Matsumoto, K., Watanabe, M., Nakagama, H., Ochiya, T., Yokota, J., Kohno, T., Tsuchiya, N., 2014. NEK9-dependent proliferation of cancer cells lacking functional p53. *Scientific Reports*, **4,** 6111.

Lara-Gonzalez, P., Westhorpe, F. & Taylor, S., 2012. The spindle assembly checkpoint. *Current Biology,* **22,** 966–980.

Le Clainche & C., Carlier, M-F., 2008. Regulation of actin assembly associated with protrusion and adhesion in cell migration. *Physiological reviews*, **88,** 489-513.

Ligon, L.A., Shelly, S.S., Tokito, M., Holzbaur, E.L.F., 2003. The microtubule plus-end proteins EB1 and dynactin have differential effects on microtubule polymerization. *Molecular Biology of the Cell*, **14,** 1405–1417.

Mahjoub, M.R., Trapp, M.L., Quarmby, L.M., 2005. NIMA-related kinases defective in murine models of polycystic kidney diseases localize to primary cilia and centrosomes. *Journal of the American Society of Nephrology*, **16,** 3485–3489.

Mandelkow, E. & Mandelkow, E-M., 1994. Microtubule structure. *Current Opinion in Structural Biology*, **4,** 171–179.

Manning, A.L., Longsworth, M.S., Dyson, N.J., 2012. Loss of pRB causes centrosome dysfunction and chromosome instability. *Genes and Development*, **24,** 1364-1376.

Maresca, T.J. & Salmon, E.D. 2010. Welcome to a new kind of tension: translating kinetochore mechanics into a wait-anaphase signal. *Journal of Cell Science*, **123,** 825-835.

Masson, D. & Kreis, T.E., 1995. Binding of E-MAP-115 to microtubules is regulated by cell cycle-dependent phosphorylation. *The Journal of Cell Biology*, **131,** 1015 –1024.

Mayer, M.P. & Bukau, B., 2005. Hsp70 chaperones: cellular functions and molecular mechanism. *Cellular and Molecular Life Sciences*, **62,** 670–684.

Meng, L., Carpenter, K., Mollard, A., Vankayalapati, H., Warner, S.L., Sharma, S., Tricot, G., Zhan, F., Bearss, D.J., 2014. Inhibition of Nek2 by small molecules affects proteasome activity. *BioMed Research International*, **2014,**1–13.

Meunier, S. & Vernos, I., 2012. Microtubule assembly during mitosis - from distinct origins to distinct functions? *Journal of Cell Science*, **125,** 2805–2814.

Moniz, L.S. & Stambolic, V., 2011. Nek10 mediates G2/M cell cycle arrest and MEK autoactivation in response to UV irradiation. *Molecular and Cellular Biology*, **31,** 30–42.

Moore, A.T., Rankin, K.E., Von Dassow, G., Peris, L., Wagenback, M., Ovechkina, Y., Andrieux, A., Job, D., Wodemann, L., 2005. MCAK associates with the tips of polymerizing microtubules. *Journal of Cell Biology*, **169,** 391–397.

Moraes, E., Meirelles, G., Honorato, R., De Souza, T, De Souza, E., Murakami, M., De Oliveira, P., Kobarg, J., 2015. Kinase inhibitor profile for human Nek1, Nek6, and Nek7 and analysis of the structural basis for inhibitor specificity. *Molecules*, **20,** 1176–1191.

Morris, N.R., 1975. Mitotic mutants of Aspergillus nidulans. *Genetical research*, **26,** 237–254.

Musacchio, A. & Salmon, E.D., 2007. The spindle-assembly checkpoint in space and time. *Nature reviews Molecular cell biology*, **8,** 379–93.

Nassirpour, R., Shao, L., Flanagan, P., Abrams, T., Jallal, B., Smeal, T., Yin, M-J., 2010. Nek6 mediates human cancer cell transformation and is a potential

cancer therapeutic target. *Molecular Cancer Research,* **8,** 717–728.

Neal, C.P., Fry, A.M., Moreman, C., McGregor, A., Garcea,G., Berry, D.P., Manson, M.M., 2014. Overexpression of the Nek2 kinase in colorectal cancer correlates with beta-catenin relocalization and shortened cancer-specific survival. *Journal of Surgical Oncology*, **110,** 828–838.

Ngan, V.K., Bellman, K., Hill, B.T., Wilson, L., Jordan, M.A., 2001. Mechanism of mitotic block and inhibition of cell proliferation by the semisynthetic Vinca alkaloids vinorelbine and its newer derivative vinflunine. *Molecular Pharmacology*, **60,** 225–232.

Nigg, E. A. & Raff, J.W., 2009. Centrioles, centrosomes, and cilia in health and disease. *Cell*, **139,** 663–678.

Nishino, N., Kurasawa, Y., Evans, R., Lin, S.H., Brinkley, B.R., Yu-Lee, YL.Y., 2006. NudC is required for Plk1 targeting to the kinetochore and chromosome congression. *Current Biology*, **14,** 1414-1421.

Noguchi, K., Fukazawa, H., Murakami, Y., Uehara, Y., 2002. Nek11, a new member of the NIMA family of kinases, involved in DNA replication and genotoxic stress responses. *The Journal of Biological Chemistry*, **277,** 39655–39665.

Noguchi, K., Fukazawa, H., Murakami, Y., Uehara, Y., 2004. Nucleolar Nek11 is a novel target of Nek2A in G1/S-arrested cells. *Journal of Biological Chemistry*, **279,** 32716–32727.

O'Connor, V., Houtman, S.H., De Zeeuw, C.I., Bliss, T.V.P., French, P.J., 2004. EML5, a novel WD40 domain protein expressed in rat brain. *Gene*, **336,** 127–37.

O'Regan, L. & Fry, A.M., 2009. The Nek6 and Nek7 protein kinases are required for robust mitotic spindle formation and cytokinesis. *Molecular and Cellular Biology*, **29,** 3975–3990.

O'Regan, L., Sampson. J., Richards, M.W., Knebel, A., Roth, D., Hood, F.E., Straube, A., Royle, S.J., Bayliss, R., Fry, A.M., 2015. Hsp72 is targeted to the

mitotic spindle by Nek6 to promote K-fiber assembly and mitotic progression. *The Journal of Cell Biology*, **209,** 349–358.

Ohi, R., Sapra, T., Howard, J., Mitchison, T.J., 2004. Differentiation of cytoplasmic and meiotic spindle assembly MCAK functions by Aurora B-dependent phosphorylation. *Molecular Biology of the Cell*, **15,** 2895 –2906.

Orr, G.A., Verdier-Pinard, P., McDaid, H., Horwitz, S.B., 2003. Mechanisms of Taxol resistance related to microtubules. *Oncogene*, **22,** 7280–7295.

Osmani, A.H., McGuire, S.L. & Osmani, S. A., 1991. Parallel activation of the NIMA and p34cdc2 cell cycle-regulated protein kinases is required to initiate mitosis in A. nidulans. *Cell*, **67,** 283–291.

Pollmann, M., Parwaresch, R., Adam-Klages, S., Kruse, M-L., Buck, F., Heidebrecht, H-J., 2006. Human EML4, a novel member of the EMAP family, is essential for microtubule formation. *Experimental Cell Research*, **312,** 3241–3251.

Prigent, C., Glover, D.M. & Giet, R., 2005. Drosophila Nek2 protein kinase knockdown leads to centrosome maturation defects while overexpression causes centrosome fragmentation and cytokinesis failure. *Experimental Cell Research*, **303,** 1–13.

Prosser, S.L., Sahota, N.K., Pelletier, L., Morrison, C.G., Fry, A.M., 2015. Nek5 promotes centrosome integrity in interphase and loss of centrosome cohesion in mitosis. *Journal of Cell Biology,* **209,** 339–348.

Prota, A.E., Magiera, M.M., Kuijpers, M., Bargsten, K., Frey, D., Wieser, M., Jaussi, R., Hoogenraad, C.C., Kammerer, R.A., Janke, C., Steinmetz, M.O., 2013. Structural basis of tubulin tyrosination by tubulin tyrosine ligase. *Journal of Cell Biology*, **200,** 259–270.

Pu, R.T. & Osmani, S. A., 1995. Mitotic destruction of the cell cycle regulated NIMA protein kinase of Aspergillus nidulans is required for mitotic exit. *The EMBO journal*, **14,** 995–1003.

Pu, R.T, Xu, G., Wu, L., Vierula, J., O'Donnell, K., Ye, X.S., Osmani, S.A.,1995. Isolation of a functional homolog of the cell cycle-specific NIMA protein kinase of Aspergillus nidulans and functional analysis of conserved residues. *The Journal of biological chemistry*, **270,** 18110–6.

Ramey, V.H., Wang, H-W., Nakajima, Y., Wong, A., Liu, J., Drubin, D., Barner, G., Nogales, E., 2011 The Dam1 ring binds to the E-hook of tubulin and diffuses along the microtubule. *Molecular Biology of the Cell*, **22,** 457–466.

Rankin, K.E. & Wordeman, L., 2010. Long astral microtubules uncouple mitotic spindles from the cytokinetic furrow. *Journal of Cell Biology*, **190,** 35–43.

Rapali, P., Radnai, L., Süveges, D., Harmat, V., Tölgyesi, F., Wahlgren, W.Y., Katona, G., Nyitray, L., Pál, G., 2011. Directed evolution reveals the binding motif preference of the LC8/DYNLL hub protein and predicts large numbers of novel binders in the human proteome. *PLoS ONE*, **6,** 1-14.

Rapley, J., Nicolàs, M., Groen, A., Regué, L., Betran, M.T., Caelles, C., Avruch, J., Roig, J., 2008. The NIMA-family kinase Nek6 phosphorylates the kinesin Eg5 at a novel site necessary for mitotic spindle formation. *Journal of Cell Science*, **121,** 3912–3921.

Regué, L., Sdelci, S., Betran, M.T., Caelles, C., Reverter, D., Roig, J., 2011. DYNLL/LC8 protein controls signal transduction through the Nek9/Nek6 signaling module by regulating Nek6 binding to Nek9. *Journal of Biological Chemistry*, **286,** 18118–18129.

Richards, M.W., O'Regan, L., Mas-Droux, C., Blot, J.M.Y., Cheung, J., Hoelder, S., Fry, A.M., Bayliss, R., 2009. An autoinhibitory tyrosine motif in the cell-cycle-regulated Nek7 kinase is released throughbBinding of Nek9. *Molecular Cell*, **36,** 560–570.

Richards, M.W., Law, E.W.P., Rennalls, L.P., Busacca, S., O'Regan, L., Fry, A.M., Fennell, D.A., Bayliss, R., 2014. Crystal structure of EML1 reveals the basis for Hsp90 dependence of oncogenic EML4-ALK by disruption of an atypical β-propeller domain. *Proceedings of the National Academy of Sciences of the United States of America*, **111,** 5195–200.

Richards, M., O'Regan, L., Roth, D., Montgomery, J.M., Straube, A., Fry, A.M., Bayliss, R., 2015. Microtubule association of EML proteins and the EML4-ALK variant 3 oncoprotein require an N-terminal trimerization domain. *Biochemical Journal*, **536,** 529–536.

Roberts, R.L., Mösch, H.U. & Fink, G.R., 1997. 14-3-3 proteins are essential for RAS/MAPK cascade signaling during pseudohyphal development in S. cerevisiae. *Cell*, **89,** 1055–1065.

Roig, J., Groen, A., Caldwell, J., Avruch, J., 2005. Active Nercc1 protein kinase concentrates at centrosomes early in mitosis and is necessary for proper spindle assembly. *Molecular Biology of the Cell*, **16,** 4827–4840.

Roig, J., Mikhailox, A., Belham, C., Avruch, J., 2002. Nercc1, a mammalian NIMA-family kinase, binds the Ran GTPase and regulates mitotic progression. *Genes and Development*, **16,** 1640–1658.

Roll-Mecak, A., 2014. Intrinsically disordered tubulin tails: Complex tuners of microtubule functions? *Seminars in Cell & Developmental Biology*, **37,** 11–19.

Rubio, P.M., Geraghty, K.M., Wong, B.H., Wood, N.T., Campbell, D.G., Morrice, N., Mackintosh, C., 2004. 14-3-3-Affinity purification of over 200 human phosphoproteins reveals new links to regulation of cellular metabolism, proliferation and trafficking. *Biochemistry Journal*, **379,** 395–408.

Sabir, S.R., Sahota, N.K., Jones, G.D.D., Fry, A.M., 2015. Loss of Nek11 prevents G2/M arrest and promotes cell death in HCT116 colorectal cancer cells exposed to therapeutic DNA damaging agents. *Plos One*, **10,** 1-19.

Sanhaji, M., Friel, C.T., Wordemann, L., Louwen, F., Yuan, J., 2011. Mitotic centromere-associated kinesin (MCAK): a potential cancer drug target. *Oncotarget*, **2,** 935–947.

Schmid-Burgk, J.L., Chauhan, D., Schmidt, T., Ebert, T.S., Reinhrdt, J., Endl, E., Hornung, V., 2015. A genome-wide CRISPR screen identifies NEK7 as an essential component of NLRP3 inflammasome activation. *Journal of Biological Chemistry*, **291,** 103–109.

Schober, J.M., Cain, J.M., Komarova, Y.A., Borisv, G.G., 2009. Migration and actin protrusion in melanoma cells are regulated by EB1 protein. *Cancer Letters,* **284,** 30-36.

Schweitzer, B. & Philippsen, P., 1992. Short communication NPK1 , a nonessential protein kinase gene in Saccharomyces cerevisiae with similarity to Aspergillus nidulans nimA. *Molecular and General Genetics*, **234,** 164–167.

Sharma, N., Bryant, J., Wloga, D., Donaldson, R., Davis, R.C., Jerka-Dziadosz, M., Gaertig, J., 2007. Katanin regulates dynamics of microtubules and biogenesis of motile cilia. *Journal of Cell Biology*, **178,** 1065–1079.

Shi, H. Wang, Y., Li, X., Zhan, X., Tang, M., Fina, M., Su, L., Pratt, D., Cu, C.H., Hildebrand, S., Lyon, S., Scott, L., Quan, J., Sun, Q., Russell, J., Arnett, S., Jurek, P., Chen, D., Kraychenko, V.V., Mathison, J.C., Moresco, E.M.Y., Monson, N.L., Ulevitch, R.J., Beutler, B., 2015. NLRP3 activation and mitosis are mutually exclusive events coordinated by NEK7, a new inflammasome component. *Nature Immunology*, **(December)**, 1–12.

Sirajuddin, M., Rice, L.M. & Vale, R.D., 2014. Regulation of microtubule motors by tubulin isotypes and post-translational modifications. *Nature Cell Biology*, **16,** 335–344.

Soda, M. Choi, L.M., Enomoto, M., Takada, S., Yamashita, Y., Ishikawa, S., Fujiwara, S-I., Wantanabe, H., Kurashina, K., Hatanaka, H., Bando, M., Ohno, S., Ihikawa, Y., Aburatani, H., Niki, T., Sohara, Y., Sugiyama, Y., Mano, H., 2007. Identification of the transforming EML4–ALK fusion gene in non-small-cell lung cancer. *Nature*, **448,** 561–566.

Straube, A., 2011. *Microtubule dynamics - Methods and Protocols* 1st ed., Springer, 174.

Su, T.T., Parry, D.H., Donahoe, B., Chien, C., Farrell, P.H.O., Purdy, A., 2009. Cell cycle roles for two 14-3-3 proteins during Drosophila development. *Journal of Cell Science,* **114,** 3445–3454.

Suprenant, K.A., Dean, K., McKee, J., Hake, S.,1993. EMAP, an echinoderm microtubule-associated protein found in microtubule-ribosome complexes. *Journal of Cell Science*, **104,** 445–50.

Swailes, N.T., Colegrave, M., Knight, P.J., Peckham, M., 2006. Non-muscle myosins 2A and 2B drive changes in cell morphology that occur as myoblasts align and fuse. *Journal of Cell Science*, **119,** 3561-3570.

Tanaka, T., Sereno, F.F., Tseng, H-C., Kulkarni, A.B., Tsai, L-H., Gleeson, J.G. 2004. Cdk5 phosphorylation of doublecortin Ser297 regulates its effects on neuronal migration. *Cell.* **41,** 215-225.

Tegha-Dunghu, J., Neumann, B., Reber, S., Krause, R., Erfle, H., Walter, T., Held, M., Rogers, P., Hupfield, K., Ruppert, T., Ellenburg, J., Gruss, O.J., 2008. EML3 is a nuclear microtubule-binding protein required for the correct alignment of chromosomes in metaphase. *Journal of Cell Science*, **121,** 1718–1726.

Thiel, C., Kessler, K., Giessl, A., Dimmler, A., Shalev, S.A., Von der Haar, S., Zenker, M., Zahnleiter, D., Stöss, H., Beinder, E., Abou Jamra, R., Ekici, A.B., Schröder-Kreß, N., Aigner, T., Kirchner, T., Reis, A, Brandstätter, J.H., Rauch, A., 2011. NEK1 mutations cause short-rib polydactyly syndrome type majewski. *The American Journal of Human Genetics*, **88,** 106–114.

Tirnauer, J.S. & Bierer, B.E., 2000. EB1 proteins regulate microtubule dynamics, cell polarity, and chromosome stability. *Journal of Cell Biology*, **149,** 761–766.

Tokuraku, K., Okuyama, S., Matsushima, K., Ikezu, T., Kotani, S., 2010. Distinct neuronal localization of microtubule-associated protein 4 in the mammalian brain. *Neuroscience Letters*, **484,** 143–7.

Torivama, M., Mizuno, N., Fukami, T., Iguchi, T., Torivama, M., Tago, K., Itoh, H., 2012. Phosphorylation of doublecortin by protein kinase A orchestrates microtubule and actin dynamics to promote neuronal progenitor cell migration. *Journal of Biological Chemistry.* **16,** 12691-12702.

Tournebize, R., Popov, A., Kinoshita, K., Ashford, A.J., Rybiana, S., Mayer, T.U., Walczak, C.E., Karsenti, E., Hyman, A.A., 2000. Control of microtubule dynamics by the antagonistic activities of XMAP215 and XKCM1 in Xenopus egg extracts.

Nature Cell Biology, **2,** 13-19.

Uhlén, M., Björling, E., Agaton, C., Szigyarto, C.A-K., Amini, B., Andersen, E., Andersson, A-C., Angelidou, P., Asplung, A., Asplund C., Berglund, L., Bergström, K., Brumer, H., Cerjan, D., Ekström, M., Elobeid, A., Eriksson, C., Fagerberg, L., Falk, R., Forsberg, M., Björklund, M.G., Gumbel, K., Halimi, A., Hallin, I., Hamsten, C., Hansson, M., Hedhammar, M., Hercules, G., Kampf, C., Larsson, K., Lindskog, M., Lodewyckx, W., Lund, J., Lundenberg, J., Magnusson, K., Malm, E., NIlsson, P., Odling, J., Oksvold, P., Olsson, I., Oster, E., Ottosson, J., Paavilainen, L., Persson, A., Rimini, R., Rockberg, J., Runeson, M., Sivertsson, A., Sköllermo, A., Steen, J., Stenvall, M., Sterky, F., Strömberg, S., Sundberg, M., Tegel, H., Tourle, S., Wahlund, E., Waldén, A., Wan, J., Wernérus, H., Westburg, J., Wester, K., Wrethagen, U., Xu, L.L., Hober, S., Pontén, F., 2005. A human protein atlas for normal and cancer tissues based on antibody proteomics. *Molecular & Cellular Proteomics,* **4,** 1920–1932.

Uhlen, M., Oksvold, P., Fagerberg, L., Lundberg, E., Jonasson, K., Forsberg, M., Zwahlen, M., Kampf, C., Westerm K., Hober, S., Wernerus, H., Björling, L., Ponten, F., 2010. Towards a knowledge-based Human Protein Atlas. *Nature Biotechnology*, **28,** 1248–1250.

Upadhya, P., Birkenmeier, E.H., Birkenmeier, C.S., Barker, J.E., 2000. Mutations in a NIMA-related kinase gene, Nek1, cause pleiotropic effects including a progressive polycystic kidney disease in mice. *Proceedings of the National Academy of Sciences of the United States of America*, **97,** 217–221.

Uto, K. & Sagata, N., 2000. Nek2B, a novel maternal form of Nek2 kinase, is essential for the assembly or maintenance of centrosomes in early Xenopus embryos. *The EMBO Journal*, **19,** 1816–1826.

Vasquez, R.J., Gard, D.L. & Cassimeris, L., 1994. XMAP from Xenopus eggs promotes rapid plus end assembly of microtubules and rapid microtubule polymer turnover. *Journal of Cell Biology,* **127,** 985–993.

Vasquez, R.J., Gard, D.L. & Cassimeris, L., 1999. Phosphorylation by CDK1 regulates XMAP215 function in vitro. *Cell Motility and the Cytoskeleton*, **43,** 310–21.

Velonas, V., Woo, H., Remedios, C., Assinder, S., 2013. Current status of biomarkers for prostate cancer. *International Journal of Molecular Sciences*, **14,** 1034–11060.

Verhey, K.J. & Gaertig, J., 2007. The tubulin code. *Cell cycle,* **6,** 2152–60.

Vincent, M.D., Kuruvilla, M.S., Leighl, N.B., Kamel-Reid, S., 2012. Biomarkers that currently affect clinical practice: EGFR, ALK, MET, KRAS. *Current Oncology*, **19,** 33–44.

Vitre, B., Coquelled, F.M., Heichette, C., Garnier, C., Chrétien, D., Arnal, I., 2008. EB1 regulates microtubule dynamics and tubulin sheet closure in vitro. *Nature Cell Biology*, **10,** 415–421.

Walczak, C.E., Cai, S. & Khodjakov, A., 2010. Mechanisms of chromosome behaviour during mitosis. *Nature Reviews Molecular Cell Biology*, **11,** 91–102.

Walczak, C.E., Gan, E.C., Desai, A., Michison, T.J., Kline-Smith, S.L., 2002. The microtubule-destabilizing kinesin XKCM1 is required for chromosome positioning during spindle assembly. *Current Biology*, **12,** 1885–9.

Walther, A., Houlston, R & Tomlinson, I., 2008. Association between chromosomal instability and prognosis in colorectal cancer: a meta-analysis. *Gut,* **57,** 941-950.

Wang, R., Song, Y., Xu, X., Wu, Q., Liu, C., 2013. The expression of Nek7, FoxM1, and Plk1 in gallbladder cancer and their relationships to clinicopathologic features and survival. *Clinical and Translational Oncology*, **15,** 626–632.

Wehenkel, A. & Janke, C., 2014. Towards elucidating the tubulin code. *Nature Cell Biology*, **16,** 303–5.

Whipple, R.A., Cheung, A.M., Martin, S.S., 2007. Detyrosinated microtubule protrusions in suspended mammary epithelial cells promote reattachment. *Experimental Cell Research*, **7,** 1326-1336

Widlund, P.O., Stear, J., H.Pozniakovsky, A., Zanic, M., Reber, S., Brouhard, G.J., Hyman, A.A.,Howard, J., 2011. XMAP215 polymerase activity is built by combining multiple tubulin-binding TOG domains and a basic lattice-binding region. *Proceedings of the National Academy of Sciences*, **108,** 2741–2746.

Wordeman, L. & Asbury, C., 2001. A short history of mitosis : the early days. *Concepts and Mechaisms in Mitosis.*

Wu, W., Baxter, J.E., Wattam, S.L., Hayward, D.G., Fardilha, M., Knebel, A., Ford, E.M., Da Cruz de Silva, E.F., Fry, A.M., 2007. Alternative splicing controls nuclear translocation of the cell cycle-regulated Nek2 kinase. *Journal of Biological Chemistry*, **282,** 26431–26440.

Yang, S.W., Gao, C., Chen, L., Song, Y.L., Zhu, J.L., Qi., S.T., Jiang, Z.Z., Wang, Z.W., Lin, F., Huang, H., Xing, F.Q., Sun, Q.Y., 2012. Nek9 regulates spindle organization and cell cycle progression during mouse oocyte meiosis and its location in early embryo mitosis. *Cell Cycle*, **11,** 4366–4377.

Yang, J. & Weinberg, R.A., 2008. Epithelial-Mesenchymal transition: at the crossroads of development and tumor metastasis. *Developmental Cell*, **14,** 818–829.

Yao, D., Dai, C. & Peng, S., 2011. Mechanism of the mesenchymal-epithelial transition and its relationship with metastatic tumor formation. *Molecular Cancer Research*, **9,** 1608–1620.

Yen, T.J., Li, G., Schaar, B.T., Szilak, I., Cleveland, D.W., 1992. CENP-E is a putative kinetochore motor that accumulates just before mitosis. *Nature*, **359,** 536–539.

Yin, M-J., Shao, L., Voehinger, D., Smeal, T., Jallal, B., 2003. The serine/threonine kinase Nek6 is required for cell cycle progression through mitosis. *The Journal of Biological Chemistry*, **278,** 52454–52460.

Zalli, D., Bayliss, R. & Fry, A.M., 2012. The Nek8 protein kinase , mutated in the human cystic kidney disease nephronophthisis, is both activated and degraded during ciliogenesis. *Human Molecular Genetics,* **21,** 1155–1171.

Zanic, M., Widlund, P.O., Hyman, A.A., Howard, J., 2013. Synergy between XMAP215 and EB1 increases microtubule growth rates to physiological levels. *Nature Cell Biology*, **15,** 688–693.

Zeng, Y., Han, Z-D., Wang, C., Cai, C., Huang, Y-Q., Luo, H-W., Liu, Z-Z., 2015. Overexpression of NIMA-related kinase 2 is associated with progression and poor prognosis of prostate cancer. *BMC Urology*, **15,** 1–8.

Zhang, C.C., Yang, J.M., Bash-Babula, J., White, E., Murphy, M., Levine, A.J., Hait, W.N.,1999. DNA damage increases sensitivity to vinca alkaloids and decreases sensitivity to taxanes through p53-dependent repression of microtubule-associated protein 4. *Cancer Research*, **59,** 3663–70.

Zhu, Z.C., Gupta, K.K., Slabberkoorn, A.R., Paulson, B.A., Folker, E.S., Goodson, H.V., 2009. Interactions between EB1 and Microtubules: Dramatic effect of affinity tags and evidence for cooperative behaviour. *Journal of Biological Chemistry*, **284,** 32651–32661.

Appendix

pFLAG-CMV-2
4.7 kb

4662
4219
f1 IG
419
CMV
FLAG

Hind III
Not I
EcoR I
Cla I
Bgl II
EcoR V
Kpn I
Sal I
Xba I
Bam HI
Sma I

hGH poly A
1638
SV40 ori
E.coli ori/b-lact
2029

pLEICS-12
7481 bp

SpeI (250)
NdeI (485)
CMV Promoter
NcoI (611)
HindIII (890)
NcoI (903)
His-Tag
T7 Promoter
3 x Flag
TEV Site
EcoRV (1044)
NotI (1111)

Amp
ColE Origin
SV40 poly A
NcoI (4747)
Neomycin
SmaI (4128)
XmaI (4126)
SV40 Origin
NcoI (4012)
SV40 Promoter

SacB
HindIII (2904)
EcoRI (2992)
XhoI (3007)
XbaI (3019)
SP6 Promoter
BGH Poly A